



# Calculation and Simulation of Turbogenerators Using Permeance Network. Optimization Application.

Dmitry Petrichenko

## ► To cite this version:

Dmitry Petrichenko. Calculation and Simulation of Turbogenerators Using Permeance Network. Optimization Application.. Electric power. Ecole Centrale de Lille, 2007. English. NNT : . tel-00346766

**HAL Id: tel-00346766**

**<https://theses.hal.science/tel-00346766>**

Submitted on 12 Dec 2008

**HAL** is a multi-disciplinary open access archive for the deposit and dissemination of scientific research documents, whether they are published or not. The documents may come from teaching and research institutions in France or abroad, or from public or private research centers.

L'archive ouverte pluridisciplinaire **HAL**, est destinée au dépôt et à la diffusion de documents scientifiques de niveau recherche, publiés ou non, émanant des établissements d'enseignement et de recherche français ou étrangers, des laboratoires publics ou privés.

ÉCOLE CENTRALE DE LILLE

**THESE**

Présenté en vue d'obtenir le grade de

**DOCTEUR**

en

Génie Électrique

par

Dmitry PETRICHENKO

Doctorat délivré par l'École Centrale de Lille.

Titre de la thèse :

**Contribution à la modélisation et à la conception optimale des turbo-alternateurs de faible puissance**

Soutenu le 10 juillet 2007 devant le jury d'examen :

Rapporteurs :	L.GERBAUD	Professeur au LEG (Grenoble)
	B.VANDEPUT	Professeur à l'Université d'Eindhoven
Examineurs :	P.BROCHET	Professeur à l'Ecole Centrale de Lille
	M.HECQUET	MdC-HDR à l'IUT à Lille
	V.KUZNETSOV	Professeur au MPEI (Moscou)
	D.LALOY	Resp. R&D Jeumont Framatome
	H.LOMONOVA	Professeur à l'Université d'Eindhoven
Directeur de recherche :	P.BROCHET	Professeur à l'Ecole Centrale de Lille
Co-encadrant :	M.HECQUET	MdC-HDR à l'IUT A Lille

Thèse préparée dans le laboratoire, L2EP, à l'École Centrale de Lille.



Calculation and Simulation of Turbogenerators Using  
Permeance Network.  
Optimization Application.

Dmitry Petrichenko

22 May 2007

# Preface

The presented work was realized in Ecole Centrale de Lille in the laboratory of Electrotechnics and Power Electronics (Laboratoire d'Electrotechnique et d'Electronique de Puissance, L2EP) of Lille, team COME (Conception et Optimisation de Machines Electriques) with participation of CNRT (Centre National de Recherche Technologique de la France) in collaboration with Jeumont Framatome Areva Nuclear Power, region Nord – Pas de Calais and Moscow Power Engineering Institute.

## Acknowledgments

I wish to express my grateful acknowledgments to professor Pascal BROCHET, the professor of Ecole Centrale de Lille and the responsible of the COME team who heartily welcomed me in his team, for his belief in me. His human qualities created a perfect team and working among such people helped me a lot in my research.

I wish to express my gratitude to doctor Michel HECQUET, the associate professor of l'IUT de Lille, for his valuable advices, extraordinary energy, powerful support and very nice personality. Without his help and encouragement I wouldn't have finished my work and definitely wouldn't have spoken french.

I wish to acknowledge professor Vyacheslav KUZNETSOV, the professor of the department of Electromechanics, Moscow Power Engineering Institute. His passion of science, amicability, his personality made me choosing the way of researcher in electromechanics after the studentship and led me through hardship to the desired result while working on thesis.

I want to thank Mr. Patrick Brutsaert, engineer of the turbogenerator department of Jeumont-Framatome for his valuable remarks, advices and sharing his experience during my work.

I want to thank Mr. David BONNET (and Mr. Rith LY, the student-interns who made valuable contribution to the development and validation of our approach and software.

I would like to express my hearted acknowledgments to Mr. Andre Vandenput, the Professor of the Eindhoven University of Technology, Electrical Engineering Department, and Mr. Laurent GERBAUD, the Professor of the National Polytechnic Institute of Grenoble, who do us the honor of participating in the jury as reporters.

I want to express my sincere acknowledgments to Mr. Daniel LALOY, the coordinator of R&D department of electrotechnics and electronics laboratory of Jeumont-Framatome in the equipments business unit of AREVA, Mr. Jean-Louis COUDERT and Mr. Damien VERBEKE, the engineers of Jeumont-Framatome, for their valuable help.

I also thank all the administrative, technical and professor staff of Ecole Centrale de Lille and my colleagues for perfect working conditions and support. Among them I would like to thank personally Darius VIZIREANU, Frédéric GILLON, Bellemaine NAPAME, Xavier CIMETIERE, Olivier BARRE for their help and support.

And finally I want to thank my wife, my mother, my relatives for the tonnes of patience and firm belief in me.

*To my mother Vera*

*To my wife Julie*

*To my aunt Kate*

*To my wife's mother Elena*

# Abstract

Huge recent growth of electric energy consumption all over the world applies higher demands to turbogenerator performances and characteristics. The activities of different turbogenerator manufactures are being invested in order to ameliorate the products and increase the speed of project development.

An electrical machine is one of the most complicated parts of any electromechanical converter and can be itself considered as a complex system characterized by magnetic, electrical, wave, thermal, mechanical air- and hydrodynamic phenomena. For these reasons the main attention of a scientific researcher has been focused on the development of reliable multiphysical and coupled models and methods of electrical machines simulation and optimization.

For the purpose of turbogenerator optimization its model using parameterized electromagnetic coupled permeance network approach was created. Different phenomena like axial heterogeneity of the machine were taken into account. The model and developed software were tested in different cases to perform rapid calculation of the turbogenerator characteristics and operating modes. The calculation core of the software was coupled with the optimization tool to perform the machine's parameter influence study.

The developed approach and the flexibility of the software give the possibilities to further development and extension of the model by multi-physical phenomena, coupling realized model with vibrational, acoustic and especially thermal ones.

# Keywords

Multi-physical model  
Turbogenerator  
Electro-magnetic coupling  
Permeance network  
Optimization model

# Contents

<b>Introduction</b>	<b>1</b>
<b>1 Problem definition and overview</b>	<b>5</b>
1.1 Existing methods . . . . .	6
1.1.1 Conventional methods of calculations . . . . .	8
1.1.2 Field calculation methods . . . . .	15
1.1.3 Permeance network methods . . . . .	19
1.2 Conclusion . . . . .	23
<b>2 Used Approach</b>	<b>25</b>
2.1 Theoretical basis . . . . .	26
2.1.1 Calculating magnetic fields using vector or scalar magnetic potentials	26
2.1.2 Magnetic charges approach . . . . .	28
2.1.3 Coils in ferromagnetic systems . . . . .	31
2.1.4 Idea of a tooth contour and special boundary conditions . . . . .	33
2.1.5 Magnetic charges and permeance network . . . . .	37
2.2 Machine's permeance network . . . . .	39
2.2.1 General approach for zones' division of the machine . . . . .	40
2.2.2 Stator network . . . . .	43
2.2.3 Rotor network . . . . .	46
2.2.4 Airgap characteristics calculation . . . . .	49
2.3 Taking into account axial heterogeneity . . . . .	55
2.3.1 Steel zones . . . . .	56
2.3.2 Air-gap zone . . . . .	59
2.3.3 Slots zone . . . . .	60
2.4 Permeance Network Equations . . . . .	62
2.4.1 PN equations in matrix form . . . . .	62
2.4.2 Tableau formulation . . . . .	64
2.4.3 Taking into account nonlinearities . . . . .	66
2.5 Steady-state fixed-rotor model . . . . .	67
2.5.1 Basic equations . . . . .	67
2.5.2 Characteristics calculation . . . . .	69
2.6 Model taking into account rotation . . . . .	71
2.7 Conclusion . . . . .	71



<b>3</b>	<b>Software implementation</b>	<b>73</b>
3.1	General Information . . . . .	73
3.2	Software structure and approach . . . . .	74
3.2.1	Circuit Description Tools overview . . . . .	76
3.2.2	Matlab Solver general approach . . . . .	78
3.2.3	Matlab Solver structure . . . . .	79
3.3	Graphical User Interface . . . . .	81
3.3.1	Program Main Window . . . . .	81
3.3.2	Setting up project data . . . . .	81
3.3.3	Model generation and its characteristic view . . . . .	88
3.3.4	Calculating the modes and characteristics of turbogenerator . . . . .	89
3.4	Conclusion . . . . .	97
<b>4</b>	<b>Application</b>	<b>99</b>
4.1	Synchronous machine of 3kW . . . . .	99
4.1.1	Machine description . . . . .	99
4.1.2	Machine's permeance network . . . . .	101
4.1.3	Calculation results . . . . .	101
4.2	Two pole turbogenerator . . . . .	107
4.2.1	Machine description and its permeance network . . . . .	107
4.2.2	Calculation results . . . . .	107
4.3	Multi-pole turbogenerator . . . . .	114
4.3.1	Jeumont 4-pole turbogenerator . . . . .	114
4.4	Optimization application example . . . . .	117
4.4.1	Objective . . . . .	117
4.4.2	Calculation results . . . . .	118
4.5	Conclusion . . . . .	118
	<b>Conclusion and perspectives</b>	<b>121</b>
<b>A</b>	<b>Matlab Solver functions</b>	<b>125</b>
A.1	General functions . . . . .	125
A.2	Calculation functions . . . . .	126
A.2.1	Mode calculation functions . . . . .	126
A.2.2	Characteristic calculation functions . . . . .	126
A.3	Low-level calculation functions . . . . .	127
A.4	Post-processing functions . . . . .	127
<b>B</b>	<b>2-pole turbogenerator result comparison</b>	<b>129</b>

# List of Figures

1	4-poles rotor and stator . . . . .	2
2	2-poles rotor of turbogenerator . . . . .	2
1.1	Synchronous model equivalent circuit . . . . .	8
1.2	Synchronous model phasor diagram . . . . .	9
1.3	Equivalent circuit for Pottier diagram . . . . .	10
1.4	Potier diagram . . . . .	10
1.5	Frame conversion diagram . . . . .	11
1.6	Phasor diagram of a synchronous generator working on an active-inductive load . . . . .	13
1.7	Flux density in the air-gap of a big generator . . . . .	14
1.8	Variation of $x_d$ and $x_q$ parameters . . . . .	14
1.9	A 2D mesh of a synchronous machine and a 3D mesh of a claw-pole machine	20
1.10	Flux tube . . . . .	21
1.11	Permeance network of a synchronous generator . . . . .	22
1.12	Different calculation approaches groups . . . . .	24
2.1	A part of magnetic system's equivalent circuit in terms of SMP . . . . .	27
2.2	A part of magnetic system's equivalent circuit in terms of VMP . . . . .	28
2.3	Magnetic shell and its potential. . . . .	30
2.4	Magnetic charges field in air . . . . .	31
2.5	Forms of magnetic leaves . . . . .	32
2.6	Distribution of SMP and magnetic charges density for a coil with current . .	33
2.7	Stator and rotor tooth contours . . . . .	35
2.8	Tooth contour . . . . .	36
2.9	A magnetic shell stretched on tooth . . . . .	38
2.10	Other configuration of magnetic shells. . . . .	38
2.11	Magnetic shells in case of two layers of PN. . . . .	39
2.12	Main zones of a machine . . . . .	40
2.13	Characteristic zones of machine's magnetic core . . . . .	41
2.14	Zone definition . . . . .	42
2.15	Full stator scheme . . . . .	43
2.16	Tooth scheme . . . . .	44
2.17	Tooth division . . . . .	45
2.18	The stator yoke element . . . . .	45
2.19	Concentric rotor PN . . . . .	47
2.20	2-pole rotor PN . . . . .	47

2.21	Adaptive rotor PN. . . . .	48
2.22	TC field under SBC . . . . .	50
2.23	Tooth contour unipolar permeance calculation . . . . .	52
2.24	Finite element solution for air-gap unipolar permeance calculation . . . . .	54
2.25	TC permeance calculation comparison . . . . .	54
2.26	Stator magnetic system cross-section in axial direction . . . . .	55
2.27	Flux buging in the air of machine . . . . .	56
2.28	BH curve modification . . . . .	57
2.29	Flux displacement to the ventilation duct area in case of high saturation . . . . .	58
2.30	Field in the airgap of a machine . . . . .	59
2.31	Field in the slot zone of the machine. . . . .	61
2.32	Synchronous machine vector diagram . . . . .	68
2.33	Mutual chracteristics between stator and rotor teeth. . . . .	72
3.1	General structure of TurboTCM . . . . .	75
3.2	Interaction between TCMLib and Matlab . . . . .	77
3.3	Collaboration between different parts of the software . . . . .	79
3.4	Input data specification . . . . .	80
3.5	Program main window . . . . .	82
3.6	Setting up rated data . . . . .	83
3.7	Stator parameters setup . . . . .	84
3.8	Setting up stator slot parameters . . . . .	84
3.9	Defining slot parameters . . . . .	85
3.10	Slot distribution window for the rotor . . . . .	86
3.11	Rotor slot distribution . . . . .	87
3.12	Simulation parameters window . . . . .	88
3.13	Calculation of excitation current . . . . .	89
3.14	Air-gap characteristic viewer . . . . .	90
3.15	All characteristics viewer . . . . .	91
3.16	Operating mode calculation window . . . . .	92
3.17	Ampere-turns of PN elements (top) and air-gap flux density (down) . . . . .	93
3.18	Input data for no-load characteristic . . . . .	94
3.19	Input data for load characteristic . . . . .	95
3.20	Input data for regulation characteristic . . . . .	96
3.21	Input data for V-shaped characteristic calculations . . . . .	96
3.22	Input data for angular characteristic . . . . .	98
3.23	Results of angular characteristic calculation . . . . .	98
4.1	Rotor dimensions . . . . .	100
4.2	Steel BH-curves: rotor (left), stator(right) and shaft (bottom). . . . .	101
4.3	Rotor simplified scheme . . . . .	102
4.4	OPERA-RM model (fragment). . . . .	102
4.5	Fluxes comparison: TurboTCM – OPERA RM . . . . .	103
4.6	Noload (left) and load (right) characteristics: TurboTCM – OPERA RM . . . . .	104
4.7	Dynamic calculation: TurboTCM – OPERA RM . . . . .	104
4.8	Experimental workbench . . . . .	105
4.9	Static characteristics: comparison with experiment . . . . .	106

4.10	Rotation effect: experimental comparison . . . . .	106
4.11	Regulation characteristic of machine 1. . . . .	111
4.12	V-shaped characteristic of machine 1. . . . .	111
4.13	Regulation characteristic of machine 1 and variation of its $x_d$ and $x_q$ parameters. . . . .	112
4.14	No-load air-gap flux density distribution. . . . .	112
4.15	Rated mode air-gap flux density distribution. . . . .	113
4.16	Short-circuit mode air-gap flux density distribution. . . . .	113
4.17	Rotor of the 4-pole turbogenerator. . . . .	114
4.18	Taking into account rotor arms . . . . .	115
4.19	4-pole rotor permeance network. . . . .	115
4.20	No-load characteristic comparison for 4-pole machine. . . . .	116
4.21	$K_{hB3}$ for $T_{p1}$ min (left) and $K_{hB3}$ for $T_{p1}$ max (right) . . . . .	118
4.22	$K_{hE3}$ (left) and $K_{hE1}$ (right) for different $T_{p1}$ . . . . .	119
4.23	$I_f$ for $D_{i1}$ min (left) and $D_{i1}$ max for different $T_{p1}$ . . . . .	119
B.1	No-load characteristic comparison: Machine 1. . . . .	132
B.2	No-load characteristic comparison: Machine 2. . . . .	132
B.3	No-load characteristic comparison: Machine 3. . . . .	133
B.4	No-load characteristic comparison: Machine 4. . . . .	133
B.5	No-load characteristic comparison: Machine 5. . . . .	134
B.6	No-load characteristic comparison: Machine 6. . . . .	134
B.7	No-load characteristic comparison: Machine 7. . . . .	135
B.8	No-load characteristic comparison: Machine 8. . . . .	135
B.9	Short circuit characteristic comparison: Machine 1. . . . .	138
B.10	Short circuit characteristic comparison: Machine 2. . . . .	138
B.11	Short circuit characteristic comparison: Machine 3. . . . .	139
B.12	Short circuit characteristic comparison: Machine 4. . . . .	139
B.13	Short circuit characteristic comparison: Machine 5. . . . .	140
B.14	Short circuit characteristic comparison: Machine 6. . . . .	140
B.15	Short circuit characteristic comparison: Machine 7. . . . .	141
B.16	Short circuit characteristic comparison: Machine 8. . . . .	141



# Introduction

The development of new methods of investigation of electromechanical systems, consisting of different electromechanical converters, electrical, mechanical elements and semiconductor devices, and methods of representing magnetic fields and processes in electromechanical converters are among the most important problems of contemporary electromechanics. Historically, these two problems have been rather separated from one another and different methods have been used to solve them. This can be explained both by the diversity of the phenomena that occur in these systems and the modest capability of the computer equipment which has been used over many decades. The situation has changed. During the last 20-25 years a lot of new mathematical methods for analyzing phenomena and processes in electromechanical devices and systems have been developed and have become available. The growth of computer technologies and calculation speed has become an important event which made it possible the optimization problems to be shown for any objective function and the behavior of electromechanical systems and their elements to be analyzed both under nominal and extreme operating conditions.

An electrical machine is one of the most complicated parts of any electromechanical converter and can be itself considered as a complex system characterized by magnetic, electrical, wave, thermal, mechanical air- and hydrodynamic phenomena. For these reasons the main attention of a scientific researcher has been focused on the development of reliable multiphysical and coupled models and methods of electrical machines simulation and optimization.

The production and maintenance of turbogenerators currently constitute one of the main activities of *Jeumont S.A.*<sup>1</sup>. This activity is being invested in order to ameliorate the products and increase the speed of project development. The following figures present examples of 4-poles and stator (Figure 1) and 2-poles (Figure 2) rotors of turbogenerators produced in Jeumont.

The main objective of that study was to create a rapid model (and a software) of a turbogenerator which allows to calculate its characteristics and can be used together with optimization software.

This work consists of several chapters:

Chapter 1 presents the problem definition and overview of existing approaches used to calculate electrical machine characteristics. Describing conventional, numerical and combined methods we define our solution based on permeance network approach in order to obtain a rapid model which anyway can represent internal processes in an electrical machine in details.

In chapter 2 we thoroughly describe theoretical basis and realization of the approach

---

<sup>1</sup>Jeumont S.A. is a part of Framatome ANP - AREVA group. ANP - Advanced Nuclear Power

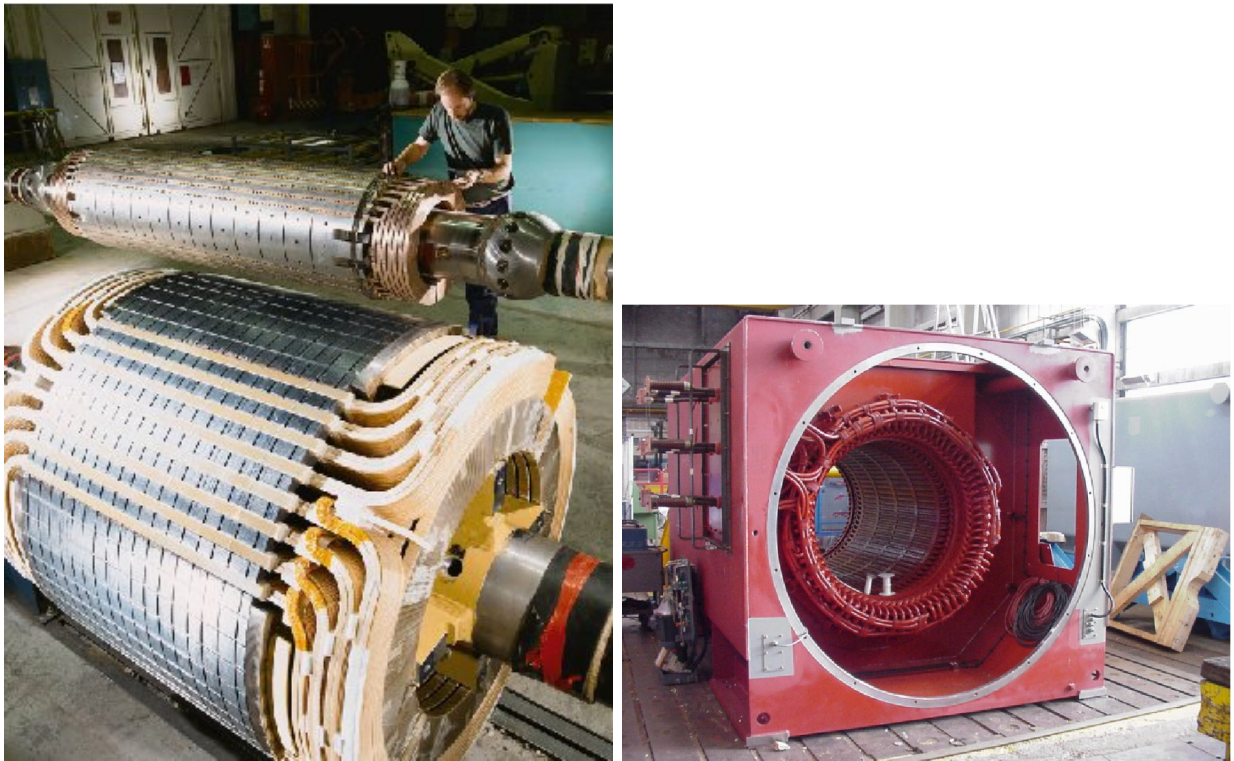


Figure 1: 4-poles rotor and stator



Figure 2: 2-poles rotor of turbogenerator

that we use. The description of the permeance network, the method of its construction and calculation of its parameters are given. The use of adaptive permeance network con-

struction give wide flexibility in implementation of different slot and yoke configurations. The proposed method of taking into account axial heterogeneity of turbogenerators can be spread on any type of machines having irregular axial structure; it can be used with any other calculation technique besides permeance networks. The fixed rotor algorithm shows high performance while calculating static characteristics of synchronous machines.

Chapter 3 gives the explanation of the way how our approach was realized in software, called **TurboTCM**. The tool is written in **Matlab** with some core objects written in **C++** using efficient object-oriented approach and component object model technique. Splitting the software on two levels – calculation core and graphical interface – gives the flexibility in use both in project definition with general calculations and in using specific features. The last allow extracting any available information about the internal networks from within **Matlab**. That last feature helps coupling **TurboTCM** with *any* calculation software and user-defined scripts in **Matlab** giving possibility to use the software with external optimization tools. The description of the internal software structure is followed by graphical user interface presentation.

Chapter 4 shows the results of model application to different machines. First the method was tested on a small 3 kW synchronous machine and compared with finite elements calculation. Then we present a 2-pole turbogenerator case with experimental validation. The 4-pole turbogenerator, its particularities and model realization are shown later. And in the end of the chapter we present the use of **TurboTCM** coupled with optimization supervisor **Sophemis** performing some results of screening and influence factor studies.

Finally, the main conclusions are presented with the perspective future use, development and application of our model and software.





# Chapter 1

## Problem definition and overview

This chapter gives a view on the aim of the thesis, the overview of several methods of electrical machine calculation, the choice of the method of simulation or so-called “virtual prototyping” applied to the case of turbogenerators.

The most part of the electrical machines are well-known and everything seems to be already done and studied in this area.

The scientific and technological progress in such areas like electrotechnics, permanent magnets, steels, composite and powder ferromagnetic materials, power electronics, converters, controllers delivers exceptional opportunities for further development and innovations in electromechanics. The same situation can be found also in further development of the structure of electrical machines and simplification and quality of their production process.

The objective of the project is to develop a *turbogenerator calculation tool* which can be used as a part of an *optimal design software*.

This tool must be able to perform all possible steady-state analysis of turbogenerators. For Jeumont it is necessary to obtain rapidly steady-state no-load and load characteristics of a machine, calculate its parameters in any operating mode:

- Any steady-state operating modes given by  $U$ ,  $I$  and Power Factor (PF) angle.
- Regulation, V-shape and Power-load angle characteristics.
- P-Q diagrams for different restrictions.
- Parameters and time constants, masses of active materials, losses and efficiency.
- Flux density distribution in the air-gap, stator and pole teeth, and stator yoke.
- $X_d$ ,  $X_q$  parameters for every calculated mode.

A modern turbogenerator is a complex, high-technological product which is described by hundreds of parameters starting from the basic geometry and structure and finishing by the material properties. Jeumont produces several series of turbogenerators of basically 2-poles and 4-poles construction for the power of 10-100MW. But also the production of machines up to 10 poles is under consideration. This fact demands rather flexible tool and mathematical model, which allows taking into account the special features of the turbogenerators, like:

- complex geometry of the turbogenerator's rotor, its tooth zone;
- complex geometry of the slots;
- complex distribution of the wires both in stator and rotor winding;
- winding cooling system;
- axial heterogeneity of a machine caused by stator and/or rotor ventilation ducts.

A lot of different methods which allow calculation of the characteristics listed above. Some of them can give only the estimations, some of them provide the redundant information. While creating a software for an engineer we should balance between them and use all the possible knowledge to obtain a model *not too general to be faulty and not too precise to be useless*.

But first of all let's take a glance on the existing methods of calculations.

## 1.1 Existing methods

The equations of electrical and magnetic circuits, which describe the processes in electrical machines, are obtained from the electromagnetic field equations according to the several assumptions.

The second Maxwell equation

$$\text{rot } \vec{E} = -\frac{\partial \vec{B}}{\partial t}, \quad (1.1)$$

written in an integral form links together the electrical field in a machine's winding and the changing speed of the magnetic field linked with the winding. This equation can be simply converged to the differential equations of voltages for separate electrical circuit contours

$$u_k + e_k = R_k i_k, \quad (1.2)$$

which link together the parameters of the electrical circuit's contour  $k$  ( $i_k$  – winding current,  $u_k$  – external voltage,  $R_k$  – winding's active resistance,  $e_k = -d\Psi_k/dt$  – an EMF induced in the winding) and magnetic circuit parameters – the winding flux linkage  $\Psi_k$ .

Contrary, the first Maxwell's equation, which determines the relation between magnetic field (with the strength  $\vec{H}$ ) and electrical field (with the winding's current density  $\vec{J}$ ),

$$\text{rot } \vec{H} = \vec{J}, \quad (1.3)$$

written in an integral form, is much more difficult to be transformed into the magnetic circuit equations

$$\Phi_i = \Lambda_i F_i \quad (1.4)$$

where  $\Phi_i$  – magnetic flux;  $F_i$  – magneto-motive force;  $\Lambda_i$  – magnetic permeance of the  $i$ -th branch.

The difficulties of that transform have the following reasons:

- the borders of the cores have rather complex form, for example, teeth zones of stator and rotor;
- the geometry of the air-gap between stator and rotor is variable according to their mutual movement;
- the magnetization characteristic of the stator and rotor cores are nonlinear.

Thus, in order to be able to calculate analytically the magnetic field in such a complex object, a set of assumptions has been defined. The main of them are as follows:

- the processes of the electromagnetic energy transform are determined mostly using the main harmonic of the air-gap flux density;
- the salient surfaces of the magnetic cores can be replaced with the non-salient air-gap, which is equivalent for the unipolar field;
- the main field of a saturated machine (the field of the first harmonic of flux density) can be considered as a sum of two independent fields – directed along longitudinal and transverse axes;
- the field factors for the basic harmonics of the flux density along longitudinal and transverse axes, found in linear approximation, can be applied to the saturated machine;
- the main field and the leakage fields of a saturated machine can be considered independently;
- the fields of the higher and lower spacial harmonics of flux density can be considered independently both on each other and on the main flux density harmonic.

The assumptions listed above, were formulated more than 70 years ago during the period of the basic creation of the electrical machine theory and were well presented in the fundamental monograph of R. Richter.

These assumptions allowed to divide the area of the field of an electrical machine into a set of zones with rather simple borders' geometry which does not depend on the rotor's movement (for example, an air-gap zone on a half-period of the first harmonic of flux density; zones corresponding to the slots, teeth and half-period of the field in the stator and rotor yokes). Using the *magneto-motive force* (MMF) makes it possible to calculate the magnetic field in such zones analytically and to find analytical equations determining the magnetic permeances of the specified branches  $\Lambda_i$ .

Thus, these assumptions helps to transform the description of the magnetic field in the machine in the form of Maxwell's equations (1.1), (1.3), fulfilled with the boundary conditions and complementary equations, into the description of the processes in the machine by means of its electrical and magnetic circuits (1.2), (1.4). Based on these equations and these assumptions a lot of different analytical methods of electrical machines calculations were developed.

### 1.1.1 Conventional methods of calculations

The methods developed during the period of basic development of the electrical machine theory, as it has been shown above, were based on rather strong assumptions, but even nowadays they are widely used in the design practice. The behavior of electrical machines both in steady-state and transient regimes is estimated using these methods. All of them are based on a determination of special parameters of the machines, which are used to calculate the characteristics of the last ones later on. For the moment there is a big variety of analytical methods of electrical machine calculations but here only some models concerning synchronous electrical machines will be discussed.

#### General methods

The synchronous reactance model is the simplest one. This model can be applied only for the first estimation of the behavior of machines with rather low level of saturation. Additional assumptions are used in this model:

- magnetic circuit saturation is neglected;
- hysteresis and eddy currents effects are neglected;
- electromotive forces (EMF) are supposed to be proportional to the excitation current;
- the machine is supposed to have non-salient poles.

Figure 1.1 shows the equivalent electrical circuit of the machine according to this model. The circuit is presented for one stator phase.

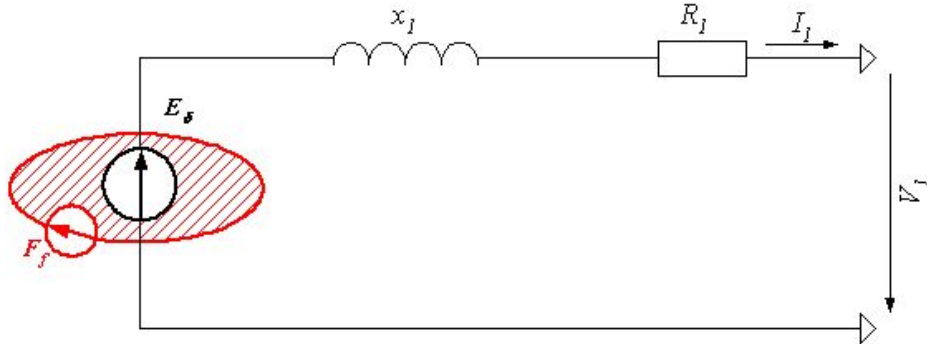


Figure 1.1: Synchronous model equivalent circuit

This model allows using the following equation in a complex form:

$$\dot{E}_1 - R_1 \dot{I}_1 - jx_1 \dot{I}_1 - \dot{V}_1 = 0 \quad (1.5)$$

$R_1$  – active resistance of a stator phase;

$x_1 = x_a + x_{1\sigma}$  – full synchronous reactance of a stator phase, where  $X_a$  – stator winding reactance,  $X_{1\sigma}$  – stator leakage reactance;

$\dot{E}_1$  – EMF of a stator phase;

$\dot{I}_1$  – stator current;

$\dot{V}_1$  – external phase voltage.

This scheme corresponds to the following phasor diagram (Figure 1.2):

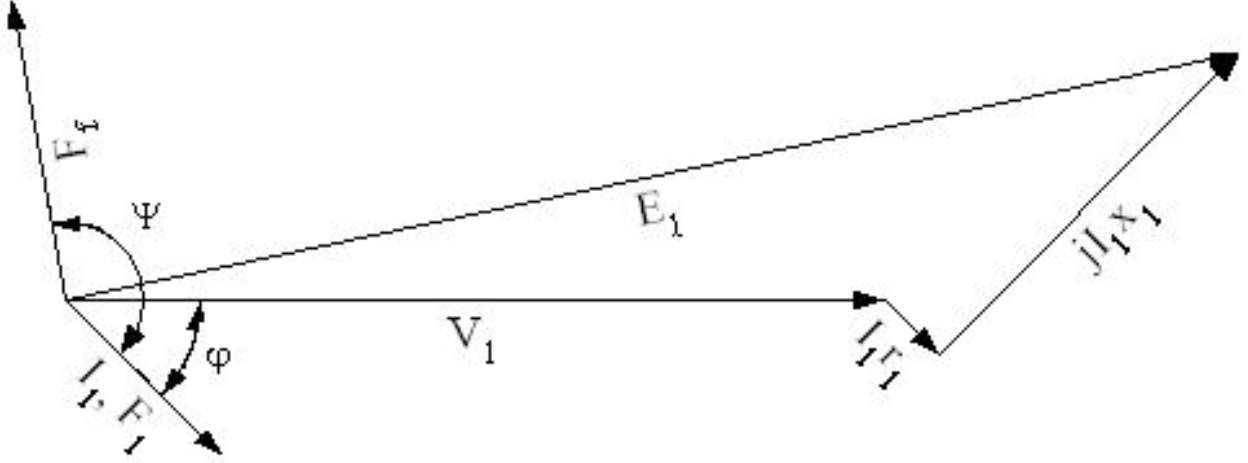


Figure 1.2: Synchronous model phasor diagram

The EMF  $\dot{E}_1$  is determined from the linear no-load characteristic. The model represents separate MMFs induced by stator and rotor windings ( $\dot{F}_f$  and  $\dot{F}_1$  respectively), while in reality there is only a full magnetic field in the machine produced by two windings simultaneously.

To take into account the saturation a real no-load curve must be used. Anyway, in this case the influence of slot, differential and end-winding leakages is neglected. That means that the value of  $x_{1\sigma}$  is considered linear and not depending on the magnetic state of the machine. This can be easily assumed for differential and end winding leakages but not so evident for the slot one.

$$x_{1\sigma} = x_{\sigma slot} + x_{\sigma diff} + x_{\sigma end} \quad (1.6)$$

Figures 1.3 and 1.4 show the equivalent circuit and the phasor diagram respectively, representing that one approach. In this case the EMF source  $\dot{E}_\delta$  represents the EMF caused by the interaction of both stator and rotor MMF-s:  $\dot{F}_f$  and  $\dot{F}_1$ .  $\dot{E}_\delta$  is so-called “EMF beyond the leakage”.

The diagram 1.4 is also called *Pottier diagram* and is widely used to calculate the excitation MMF (thus, field winding current) for the particular operating mode. Knowing the value of  $x_{1\sigma}$  (1.6) and the values of the mode:  $\dot{V}_1$ ,  $\dot{I}_1$  and  $\cos\phi$ , one can calculate the EMF  $\dot{E}_\delta$  and the value of corresponding  $\dot{F}_\delta$  using the precalculated no-load characteristic. Using the vector sum of  $\dot{F}_\delta$  and the referred value of stator winding MMF  $\dot{F}'_1$ , the value of excitation MMF  $F_f$  can be found.

The reduction of stator MMF  $F_1$  to  $F'_1$  is usually realized by armature reactance factor  $k_a$ :

$$F'_1 = k_a F_1 = \frac{F_1}{k_f} \quad (1.7)$$

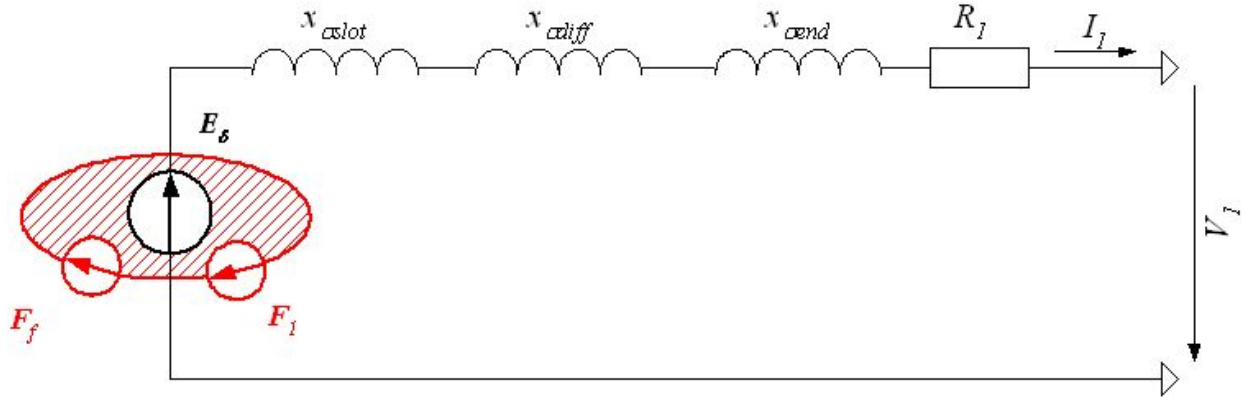


Figure 1.3: Equivalent circuit for Pottier diagram

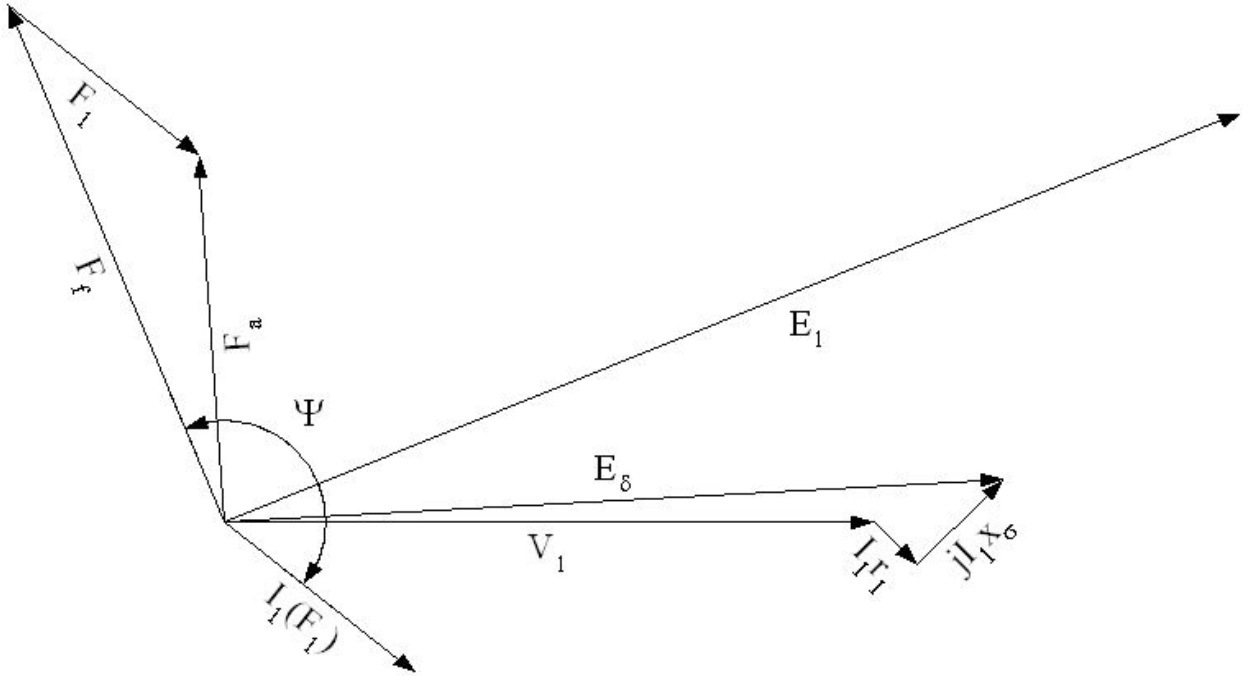


Figure 1.4: Potier diagram

where  $k_f$  – excitation field form factor. It's value for non-salient pole machines can be found in general [22]:

$$k_f = \frac{B_{\delta 1m}}{B_\delta} = \frac{F_{f1m}}{F_{fm}} = \frac{4}{\pi} k_{pf} = \frac{8 \sin \frac{\rho\pi}{2}}{\pi^2 p} \quad (1.8)$$

where:  $F_{fm} = I_f w_f$  – field winding MMF (on the pole axis);  $F_{f1m} = \frac{4}{\pi} k_{pf} F_{fm}$  – the amplitude of the field winding MMF first harmonic;  $k_{pf} \approx \sin \frac{\rho\pi}{2} / \frac{\rho\pi}{2}$  – distribution factor for the first harmonic of MMF. This factor realizes the reduction of the distributed stator winding to the rotor winding according to their first harmonics.

Sometimes the Pottier reactance  $x_{1\sigma}$  is multiplied by a factor of 1.1 to take into account the increase of the EMF of slot leakage due to saturation.

### DQ-frame methods

The method is based on the determination of the inductances of a machine in linear mode for the transient or steady-state operational conditions and though this method is mostly used for salient pole machines, we should mention it here, since its “philosophy” affects other methods of calculations.

The dq-frame is connected with the rotor axes:  $d$ -axis is aligned with the one of excitation winding, while  $q$ -axis leads the  $d$ -axis on  $\pi/2$  electrical radians. After that all the currents, fluxes, flux densities, voltages, EMFs, MMFs both of stator and rotor are projected to these axes and converted from a three-phase frame to dq-frame (see Figure. 1.5).

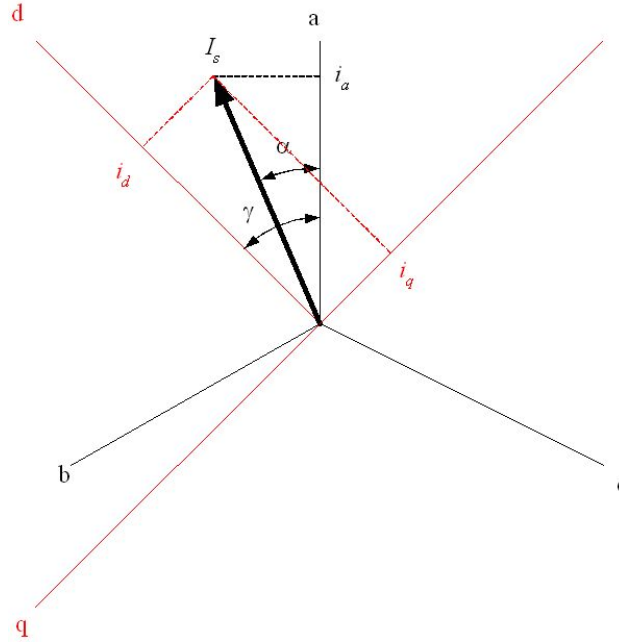


Figure 1.5: Frame conversion diagram

The coordinate transform of the currents can be performed using the Park-transform:

$$\left. \begin{aligned} i_d &= \frac{2}{3} (i_a \cos \gamma + i_b \cos(\gamma - 2\pi/3) + i_c \cos(\gamma + 2\pi/3)) \\ i_q &= -\frac{2}{3} (i_a \sin \gamma + i_b \sin(\gamma - 2\pi/3) + i_c \sin(\gamma + 2\pi/3)) \end{aligned} \right\} \quad (1.9)$$

$i_a, i_b, i_c$  – stator phase currents;

$i_d, i_q$  – stator currents in dq-frame.

The reverse transform can be performed using the following equations:

$$\left. \begin{aligned} i_a &= i_d \cos \gamma - i_q \sin \gamma \\ i_b &= i_d \cos(\gamma - 2\pi/3) - i_q \sin(\gamma - 2\pi/3) \\ i_c &= i_d \cos(\gamma + 2\pi/3) - i_q \sin(\gamma + 2\pi/3) \end{aligned} \right\} \quad (1.10)$$

If the stator winding of a synchronous machine is connected in star with neutral or triangular, it is possible that  $i_a + i_b + i_c \neq 0$ . In that case it is necessary to add an equation for the zero sequence currents:

$$i_0 = \frac{1}{3} (i_a + i_b + i_c). \quad (1.11)$$



The equations (1.9) and (1.10) set up the direct and reverse correspondence between the real currents in stator phases and new variables in the axes  $d, q$ . The equations for the flux linkages and voltages of the stator winding are obtained in the same manner:

$$\left. \begin{aligned} \Psi_d &= \frac{2}{3} (\Psi_a \cos \gamma + \Psi_b \cos(\gamma - 2\pi/3) + \Psi_c \cos(\gamma + 2\pi/3)) \\ \Psi_q &= -\frac{2}{3} (\Psi_a \sin \gamma + \Psi_b \sin(\gamma - 2\pi/3) + \Psi_c \sin(\gamma + 2\pi/3)) \\ \Psi_0 &= \frac{1}{3} (\Psi_a + \Psi_b + \Psi_c) \end{aligned} \right\} \quad (1.12)$$

To determine the correspondence between flux linkages and currents, including the rotor excitation winding, the following equations are used:

$$\left. \begin{aligned} \Psi_d &= L_d i_d + L_{afd} i_f = x_d i_d + x_{afd} i_f \\ \Psi_q &= L_q i_q = x_q i_q \\ \Psi_0 &= L_0 i_0 = x_0 i_0 \\ \Psi_f &= \frac{3}{2} L_{afd} i_d + L_f i_f = x_{afd} i_d + x_f i_f \end{aligned} \right\} \quad (1.13)$$

$\Psi_f, i_f$  – Rotor excitation winding flux linkage and current respectively.

$L_d$  – An inductance of a stator phase with symmetric sinusoidal current for a synchronous rotation speed, *while the stator field axis is aligned with the longitudinal axis of rotor*. The corresponding reactance  $x_d$  is called *synchronous longitudinal reactance*.

$L_q$  – An inductance of a stator phase with symmetric sinusoidal current for a synchronous rotation speed, *while the stator field axis is aligned with the transverse axis of rotor*. The corresponding reactance  $x_q$  is called *synchronous transverse reactance*.

$L_0$  – An inductance of a stator phase with *zero-sequence current*. The corresponding reactance  $x_0$  is called *zero-sequence reactance*.

$L_{afd}$  – A mutual inductance between a stator phase with symmetric sinusoidal current for a synchronous rotation speed, while the stator field axis is aligned with the longitudinal axis of rotor, and an excitation winding;  $x_{afd}$  – its corresponding reactance.

The voltages can be described by the following system of equations:

$$\left. \begin{aligned} u_d &= d\Psi_d/dt - \omega\Psi_q + r_1 i_d \\ u_q &= d\Psi_q/dt + \omega\Psi_d + r_1 i_q \\ u_0 &= d\Psi_0/dt + r_1 i_0 \\ u_f &= d\Psi_f/dt + r_f i_f \end{aligned} \right\} \quad (1.14)$$

The equations (1.14) are the well-known *Park-Gorev* ones. If the saturation of a magnetic circuit and the rotation speed are constant, then these equations become the linear differential ones. Figure 1.6 shows the phasor diagram corresponding to synchronous machine working as a generator on an active-inductive load.

The inductive parameters of the machines, which can be used in this model, are usually obtained analytically based on geometrical configuration and normal operational conditions of a machine. But this model doesn't take into account the variation of  $x_d$  and  $x_q$  according to the particular operational conditions, different loads and different load types, thus it's not really suitable for turbogenerators, which are known to work in wide variety of loads.

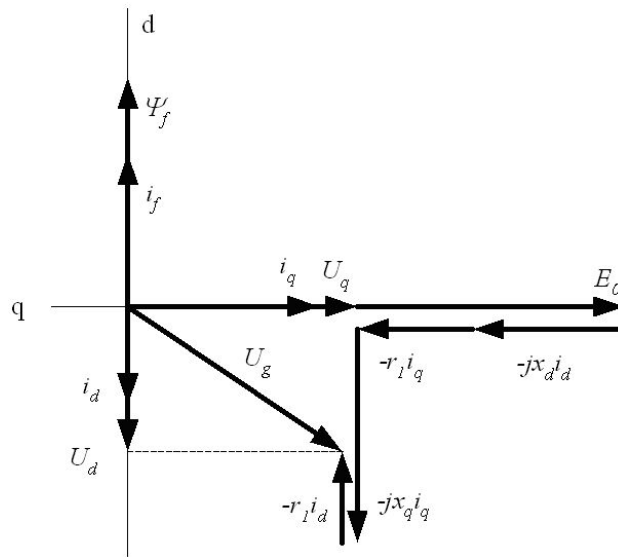


Figure 1.6: Phasor diagram of a synchronous generator working on an active-inductive load

The appropriate precision of the electromagnetic calculations is achieved using special coefficients which are obtained from comparison of experimental and calculated data. Applied to the special modes and electrical machines with non-typical dimensions, these methods give too big errors of calculations.

The set of assumptions, which the existing methods are based on, cannot be fully applied to such spread electrical machines like salient and non-salient poles synchronous machines with non-integer number of slots per pole and per phase. The field in the air-gap for both of them has very non-sinusoidal form and contains both high and low spatial harmonics. This effect is significantly expressed in big turbo- and hydrogenerators of extra power with high electromagnetic loads (Figure 1.7).

A lot of parameters and characteristics of electrical machines, which are significantly influenced by double-sided saliency of stator and rotor, by changes of geometrical configuration of the magnetic field caused by the rotation and saturation, cannot be absolutely estimated, applying the assumptions above. For instance, it concerns the harmonic factor of the synchronous generators' line voltage. Its value is limited by the standards of the network but cannot be precalculated for a machine taking into account the influence of saliency, saturation and damper winding currents in no-load mode.

Such well-known parameters as  $x_d$  and  $x_q$ , being used in many contemporary models of electrical machines, are in fact nonlinear, contrary to the assumptions. Even for non-salient poles synchronous generators  $x_d$  and  $x_q$  vary a lot according to the operating mode of a machine (Figure 1.8).

Finally, a big disadvantage of the existing conventional methods is their “*non-universality*”, that leads to the development of the methods for each significantly new implementation of an electrical machine.

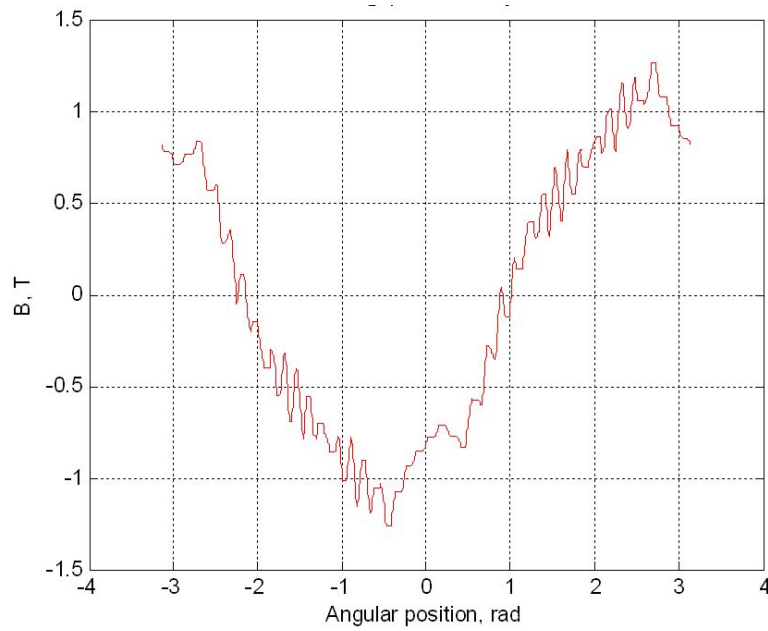


Figure 1.7: Flux density in the air-gap of a big generator

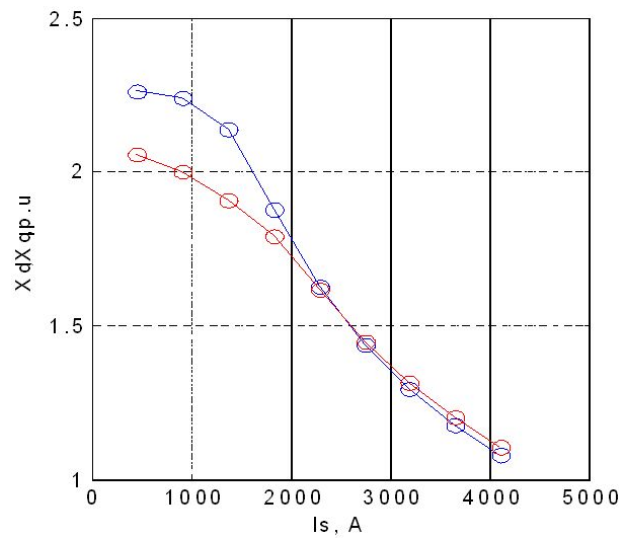


Figure 1.8: Variation of  $x_d$  and  $x_q$  parameters

### 1.1.2 Field calculation methods

The development of electrical machinery, growth of their power, especially that of turbo- and hydrogenerators, highlighted the disadvantages of existing methods of electromagnetic calculations. From the other hand, as it has been mentioned above, the evolution of the information technologies and computing facilities allows the creation of the methods which numerically solve Maxwell's equations in two-dimensional and even three-dimensional representation.

Many different techniques are realized to calculate the electromagnetic field in machines. The main of them are *Finite Difference Method* (FDM), *Finite Element Method* (FEM), *Finite Integration Technique* (FIT). All of them are based on a principle of application of a mesh on an object of calculation and further determination of the solution variable in the nodes of the mesh. While FDM has a rectangular mesh (grid), the others represent the geometry using the elements of different shapes starting from triangular.

These methods allow calculation of the equations of any complexity, taking into non-linearity of the cores, account movement of rotor, eddy currents, performing resolution of the coupled thermal and mechanical problems simultaneously. Since we always have to solve the "direct task", the solution involves many mutually linked iterative processes and the bigger the complexity of the problem, the greater the time of calculation.

For general time-varying fields, the original first-order full Maxwell equations can be written as follows [25]:

$$\nabla \times \vec{E} + \frac{\partial \vec{B}}{\partial t} = 0 \quad (\text{Faraday's Law}) \quad (1.15a)$$

$$\nabla \times \vec{H} - \frac{\partial \vec{D}}{\partial t} - \vec{J} = \vec{J}^{imp} \quad (\text{Maxwell-Ampere's Law}) \quad (1.15b)$$

$$\nabla \cdot \vec{D} = \rho^{imp} \quad (\text{Gauss's Law - electric}) \quad (1.15c)$$

$$\nabla \cdot \vec{B} = 0 \quad (\text{Gauss's Law - magnetic}) \quad (1.15d)$$

$$\vec{D} = \varepsilon \vec{E} \quad (1.15e)$$

$$\vec{B} = \mu \vec{H} \quad (1.15f)$$

$$\vec{J} = \sigma \vec{E} \quad (1.15g)$$

where:  $\vec{E}$  and  $\vec{H}$  are the electric and magnetic field intensities, respectively;  $\rho^{imp}$  is the imposed source of electric charge density;  $\vec{J}^{imp}$  is the imposed source of electric current density;  $\vec{D}$  and  $\vec{B}$  are the electric and magnetic flux densities respectively;  $\vec{J}$  is the electric (eddy) current density;  $\varepsilon$ ,  $\mu$ ,  $\sigma$  are the constitutive parameters: permittivity, permeability and conductivity of the medium, respectively.

All the imposed sources in the equations (1.15) are five functions of the space and time coordinates. Generally, the medium constitutive parameters can be nonlinear and anisotropic, as well.

At the interface between two media, for example, medium (+) and medium (-), the

boundary conditions can be expressed electric fields as

$$n \times (\vec{E}^+ - \vec{E}^-) = 0, \quad (1.16a)$$

$$n \cdot (\vec{D}^+ - \vec{D}^-) = \rho_s^{imp} \quad (1.16b)$$

And similarly for magnetic fields as

$$n \times (\vec{H}^+ - \vec{H}^-) = \vec{J}_s^{imp}, \quad (1.17a)$$

$$n \cdot (\vec{B}^+ - \vec{B}^-) = 0 \quad (1.17b)$$

where  $n$  is the unit vector normal to the interface, pointing from medium (-) to medium (+),  $\rho_s^{imp}$  is the imposed surface charge density and  $\vec{J}_s^{imp}$  is the imposed surface electric current density.

The boundary conditions can be reduced to a spacial case when one of the media becomes a perfect conductor wall:

$$n \times \vec{E} = 0, \quad (1.18a)$$

$$n \cdot \vec{B} = 0 \quad (1.18b)$$

or a perfect magnetic wall:

$$n \times \vec{H} = 0, \quad (1.19a)$$

$$n \cdot \vec{D} = 0 \quad (1.19b)$$

To look through the finite element solution let's simplify the equation set (1.15), neglecting the eddy currents and electric charge density. The system of equations (1.15) becomes as follows:

$$\nabla \times \vec{E} = -\frac{\partial \vec{B}}{\partial t} \quad (1.20a)$$

$$\nabla \times \vec{H} = \vec{J}^{imp} \quad (1.20b)$$

$$\nabla \cdot \vec{B} = 0 \quad (1.20c)$$

$$\vec{B} = \mu \vec{H} \quad (1.20d)$$

In order to simplify the solution, a special dummy variable is introduced to the system - a *vector magnetic potential*:

$$\vec{B} = \nabla \times \vec{A} \quad (1.21)$$

After putting (1.17) to (1.16) we obtain:

$$\nabla \times \vec{B} = \nabla \times (\nabla \times \vec{A}) = \nabla (\nabla \cdot \vec{A}) - \nabla^2 \vec{A} = \mu \vec{J}^{imp} \quad (1.22)$$

or, considering that  $\nabla \cdot \vec{A} = 0$ :

$$\nabla^2 \vec{A} = -\mu \vec{J} \quad (1.23)$$

For 2D sinusoidally time varying magnetic field can be described with the aid of the magnetic vector potential in scalar form [15]:

$$\frac{\partial}{\partial x} \left( \frac{1}{\mu} \frac{\partial \vec{A}}{\partial x} \right) + \frac{\partial}{\partial y} \left( \frac{1}{\mu} \frac{\partial \vec{A}}{\partial y} \right) = -\vec{J} + j\omega\sigma \vec{A}. \quad (1.24)$$

where  $\omega$  is the angular frequency of the magnetic field.

Similar equation can be written for the 2D magnetostatic field:

$$\frac{\partial}{\partial x} \left( \frac{1}{\mu} \frac{\partial \vec{A}}{\partial x} \right) + \frac{\partial}{\partial y} \left( \frac{1}{\mu} \frac{\partial \vec{A}}{\partial y} \right) = -\vec{J}. \quad (1.25)$$

The further solution of the equations can be found using one of the field calculation methods, mentioned above, or any of their modifications. Let's discuss a little bit one of the most spread method in this area.

### Finite Element Method

As it has been mentioned above, the in FEM we obtain the values of variables in the nodes of a mesh, which is usually triangular, but generally can have any polygonal form. The mesh is applied to the geometry of a real object.

Minimization of the magnetic energy functional over a set of elements (mesh) leads to a matrix equation that has to solve for the magnetic vector potential  $\vec{A}$ . It is in fact the minimization of  $\vec{A}$  throughout the mesh. A planar mesh is represented by a set of elements: triangles or quadrilaterals, each of them having at least three vertices called nodes or grid points. The number of nodes corresponding to each element depends on the shape of the element and also on the type of function used to model the potential within the element. This function is called the shape function and can be of any order depending on the desired complexity. Usually linear or second-order shape functions are used. Assuming a linear shape function of  $\vec{A}$  within an element, the vector potential inside each element is described as:

$$A = \alpha_1 + \alpha_2 x + \alpha_3 y \quad (1.26)$$

If considering a triangular element with nodes  $l$ ,  $m$  and  $n$ , the values of  $A$  at each node are:

$$\begin{aligned} A_l &= \alpha_1 + \alpha_2 x_l + \alpha_3 y_l \\ A_m &= \alpha_1 + \alpha_2 x_m + \alpha_3 y_m \\ A_n &= \alpha_1 + \alpha_2 x_n + \alpha_3 y_n \end{aligned} \quad (1.27)$$

where  $A_l = A(x_l, y_l)$ ,  $A_m = A(x_m, y_m)$  and  $A_n = A(x_n, y_n)$ .

In matrix form the equation set (1.26) is:

$$\begin{vmatrix} A_l \\ A_m \\ A_n \end{vmatrix} \begin{vmatrix} 1 & x_l & y_l \\ 1 & x_m & y_m \\ 1 & x_n & y_n \end{vmatrix} = \begin{vmatrix} \alpha_1 \\ \alpha_2 \\ \alpha_3 \end{vmatrix} \quad (1.28)$$

The solution of the equation (1.27) yields:

$$\begin{aligned} \alpha_1 &= \frac{1}{2\Delta} \begin{vmatrix} A_l & x_l & y_l \\ A_m & x_m & y_m \\ A_n & x_n & y_n \end{vmatrix} & \alpha_2 &= \frac{1}{2\Delta} \begin{vmatrix} 1 & A_l & y_l \\ 1 & A_m & y_m \\ 1 & A_n & y_n \end{vmatrix} \\ \alpha_3 &= \frac{1}{2\Delta} \begin{vmatrix} 1 & x_l & A_l \\ A_m & x_m & A_m \\ A_n & x_n & A_n \end{vmatrix} & 2\Delta &= \begin{vmatrix} 1 & x_l & y_l \\ 1 & x_m & y_m \\ 1 & x_n & y_n \end{vmatrix} \end{aligned} \quad (1.29)$$

where  $\Delta$  is the surface area of a triangle with nodes  $l, m, n$ . Putting the equation (1.29) into equation (1.26) the linear interpolation polynomial function is:

$$A = \frac{1}{2\Delta} \sum_{k=l,m,n} [a_k + b_k x + c_k y] A_k = [N_l \quad N_m \quad N_n] \begin{bmatrix} A_l \\ A_m \\ A_n \end{bmatrix} \quad (1.30)$$

where  $N_l = (a_l + b_l x + c_l y)/(2\Delta)$ ,  $N_m = (a_m + b_m x + c_m y)/(2\Delta)$  and  $N_n = (a_n + b_n x + c_n y)/(2\Delta)$

The flux density is constant within a particular triangular finite element:

$$\vec{B}(x, y) = \frac{1}{2\Delta} \sum_{k=l,m,n} (\vec{1}_x c_k - \vec{1}_y b_k) A_k \quad (1.31)$$

where  $\vec{1}_x$  and  $\vec{1}_y$  are the unit vectors.

The node point potentials  $A_k$  can be calculated by minimizing the energy functional that is the difference between the stored energy and the input (applied) energy in the system volume. For magnetic systems and 2D problem the minimization functional is:

$$F = \int_S \left( \frac{B^2}{2\mu} - \vec{J} \cdot \vec{A} + j\omega \frac{1}{2} \sigma \vec{A}^2 \right) dS. \quad (1.32)$$

The functional is minimized when  $\frac{\partial F}{\partial A} = 0$ . Considering a single triangular finite element, we can write:

$$\int_S \frac{\partial}{\partial A_k} \left[ \frac{B^2}{2\mu} - \vec{J} \cdot \vec{A} + j\omega \frac{1}{2} \sigma \vec{A}^2 \right] dS = 0 \quad (1.33)$$

or

$$\begin{aligned} \int_S \left\{ \frac{1}{2\mu} \frac{\partial}{\partial A_k} \left[ \left( \frac{\partial A}{\partial x} \right)^2 + \left( \frac{\partial A}{\partial y} \right)^2 \right] - \frac{\partial}{\partial A_k} (\vec{J} \cdot \vec{A}) \right\} dxdy \\ + j \int_S \left[ \omega \frac{1}{2} \sigma \frac{\partial}{\partial A_k} \vec{A}^2 \right] dxdy = 0 \end{aligned} \quad (1.34)$$

where  $dS = dxdy$ .

The minimization of the functional with respect to the magnetic vector potential can be approximated by the following set of equations:

$$[G][A] = [I] \quad (1.35)$$

where  $[G]$  is the global coefficient matrix,  $[A]$  is the matrix of nodal magnetic vector potentials and  $[I]$  matrix represents nodal currents (forcing functions).

The elements of  $[G]$  and  $[I]$  matrices are expressed as follows:

$$[S] = \frac{1}{4\mu\Delta} \begin{bmatrix} b_l b_l + c_l c_l & b_l b_m + c_l c_m & b_l b_n + c_l c_n \\ b_m b_l + c_m c_l & b_m b_m + c_m c_m & b_m b_n + c_m c_n \\ b_n b_l + c_n c_l & b_n b_m + c_n c_m & b_n b_n + c_n c_n \end{bmatrix} + j \frac{\omega \sigma \Delta}{12} \begin{bmatrix} 2 & 1 & 1 \\ 1 & 2 & 1 \\ 1 & 1 & 2 \end{bmatrix} \quad (1.36)$$

$$[I] = J \frac{\Delta}{3} \begin{bmatrix} 1 \\ 1 \\ 1 \end{bmatrix} \quad (1.37)$$

The equations (1.34)-(1.36) are solved for the potential  $\vec{A}$  in a region containing the triangle with nodes  $l$ ,  $m$  and  $n$ . For the real problems with many elements this solution is repeated for each one.

In order to obtain the EMF using these methods, a *direct task* must be solved: determination of the phase EMF-s from the defined current distributions in stator and rotor windings. That means, that the steady-state operating mode must be defined by *three variables*: excitation current  $I_f$ , stator current  $I_s$  and the angle between them  $\Psi$ . The full period must be calculated to take into account double saliency of the magnetic cores. Practically, one has to solve the problem defined by stator voltage  $U_s$ , stator current  $I_s$  and angle  $\phi$  between them. That leads to the iterative process of the solution and in most cases the steady-state mode must be determined from solving the transient one.

A FEM 2D mesh is presented on Figure 1.9, left. One can see a huge amount of elements of the mesh, especially in the air-gap zone of the machine. While modeling machines with rather complex geometry, the number of elements can exceed even 100000. It means that a lot of redundant information is calculated for each step of each iteration, while practically one needs *only windings' flux linkages* to be obtained.

Besides, the most of calculations are performed on 2D models without proper taking into account axial heterogeneity of the cores, like ventilation ducts and end effects. Generally, only the real lengths of stator and rotor cores are taken into account, while the influence of that axial structure of the machine on the zones of air-gap and slots are neglected. When these neglects significantly decrease the accuracy of the calculations, usually 3D FEM solutions are proposed (Figure 1.9, right), thus more exceeding information is calculated.

All these facts leads to tremendous time of calculations and show the useless of these techniques in case of general optimization of electrical machines and entire electromechanical systems (drives). Thus these methods can find their best application in the problems of investigation of particular phenomena in the electrical machines, like thorough end-windings' forces calculations, edge losses and etc.

### 1.1.3 Permeance network methods

To decrease the waste of time while calculating each time a lot of redundant information, a lot of methods were proposed. They can be combined together as the methods, which



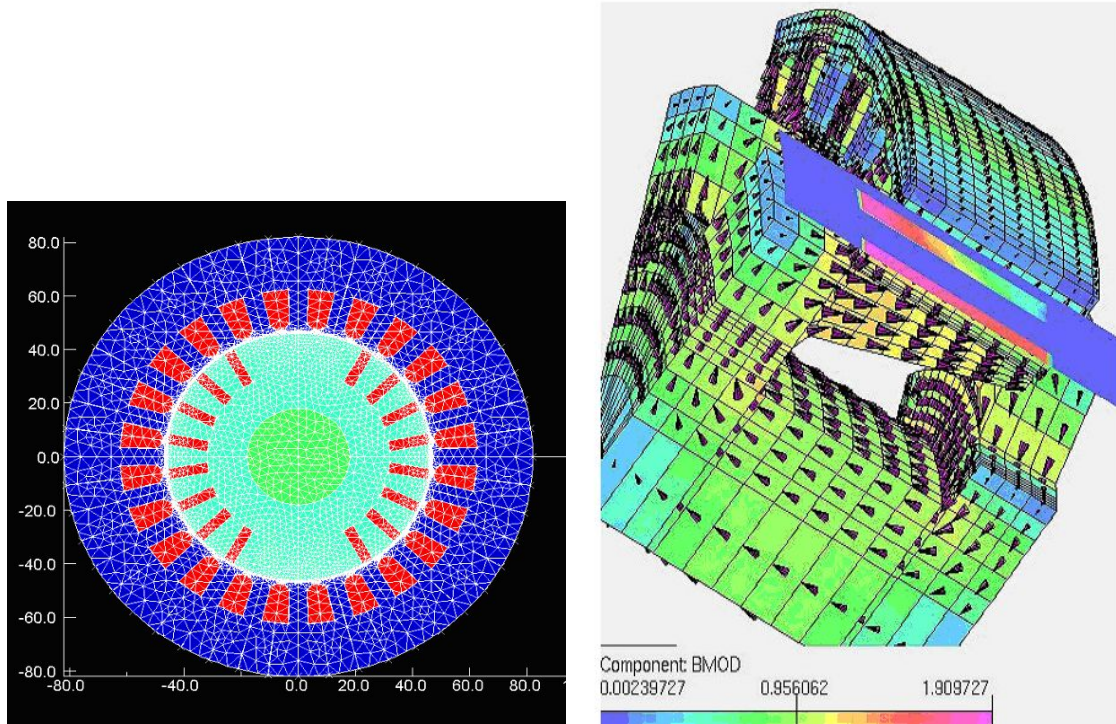


Figure 1.9: A 2D mesh of a synchronous machine and a 3D mesh of a claw-pole machine

use *the particularities* of electrical machines, such as their peridicity, a lot of areas of their magnetic system with well determined flux orientation. These methods exploit the idea of calculating the parameters of the equivalent lumped elements which represent the particular parts of the magnetic system. This group of methods is called *Permeance Network Methods* (PNM).

The main advantage of the PNM approach is that comparing with the field-based methods one obtains much less amount of elements describing the field inside the electrical machine with the sufficient accuracy.

The PNM approach has been in use since the works of Roters [48], Carpenter [8] and later of Ostovic [35], Latreche [30], Slemon [53], Ivanov-Smolenskii [21], Khvostov [26], Kuznetsov [23] and others.

In CEGELY several works are devoted to the development of dynamic flux tubes taking into account saturation and hysteresis applied to loss estimation problem [33, 14, 52]. The works of LEEI [12] and LEF [24] use PNM approach in diagnostic domain. The works of LEG [45, 2] present the PNM coupled with different optimization methods; some works are oriented to design of electromechanical devices and optimization of their static characteristics [9, 13].

Some international references also are of of the PNM approach [56, 36, 37, 11, 34, 54].

In L2EP such works have been conducted for many years using coupling of that method with finite element analysis. Michel Hecquet applied it to a claw-pole machine [17]; C. Delmotte-Delforge [10] realized a model of AC motor associated with its control system; H. Roisse [47] worked on a synchronous permanent magnet machine. In order to enforce the idea of using PNM in optimal design of electrical machines several works were devoted to

couple the approach with response surface method. From the other hand, L2EP is trying to implement a *multi-physical* approach, taking into account mechanical (vibro-acoustic) and thermal processes along with electro-magnetic one, applied to optimal design of electrical machines. The work of M. Hecquet [18] comprises all the efforts done in L2EP in the domain of PNM.

### Flux tubes method

Method of *flux tubes* is one of the most popular implementations of PNM method. It was proposed by V. Ostovic [35].

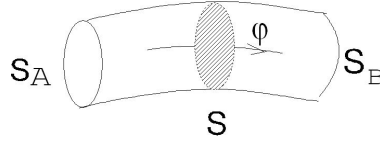


Figure 1.10: Flux tube

The magnetic circuit of an electrical machine is decomposed on several parts. Each of the parts is represented by the *permeance* limited by the contours of a flux tube (Figure 1.10). For these small regions the following conditions are applied:

- the flux  $\phi$  is considered to be constant inside the tube;
- the surfaces  $S_a$  and  $S_b$  are the magnetic equipotentials.

In this case, the permeance:

$$P = \frac{\phi}{\epsilon_A - \epsilon_B} \quad (1.38)$$

where  $\epsilon_A$  and  $\epsilon_B$  – the scalar magnetic potentials of the surfaces  $A$  and  $B$  respectively.

The equation (1.38) and the condition above lead to another assumption that the magnetic fluxes in the cores and even in the air regions of the magnetic system “*are frozen*”, i.e. *they do not change their shape in all operating modes*.

The method was realized in many different models. For example, it was realized in the software Sirepce developed at L2EP (Herve Roisse) [47], and validated by the model of a salient-pole synchronous generator (Michel Hecquet, [17]). A simplified equivalent circuit (permeance network) of that generator is shown on Figure 1.11.

Nonlinear permeances  $P_{sd}$  and  $P_{sy}$  represent stator tooth and yoke parts, nonlinear permeances  $P_{rp}$  and  $P_{ry}$  represent rotor pole and yoke parts. Stator slot leakage is represented by linear permeances  $P_{sl}$  while rotor linear permeance  $P_{rl}$  represents inter-pole leakage. MMF sources  $F_{sd}$  and  $F_{rp}$  are placed in stator teeth and rotor poles, they implement stator and rotor currents, realizing the coupling of the electric and magnetic parts of the model.

The air-gap is implemented by means of permeances  $P_{agg}$  from each rotor pole to each stator tooth. These permeances are obtained by FEM analysis of the machine as functions of the rotor angular position [19, 20]. It allows to take into account the rotation, performing transient analysis.

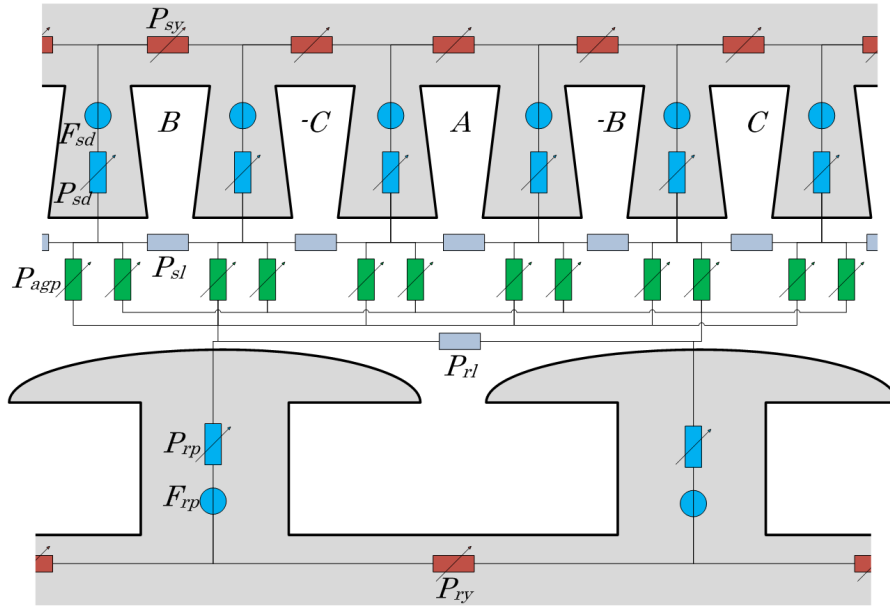


Figure 1.11: Permeance network of a synchronous generator

### Tooth Contour Method

In order to generally take into account the influence of such factors in electrical machines as double sided saliency of the stator and rotor cores, the change of the form of air-gap due to rotor rotation and the saturation of the elements of the cores, the *Tooth Contour Method* (TCM) was designed, theoretically proved and developed at the department of Electromechanics of Moscow Power Engineering Institute (MPEI).

The basis of TCM was generalized in a monograph by Doctor of Technical Sciences, Professor A. Ivanov-Smolenskii in [21] and generalized in [23]. Further development of TCM was made in the Technical Sciences Doctoral thesis of Professor V. Kuznetsov [28]. The TCM was applied to different types of machine including turbogenerators [26].

The TCM is based on theoretically validated representation of the total magnetic field in the air-gap as the sum of local magnetic fields of the particular elements of the so-called tooth contours. Usually the tooth contour is considered to be an element formed by the conductors located in adjacent slots, but it may be also represented as any part of the core surface e.g., the pole-shoe may be divided into several “tooth contours”.

The local magnetic fields of tooth contours are to be calculated under the artificial boundary conditions, called by the authors of the method *the Special Boundary Conditions* (SBC), supposing that the permeability both of stator and rotor iron is infinitely large. This special field is localized in a small region, which usually does not exceed three or four tooth pitches and so it could be easily calculated. As a result, a mutual permeance between excited contour of a stator and one of a non-excited rotor contours are obtained as a function of their relative position. The total air gap field may be represented with non-planar *permeance network* with relatively small number of branches.

The calculation of the air gap magnetic field in the absence of iron saturation is carried out on the basis of this PN without any assumptions. We have to calculate the field only

inside the small area of air gap, limited by 3 – 4 tooth contours. Thus the calculation time is extremely reduced.

More detailed description of the method and approach is given in Chapter 2.

## 1.2 Conclusion

So, one can easily find that the conventional methods listed in the beginning of the chapter with all the assumptions applied to them, cannot now serve to satisfy the needs of contemporary electrical machinery. The following reasons limit the use of these methods nowadays:

- non-sinusoidal distributions of both stator and rotor MMF;
- weak taking into account the influence of double sided saliency;
- impossibility to completely take into account the variation of the machines' parameters as a function of magnetic saturation and mutual stator-rotor angular position;
- huge amount of “adjusting” coefficients, developed for each new kind of a machine leading to non-universality.

The growth of the part of numerical modeling, numerical methods of direct solution of Maxwell problem seems to significantly increase the accuracy of calculations. But tremendous amount of redundant information about the magnetic field in each moment of the simulation and in each point of the machine's volume, while using these methods, leads to tremendous time of calculation. It makes it almost impossible to use the methods in rapid tasks of electric machine's optimization. In most cases, the field calculations are used in 2D, neglecting the biggest part of information on the axial structure of the machines.

Some works are devoted to coupling of FEM calculations with conventional models in order to obtain steady-state characteristics of a machine, as it was done in [46] for a turbogenerator case. Parameters  $X_d$  and  $X_q$  were obtained from FEM calculations and then regular  $dq$ -model was used. It helps to win calculation time comparing to pure FE-models and gives a big advantage of taking into account induced currents comparing to conventional approach.

Permeance network methods seem to show the good compromise between these two approaches (Figure 1.12). Using the particularities of electrical machines' magnetic fields, these methods represent the magnetic fields with accuracy enough for the most of contemporary practical calculations.

The proposed approach is based on a theoretically validated tooth contour method. The method was developed having the following aims:

- implement the complex geometrical structure of modern turbogenerators;
- take into account their particularities;
- generalize and automatize the approach of PN generation;
- create the model which can be used as a part of optimal design software.

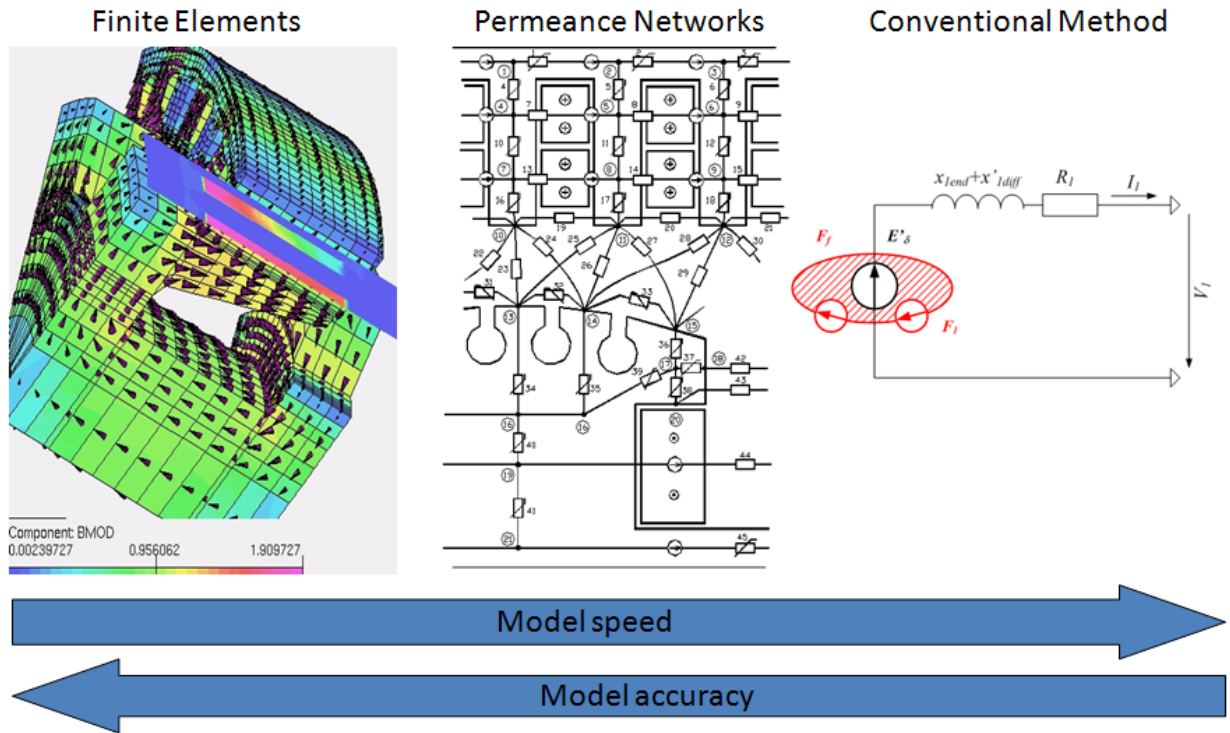


Figure 1.12: Different calculation approaches groups

The basis of the calculation of magnetic field in an electrical machine using this method was a little bit discussed above and will be detailed in the following chapter. Here it is necessary to remind, that using this method, one solves the direct problem, defined by stator and rotor currents and the spacial angle between them. So, the iterative process is needed to calculate the particular operating mode.

For each calculated point in steady state mode, a real distribution of the windings' FMM-s and fluxes is represented. And finally the flux linkages of the windings are obtained. These flux linkages already *include* the influence of *differential and slot leakages*.

Besides, the influence of axial heterogeneity of the machine on the magnetic field in different regions is taken into account. It is shown, that the radial ducts distributed axially in the stator and/or rotor cores *differently* influence the following *different* areas of the machine:

- stator tooth and yoke zones;
- stator slot air zone;
- air gap zone between stator and rotor;
- rotor slot air zone;
- rotor tooth and yoke zones.

The calculation of permeance network model can be rather fast and performed both in steady-state and transient mode.

The following chapter presents thoroughly the chosen calculation approach.

# Chapter 2

## Used Approach

As it has been mentioned in Chapter 1, the growth and development of the computer technics nowadays permits to numerically modelize any phenomenon in an electrical machine. For instance, the FEM models of electromagnetic, mechanical, thermal and other phenomena in electrical machine might contain dozens and hundreds thousand elements. Anyway, the increase of the detailing of EM is limited since now it is not enough just to investigate some processes in EM but what is more important – to find the solutions close to optimal ones. Moreover, modern optimization strategy has a multiphysical orientation, i.e. it concerns thermal, aerodynamic, vibroacoustic problems along with electromagnetic one.

In this case the electromagnetic model must be modified in order to have *enough accuracy* with as less number of elements as possible. It can be achieved exploiting and taking into account the particularities which can be found in electrical machines:

1. linear zone of air-gap;
2. high permeability of stator and rotor cores ( $\mu_r \geq 10$  even if saturated);
3. well-defined direction of the flux in magnetic cores.

The proposed approach uses these particularities to construct a general *permeance network* (PN) of a turbogenerator and calculate its parameters. The approach is based on a further development of the *Tooth Contour Method* (TCM). The last one was designed, theoretically proved and developed at the department of Electromechanics of Moscow Power Engineering Institute (MPEI).

The basis of TCM was generalized in a monograph by Doctor of Technical Sciences, Professor A. Ivanov-Smolenskii and his co-authors [23]. Further development of TCM was made in the Technical Sciences Doctoral thesis of Professor V. Kuznetsov [28].

The idea of TCM is to divide a two-dimensional field of an electrical machine into a set of small sub-areas where the field can be easily calculated. So-called “tooth contours” can be chosen as such sub-areas. A “tooth contour” is a contour which embraces one tooth of a machine’s core. Its field is being calculated under the special boundary conditions, which diminish the size of a tooth contour down to only several tooth pitches. Since the zone of the air-gap is linear, the sum of the magnetic fields of these contours gives a full magnetic field in the active zone of a machine (air-gap), including both main field and the fields of slot and differential leakage. The field of the coil end leakage must be taken into account on the stage of the electrical calculations by means of corresponding inductances.

The calculation of the electromagnetic processes in a machine can be generally divided into several stages. On the first stage the calculation of the tooth contours' fields is being performed while exciting only one contour of all. That calculation is repeated for different possible mutual positions of the stator and rotor contours. As a result one obtains the dependency of the permeance between an excited tooth and one of non-excited teeth.

On the second stage a full magnetic equivalent circuit is constructed including non-linear parts of the machine (in the cores) and the permeances of the air-gap mentioned above. By means of this PN the branch fluxes and coils flux linkages can be calculated for the defined distribution of the stator and rotor currents and their mutual position.

The calculation of the electromagnetic processes in the coupled electrical and magnetic circuits is performed on the third stage.

Some works use a 3D permeance networks in order to take into account the configuration of magnetic field in all dimensions like it was performed for claw-pole machine in [17]. In the case of more conventional machines (like turbogenerators, large synchronous machines) and considering the use of the model in optimal design software, the obtained PN is the one in-plane. Thus, in order to take into account axial heterogeneity of a machine, its three-dimensional peculiarities and edge-effects, special techniques must be involved. Actually, all these effects have to be considered on the stage of the PN creation, i.e. during the calculation of the parameters of the PN. By means of obtained PN both dynamic and steady-state calculations can be performed.

This chapter presents theoretical basis of the approach, strategy of machine's PN construction and calculation of its parameters. Section 2.1 discusses magnetic charges approach in application to PN construction and gives an idea of a "tooth contour". The PN of an electric machine is presented in section 2.2, showing the approach to its construction. The particularities of taking into account axial heterogeneity of a machine are shown in section 2.3. Section 2.4 highlights the equations of the PN and the methods used to solve them. The method of steady-state operating mode and characteristic calculation is given in section 2.5 while the approach of taking into account rotation is observed in section 2.6.

## 2.1 Theoretical basis

This section describes basic hypotheses and theoretical approach to creation of a mathematical model of an electric machine using PN.

### 2.1.1 Calculating magnetic fields using vector or scalar magnetic potentials

Generally, electrical machines can be decomposed on three characterized zones: ferromagnetic cores, nonmagnetic areas filled with conductors having electrical current and nonmagnetic areas without conductors. In the linear approximation the permeability of the cores can be assumed infinite, thus the calculation can be performed only in the nonmagnetic areas solving the Maxwell equations for electromagnetic field. While using a *vector magnetic potential* (VMP), the field is found solving the Poisson's equation (1.25) with Neuman boundary conditions. Nowadays VMP is widely used in field calculation methods (section 1.1.2) since it easily permits to take into account the areas conducting current.



The better convergence of the solution gives Dirichlet problem, for which a harmonic function must be found while its boundary values are known. In this case the problem is solved using *scalar magnetic potential* (SMP). Its use naturally corresponds to the ideas of electrical potential (analogy with SMP) and current (analogy with magnetic flux) in electrical circuits. Very well developed theoretical methods of electrical circuit calculations are easily transposed to the magnetic area. Under several conditions a magnetic system equivalent circuit with lumped parameters can be built, taking into account the saturation of the cores, using SMP.

A fragment of a regular simple magnetic scheme representing the part of a stator using SMP is given on Figure 2.1. There are three slots presented with the windings holding the full currents  $i_{k-1}$ ,  $i_k$  and  $i_{k+1}$ . The yoke permeances  $\Lambda_{yk-1}$ ,  $\Lambda_{yk}$ ,  $\Lambda_{yk+1}$  and tooth permeances  $\Lambda_{tk}$ ,  $\Lambda_{tk+1}$  are nonlinear. The slot leakages are represented by  $\Lambda_{sk-1}$ ,  $\Lambda_{sk}$  and  $\Lambda_{sk+1}$ . The sources of MMF  $F_k = i_k - i_{k-1}$  and  $F_{k+1} = i_{k+1} - i_k$  are placed in tooth branches. The air-gap permeances  $\Lambda_{gkm}, \Lambda_{gkm+1}, \Lambda_{gk+1m}$  and  $\Lambda_{gk+1m+1}$  connect stator teeth  $k$  and  $k+1$  with rotor teeth  $m$  and  $m+1$ , which are not shown on the picture.

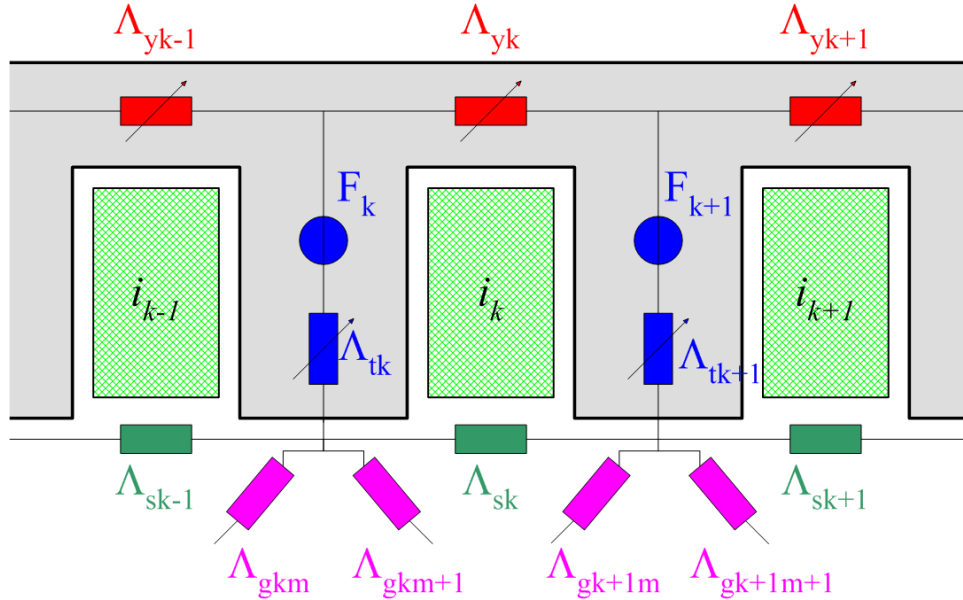


Figure 2.1: A part of magnetic system's equivalent circuit in terms of SMP

In the circuit on Figure 2.1 the node potentials correspond to SMP and currents – to magnetic fluxes. The MMF sources are represented by their electrical analogies – EMF sources.

Actually, the magnetic equivalent circuit can be built using a VMP as well (Figure 2.2). In this case we have to “rotate” the previous scheme on  $90^\circ$ . Now the *flux*, transversing the branch, will be determined by *potential difference* between its nodes. If in case of SMP the excitation was created by the scalar potential difference – MMF –, here its created by the corresponding “external” currents imposed to the nodes in the area of the conductors  $i_{k-1}$ ,  $i_k$  and  $i_{k+1}$ , taking into account a scaling factor. On the external border of the yoke (blue line on the Figure 2.2) the radial component vector  $\vec{B}_y = \frac{\partial A}{\partial x} = 0$ , i.e.  $A_x = \text{const}$ . That leads this line to be equipotential in the scheme thus implementing Neumann boundary condition.



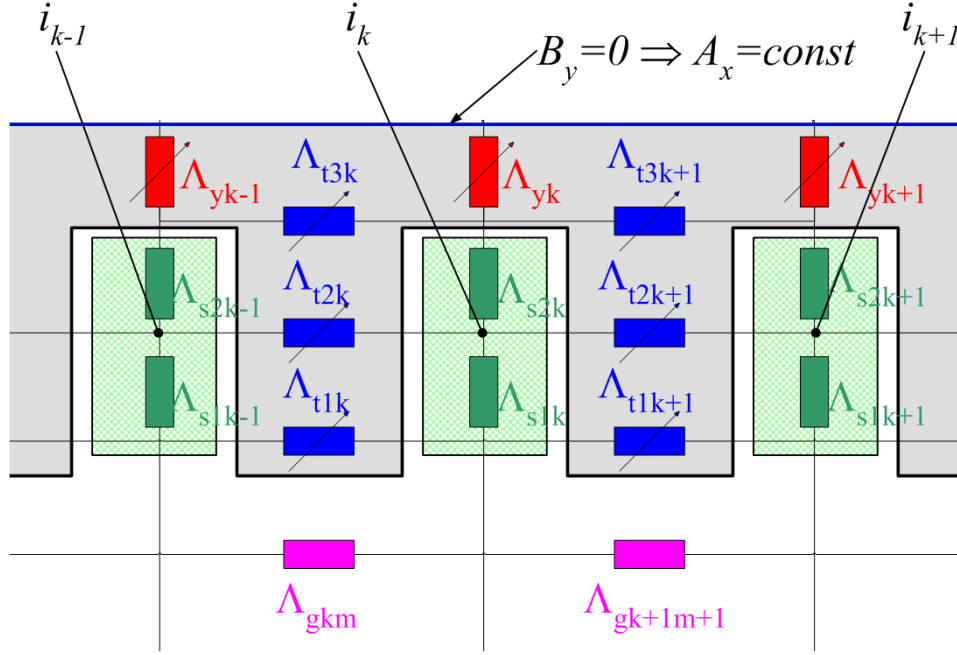


Figure 2.2: A part of magnetic system's equivalent circuit in terms of VMP

One should pay attention on the representation of the air-gap permeances. Like all the other branches of the circuit they must be oriented transversely to the flux. But the flux in the area of air-gap *has no evident limits* – the last ones depend on the mutual positions of rotor and stator as well as on the operating mode of the entire machine. This is an important obstacle which prevented the use of VMP in computations according to the models with lumped parameters, like permeance networks.

In our model we use the PN based on SMP representation of magnetic field. The *magnetic charges approach* permits to theoretically prove the process of PN construction.

### 2.1.2 Magnetic charges approach

The magnetic systems with current-carrying areas can also be handled by means of SMP applying the *magnetic charges approach* even including zones inside the conductors with current [23].

The magnetic field  $\vec{H}$  can be presented as a result of overlapping of two fields

$$\vec{H} = \vec{H}_1 + \vec{H}_2. \quad (2.1)$$

The resultant field complies to the well-known equations (1.20) rewritten in a differential form:

$$\text{rot} \vec{E} = -\frac{\partial \vec{B}}{\partial t} \quad (2.2a)$$

$$\text{rot} \vec{H} = \vec{J} \quad (2.2b)$$

$$\text{div} \vec{B} = 0 \quad (2.2c)$$

$$\vec{B} = \mu\mu_0 \vec{H} \quad (2.2d)$$

The field intensity  $\vec{H}_2$  is chosen to comply two equations:

$$\text{rot} \vec{H}_2 = \vec{J} \quad (2.3a)$$

$$\vec{B}_2 = \mu\mu_0 \vec{H}_2 \quad (2.3b)$$

where magnetic permeability must be the same as in the real field. The divergence of that field is now not equal to zero since the *magnetic charges* were introduced:

$$\text{div} \vec{B}_2 = -\rho, \quad (2.4)$$

where  $\rho$  – magnetic mass density,  $Wb/m^3$ .

The curl of the component vector  $\vec{H}_1$  turns out to be zero:

$$\text{rot} \vec{H}_1 = \text{rot} (\vec{H} - \vec{H}_2) = 0. \quad (2.5)$$

Thus, the field  $\vec{H}_1$  is potential and defined by SMP  $\varphi$ , which depends on the introduced magnetic charges:

$$\vec{H}_1 = -\text{grad} \varphi. \quad (2.6)$$

The divergence of the field  $\vec{H}_1$  along with the field  $\vec{H}_2$  depends on the sources of the field

$$\text{div} \vec{B}_1 = \text{div} (\vec{B} - \vec{B}_2) = -\text{div} \vec{B}_2 = \rho. \quad (2.7)$$

Considering that  $H = -\text{grad} \varphi$  and (2.7) it's possible to obtain the equation for SMP:

$$\text{div} (\mu\mu_0 \text{grad} \varphi) = -\rho. \quad (2.8)$$

The equation  $\text{rot} \vec{H}_2 = J$  is complied automatically if:

$$\vec{H}_2 = \int \vec{J} \times \vec{dl}_{l_0}, \quad (2.9)$$

where  $\vec{dl}$  – arbitrary directed vector.

Thus, on the first stage vector  $\vec{dl}$  must be chosen and field  $H_2$  is calculated in each point. Further, the volumetric (or surface) magnetic charge density can be found and solving equation (2.6), we can find  $\vec{H}_1$ . The sought field  $\vec{H}$  is equal to  $\vec{H}$  in the areas without current and equal to the sum of  $\vec{H}_1$  and  $\vec{H}_2$  in those carrying current.

Let's consider a contour  $l$  carrying current  $I$  (Figure 2.3). The magnetic potential in any point  $M$  of ambient space is created by a double magnetic layer, situated on surface  $S$  stretched on the contour  $l$ . Moreover, the potential of the point  $M$  depends only on the product of the current  $I$  and the space angle  $\Omega$  – the angle of observation of the contour  $l$  from the point  $M$ ,

$$\varphi = \frac{I\Omega}{4\pi} \quad (2.10)$$

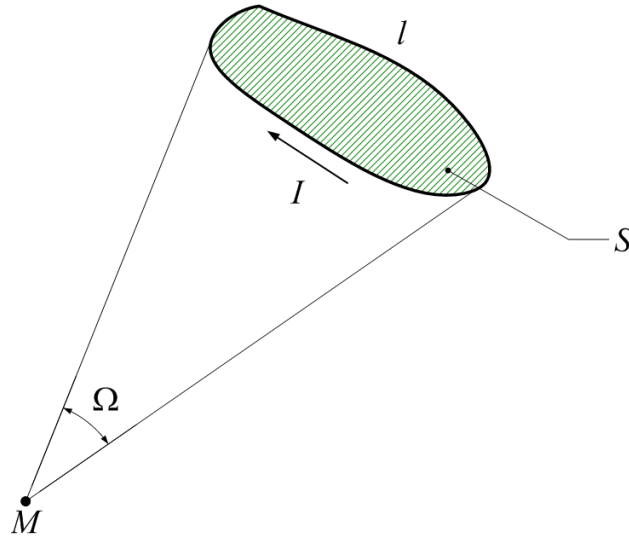


Figure 2.3: Magnetic shell and its potential.

and doesn't depend on the form of the surface stretched on the contour.

The fact that the form of the surface stretched on the contour with current can be chosen arbitrary is very important and gives wide possibilities and flexibility in simplifying the boundaries and achieving better convergence of a solution.

The equation (2.10) is similar to that of electric field potential, created by a double layer of electric charges. Generally, all the equations describing electrical charges are similar to those of magnetic charges. The application of Gauss theorem to magnetic charges leads to the following:

$$H_{Bn} - H_{An} = \frac{\sigma}{\mu_0}, \quad (2.11)$$

where  $H_{An}$ ,  $H_{Bn}$  – are the projections of  $\vec{H}_A$  and  $\vec{H}_B$  onto a normal line to surface  $S$ . The magnetic charge density  $\sigma$  is evident to be both positive and negative.

The equation (2.11) gives the most correct interpretation of the nature of magnetic charges. The surfaces with distributed magnetic charges are neither equipotential surface nor the ones with equal potential difference between them. The imposed condition (2.11) determines only a sudden change, a discontinuity of the magnetic field strength while crossing the surface. The value of that change for the medium with permeability of  $\mu_0$  concurs with the magnetization. Thus the magnetic charge density can be found like

$$\sigma = \frac{\mu_0 I}{b} = \mu_0 J a, \quad (2.12)$$

where  $a$  and  $b$  – are the dimensions of the cross-section of a rectangular conductor with current density  $J$  (Figure 2.4).

The sign of  $\sigma$  is determined by the sign of magnetic mass, which forms the surface layer, i.e. it is determined by the fact whether that one magnetic mass is a “source” or a “sink” of the field. The magnetic mass density inside the magnetic layer

$$\rho = \frac{\sigma}{b} = \frac{\mu_0 J a}{b}. \quad (2.13)$$

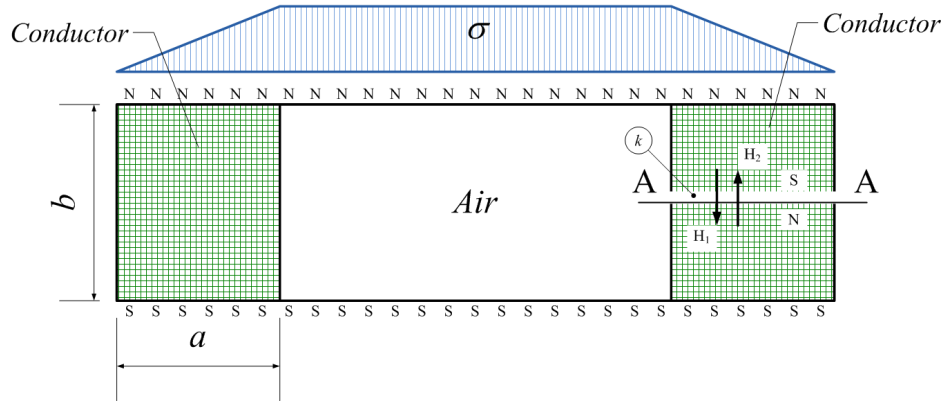


Figure 2.4: Magnetic charges field in air

The magnetic charges distributed on the surface of magnetic layer create the magnetic field not only outside the layer but also inside. It is evident that since the property of field line continuity is broken on the double magnetic layer surface, then the field inside the layer is not reproduced neither by sign nor by value. For example, for a contour in the air the magnetic charges on the surfaces of the layer stretched on that contour create field which has an opposite sign and is much stronger inside the contour than the one outside (Figure 2.4). The property of potentiality of the field is broken while crossing the layer. It is not physically justified. Thus, it is necessary to consider the layer impermeable. The field in any point  $k$  can be found also by adding two fields:  $\vec{H}_1$  – the field of initial magnetic charges distribution and  $\vec{H}_2$  – the field of the charges, formed by a “cut”  $AA$ :  $\vec{H} = \vec{H}_1 + \vec{H}_2$ .

The surface magnetic charge density in the zone of the cut doesn't depend on the position of that surface (everywhere except the transverse section of the contour) and is determined by (2.12), i.e.:

$$H_2 = \frac{I}{b} = Ja = \frac{\sigma}{b}. \quad (2.14)$$

In the transverse section zone the surface magnetic charge density can be considered linearly decreasing in the line of external part of the contour if the current density is equal in all the points of the contour.

For the chosen form of the surface stretched on the contour (Figure 2.4), the field vector  $\vec{H}_1$  inside the coil has opposite sign relative to the real field, while vector  $\vec{H}_2$  has the same direction.

### 2.1.3 Coils in ferromagnetic systems

The assumption that the steel permeability of EM magnetic cores  $\mu_{Fe} = \infty$  leads to the assumption that tangential component vector of magnetic field on the edge between air and steel is almost zero:

$$H_t = -\frac{\partial \varphi_m}{\partial t} = 0, \quad (2.15)$$

i.e.  $\varphi_m|_t = \text{const.}$

In other words, since the magnetic field lines “come” to the air-steel edge at angle of  $90^\circ$ , the SMP of the cores on these edges can be assumed *constant*, i.e. these edges are the *equipotential lines of scalar magnetic potential*. Actually, the equation (2.15) is true even if the relative permeability of the core  $\mu_r \geq 10$  [23].

The principle of magnetic charges (leaves, layers, shells) applied to a single contour can be spread on multicoil windings. The windings can be divided into the contours, each of them being replaced by a magnetic leaf. If the leaf surface coincides with the ferromagnetic core’s surface, then the SMP of the core obtains a sudden change in the place of contact equal to the magnetic charge density.

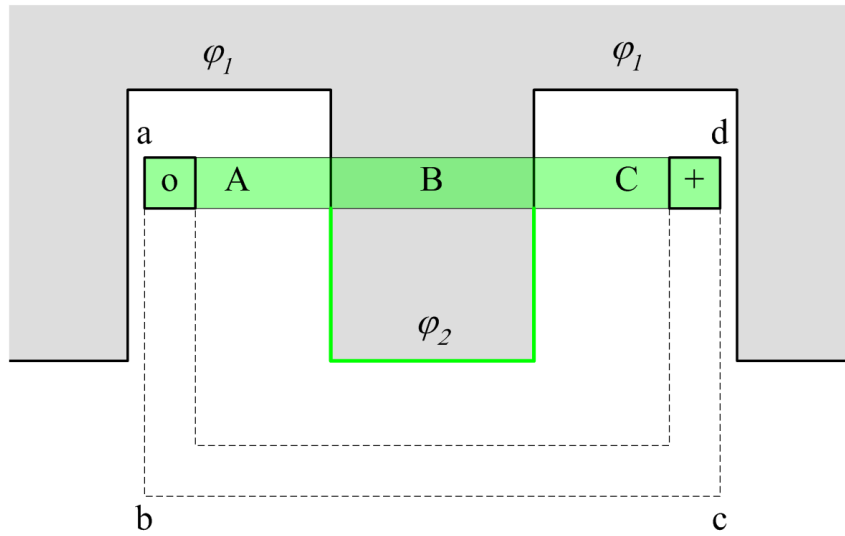


Figure 2.5: Forms of magnetic leaves

The contour embracing the tooth (Figure 2.5) is divided into 3 parts (A, B and C). Two of them (A and C) are placed completely in air and are formed by real sections of the contour and infinitively thin current layers carrying the full current of the contour. The part of a contour B crosses the ferromagnetic surfaces and creates the sudden change of SMP in the points of contacts:

$$\varphi_2 - \varphi_1 = i \quad (2.16)$$

Actually, the surface stretched on the contour can have any form, not necessarily rectangular one. It is possible create a surface, which doesn’t cross ferromagnetic core, like shown in Figure 2.5 as dash line. In this case there is no necessity to assign the potential on ferromagnetic cores, the last one is always zero.

As an example, let’s consider a coil with number of turns  $w_k$ , current  $i_k$ , which is placed on a tooth with infinite permeability (Figure 2.6). Dividing the coil onto three parts A, B, C as it was discribed above, we can calculate the field as a sum of fields of different parts. The distribution diagrams of sufrage magnetic charges on the end surfaces of the coil is shown on Figure 2.6; the maximum value of surface magnetic charge density is:

$$\sigma_{max} = \frac{\mu_0 i_k w_k}{b}. \quad (2.17)$$

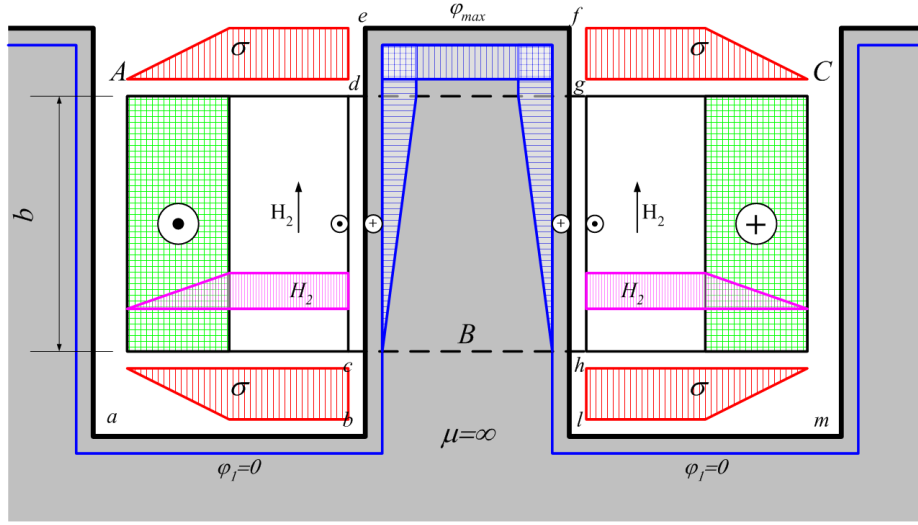


Figure 2.6: Distribution of SMP and magnetic charges density for a coil with current

If the density of turns of the coil is constant, then in the zone of its cross-section  $\sigma$  increases linearly starting from the external border of the coil. Similarly to the magnetic charge density changes the field strength  $H_2$  inside the coil. Its maximum value inside the coil is:

$$H_{2max} = \frac{i_k w_k}{b}. \quad (2.18)$$

In the shown version of the allocation of the surface stretched on the contour vector  $\vec{H}_2$  is directed strictly vertically, i.e. its horizontal component is zero in all the points of magnetic layer.

On a ferromagnetic surface in zones  $abc$  and  $hlm$  magnetic potential can be considered as zero. It changes linearly along the lines  $cd$  and  $gh$ . Its maximum value takes place on the line  $defg$  and is equal to  $i_k w_k$ . According to (2.15) the ferromagnetic surface is equipotential what is complied only taking into account  $\vec{H}_2$  or *current layers on the ferromagnetic surface*.

#### 2.1.4 Idea of a tooth contour and special boundary conditions

To obtain the magnetic field of an electrical machine and its parameters, a method of scalar magnetic potential can be used. To do this let's replace the machine winding with a magnetic leaf which is partially aligned with the surface of the core, that the winding is placed on. Real conductors of the windings will be considered to be formed by an infinitively big amount of thin current fibers. Further, let's divide the leaf surface on the parts of equal magnetic charges densities. Since the task is linear (in the air-gap) the full magnetic field of a machine can be considered to be formed by different magnetic leaves' fields of equal densities. Thus, each equal density part of the magnetic leaf can be considered to be formed by its current. So, the complex winding of an electrical machine can be divided into the contours. The coil ends form additional contours. Now let's consider the magnetic field in the air-gap of a machine without coil ends, which are replaced by the boundaries of the magnetic leaves formed by thin current fibers. The air-gap field will not change much in this

case, if the length of a machine is much bigger than the value of the air-gap. The equal density parts of the magnetic leaf are aligned with the teeth surfaces and are limited by two adjacent slot currents. The change of the magnetic potential while moving from the surface of one tooth to the surface of another one is equal to the change of a magnetic charge density, i.e. the slot current. Each equal density part of a magnetic leaf is stretched on the contour formed by two adjacent slot currents and a current fiber replacing the coil-end part. The current of the contour is equal to the magnetic charges density of the leaf's part.

Let's call such contour a *Tooth Contour* (TC). The currents of tooth contours certainly must follow the condition:

$$i'_{k+1} - i'_k = i_{sk} \quad (2.19)$$

The currents can be determined up to a constant value. For instance, if we assume the current of the first TC to be zero, then for the  $k^{th}$  TC we obtain according to (2.19):

$$i'_k = \sum_{j=1}^{k-1} i_{sj} \quad (2.20)$$

The magnetic potentials of teeth are the sum of the core's potential and that of the magnetic charges density of the corresponding TC.

Let's consider two tooth contours: on stator and rotor (Figure 2.7). The permeability of stator  $\mu_S$  and rotor  $\mu_R$  cores is infinite. The stator TC  $k$  is *excited*, i.e. its current  $i'_k \neq 0$ . The magnetic leaf, stretched on the tooth, produces the potential of the tooth's surface  $\varphi = i'_k$ . All the other surfaces have *zero potentials*. Such conditions of potential distribution are called *Special Boundary Conditions* (SBC). The field calculated under SBC permits to obtain the flux of a non-excited TC produced by the excited one. The flux of a rotor TC  $m$  is obtained on the surface stretched on that contour – surface *abcdef*.

In order to determine the permeance  $\Lambda_{km}$  between stator TC  $k$  and rotor TC  $m$  one should excite the TC  $k$  with a unit current  $i'_k = 1$  and calculate the flux  $\Phi_m$  on the surface *abcdef*. The permeance then will be

$$\Lambda_{km} = \frac{\Phi_m}{\varphi_k - \varphi_m} = \frac{\Phi_m}{i'_k} = \Phi_m. \quad (2.21)$$

### Tooth Contour deep in slots

Along with the assumptions which are accepted in general theory of electrical machines and which allow to consider the task of the calculation of a magnetic field as a quasistationary one, let's assume the following:

1. the field in the air-gap of the machine is an in-plane one and the coil end field can be considered independently;
2. the tooth contours of the machine are wide and deep in slots;
3. the saturation of the cores stays in limits when the air-gap surfaces of the teeth can be considered as equipotentials for the scalar magnetic potential (this requirement is usually satisfied for existing electrotechnical steels since they usually have  $\mu_r > 10$  even in high saturation).

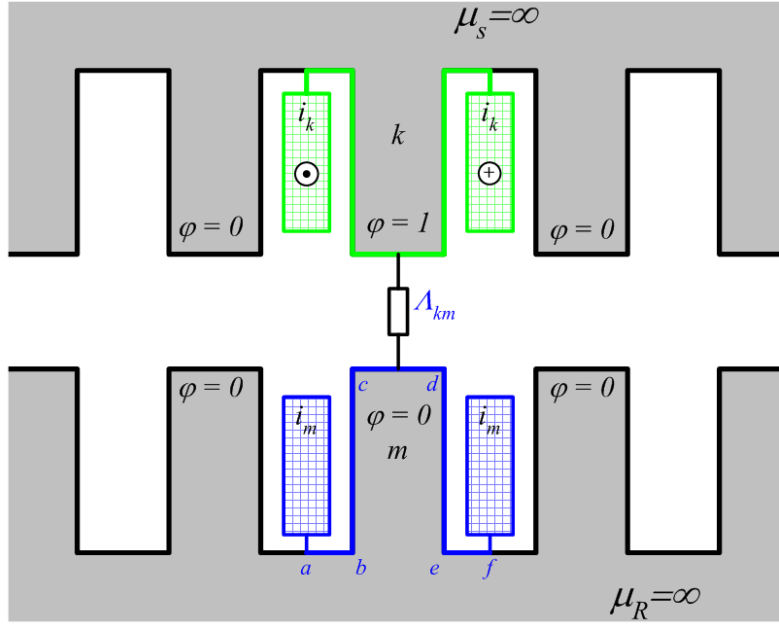


Figure 2.7: Stator and rotor tooth contours

The first assumption is the conventional one and the axial heterogeneity of the machine caused by coil ends and ventilation ducts, is taken into account separately.

The idea of “wide and deep in slots” contour is given in [23]. One of its properties making it deep in slots lies in the fact that the field’s force lines, which cross the air-gap, are completely linked with the slot’s conductor, i.e. they do not cross the latter. According to [23, pp. 62-63] a contour can be considered as *deep in slots* if the relative immersion of a conductor into a slot  $h/b_s$  is equal or bigger than the value given in table below, depending on the relative slot opening  $b_s/\delta$ <sup>1</sup>. Most of turbogenerators do satisfy these conditions.

$b_s/\delta$	0.5	1.0	2.0	4.0	6.0	$\geq 8.0$
$h/b_s$	0.00	0.15	0.35	0.50	0.57	0.6

The third assumption is the most important one, since it allows applying the TCM to the saturated machines. The influence of the saturation on the air-gap permeance has been investigated in several works ([23], [26], [31]). In [26] it is shown that for the typical tooth zone proportions of turbogenerators, the unipolar air-gap permeance can be considered not depending on the saturation.

According to the second and third assumptions the air-gap field of an electric machine, being completely linked with the contours, is formed by a system of equipotential teeth surfaces. At the same time, the slot’s field located deeper in the slot than a conductor, doesn’t depend on the field of the air gap. Thus, the air-gap field can be considered independently of the slot’s one.

<sup>1</sup>Here:  $h$  – immersion of a conductor in slot,  $b_s$  – slot opening,  $\delta$  – air-gap value.



### SBC and limits of the zone

The calculation of the mutual permeances between the teeth (tooth contours) of stator and rotor is one of the most important stages of the PN parameters' calculation, since its accuracy is the one that the representation of a total magnetic field of an electrical machine depends on.

To determine these permeances a magnetic field created by the current of a tooth contour must be considered. Let's consider a tooth contour with index  $s$  presented on Figure 2.8<sup>2</sup>. It's field is created by the wires with current placed in the slots between the tooth  $s$  and adjacent teeth  $s - 1$  and  $s + 1$ .

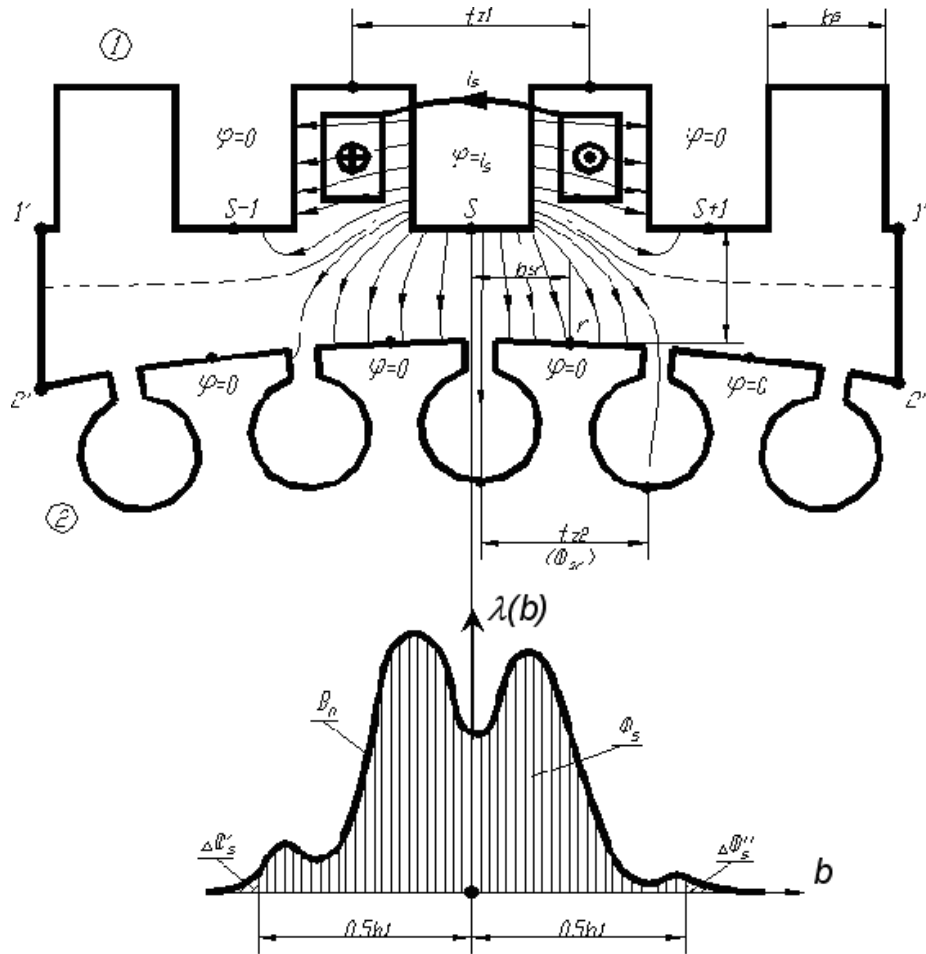


Figure 2.8: Tooth contour

The magnetic field of the current  $i_s$  is calculated applying the following assumptions:

- all other currents in the magnetic system are equal to zero;
- the current is distributed regularly inside the wires;
- the permeability of the steel of both cores (stator and rotor) is infinite ( $\mu_c = \infty$ );

<sup>2</sup>In order to show more spectacular slot effects an interaction of a hydro-generator pole and stator tooth was chosen [27].

- the magnetic field is two-dimensional.

The mutual position of the stator (1) and rotor (2) cores is set by the distance  $b_{sr}$  between the axis of an excited tooth placed on the core 1 and the axis of a tooth placed on the core 2.

The boundary conditions are chosen in the manner that the magnetic field lines have only one direction in the air-gap and the consumption of the magnetic potential in the airgap is equal to the tooth contour current  $i_s$ . This is reachable if the tooth  $s$  has the magnetic potential  $\phi = i_s$ , while all the other teeth of both cores have potential  $\phi = 0$ .

The results of a field calculation of the tooth contour are presented on Figure 2.8 by a distribution of normal part of flux density  $B_n$  on a middle line of an air gap. As one can see, the magnetic flux density of a tooth contour in the air gap, being calculated with special boundary conditions, fades out rather not too far away from the excited tooth contour's axis.

The most part of the contour's mutual flux

$$\Phi_s = l_\delta \int_{-\infty}^{\infty} B_n dx, \quad (2.22)$$

where  $l_\delta$  is an effective length of a machine, is concentrated in the zone of [23, p.69]

$$b_1 = t_{z1} + 2\frac{\delta}{\pi} \ln \frac{2\delta}{\pi g t_{z1}} \cong t_{z1} + b_s + 3\delta, \quad (2.23)$$

where  $t_{z1}$  is a tooth pitch of an excited contour;  $\delta$  is an air gap;  $g = (\Delta\Phi'_s + \Delta\Phi''_s) / \Phi_s = 0.01 \div 0.001$  is a relative tolerance of flux determination.

In order to form the limits of the zone of calculation a special, special "magnetic shunts" can be used. These shunts are shown on Figure 2.8 as lines  $1' - 2'$  and  $1'' - 2''$ . They have infinitely big permeability and thus connect two magnetic cores (stator and rotor) into one zone of a tooth contour.

### 2.1.5 Magnetic charges and permeance network

A permeance network is a representation of a continuous magnetic system by a discrete one having lumped parameters. As it was shown in Section 2.1.2, the magnetic charge surface can have any form. For a permeance network based on SMP it is necessary to have well determined boundaries with determined values on them. The best way to provide that determinancy is to make magnetic shell to cross ferromagnetic surface.

Let's consider a ferromagnetic tooth (Figure 2.9) surrounded by conductuctors carrying currents  $i_k$  and  $i_{k+1}$  with a very simple magnetic circuit. In the magnetic circuit the tooth  $k$  is represented by one branch, containing MMF source  $F_k$  and nonlinear permeance  $\Lambda_{tk}$ ; the yoke parts under the adjacent slots are represented by permeances  $\Lambda_{yk}$  and  $\Lambda_{yk+1}$ .

The magnetic shell stretched on the tooth will produce a change of SMP on its surface at it was described in section 2.1.3. Since the whole tooth is represented by only one branch that branch obtains the full change of SMP  $F_k = i_k - i_{k+1}$ .

Generalizing, we can say that *the branch of a permeance network being crossed by a magnetic shell obtains an MMF equal to the change of SMP produced by that shell.*

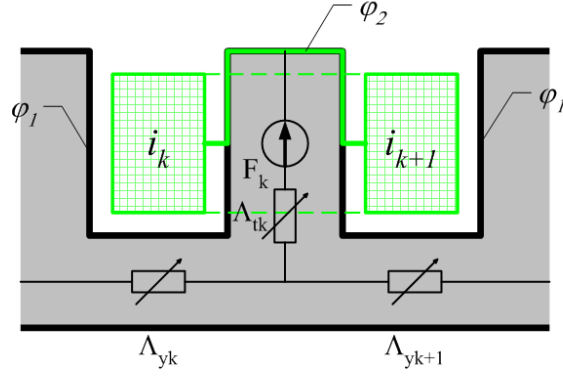


Figure 2.9: A magnetic shell stretched on tooth

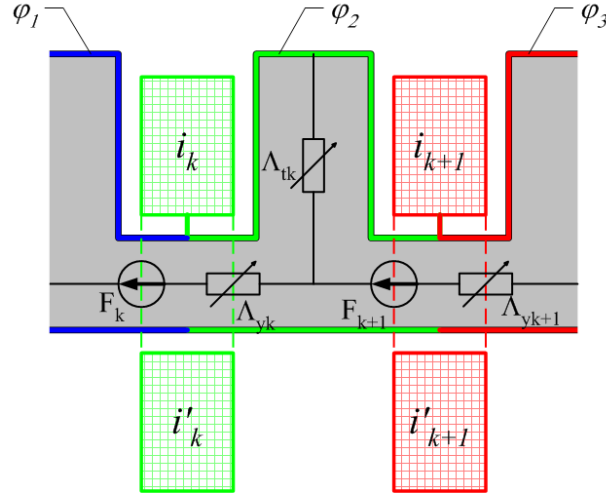


Figure 2.10: Other configuration of magnetic shells.

A magnetic shell can be stretched also in the direction crossing the yoke part. Let's consider now the same magnetic system but with the configuration of magnetic shells, shown on Figure 2.10. In this case we can introduce fake currents outside the magnetic system which correspond to the currents in slots:  $i'_k = -i_k$  and  $i'_{k+1} = -i_{k+1}$ . Now the magnetic shells stretched between these currents cross the yoke branches producing in them potential differences  $F_k = i_k$  and  $F_{k+1} = i_{k+1}$ . This corresponds to a well-known electrotechnical principle of transference of EMF sources over a circuit node.

The scheme on Figure 2.10 is easier to be realized since each source of MMF corresponds to a full slot current. Let's introduce then another layer of PN between teeth (Figure 2.11). The PN now obtains additional tooth permeance  $\Lambda'_{tk}$ . Branch  $F_{sk} - \Lambda_{sk}$  correspond to the slot leakage of the left slot and branch  $F_{sk+1} - \Lambda_{sk+1}$  - of right slot. The branch  $k$  will still be crossed by the shell stretched on a full winding carrying slot current  $i_k$  while the new branch  $sk$  will be crossed by the shell stretched *only on the top half of the winding* thus having the value of MMF slot  $F_{sk} = i_k/2$ . The same effect is observed on the right slot.

Thus, according the chosen configuration of magnetic shells (like on figures 2.10 and 2.11) one can formulate the following principles:

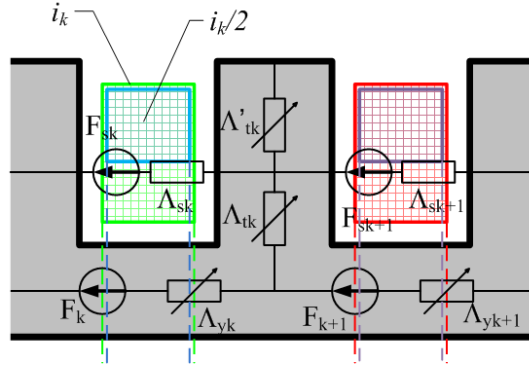


Figure 2.11: Magnetic shells in case of two layers of PN.

1. MMF sources are placed in azimuthal branches of the PN.
2. The value of the source is equal to *the part of the slot current which embraces the branch*.
3. The higher the number of azimuthal branches the better the precision of the PN.

## 2.2 Machine's permeance network

The space of an electrical machine can be divided into several main zones (Figure 2.12):

- stator tooth and yoke zones;
- stator slot zone;
- air gap;
- rotor tooth and yoke (central part) zones;
- rotor yoke zone (central part of the rotor).

Generally, any PN describing the magnetic system of an electrical machine consists of the elements of following types:

- linear passive elements (permeances or reluctances);
- nonlinear passive elements (permeances or reluctances) which depend on a solution variable (flux or ampere-turns);
- sources of MMF;
- special linear elements which depend on an independent parameter (mutual position between stator and rotor).

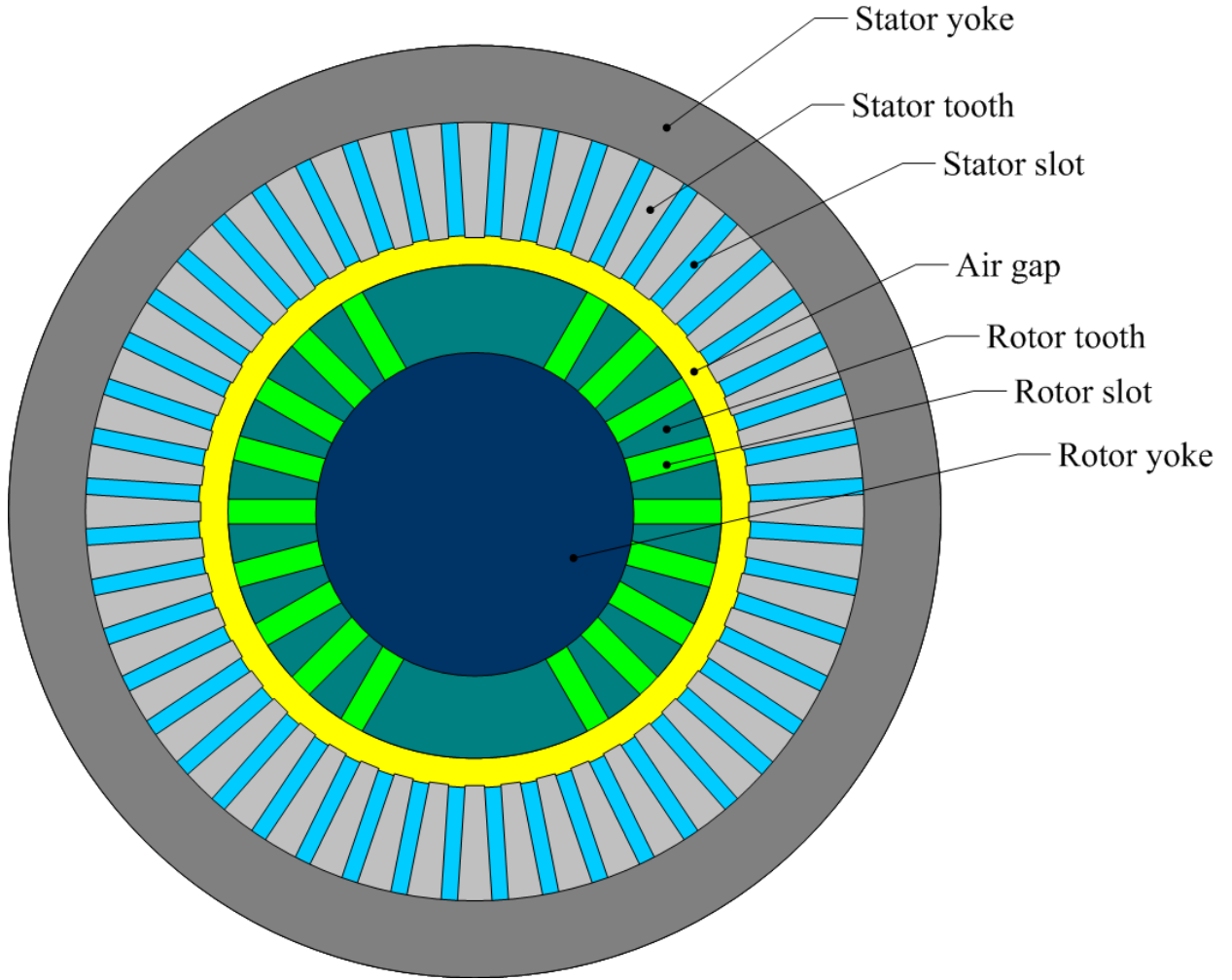


Figure 2.12: Main zones of a machine

The *linear elements* represent the fluxes in the air-zones of stator or rotor - the slot leakages. Their values are calculated and fixed during the calculation process.

The *nonlinear elements* represent the parts of the cores of stator or rotor, i.e. stator and rotor teeth and yokes. The values of these elements are given as weber-ampere characteristics  $\Phi(U_m)$ , where  $\Phi$  – the element's flux and  $U_m$  – the element's magnetic potential difference corresponding to that flux.

The *dependent linear elements* are the ones that represent the mutual permeances between stator and rotor teeth. They are given by characteristics  $\Lambda(\Theta)$ , where  $\Lambda$  – the element's permeance and  $\Theta$  – the mutual position between stator and rotor (angle). These characteristics are calculated on the preparation stage. The values of these elements are fixed during the calculation process for the particular rotor position.

### 2.2.1 General approach for zones' division of the machine

In order to divide the volume of an electrical machine onto discrete elements and calculate their characteristics, we must determine the geometrical limits of the zones represented by the elements and assume the direction of the flux in these zones. Figure 2.13 shows a part

of a magnetic system (stator or rotor) of a machine and we shall explain the process of zone determination on that example.

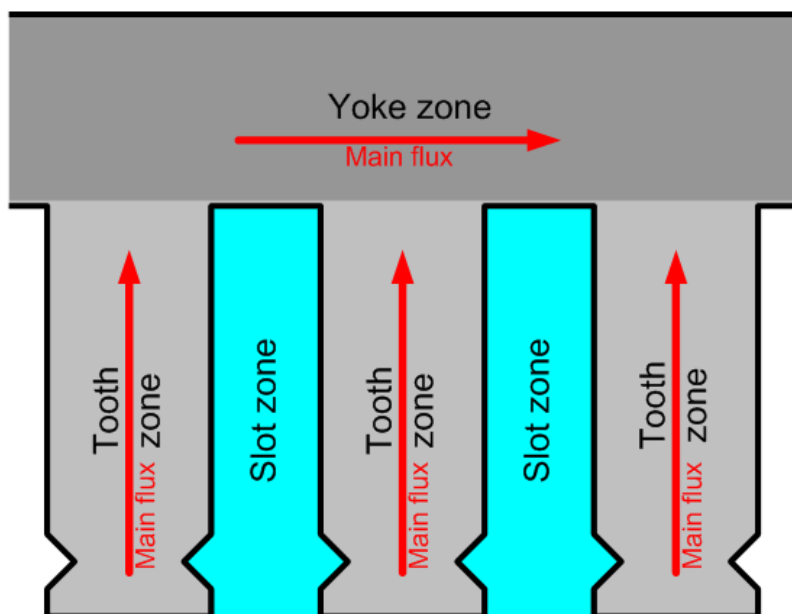


Figure 2.13: Characteristic zones of machine's magnetic core

The characteristic zones of any machine's core are the following:

**Tooth zone** – the one representing a tooth of a magnetic system. The tooth is made of magnetic material and according to the assumption that the permeability even in saturation is relatively high, we can say that *generally the flux in that zone has radial direction only*. Let's call such a zone *radial zone*.

**Yoke zone** – the one representing a yoke of a magnetic system. The material of that zone is also magnetic and the flux goes in the direction from one tooth to another. That zone will be called *tangential zone*.

**Slot zone** – the one representing the air between teeth. In these zones the flux is also directed from one tooth to another, thus it is also the *tangential zone*.

### Zone definition

Each zone of a machine is defined with two pairs of vectors:  $[h_l, w_l]$  and  $[h_r, w_r]$ . These vectors define the points of the *left* and *right* borders of the zone relative to its flux axis (Figure 2.14). Vectors  $h_l$  and  $h_r$  represent the height from the top of the zone, while vectors  $w_l$  and  $w_r$  represent the *half-width*, i.e. the distance between the point and the flux axis.

According to the specification of the machine, slot zones are defined. Tooth zones are obtained as a geometrical differences between adjacent slots. For these radial zones the vectors  $w_r$  and  $w_l$  represent actually the arc lengths of the corresponding segments.

According to the chosen number of layers, slot zones and tooth zones are divided into *elementary zones* corresponding to the elements of the network. Each elementary zone is also represented by vectors  $[h_l, w_l]$ ,  $[h_r, w_r]$ .

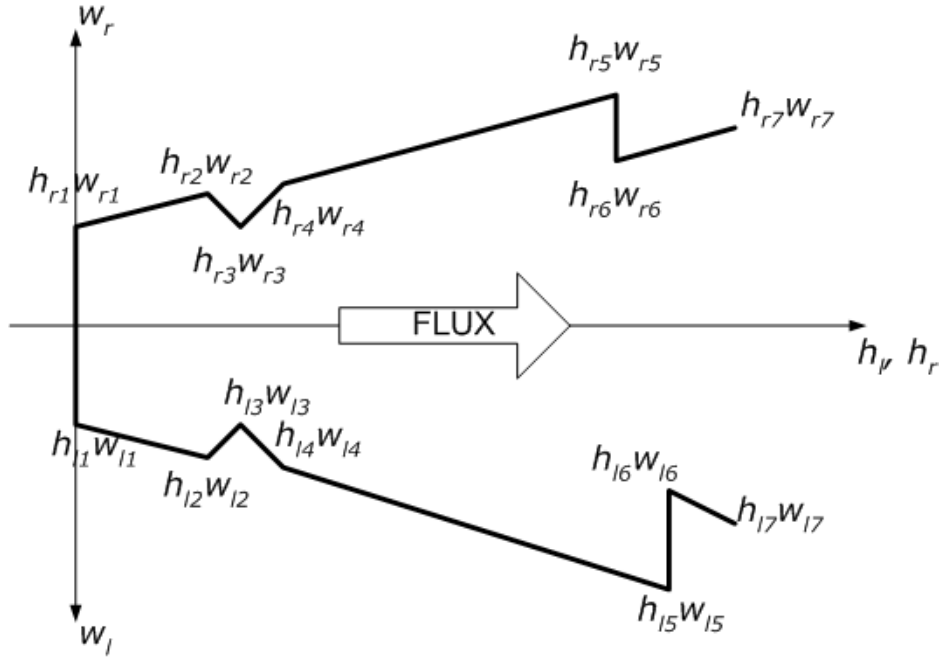


Figure 2.14: Zone definition

This principle of zone definition is used to represent all the zones of an electrical machine corresponding to the elements of PN, except air-gap permeances, since the latter have no well-defined boundaries.

### Automatic PN generation – Variable Topology Network

The method of general zone description of a machine discussed above gives a possibility to implement automatic network generation according to demanded precision abstracting from the structure of the machine.

The network generation is realized separately for three different parts: air-gap, stator and rotor. The topology of air-gap is always fixed and determined by the number of stator and rotor teeth. Stator and rotor magnetic systems networks are generated using the same method and the same algorithm. The latter can be described as following:

1. Distinguishing tooth and yoke zones.
2. Tooth zone: describing the dimensions of each tooth using zone definition shown above. Used zones are radial.
3. Tooth zone: splitting the zone of each tooth into layers one obtains a set of radial (teeth) and tangential (slots) zones.
4. Tooth zone: forming the network of the tooth zone according to that set of zones – each element of the network has a corresponding zone.
5. Yoke zone (central part in case of rotor): splitting the zone of yoke into sub-zones placed between the teeth.

6. Yoke zone: forming the yoke network according to the set of zones obtained on step 5.
7. Linking tooth and yoke networks together.

The obtained networks of stator and rotor are linked together by means of air-gap network. The resulting PN has a *variable topology* which depends on particular geometrical structure of the components (rotor and stator)<sup>3</sup>.

### 2.2.2 Stator permeance network

The total stator PN is presented on Figure 2.15. It consists of nonlinear radial tooth

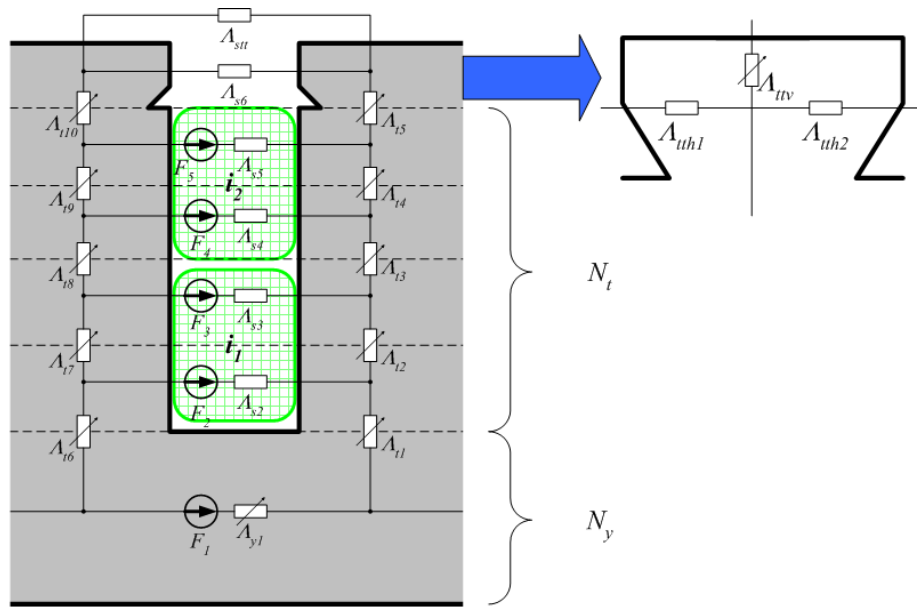


Figure 2.15: Full stator scheme

permeances  $\Lambda_{t1}$ - $\Lambda_{t10}$ , azimuthal yoke permeances  $\Lambda_y$  and linear slot leakage permeances  $\Lambda_{s2}$  -  $\Lambda_{s6}$ . The number of elements and, thus, the precision of the network depends on the number of layers in tooth and yoke zones. For  $N_y$  greater than 1 the layers of azimuthal yoke permeances are added connected by additional radial yoke permeances. Tooth top slot permeance  $\Lambda_{stt}$  represents inter tooth top flux.

The zoom of the tooth top on Figure 2.15 presents the permeance network of that one part of the tooth. It has additional azimuthal nonlinear branches which represent the saturation of that part of a tooth.

Let's further consider the calculation of the parameters of the stator elements.

#### Tooth permeances

Each stator tooth is presented by several permeances radially directed. A simplified scheme of a stator tooth is shown on Figure 2.16.

<sup>3</sup>Topology variation is discussed in rotor network section 2.2.3.



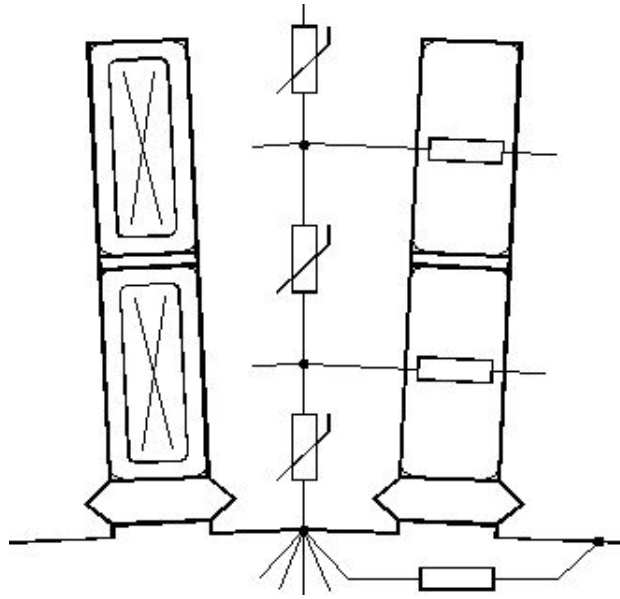


Figure 2.16: Tooth scheme

The scheme consists of radial passive nonlinear elements connected in series. The number of branches is determined by the number of layers which the tooth zone of stator is divided in. For rectangular slots the teeth have a trapezoidal form. The magnetization curve  $\Phi(U_m)$  of each zone is being calculated from the BH-curve of the steel. In order to take into account the variable cross-section of the tooth, the last one is divided into several elementary parts (Figure 2.17). For each point of the BH-curve the flux  $\Phi$  is calculated as following:

$$\Phi = B \cdot l_{eff} \cdot b_{min} \quad (2.24)$$

where  $l_{eff}$  – effective core length;  $b_{min}$  – minimal part's width. The magnetic potential difference of the part is obtained from that flux as a sum of the ampere-turns of elementary subdivisions:

$$U_{m.el.} = h_{el} \cdot \frac{H_1 + 4H_3 + H_2}{6} \quad (2.25)$$

where  $h_{el}$  – the elementary part's height;  $H_1$ ,  $H_2$ ,  $H_3$  – the magnetic strength in the top, bottom and middle sections of the elementary part respectively. These magnetic strengths are determined of the corresponding values of flux densities taking into account the flux displacement into the air part: both in the slot areas between the teeth and the ventilation duct areas between the steel packs in axial direction. The approach is described later in Section 2.3.1. That approach allows a precise calculation of weber-ampere characteristic of any part of a tooth even with rather complex geometrical configuration.

### Stator yoke permeances

The stator yoke can be also presented by several layers of permeances. But it is sufficient to use only one layer for that part. The magnetic scheme parts are limited in azimuthal direction by the axes of adjacent teeth. The magnetization curve of a yoke part is calculated the same

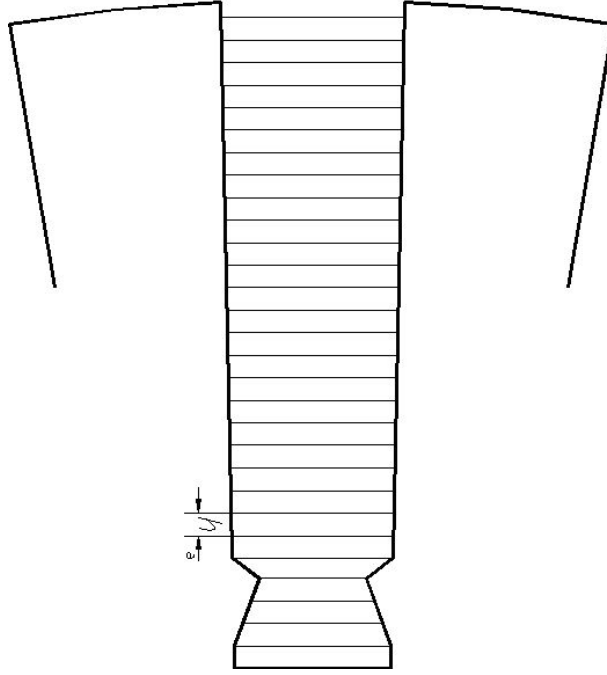


Figure 2.17: Tooth division

manner as for the tooth zone while the length of each zone is obtained by the middle line of the flux in that one. This means that we represent the curved elements as rectangular ones (Figure 2.18).

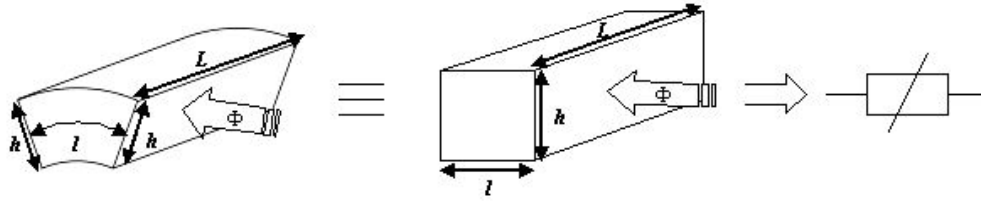


Figure 2.18: The stator yoke element

### Slot slot leakage permeances

As it has been mentioned above the tooth zone of a stator is divided into several layers. The slot leakage fluxes are calculated with a definite precision. The bigger the number of the layers, the higher the precision of that calculation. But even if the winding layer is represented by only one zone, the calculation error is less than 4% [23].

The slot leakage permeances for the zones with the winding in case of the rectangular slot can be found as follows:

$$\Lambda_{\sigma i} = \frac{\mu_0 l_x h_i}{b_s} \quad (2.26)$$

where  $h_i$  – zone height;  $l_x$  – the effective length taking into account radial ventilation ducts (see further);  $b_s$  – the slit height.

The slit zone permeance can be found as follows:

$$\Lambda_{\sigma s} = \frac{\mu_0 l_x h_s}{b_s} + \Lambda_h \quad (2.27)$$

where  $\Lambda_h$  – the permeance between top surfaces of adjacent teeth in special boundary conditions [23]:

$$\Lambda_h = \frac{\mu_0 l_\delta}{\pi} \left[ \frac{2\delta}{b_s} \arctg \frac{b_s}{2\delta} + \ln \frac{\sqrt{1 + (2\delta/b_s)^2}}{2} - \ln 2 \right] \quad (2.28)$$

where  $\delta$  – air-gap,  $b_s$  – slot opening.

Other formulas for slot leakage permeances can be implemented in future, like, for instance, presented in [16, 32].

### 2.2.3 Rotor permeance network

As it has been mentioned in the beginning of this section the permeance networks of tooth zones of stator and rotor are the same. So, here we shall discuss the representation of the central part of a rotor.

#### General case

First, we have constructed a concentric rotor network, in which the central part layers are formed by circular segments. Figure 2.19 shows a simplified example of that PN, outlining the position of its elements. Each radial elements of the yoke is formed by a *trapezoidal* segment like the one of radial tooth zone. Azimuthal elements have curved rectangular form like the ones of azimuthal stator yoke zones. The methods of their calculation are the same.

**Remark.** For multipole machines PN is constructed only for 2 adjacent poles, since all the processes are same. But in cases of non-integer number of tooth per pole per phase  $q$ , the PN cannot be reduced to 2 poles: a whole machine must be calculated leading to higher discretization and greater time of calculation.

#### 2-pole specific case

The calculations for a 2-pole machines showed that the model presented above is not adequate. Indeed, the flux in multipole machines flows usually in the segments close to tooth zone and angular distance between poles is much less than  $180^\circ$ . The 2-pole machine's flux have direct flow from radially opposite poles. Thus another PN of the 2-pole rotor was proposed.

Figure 2.20 presents the PN of the central part of the rotor. Permeances  $\Lambda_{yh1} - \Lambda_{yh8}$  represent d-axis flux, while permeances  $\Lambda_{yv1} - \Lambda_{yv4}$ . Tooth zone of the machine and MMF sources are not shown in details on the figure. D-axis directed elements correspond to trapezoidal zones, q-axis – rectangular zones. The methods of their characteristics calculation is the same as presented above.

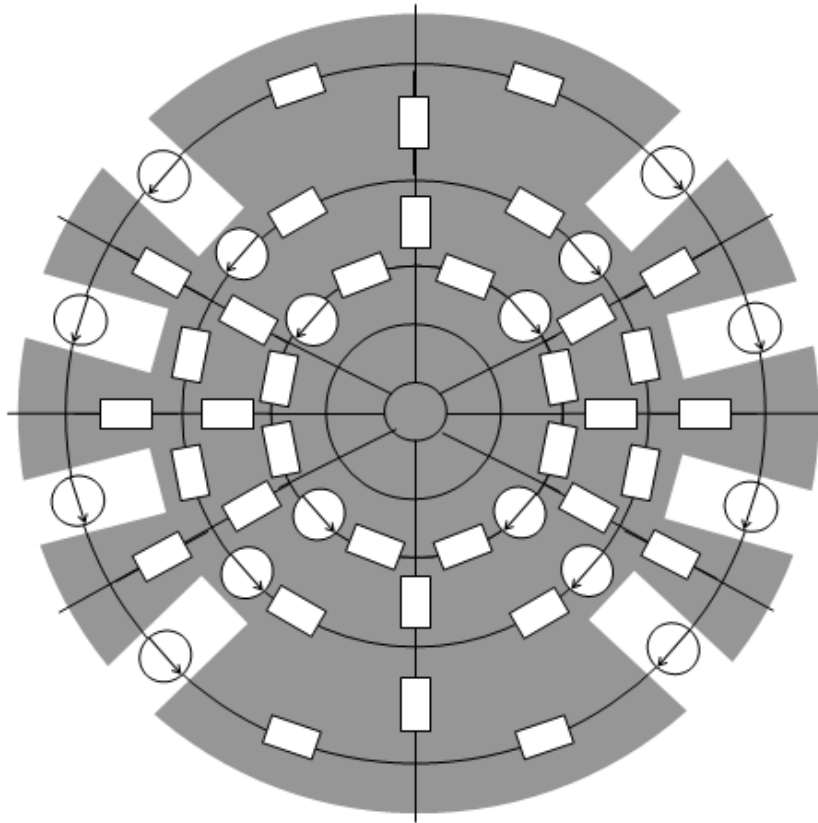


Figure 2.19: Concentric rotor PN

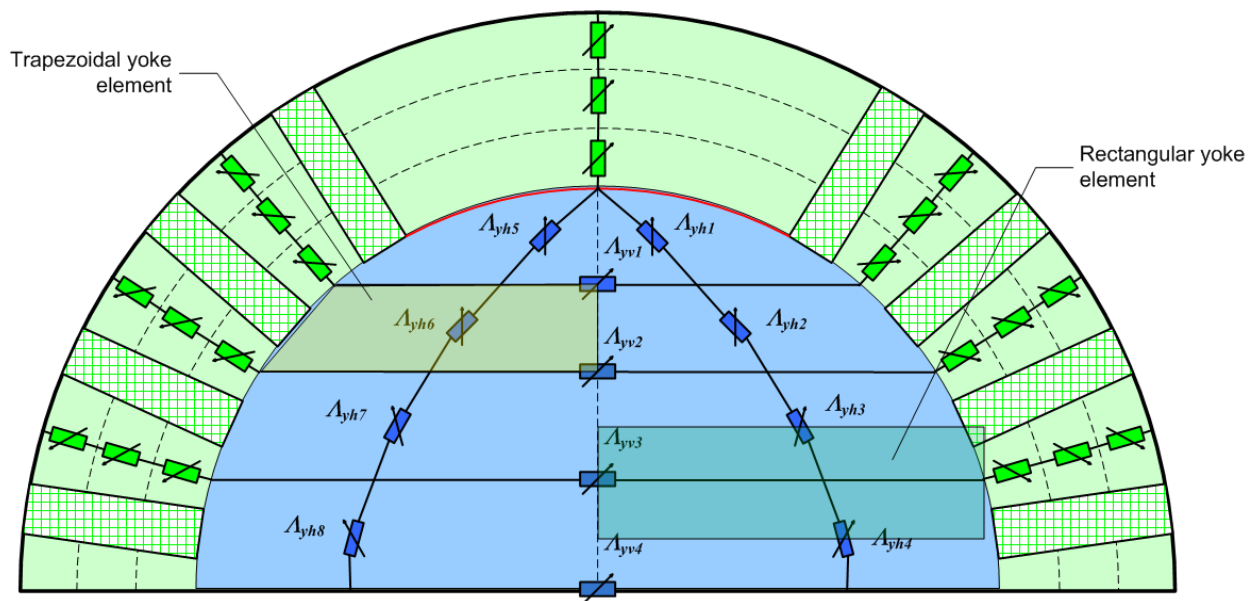


Figure 2.20: 2-pole rotor PN

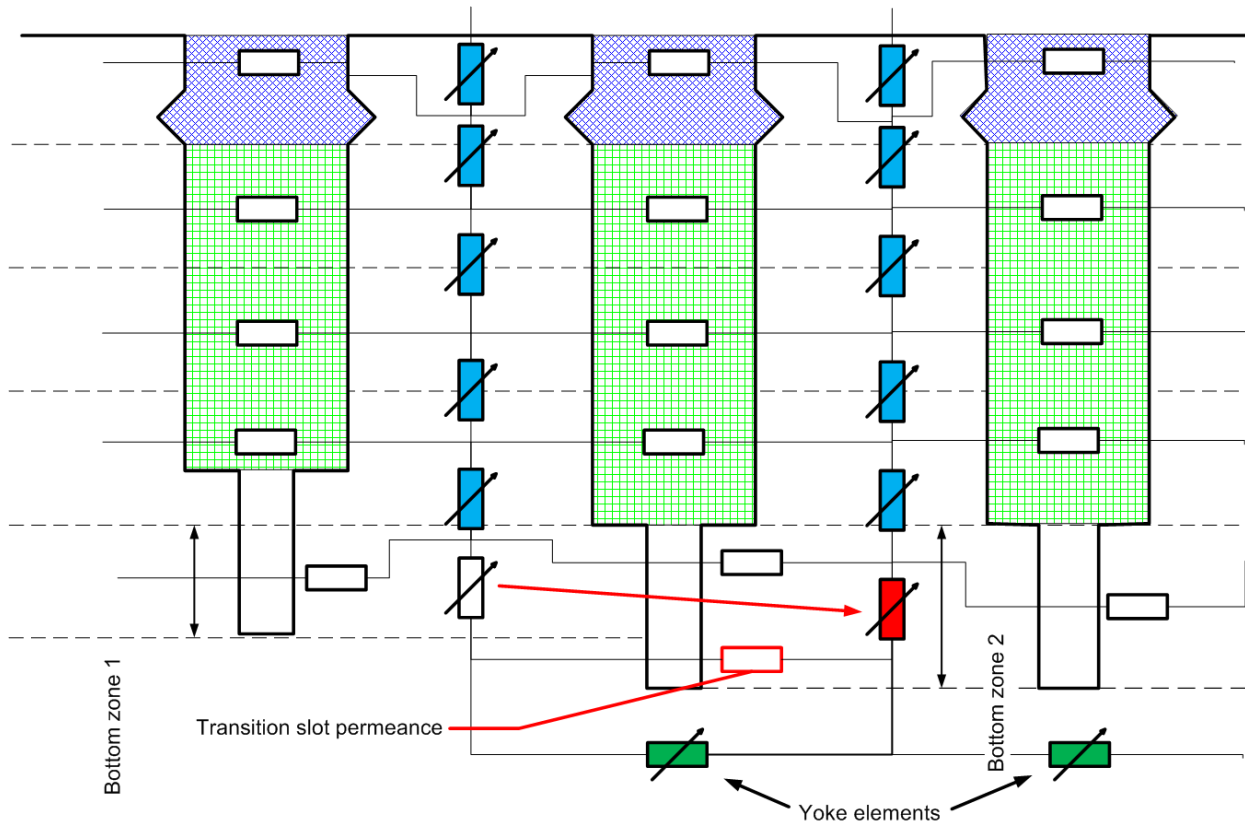


Figure 2.21: Adaptive rotor PN.

### Adaptive junction between tooth and yoke zones

In general, rotor can have different slot characteristics, like height, width, different ventilation ducts, etc. It leads to different PN construction for different slots. From the other hand, all of them must be joint to the yoke PN. Thus, an adaptive *variable topology PN* principle was proposed.

Figure 2.21 presents the permeance network of the tooth zone (MMF sources are skipped). One can see that left and central slots have different heights. The general idea is to add special *transitional* permeances between adjacent slots in order to pass from one dimensioned PN to another.

Regular assumptions discussed in Section 2.1 allow to think that the border between core and slot is an equipotential line, thus the zone of tooth is independent regarding adjacent tooth. It gives us the possibility to apply different (modified) permeance networks to different teeth. On the figure 2.21 “Bottom zone 1” is different of “Bottom zone 2”. The nonlinear bottom element of the zone 1 is replaced in zone 2 by another one having different characteristic (shown in red). Transition slot linear permeance (red) represents additional slot flux from the right tooth to the left.

If adjacent slots have same heights (like central and right slots on Figure 2.21), no transition layers are needed.

### 2.2.4 Airgap characteristics calculation

According to the principle of TCM, the air-gap permeances should be calculated between the tooth contours of stator and rotor under SBC (section 2.1.4). The calculation of the permeance can be realized using any available methods: FEM, FDM, FIT, MCM, analytical, approximative, etc.

The field of an excited TC is shown on Figure 2.22. It was calculated using FEM under SBC: the zone of calculation was limited, only one tooth was excited by means of the current  $i_{sk}$ . The distribution of the flux density on the middle line of the air-gap is given on the same figure. Actually, it seems to be rather easy to obtain the permeance using FEM. In order to do this, the flux must be calculated on the line  $abcdef$ . All the calculations must be performed for several mutual positions between rotor and stator.

#### Calculating the permeances using analytical approach

To calculate the air-gap permeances one have to calculate the magnetic field in the air-gap region. The field calculations can be performed by many different methods. Here an analytical method of calculations is given [23, pp.72-75].

Usually the calculations in the air-gap zone are performed neglecting the curvature of the air-gap, i.e. supposing that the radiuses of the sufaces divided by air-gap are infinite. Neglecting the curvature of the air-gap is approved for rather small ratios  $\delta/D$  ( $D$  – diameter of stator bore). But turbogenerators have rather big relative air-gap and this fact can lead to increase of calculation errors.

In order to take into account the curvature of the air-gap a logarithmic conformal mapping can be used. It maps a real annular air-gap  $\delta$  in  $z$ -plane into a flat air-gap with infinite curvature in  $t$ -plane:

$$t = K \cdot \ln z, \quad (2.29)$$

where  $K$  – scale factor.

In polar coordinates of basic plane  $z = r \cdot e^{j\Theta}$ , where  $r$  and  $\Theta$  – polar radius and angle respectively. Using  $t = u + jv$  from (2.29), one can obtain:

$$\left. \begin{aligned} u &= K \cdot \ln r \\ v &= K \cdot \Theta \end{aligned} \right\} \quad (2.30)$$

It permits to pass from the polar coordinates of the basic plane in the area of annular air-gap of  $z$ -plane to rectangular coordinates of flat air-gap in  $t$ -plane. The conformal mapping is performed for the first kind boundary conditions and the mapping invariant is the magnetic flux or the permeance. Thus it doesn't matter which constant  $K$  is used for the mapping.

Let's perform the mapping for air-gap value  $\delta = const$ :

$$\delta = r_1 - r_2 = K \ln \frac{r_1}{r_2}. \quad (2.31)$$

Then the scaling factor  $K$ :

$$K = \frac{\delta}{\ln \frac{r_1}{r_2}} \quad (2.32)$$

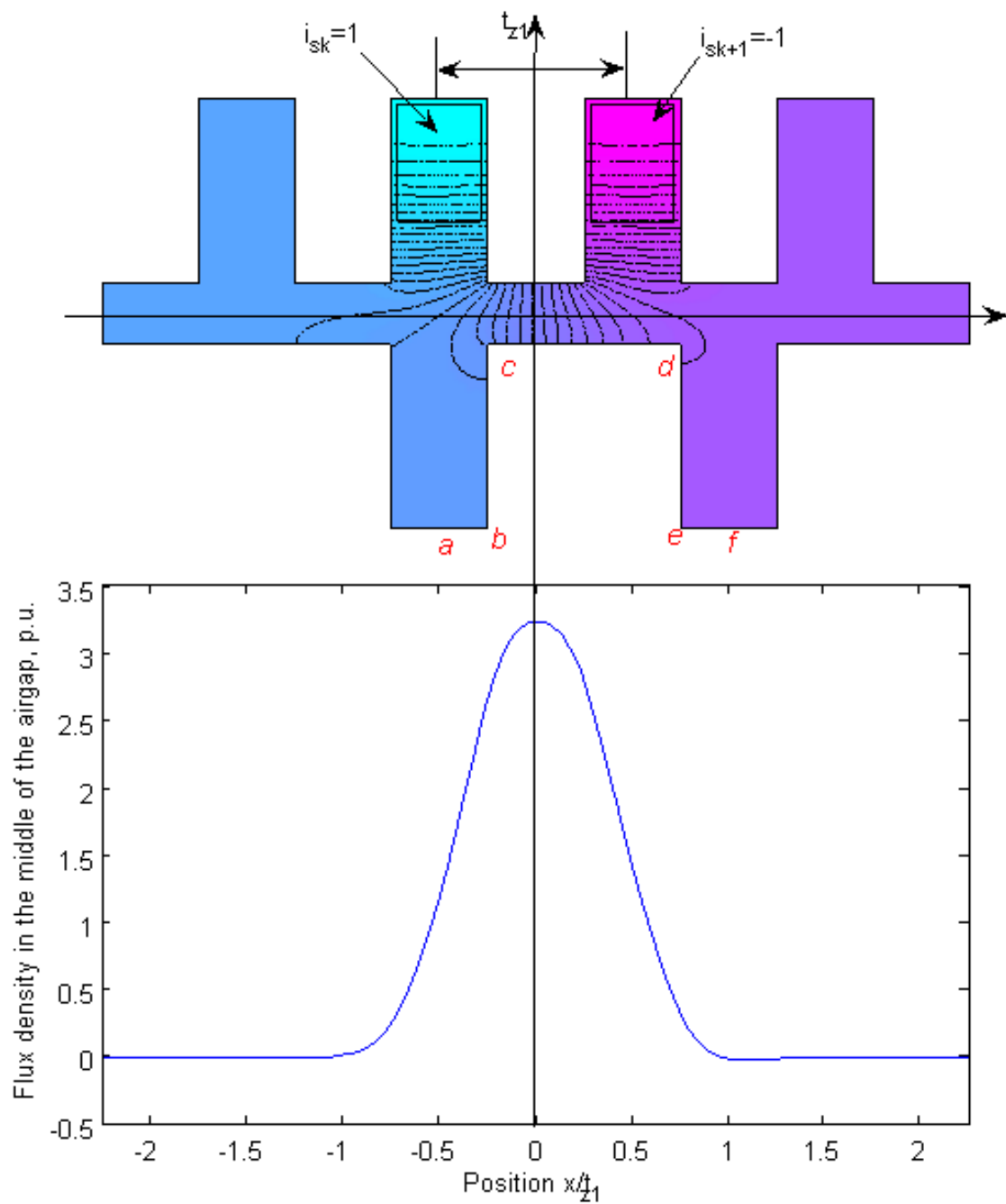


Figure 2.22: TC field under SBC

All the dimensions including slot openings, tooth pitches and etc., on the surface of the first core having radius  $r_1$  will be:

$$x'_1 = x_1 \frac{\delta}{r_1 \ln r_1/r_2}. \quad (2.33)$$

Similarly, the dimensions of the surface of the second core having radius  $r_2$  will be:

$$x'_2 = x_2 \frac{\delta}{r_2 \ln r_1/r_2}. \quad (2.34)$$

As soon as the dimensions of the stator and rotor slots and teeth are transformed using conformal mapping (2.33)-(2.34), the calculation of the permeances can be performed. The assumptions that claim the general assumptions of TCM are applied:

- the slots' form is not taken into account, they are considered to be rectangular with *the width of slot opening equal to the width of the slits*;
- the field is considered to be 2D;
- the field in the slot region is considered not to influence the neighbouring slots of the same core (stator or rotor).

The calculation process is divided into two parts. First only the salience of core opposite to the contour (stator) is taken into account (Figure 2.23). That core (rotor) of the contour is assumed to be smooth; the gap has the size  $\delta$ . The field in the air-gap can be calculated using a coefficient of a magnetic permeance of the air-gap, which is built taking into account the slots of the stator. The homopolar contour permeance of the rotor per length unit is as follows:

$$\Lambda_c = \int_{x_1}^{x_2} \lambda_c(x) dx \quad (2.35)$$

where:  $x_1, x_2$  – coordinates of the centres of the wires which form the contour.

After that the decrease of the permeance caused by the rotor salience must be taken into account, assuming now the stator being smooth. Let's set  $k_{\gamma l}$  and  $k_{\gamma r}$  as the decrease coefficients of the permeance caused by the influence of the left and right contour slots respectively. The value of  $k_{\gamma}$  depends on the position of this particular slot under the opposite tooth or the opposite slot. Thus, for each slot (left and right) the equivalent air-gap  $\delta_{eq}$  is calculated. Equivalent gap is derived based on the mean value of  $\lambda_c$  above the part of the slot which corresponds to the contour:

$$\delta_{eq l} = \frac{1}{\lambda_{ml}} = \left[ \frac{1}{x_3 - x_4} \int_{x_4}^{x_3} \lambda_c(x) dx \right]^{-1} \quad (2.36)$$

$$\delta_{eq r} = \frac{1}{\lambda_{mr}} = \left[ \frac{1}{x_2 - x_1} \int_{x_1}^{x_2} \lambda_c(x) dx \right]^{-1} \quad (2.37)$$



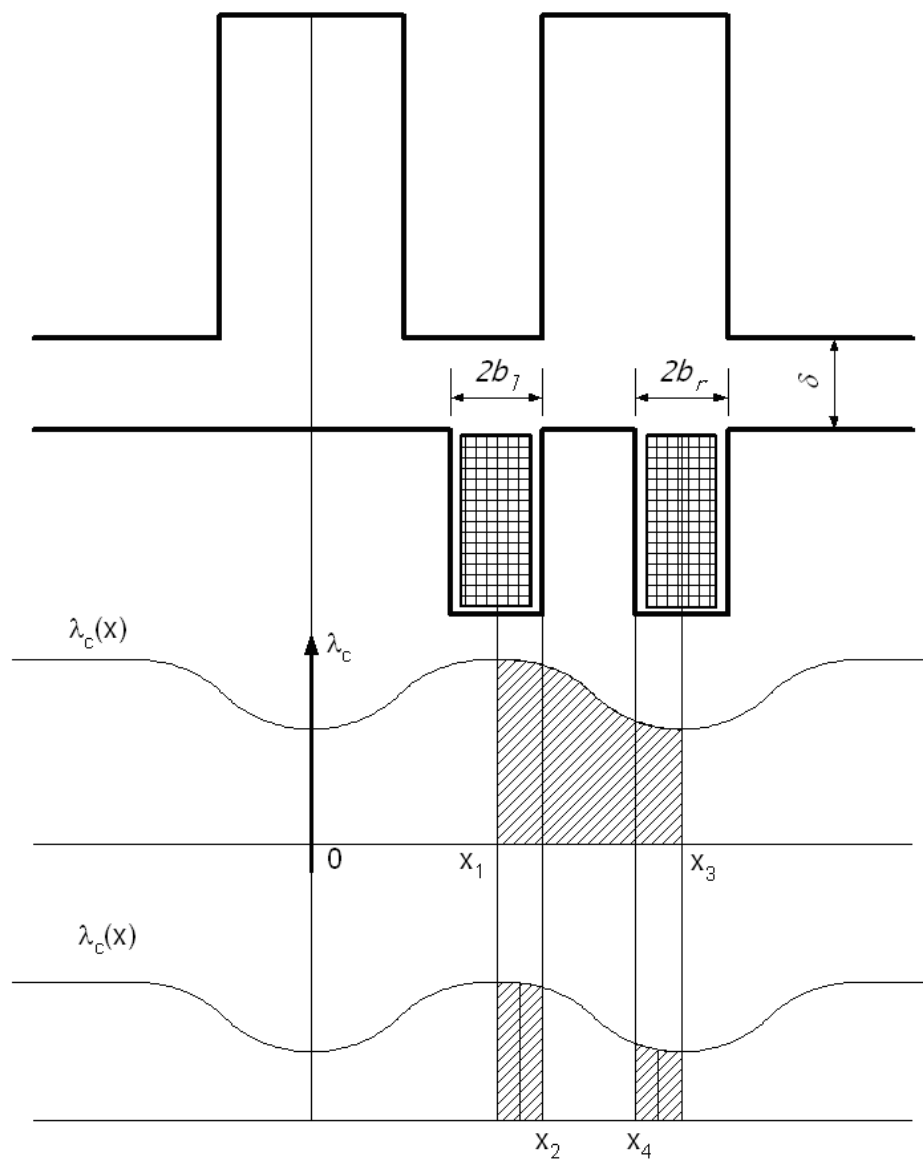


Figure 2.23: Tooth contour unipolar permeance calculation

The value of  $k_\gamma$  is derived from the curve of the air-gap permeance  $\lambda_c$ , taking into account the corresponding rotor slot and the corresponding air-gap  $\delta_{eq}$ . For a symmetrically placed wire in the slot:

$$k_\gamma = \frac{1}{2}\gamma = \frac{2}{\pi} \left[ \frac{0.5b}{\delta_{eq}} \arctan \frac{0.5b}{\delta_{eq}} - \ln \sqrt{1 + \frac{0.5b^2}{\delta_{eq}^2}} \right] \quad (2.38)$$

where  $b$  – a contour slot width.

The resulting contour permeance is obtained as:

$$\Lambda = \Lambda_c - k_{\gamma l} - k_{\gamma r}. \quad (2.39)$$

In order to calculate the function of the permeance an approximation function can be used:

$$\tilde{\lambda}(x) = \begin{cases} c + d \cosh \frac{x}{p}, & |x| \leq p \\ \lambda_{max} = \frac{1}{\delta}, & |x| > p \end{cases} \quad (2.40)$$

The approximation coefficients are obtained as following:

$$\left. \begin{aligned} x = 0, \quad \tilde{\lambda} &= \lambda_{min} = \frac{1}{b\sqrt{1+\frac{\delta^2}{b^2}}} \\ x = p, \quad \tilde{\lambda} &= \lambda_{max} = \frac{1}{\delta} \\ \int_0^p (\lambda_{max} - \tilde{\lambda}) dx &= \frac{1}{2}\gamma \end{aligned} \right\} \quad (2.41)$$

Solving equations (2.40) and (2.40) together gives:

$$\begin{aligned} c &= \frac{\lambda_{min} \cosh 1 - \lambda_{max}}{\cosh 1 - 1} \\ d &= \frac{\lambda_{max} - \lambda_{min}}{\cosh 1 - 1} \\ p &= \frac{\gamma}{2(\lambda_{max} - c - d \sinh 1)} \end{aligned} \quad (2.42)$$

That method of calculation of tooth contour permeances was compared with finite element solution (using OPERA 2D). The form of the teeth is presented on Figure 2.24. The solution was performed using TCM assumptions and SBC for  $\mu_r = 100000$ . The comparison of the results for different mutual positions is given on Figure. 2.25.

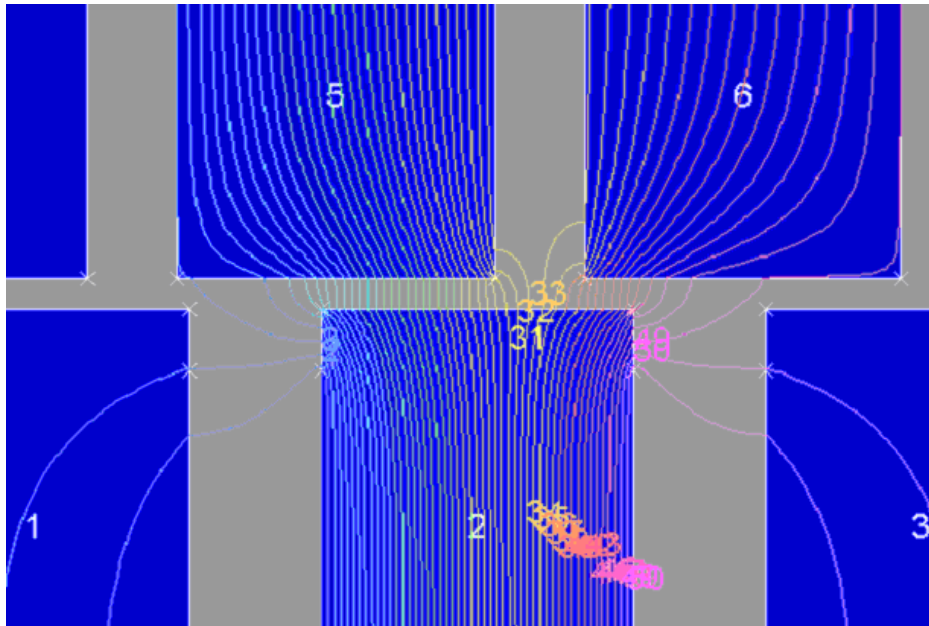


Figure 2.24: Finite element solution for air-gap unipolar permeance calculation

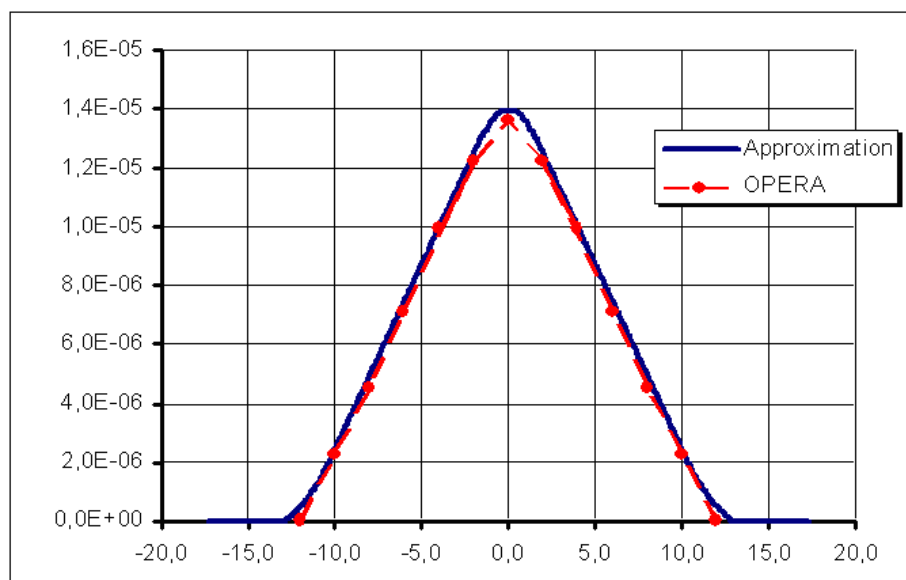


Figure 2.25: TC permeance calculation comparison

## 2.3 Taking into account axial heterogeneity

In modern turbogenerator of high power stator and/or rotor have radial ventilation ducts which should affect a lot on the magnetic permeance network of the model. Besides, stator usually is made of laminated steel with its own lamination factor. All these facts show that pure 2D representation of the fields in an electrical machine is not correct; pure cross-section without taking into account the axial heterogeneity of the machine is impossible. To take into account these effects in the permeance network the permeances must be modified in order to reflect axial effects in the network [42].

For example, the lamination factor  $K_s$  depends on the thickness of steel sheets; for example, for non-isolated or oxidized sheets the  $K_s$  can descend down to 0.86 (Table 2.3) for the sheet thickness 0.15 mm.

Sheet thickness, mm	1	0.5	0.35	0.25	0.15
Packet lamination factor	0.98	0.95	0.93	0.91	0.86

For varnished sheets the factor  $K_s$  for the thickness of 0.15 can be even 0.81 (that means the reduction of the steel's length almost on 20%). Definitely, such a reduction of the cross-section of steel severely affects the saturation of the core. Consequently this brings to the increase of the reluctances of steel parts and changes the distribution of magnetic field. In case of high saturation of several zones this circumstance influences even the field of air-gap, thus, influencing the calculated air-gap permeances.

Let's consider the magnetic system of a stator of turbogenerator shown on Figure 2.26. It consists of the support, yoke part, tooth part and a winding. The ventilation ducts of yoke part and tooth part can generally be different.

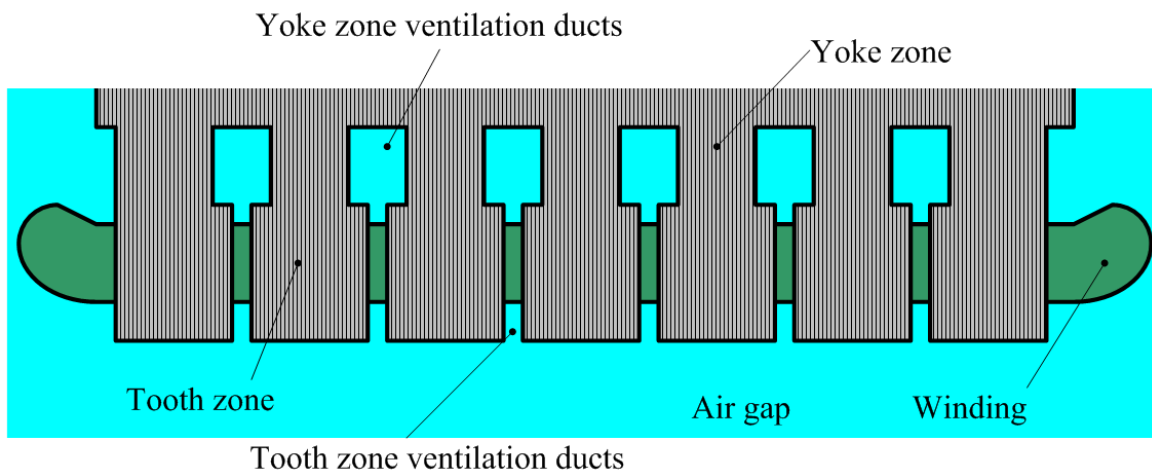


Figure 2.26: Stator magnetic system cross-section in axial direction

Several zones can be distinguished in the machine which are differently influenced by axial heterogeneity:

1. yoke layers of stator;
2. tooth layers of stator;

3. slot areas of stator;
4. air-gap area;
5. slot areas of rotor;
6. tooth areas of rotor;
7. central core areas of rotor.

In order to take into account the axial effects in a PN generated “in-plane”, the physical properties of the materials in these zones must be changed. For the nonlinear areas of steel 1 – 2 and 6 – 7 it should be BH-curve and it seems to be easy, since the flux is limited by the physical borders of magnetic packs. But the zones 3 – 5 are linear and the flux there is not limited. In the air-gap and slots the flux bulges from the magnetic system into surrounding air (Figure 2.27). For this case the permeability of these zones should be modified:  $\mu_r \neq 1$ .

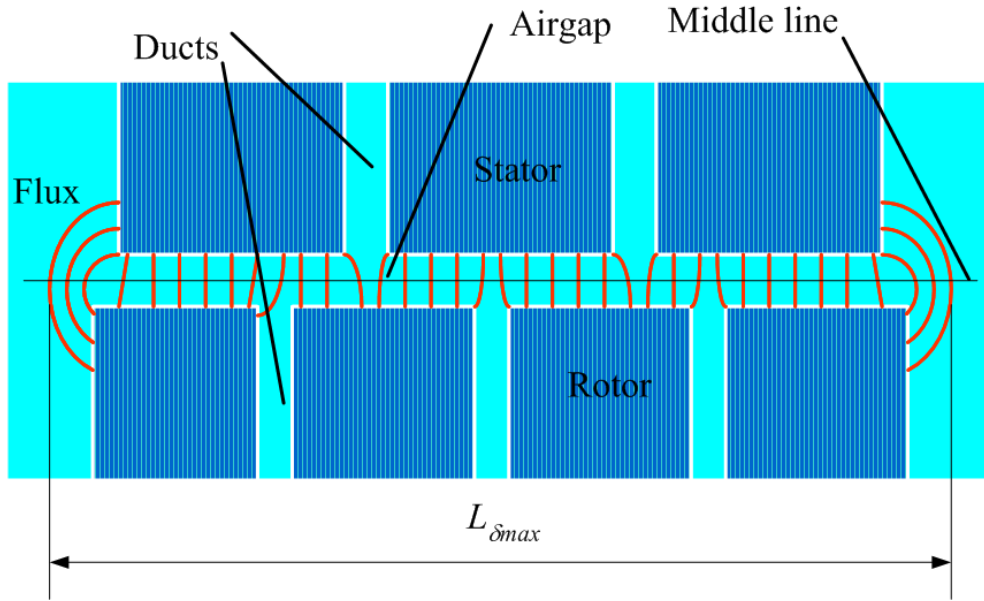


Figure 2.27: Flux bulging in the air of machine

In the PN of a machine all the elements' parameters are calculated and presented either as linear permeances  $\Lambda_k = \Phi_k / U_k = \text{const}$  or as nonlinear permeances defined by a function  $U_k = f(\Phi_k)$ . The physical properties like BH-curves and  $\mu_r$  are recalculated according to the geometry of the machine. In this case it is easier to modify the *actual length* of a machine. Moreover, this modification should be done *depending on the layer and the place of a permeance in a PN*.

### 2.3.1 Steel zones

Generally, the nonlinear permeance characteristics calculation in two-dimensional representation should be performed not for a real magnetization curve  $B(H)$  but for the one with

the reduced component  $B$  in the following proportion: the axial steel length by full axial length of the cores including the length of the ventilation ducts:

$$L_{eff} = (L - n_d \cdot w_d) \cdot k_l \quad (2.43)$$

where  $L_{eff}$  – effective length of the core;  $L$  – real physical length of the core;  $n_d$  – number of ventilation ducts;  $w_d$  – width of a duct;  $k_l$  – lamination factor.

As an example two curves – basic 1 and modified 2 – are presented on Figure 2.28. The curve was modified for the core of the length of 990 mm, which consists of 20 packets having width of 40 mm with radial ducts of 10 mm each. For the lamination factor of 0.91 the values of flux densities of the basic curve must be reduced in 1.36 times.

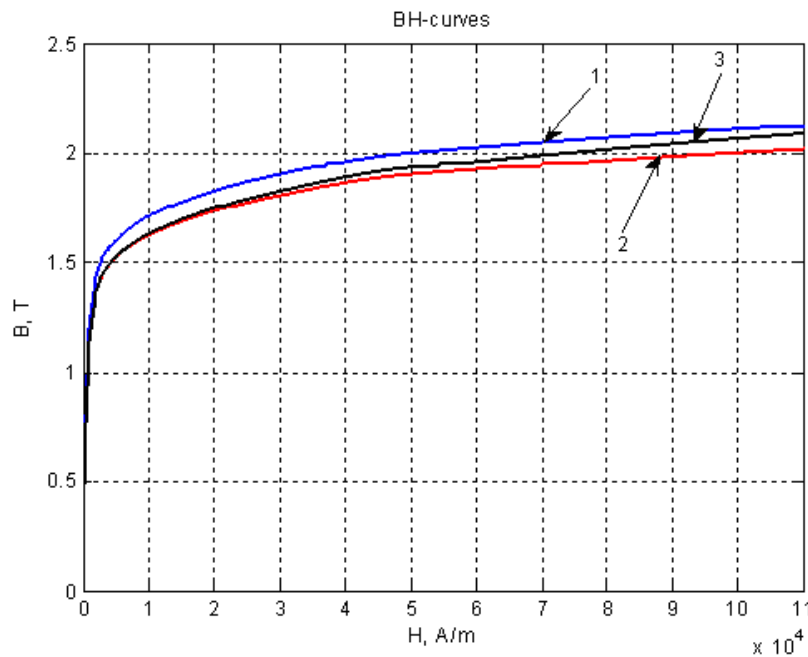


Figure 2.28: BH curve modification

For the flux densities exceeding 1.8 – 2.0 T another modification should be added to the curve 2, caused by the *flux displacement* into the inter-sheet non-magnetic space in the steel packets. The gap between the sheets being determined by the thickness of the insulation layer usually doesn't exceed 10-15% of the thickness of the sheet itself. Thus, the flux displacement plays a noticeable role only in the zone of high saturation. It can be calculated using the same method as to obtain a new magnetizing characteristic of teeth with flux displacement into slots supposing that the magnetic flux lines are parallel inside the tooth and the slot. An approximate shape of the magnetizing curve taking into account the flux displacement is presented by curve 3 on Figure 2.28.

Let's consider two adjacent packs of steel and a ventilation duct between them, as it is shown on Figure 2.29. In case of low saturation (left case on the figure), all the radial flux passes only *inside* the pack, what means that the total flux density  $B_{tot}$  passing through the core on a duct pitch  $t_d$  contains only the tooth pack component  $B_z$ ; no flux is found in the area of a duct  $w_d$ .

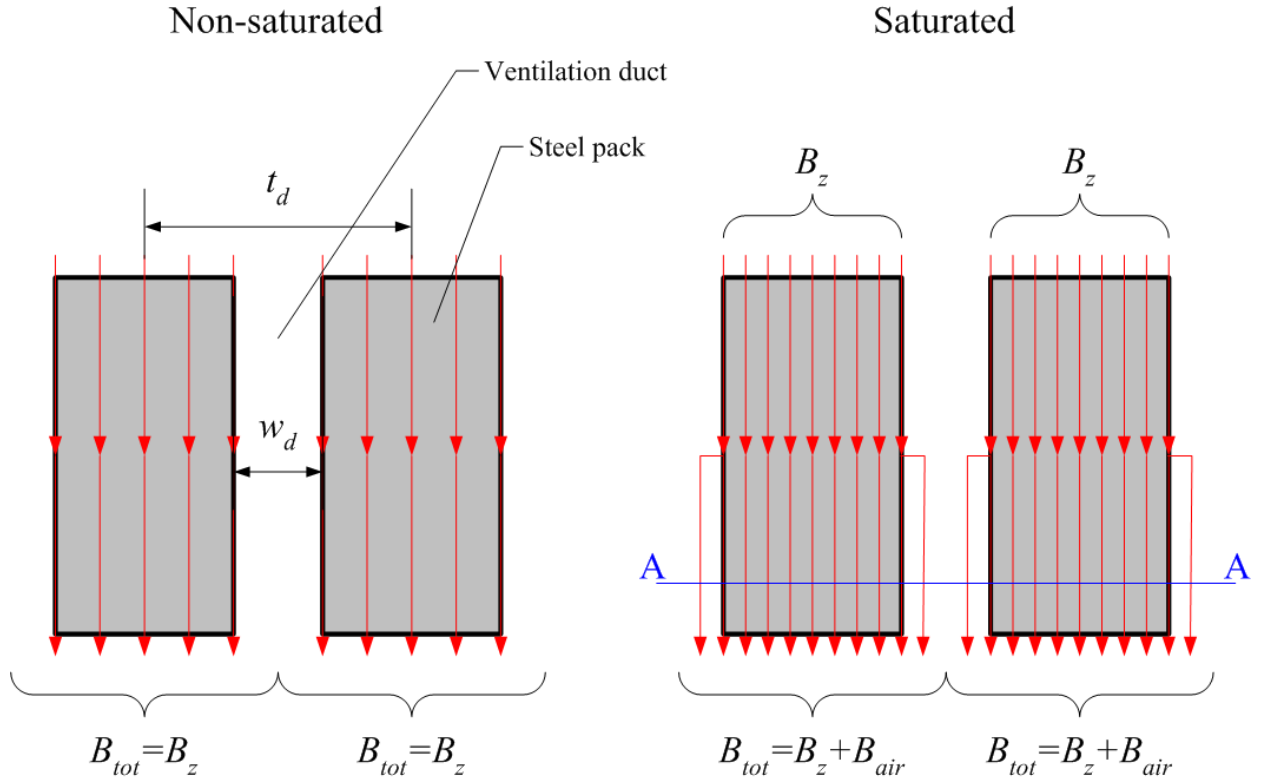


Figure 2.29: Flux displacement to the ventilation duct area in case of high saturation

But this picture changes as soon as the saturation level raises up (right case on the Figure 2.29. Total flux density on a pack pitch now contains also the part of the flux in the air of the duct:

$$B_{tot} = B_z + B_{air} = B_z + \mu_0 H_p k_l \frac{w_d}{t_d}, \quad (2.44)$$

where  $H_p$  – the field of the duct on a line  $AA$ ;  $k_l$  – lamination factor;  $w_d$  – duct width;  $t_d$  – duct pitch.

The same formula (2.44) is used to modify the BH-curve in order to taking into account the flux displacement from teeth to slots. Combining the effects of field displacement from teeth to slots and ducts, we can find that:

$$B_{tot} = B_z + B_{slot} + B_{duct} = B_z + \mu_0 H_z k_l \frac{w_d b_s}{t_d t_z}, \quad (2.45)$$

where:  $B_{tot}$  – total flux density of the element;  $B_z$  – part of flux density in the steel of tooth and pack;  $B_{slot}$  – part of the flux displaced into slot area;  $B_{duct}$  – part of the flux displaced into duct area;  $H_z$  – magnetic field;  $k_l$  – lamination factor;  $b_s$  – slot width;  $t_z$  – tooth pitch.

The modification of the BH-curve is performed for each layer of the permeance network according to the layer's dimensions like  $t_z$ ,  $t_d$ ,  $b_s$ ,  $w_d$ . Thus, the characteristic must be modified differently for different layers of PN.

The formula (2.44) is used to iteratively find the modified function  $H(B)$  for each layer. The values of  $H(B)$  are used then in (2.25) in order to calculate the characteristic of the element.

### 2.3.2 Air-gap zone

The field in air zones in axial direction is not limited by ferromagnetic cores and its distribution depends on the duct configuration both of stator and rotor and on the dimensions of air-gap and slots.

The flux distribution in the air-gap zone of a machine in axial direction is sketchly shown on Figure 2.30.

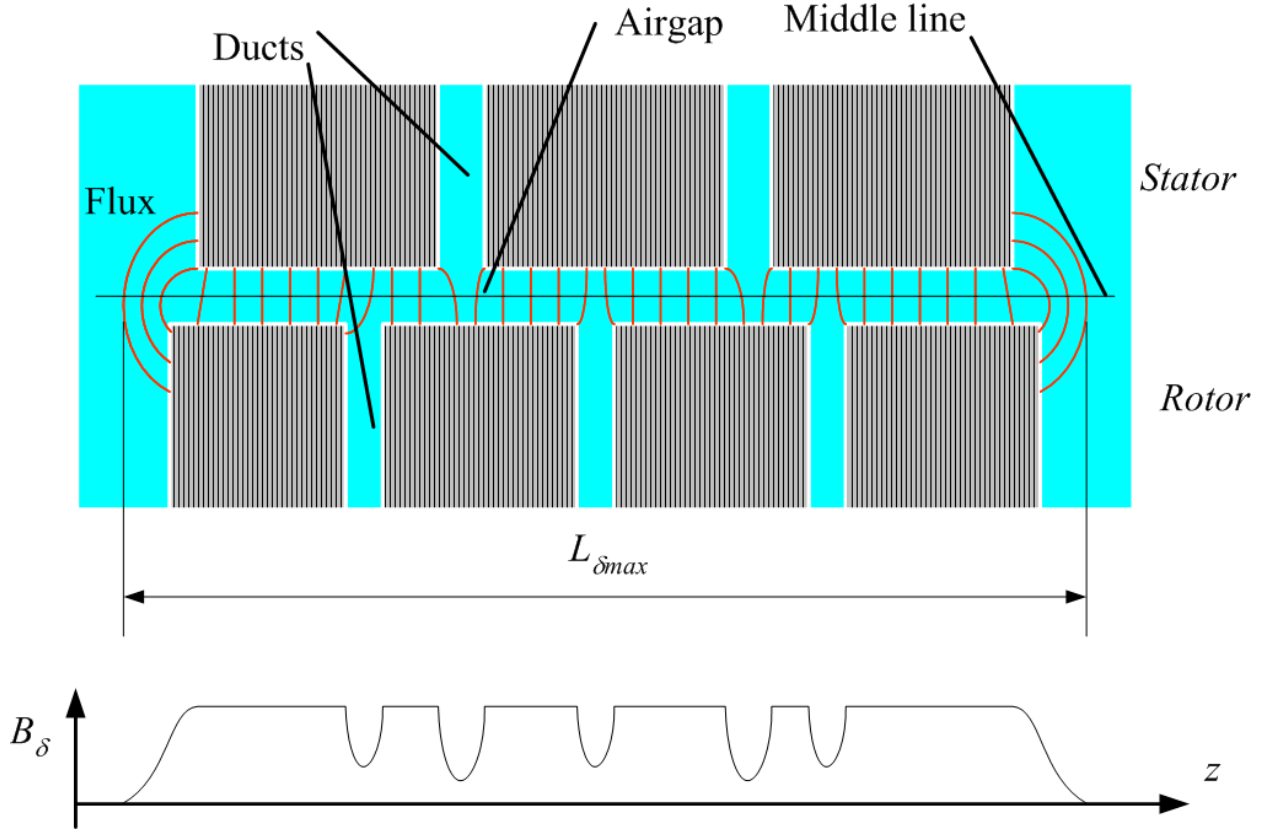


Figure 2.30: Field in the airgap of a machine

Obviously, the zone of existence of the field in the air-gap is assumed to be limited by

$$L_{\delta max} = \max(L_s, L_r) + 2 \cdot \delta, \quad (2.46)$$

where  $L_s$ ,  $L_r$  – stator and rotor physical lengths respectively;  $\delta$  – air-gap. But the flux density  $B_{\delta}$  in the air-gap has dips caused by the presence of ducts on stator and rotor and the edge effects of the cores.

As it was discussed earlier in that section, in order to take into account the influence of the ducts on the characteristics and values of the permeances in our PN, the property of the zone of air-gap must be modified. The easiest way to do it is to modify the *effective length* of the elements of air-gap:

$$L_{eff} = K_{\delta a} \cdot L_{\delta max} \quad (2.47)$$

where  $K_{\delta a}$  – a factor taking into account axial effects;  $L_{\delta max}$  – obtained by (2.46).



Generally,  $K_{\delta a}$  represents the ratio between the mean value of air-gap flux density in presence of the ducts and that of smooth cores of the same length:

$$K_{\delta a} = \frac{\langle B_{\delta} \rangle}{B_{\delta max}}. \quad (2.48)$$

The value of  $B_{\delta max}$  can be easily analytically calculated supposing that both cores are smooth and have the length  $L_{\delta max}$ .

In order to obtain the value of  $\langle B_{\delta} \rangle$  many different methods can be used: from finite element method and to analytical solutions. The easiest and rather effective way is to use Carter formula for the calculation of (2.48). For different duct distribution on stator and rotor we have:

$$K_{\delta a} = K_{\delta s} K_{\delta r} \quad (2.49)$$

The values  $K_{\delta s}$  and  $K_{\delta r}$ :

$$K_{\delta r} = t_{dr} \cdot \left( t_{dr} - \frac{\delta (b_{dr}/\delta)^2}{5 + b_{dr}/\delta} \right) \quad (2.50)$$

$$K_{\delta s} = t_{ds} \cdot \left( t_{ds} - \frac{\delta (b_{ds}/\delta)^2}{5 + b_{ds}/\delta} \right)^{-1} \quad (2.51)$$

where:  $t_{dr}$ ,  $t_{ds}$  – the step of stator and rotor steel packets respectively;  $b_{ds}$ ,  $b_{dr}$  – width of stator and rotor packets respectively;  $\delta$  – air-gap.

### 2.3.3 Slots zone

The principle of taking into account the influence of the ducts on slots is the same as for air-gap. Figure 2.31 shows the field distribution in the slot zone of the machine and the influence of the ducts.

The calculation of that influence can be performed also by Carter formulation:

$$K_{slot} = t_d \cdot \left( t_d - \frac{\delta (b_d/b'_s)^2}{5 + b_d/b'_s} \right)^{-1} \quad (2.52)$$

where:  $t_d$  – steel packet step;  $b_d$  – duct width;  $b'_s = 0.5b_s$  – half of the slot width.

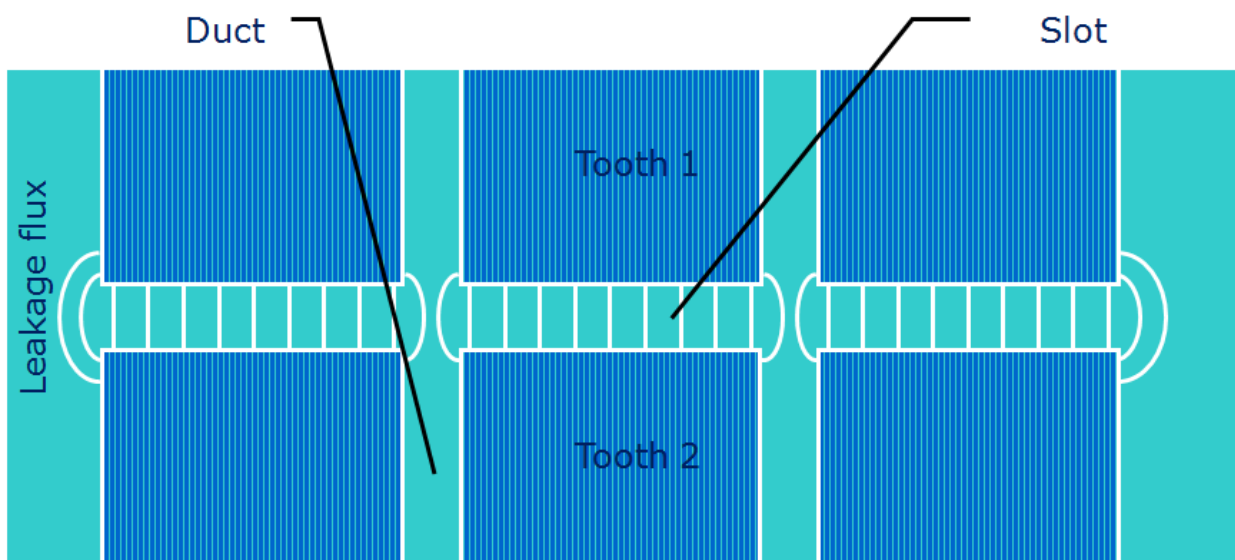


Figure 2.31: Field in the slot zone of the machine.

## 2.4 Permeance Network Equations

After the creation of the structure of PN according to the parameters of the turbogenerator and calculation of the characteristics and values of PN elements, the network is ready for magnetic state calculations. As a result of calculation we obtain the *branch fluxes* in the PN setting up the values of MMF sources in the network according to the currents of stator and rotor. Let's consider the equations of magnetic system.

### 2.4.1 PN equations in matrix form

All the information about the topology of PN, the connections between its elements is presented by the *incidence matrix* having the size  $T \times P$ , where  $T$  – number of lines in matrix corresponding to the number of nodes,  $P$  – number of columns corresponding to the number of branches in the PN:

$$\mathbf{A} = \begin{pmatrix} a_{1,1} & \dots & a_{1,P} \\ \dots & a_{i,k} & \dots \\ a_{T,1} & \dots & a_{T,P} \end{pmatrix} \quad (2.53)$$

where  $a_{i,k} = 1$ , if branch  $k$  belongs to node  $i$  and has direction from node  $i$ ;  $a_{i,k} = -1$ , if branch  $k$  belongs to node  $i$  and has direction to node  $i$ ;  $a_{i,k} = 0$  if branch  $k$  doesn't belong to node  $i$ .

The information about the permeances is stored in the diagonal matrix having size  $P \times P$ :

$$\mathbf{\Lambda} = \begin{pmatrix} \Lambda_1 & \dots & \dots \\ \dots & \Lambda_k & \dots \\ \dots & \dots & \Lambda_P \end{pmatrix} \quad (2.54)$$

where  $\Lambda_k$  – a permeance of branch  $k$  of PN. The values of this matrix are calculated according to the methods given in Section 2.2 and contains the following permeances:

1. linear constant permeances with  $\Lambda_k = \text{const}$ , for example, representing slot leakages;
2. linear permeances of air-gap which depend on the angle of between rotor and stator  $\Lambda_k = f(\alpha)$ ;
3. nonlinear permeances, which generally are defined by  $\Lambda_k = \frac{\Phi_k}{U_k} = f(\Phi_k) = g(U_k)^4$ , where  $\Phi_k$  and  $U_k$  are the flux and the potential drop of branch  $k$ .

The MMF  $f_k$  in branches of PN, produced by currents  $i_j$  in the branches of electric circuit, are defined as a vector:

$$\bar{f} = |f_1, f_2, \dots, f_k, \dots, f_P|^t, \quad (2.55)$$

where:

---

<sup>4</sup>The method of taking into account nonlinear permeances will be described later in this section.

$f_k = \sum_{j=1}^Q f_{k,j}$  – MMF of branch  $k$  of PN;

$f_{k,j} = W_{k,j} \cdot i_j$  – MMF of branch  $k$  of PN produced by current  $i_j$  in branch  $j$  of electric circuit;

$W_{k,j}$  – number of turns (bars) with current  $i_j$ , embracing branch  $k$  of PN;

$Q$  – number of branches in electric circuit.

The values  $W_{k,j}$  have zero values for the most part of the branches of PN except those of having MMF sources, i.e. tangential branches in the areas of slots and yokes.

The values of  $W_{k,j}$  are calculated according to the method described in Section 2.1.5. For the PN branches having MMF sources,  $W_{k,j}$  is the number of wires with current  $i_j$ , placed in the zone *between branch  $k$  and the air-gap*. Actually, this corresponds to the number of elementary fibers whose magnetic shells, being stretched in the yoke direction, cross the particular branch  $k$  of the PN. The sign of the value  $W_{k,j}$  corresponds to that of the current  $i_j$ .

According to (2.55) the MMF vector of the PN can be presented as follows:

$$\bar{f} = \mathbf{W} \cdot \bar{i} \quad (2.56)$$

where  $\bar{i}$  – vector of currents in electric circuit.

The matrix  $W$  is called *the transformation matrix of electric currents of electric circuit into MMF sources of magnetic circuit*:

$$\mathbf{W} = \begin{pmatrix} W_{1,1} & \dots & W_{1,Q} \\ \dots & W_{i,k} & \dots \\ W_{P,1} & \dots & W_{P,Q} \end{pmatrix} \quad (2.57)$$

The matrix (2.57) has the number of columns equal to the number of electric circuit branches  $Q$  and number of lines equal to the number of PN branches  $P$ .

In order to obtain the vector of fluxes in the branches of PN

$$\bar{\Phi} = \|\Phi_1, \Phi_2, \dots, \Phi_k, \dots, \Phi_P\|^t, \quad (2.58)$$

which are produced by MMF sources  $\bar{f}$  (2.56), a node-potential method can be used. The vector of magnetic potential drops

$$\bar{U} = \|U_1, U_2, \dots, U_k, \dots, U_P\|^t \quad (2.59)$$

can be expressed in SMP

$$\bar{\varphi} = \|\varphi_1, \varphi_2, \dots, \varphi_k, \dots, \varphi_T\|^t. \quad (2.60)$$

by means of incidence matrix (2.53):

$$\bar{U} = \mathbf{A}^t \cdot \bar{\varphi}. \quad (2.61)$$

The potential drops can be expressed for each permeance in the network:

$$\bar{U}_\Lambda = \|U_{\Lambda 1}, U_{\Lambda 2}, \dots, U_{\Lambda k}, \dots, U_{\Lambda P}\|^t = \bar{U} + \bar{f}. \quad (2.62)$$

The vector of branch fluxes can be expressed from the vector of potential drops as follows:

$$\bar{\Phi} = \mathbf{\Lambda} \cdot \bar{U}_\Lambda, \quad (2.63)$$

where  $\mathbf{\Lambda}$  – matrix of permeances (2.54). Taking into account also (2.61) the second Kirchhoff's equation can be written for a PN:

$$\bar{\Phi} = \mathbf{\Lambda} \cdot (\mathbf{A}^t \cdot \bar{\varphi} + \bar{f}). \quad (2.64)$$

In order to unambiguously determine the unknown fluxes  $\bar{\Phi}$  and node potentials  $\bar{\varphi}$  for given branches MMF-s  $\bar{f}$ , the first Kirchhoff's equation must be added in the matrix form:

$$\mathbf{A} \cdot \bar{\Phi} = 0. \quad (2.65)$$

The equations (2.64) and (2.65) completed with (2.56) describe the magnetic state of a PN for given currents in electric circuit. The solution of these nonlinear equations is realized using the methods described in sections 2.4.2 and 2.4.3.

The flux linkages of stator phases can be expressed through the branch fluxes found from the solution of the equations.

The flux linkages of branch  $j$  of electric circuit can be presented as a sum of flux linkages of all the magnetic branches with that electric branch:

$$\Psi_j = \sum \Psi_{jk_{k=1}}^P, \quad (2.66)$$

where  $\Psi_{jk} = W_{jk} \cdot \Phi_k$  – the flux linkage of the flux of branch  $k$  of magnetic circuit with the wires of branch  $j$  of electric circuit;  $W_{jk} = W_{kj}$  – number of wires of branch  $j$  which are linked with the flux  $\Phi_k$ , i.e. that of magnetic branch  $k$ .

The matrix  $W$  has the same structure as matrix (2.57). The vector of flux linkages of electric branches can be expressed:

$$\bar{\Psi} = \|\Psi_1, \Psi_2, \dots, \Psi_j, \dots, \Psi_Q\|^t = \frac{p}{a} \mathbf{W}^t \cdot \bar{\Phi}, \quad (2.67)$$

where  $p$  – number of pole paires;  $a$  – number of parallel branches of stator winding.

## 2.4.2 Tableau formulation

Let's discuss the general method to solve circuit equations, both electrical and magnetic. The equations will be considered in electrical notation. And in order to pass to the description of magnetic circuit, simple and well-known analogies can be used: electric current – magnetic flux, electric potential – SMP, voltage – magnetic potential difference.

We will use the *tableau formulation* [58] to describe the circuit equations. In this formulation, all equations describing the network are collected into one large matrix equation, involving the *Kirchhoff voltage law* (KVL), *Kirchhoff current law* (KCL) and the *constitutive equations*, CE.

For initial consideration let the network have  $b$  branches;  $n + 1$  nodes;  $R$ ,  $G$ ,  $L$ ,  $C$  elements; and sources. The KCL equation is expressed by incidence matrix means  $A$

$$\mathbf{A} \cdot \bar{I}_b = 0, \quad (2.68)$$

while KVL is given by

$$\bar{U}_b - \mathbf{A}^t \bar{V}_n = 0; \quad (2.69)$$

where:  $\bar{I}_b$  – branch currents;  $\bar{U}_b$  – branch voltages;  $\bar{V}_n$  – node potentials. The subscript  $n$  stands for nodes, the subscript  $b$  for branches, and in applications  $b$  will be replaced by the element number.

The general representation describing all possible constitutive equations has the following form:

$$\begin{matrix} \text{currents} \\ \text{voltages} \end{matrix} \begin{pmatrix} \mathbf{Y}_1 \\ \mathbf{K}_2 \end{pmatrix} \bar{U}_b + \begin{pmatrix} \mathbf{K}_1 \\ \mathbf{Z}_2 \end{pmatrix} \bar{I}_b = \begin{pmatrix} \bar{S}_{b1} \\ \bar{S}_{b2} \end{pmatrix} \quad (2.70)$$

where:  $\mathbf{Y}_1$  and  $\mathbf{Z}_2$  represent admittances and impedances, respectively;  $\mathbf{K}_1$  and  $\mathbf{K}_2$  contain dimensionless constants; and  $\bar{S}_{b1}$ , and  $\bar{S}_{b2}$  include the independent current and voltage sources, as well as the influence of initial conditions on capacitors and inductors. For notational compactness, we will use the following form:

$$\mathbf{Y}_b \bar{U}_b + \mathbf{Z}_b \bar{I}_b = \bar{S}_b. \quad (2.71)$$

In all subsequent formulations, capacitors will be entered in admittance form and inductors in impedance form, to keep the variable  $s$  in the numerator. Since the Laplace transform variable  $s$  is equivalent to the differentiation operator, we obtain a set of algebraic-differential equations when performing time domain analysis. Table (2.1) indicates the choices of  $\mathbf{Y}_b$ ,  $\mathbf{Z}_b$  and  $\mathbf{S}_b$  for various two-terminal elements including nonlinear elements.<sup>5</sup>

Element	Constitutive Equation	Value of $Y_b$	Value of $Z_b$	Value of $W_b$
Resistor	$U_b - R_b I_b = 0$	1	$-R_b$	0
Conductor	$G_b U_b - I_b = 0$	$G_b$	-1	0
Capacitor	$s C_b U_b - I_b = C_b V_0$	$s C_b$	-1	$C_b V_0$
Inductor	$U_b - s L_b I_b = -L_b I_0$	1	$-s L_b$	$-L_b I_0$
Voltage source	$U_b = E_b$	1	0	$E_b$
Current source	$I_b = J_b$	0	1	$J_b$
Nonlinear element $I(U)$	$I_b = I(U_b)$	0	1	$I(U_b)$
Nonlinear element $U(I)$	$U_b = U(I_b)$	1	0	$U(I_b)$

Table 2.1: Choices of matrices' elements

Equations (2.68)-(2.71) can be collected in the following sequence:

$$\bar{U}_b - \mathbf{A}^t \bar{V}_n = 0 \quad (2.72a)$$

$$\mathbf{Y}_b \bar{U}_b + \mathbf{Z}_b \bar{I}_b = \bar{S}_b \quad (2.72b)$$

$$\mathbf{A} \bar{I}_b = 0 \quad (2.72c)$$

---

<sup>5</sup>The method of taking into account nonlinearities will be described below.

and put into the matrix equation

$$\begin{matrix} & b & b & n \\ b & \begin{pmatrix} \mathbf{1} & \mathbf{0} & \mathbf{A}^t \end{pmatrix} \\ b & \begin{pmatrix} \mathbf{Y}_b & \mathbf{Z}_b & \mathbf{0} \end{pmatrix} \\ n & \begin{pmatrix} \mathbf{0} & \mathbf{A} & \mathbf{0} \end{pmatrix} \end{matrix} \begin{pmatrix} \bar{U}_b \\ \bar{I}_b \\ \bar{V}_n \end{pmatrix} = \begin{pmatrix} \mathbf{0} \\ \bar{S}_b \\ \mathbf{0} \end{pmatrix} \quad (2.73)$$

The matrix in (2.73) has the size of  $(b + b + n) \times (b + b + n)$ . Its size can be reduced by substituting (2.72a) into (2.72b):

$$\mathbf{Y}_b \mathbf{A}^t \bar{V}_n + \mathbf{Z}_b \bar{I}_b = \bar{S}_b \quad (2.74a)$$

$$\mathbf{A} \bar{I}_b = 0 \quad (2.74b)$$

and in matrix form:

$$\begin{pmatrix} \mathbf{Y}_b \mathbf{A}^t & \mathbf{Z}_b \\ \mathbf{0} & \mathbf{A} \end{pmatrix} \begin{pmatrix} \bar{V}_n \\ \bar{I}_b \end{pmatrix} = \begin{pmatrix} \bar{S}_b \\ \mathbf{0} \end{pmatrix} \quad (2.75)$$

The size of this matrix is now  $(b + n) \times (b + n)$ . The matrix (2.75) can be written in a simplified form:

$$\mathbf{T} \bar{x} = \bar{S} \quad (2.76)$$

where:  $\mathbf{T}$  – network matrix;  $\bar{x}$  – network variable vector;  $\bar{S}$  – network sources vector.

The matrix form (2.75) can be used to calculate both magnetic and electric circuits. The matrices  $Y_b$  and  $Z_b$  are actually diagonal matrices and represent the *permeances* and *reluctances* in magnetic network respectively.

### 2.4.3 Taking into account nonlinearities

To solve nonlinear equations a well-known *Newton-Raphson* method can be used. It gives rather good quadratic convergence and is very attractive to be used in systems with high nonlinearity. The solution of the system of equations in the following form can be found iteratively:

$$\mathbf{F}(x) = 0 \quad (2.77)$$

While solving this equation the iterations of Newton-Raphson are defined as follows:

$$\mathbf{x}^{k+1} = \mathbf{x}^k + \Delta \mathbf{x}^k \quad (2.78a)$$

$$\mathbf{J} \Delta \mathbf{x}^k = -\mathbf{F}(\mathbf{x}^k) \quad (2.78b)$$

where:  $\mathbf{F}(\mathbf{x}^k)$  – the set of equations (2.77) calculated for  $\mathbf{x} = \mathbf{x}^k$ ;  $\mathbf{J}$  – Jacobi matrix, for which  $J_{i,j} = \frac{\partial F_i}{\partial x_j}$ .

Thus, the solution of (2.78b) linearized for the step  $k$  and obtain  $\Delta \mathbf{x}^k$ . Then we obtain the new values of variables vector  $\mathbf{x}^{k+1}$  using equation (2.78a). The convergence criterion is the reduction of the norm of errors:  $\|\mathbf{F}(\mathbf{x}^{k+1})\| \leq \|\mathbf{F}(\mathbf{x}^k)\|$ . That method converges in approximately 3-5 iterations.

In order to solve nonlinear circuit equations (2.75) we must transform them to fit the form (2.77):

$$\mathbf{F}(\bar{x}) = \begin{bmatrix} \bar{U}_b - \mathbf{A}^t \bar{V}_n \\ \mathbf{Y}_b \bar{U}_b + \mathbf{Z}_b \bar{I}_b - \bar{S}_b(\bar{I}_b, \bar{U}_b) \\ \mathbf{A} \bar{I}_b \end{bmatrix} = 0 \quad (2.79)$$

Nonlinear elements are included in  $\bar{S}_b(\bar{I}_b, \bar{U}_b)$  component of equation system (2.79) as it was shown in Table 2.1. The Jacobi-matrix for the system of equations (2.79) generally has the following form:

$$\mathbf{J} = \begin{pmatrix} \mathbf{Y}'_b(I, U) \mathbf{A}^t & \mathbf{Z}'_b(I, U) \\ \mathbf{0} & \mathbf{A} \end{pmatrix} \quad (2.80)$$

The components of matrices  $\mathbf{Y}'_b$  and  $\mathbf{Z}'_b$  differ according to the type of the element in the particular branch. For linear elements:

$$\begin{cases} Y'_{i,i}(I_i, U_i) &= Y_i \\ Z'_{i,i}(I_i, U_i) &= Z_i \end{cases} \quad (2.81)$$

For nonlinear elements the components of matrices will be:

$$\begin{cases} Y'_{i,i}(I_i, U_i) &= \frac{dI_i}{dU_i} \\ Z'_{i,i}(I_i, U_i) &= \frac{dU_i}{dI_i} \end{cases} \quad (2.82)$$

The structure of Jacobi-matrix (2.80) is the same as (2.75), thus it is very easy to obtain that matrix as soon as matrix (2.75) is defined.

## 2.5 Steady-state fixed-rotor model

To calculate the steady-state mode of the machine a mathematical model with a fixed rotor can be used considering the following assumptions:

- the stator windings voltages and currents are considered to be sinusoidal;
- the calculation of the magnetic circuit is being produced for an arbitrary rotor position, considering that the calculation results for the first harmonics don't depend on that position.

### 2.5.1 Basic equations

The steady-state symmetric mode of the electrical machine is defined by an effective value of the stator current  $I_{rms}$ , excitation current  $I_f$  and an angle  $\beta$  which defines the position of the stator current vector on phasor diagram in  $d - q$ -axes (Figure 2.32). As a result we obtain phase voltage vector  $U = \sqrt{2}U_{rms}$  and angle  $\varphi$  between stator voltage and current.





$$\gamma = \arctan \frac{\Psi_d}{\Psi_q} \quad (2.86)$$

The flux linkage found by (2.85) takes into account not only the mutual inductance field but also *slot leakage field* and *differential leakage field* produced by higher harmonics of stator field without taking into account damping effect.

The vector of flux linkage can be presented in a complex plane, which real axis is aligned with  $d$ -axis and imaginary one – with  $q$ -axis:

$$\dot{\Psi}_{\delta\sigma} = \Psi_{\delta\sigma} e^{j\gamma}. \quad (2.87)$$

There is a vector of phase EMF corresponding to the vector of  $\Psi_{\delta\sigma}$ . This vector is produced by the same magnetic fields:

$$\dot{E}_{\delta\sigma} = -j\omega \dot{\Psi}_{\delta\sigma}, \quad (2.88)$$

where  $\omega = 2\pi f$  – angular frequency of stator current.

Now the stator phase voltage  $U$  can be calculated. For symmetrical steady-state operating mode and assuming that all the values change sinusoidally, the voltage  $U$  can be obtained from the voltage equation written in complex form:

$$\dot{U} + R\dot{I} + jx_{\sigma e}\dot{I} - \dot{E}_{\delta\sigma} = 0. \quad (2.89)$$

where:  $\dot{U}$ ,  $\dot{E}_{\delta\sigma}$ ,  $\dot{I}$  – complex amplitudes of stator voltage, EMF and current, respectively;  $R$  – active resistance of stator phase;  $x_{\sigma e} = \omega L_{\sigma e}$  – end-winding reactance.

Many different approaches are known to determine the value of  $x_{\sigma e}$ . Comparing different formulations, we have chosen the one giving best results for turbogenerators [7]:

$$x_{\sigma e} = 2\pi f \mu_0 \left( \frac{2}{p} \right) \left( \frac{Z_n \cdot q \cdot p}{a} \right)^2 \left( 20 + \frac{0.7 D_s}{p} \right) \xi \quad (2.90)$$

where:  $f$  – electric frequency, Hz;  $\mu_0$  – air permeability;  $p$  – pole pairs;  $Z_n$  – conductors per slot;  $q$  – slots per phase per pole;  $a$  – number of parallel circuits;  $D_s$  – stator inner diameter;  $\xi$  – winding factor.

By means of (2.89) a complex vector of phase voltage  $\dot{U}$  can be determined along with its RMS value

$$U_{rms} = |\dot{U}| / \sqrt{2} \quad (2.91)$$

and power factor angle between  $U$  and  $I$

$$\varphi = \arg \dot{U} - \arg \dot{I} = \left( -\frac{\pi}{2} - \Theta \right) - \left( -\frac{\pi}{2} - \beta \right) = \beta - \Theta. \quad (2.92)$$

### 2.5.2 Characteristics calculation

All the steady-state characteristics of the turbogenerator can be calculated using the model with fixed rotor presented above. As it was shown above the direct solution can be obtained as function of three defined variables: excitation current  $I_f$ , stator current  $I_s$  and electrical angle between them  $\beta$ . Thus, only no-load characteristic of turbogenerator can be obtained using direct solution. Any other operating mode is usually defined by other variables, like, for instance, stator voltage  $U_s$ , stator current  $I_s$ , power factor (PF) or angle  $\varphi$ . In this case the operating mode and characteristics can be obtained using iterative process.

### Calculating operating mode defined by stator voltage, stator current and power factor

The calculation of operating mode defined by stator voltage  $U^0 = \sqrt{2}U_{rms}$ , stator current  $I^0 = \sqrt{2}I_{rms}$  and angle between them  $\varphi^0$ , is usually performed in order to obtain the excitation current  $I_f$  and stator current angel  $\beta$ .

The calculation algorithm is as following:

1. set up initial values of  $I_f$ ,  $\beta$  and  $I$ ;
2. calculate complex value of stator voltage  $\dot{U}$  using (2.89) and  $|U| = f_u(I_f, \beta)$  using (2.91); angle  $\varphi = f_\varphi(I_f, \beta)$  is obtained from (2.92);
3. comparing obtained values with the defined  $U^0$  and  $\varphi^0$ , the following discrepancies can be found:

$$\left. \begin{aligned} \Delta U &= U^0 - f_u(I_f, \beta); \\ \Delta \varphi &= \varphi^0 - f_\varphi(I_f, \beta); \end{aligned} \right\} \quad (2.93)$$

4. finally, the system of nonlinear equations must be solved:

$$\left. \begin{aligned} \Delta U &= U^0 - f_u(I_f, \beta) = 0; \\ \Delta \varphi &= \varphi^0 - f_\varphi(I_f, \beta) = 0. \end{aligned} \right\} \quad (2.94)$$

The system (2.94) can be solved using any of the numerical methods, for instance, *the secant method*. According to the method, the following coefficients of linear correspondence must be determined on iteration  $j$ :

$$\left. \begin{aligned} K_{11j} &= \left. \frac{\Delta U_j}{\Delta I_{fj}} \right|_{\beta=const}; & K_{12j} &= \left. \frac{\Delta U_j}{\Delta \beta_j} \right|_{I_f=const}; \\ K_{21j} &= \left. \frac{\Delta \varphi_j}{\Delta I_{fj}} \right|_{\beta=const}; & K_{22j} &= \left. \frac{\Delta \varphi_j}{\Delta \beta_j} \right|_{I_f=const}; \end{aligned} \right\} \quad (2.95)$$

Then the increments  $\Delta I_{fj}$  and  $\Delta \beta_j$  which make vanish the discrepancies are found solving the following system:

$$\begin{aligned} K_{11j}\Delta I_{fj} + K_{12j}\Delta \beta_j &= \Delta U_j \\ K_{21j}\Delta I_{fj} + K_{22j}\Delta \beta_j &= \Delta \varphi_j \end{aligned} \quad (2.96)$$

The new values of variables are obtained:

$$I_{fj} = I_{f,j-1} + \Delta I_{fj}; \quad \beta_j = \beta_{j-1} + \Delta \beta_j. \quad (2.97)$$

The convergence criterion can be taken as the relative RMS value:

$$\sqrt{\frac{\Delta I_{fj}^2}{I_{fj}^2} + \frac{\Delta \beta_j^2}{\beta_j^2}} \leq \epsilon, \quad (2.98)$$

where  $\epsilon$  – relative error of the solution.

Described algorithm of operating mode calculation includes two iterative processes: inner process of magnetic PN calculation and outer process of excitation current calculation. It gives very good convergence of up to 4 iterations. The algorithm is used to calculate rated mode excitation current along with the regulation and V-shaped characteristics.

The same algorithms are used to obtain other characteristics of turbogenerator which depend on other variables. The examples of calculated characteristics are shown in Chapter 4.

### Calculating $x_d$ and $x_q$ parameters

Having built a vector diagram for a particular operating mode, we can easily calculate machine's  $x_d$  and  $x_q$  parameters, using following relationship:

$$\begin{aligned} x_d &= \frac{E_0 - U_q - R_s \cdot I_q}{I_d} \\ x_q &= \frac{U_d + R_s \cdot I_d}{I_q} \end{aligned} \quad (2.99)$$

where:  $U_d, U_q$  – stator voltage projections on d- and q-axis respectively;  $I_d, I_q$  – stator current projections on d- and q-axis respectively;  $R_s$  – stator active resistance;  $E_0$  – rectified no-load stator EMF corresponding to selected excitation current  $I_f$ .

## 2.6 Model taking into account rotation

The model with fixed-rotor discussed in Section 2.5 having many advantages still has its limits of use. Some applications strongly demand taking into account the real rotation of the machine's rotor. Having in mind that this thesis is devoted to big turbogenerators and the calculation of their steady-state characteristics, we should say that implementation of the rotation, especially with transient analysis, is out of scope of that study.

However, the used approach gives flexible possibility to take into account the mutual movement of the stator and rotor cores. The characteristics of air-gap elements which are precalculated on the network construction stage and determined for the whole range of possible cores' mutual positions.

As an example, Figure 2.33 presents mutual permeances between one stator tooth and all rotor teeth of a turbogenerator. The general approach of taking into account the rotation is to implement a variable which determines the mutual position between stator and rotor. That variable is then used to calculate the particular values of the permeances for the current mutual position. The algorithm was realized in the software (see Chapter 3) and some results can be found in Chapter 4.

## 2.7 Conclusion

This chapter presented the used approach, its theoretical basis and methodical implementation. The first section leads step by step to the choice of the PN configuration, the approach of its parameters' calculation. General theoretical ideas are presented.

The second section described the particularities of the PN construction and calculation of the parameters of its parts: nonlinear and linear tooth elements, air-gap elements, yoke elements. An idea of variable topology model was proposed in order to take into account geometrical peculiarities of some machines.

The method of taking into account the axial heterogeneity of magnetic cores was discussed in the third section. We showed that special techniques must be implemented to properly reflect axial effects while using a model "in-plane". Different parts of the machine are differently influenced by axial heterogeneity, characteristic zones were detected and the implementation on the level of PN was given. However, the proposed method is rather

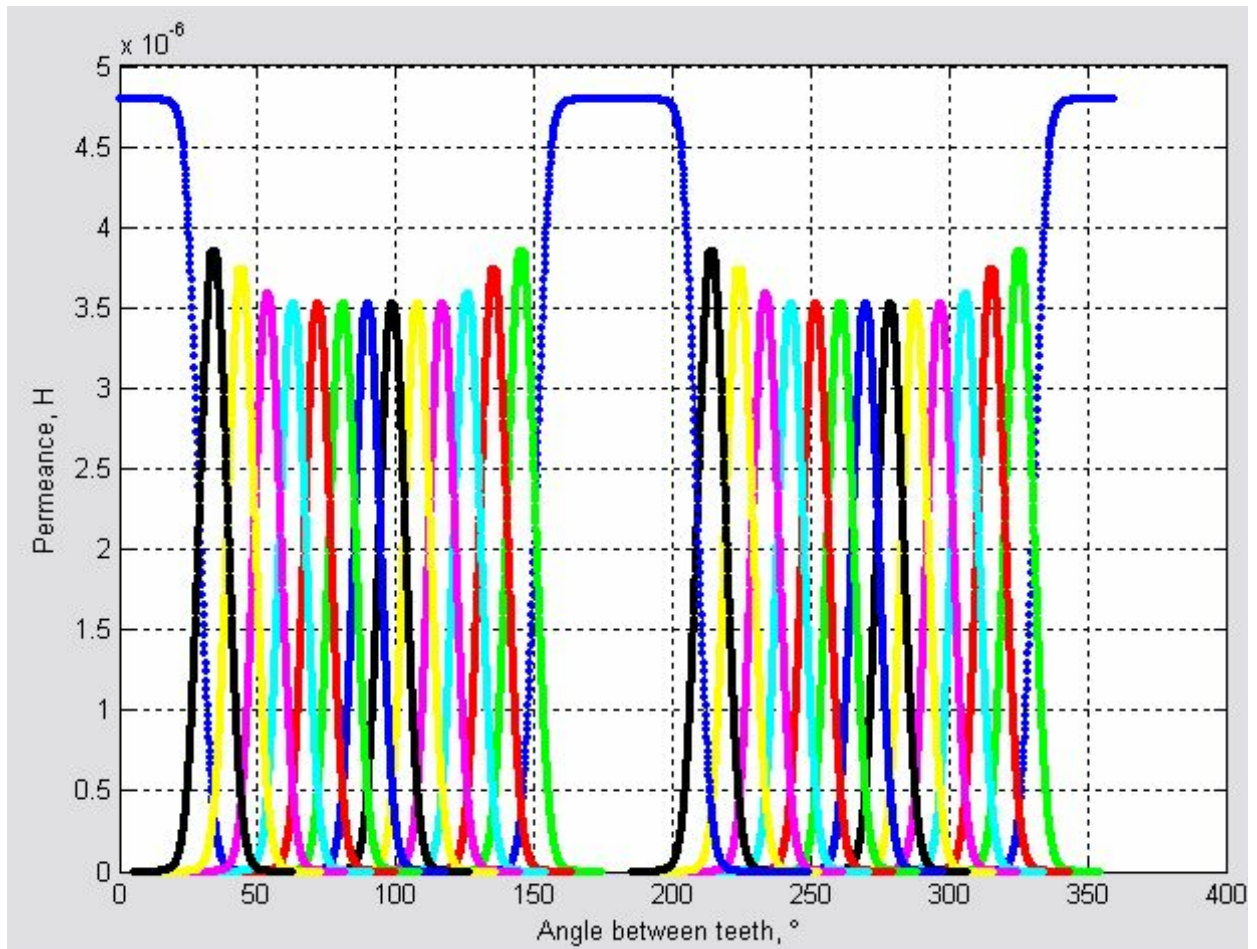


Figure 2.33: Mutual characteristics between stator and rotor teeth.

general and *can be easily used with other methods* of machine's characteristic calculations, even FEM (in plane).

Steady-state fixed rotor algorithm was presented in the fourth section. The method has very high speed of calculation since all the characteristics can be obtained without “moving” the rotor from its primary position.

Finally, we said a couple of words about the model which takes into account rotation.

# Chapter 3

## Software implementation

### 3.1 General Information

The software TurboTCM is designed for calculation of different operating modes of turbo-generators 10 – 100 MW with air-cooling. All the calculations are performed based on modified *Tooth Contour Method*, replacing the magnetic circuit of an electrical machine with rather precise permeance network, taking into account the particularities of magnetic field distribution in a machine.

The calculation is performed in two stages. On the first stage – *the generation* – the geometry of a machine is analyzed based on its parameters and the generation of a PN with calculation of its parameters is performed. As a result, a PN-model of electrical machine is created.

On the second stage – *calculation* – the generated PN-model is used for the calculation of the static operating modes or movement analysis:

- modes, defined by stator current, rotor current and power factor;
- modes, defined by stator current, stator voltage and power factor;
- machine's characteristics: no-load, load, regulation, V-shaped, angular, etc...;
- for each point of characteristic and for each calculated operating mode the complete information about magnetic and electric state of a machine can be obtained: spacial and time distribution of flux density in the air-gap, teeth, yokes, visual field distribution map in the cross-section of the machine,  $x_d$ ,  $x_q$  parameters, etc...;
- evolution of stator and rotor fluxes, flux linkages and EMFs in time (in rotation).

TurboTCM is created in Matlab and can be compiled in two ways:

1. the Matlab program;
2. separate software for Microsoft Windows with Matlab Component Runtime(MCR) module.

The software was designed using modular principle: calculation core – graphical user interface (GUI). The GUI allows to set up the input project data, generate PN-model,

verify the calculated parameters and characteristics of the model, perform the calculation of different modes and characteristics of turbogenerator.

Direct use of the calculation core gives a user more flexible capabilities<sup>1</sup>. The function of the core can be called directly from `Matlab` command line or from the user-defined scripts and programs. The functions give the following capabilities:

- create the project or read and modify the existing one, created by GUI;
- generate the PN-model based on the project;
- calculate any characteristics and modes listed above or user-defined;
- access the *complete information* about PN generated, all its elements, characteristics, etc.
- based on the full information about each element of the PN any additional calculations can be performed in order to meet the particular demands of the user.

Easy direct access to the model permits its use as a part of *turbogenerator optimization software*. The example of combined use of TurboTCM and Sophemis<sup>2</sup> is shown in the Section 4.4.

## 3.2 Software structure and approach

The software implementation of the method described earlier consists of several tasks. As an input data we have a full specification of our turbogenerator: stator and rotor sizes, number of stator and rotor slots, their dimensions, insulation, full description of the stator and excitation windings, damper winding, characteristics of the materials, specification of the electrical part, etc. Based on that information we have to:

- form the equivalent circuit of the magnetic system;
- form the circuit of the electric system;
- form the equations describing magnetic and electric circuits and mechanical system.

As soon as the system of equations is obtained, it can be solved to calculate a set of characteristics in different operating mode. The approximate structure of the software system is presented on Figure 3.1.

The design of the software was divided in two layers:

- *Circuit Description Tools*, developed in C++, which manage a network (electric or magnetic or any other) and produce its equations as well as relations between electric and magnetic parts;

---

<sup>1</sup>The direct use of the core is *not available* in the separately compiled version of the software and can be realized only from inside `Matlab`

<sup>2</sup>*Sophemis* is an optimisation software package developed by Stephan VIVIER in L2EP of Ecole Centrale de Lille

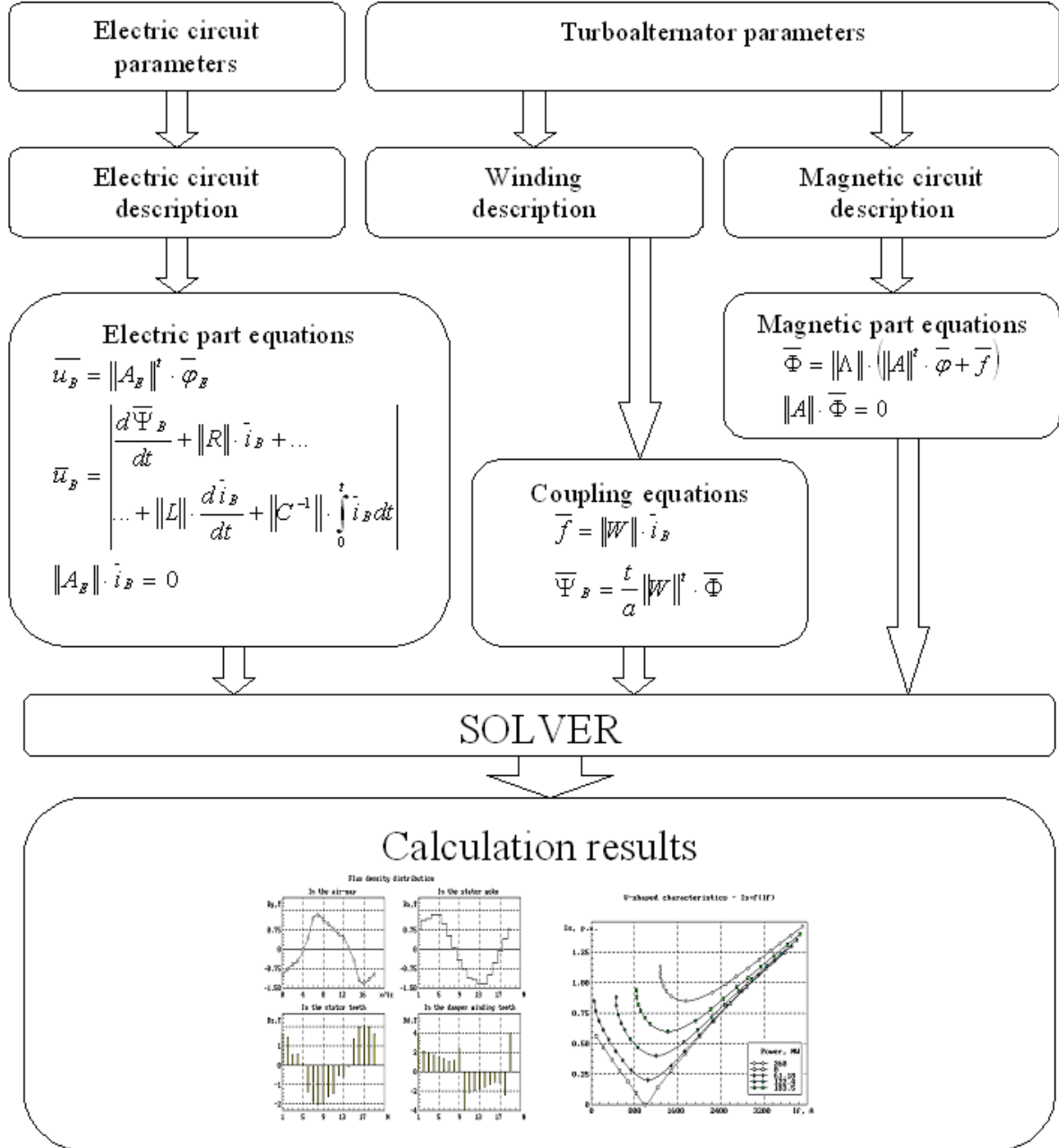


Figure 1

Figure 3.1: General structure of TurboTCM



- *Mathematical Solver and Graphical User Interface*, developed in **Matlab**, which interacts with the user and solves all the equations to obtain the results.

Further, circuit description tools will be presented followed by the general approach to construct the solver and main program application.

### 3.2.1 Circuit Description Tools overview

The circuit description tools were designed to obtain the matrices of the systems of equations to be solved. These tools have been designed in Visual C++ .NET [55, 5] using Component Object Model (COM) technology [50, 6]. COM is based on interface and object oriented programming. In a couple of words, this technology allows to combine together different software tools (which follow COM standard) in order to obtain the best of their features. Using this technique one can write the software in any preferable for the particular task language and then use it as “bricks” (COM object) from another software written on any other language. The only demand – COM support in the compiler. As it was previously said, in this work the part of the software which was dedicated to building of circuit matrices was written in C++ language using this COM technique. This part implemented the graph approach of building circuit equation matrices and special indexing technique to access as fast as possible any of the desired elements of the circuit and its parameters in any desired time during the simulation.

All these tools were compiled as a *COM type library* **TCMLib**. It provides all the components which generate and manage in real time the circuit equation matrices. Those components can be used from any solver written, for instance, in **Matlab** or **Visual Basic** or any other programming language.

Two main objects of the library – **CircuitBuilder** and **CircuitConnector** – provide the solver with the possibility to add and manage the elements and characteristics of the networks as well as the interaction between networks (Figure 3.2).

As soon as we define a network (electric or magnetic) by means of **CircuitBuilder**, it analyses the circuit and provides all the necessary matrices for the equations to the Solver. It is done both for electric and magnetic circuits. Solver, in its turn, solves the systems of equations. During the solution the Solver affects the **CircuitBuilder** object to maintain the current state of the circuit, depending on parameters specified (as, for instance, rotor angle or elements’ characteristics, etc...).

Two **CircuitBuilder** objects are linked to each other by means of **CircuitConnector** which provides the solver with correspondence matrix.

The interaction between the components of **TCMLib** and **Matlab** is shown on Figure 3.2.

#### **CircuitBuilder**

This component provides the functionality to build and manage any circuit (network) based on graph theory. This circuit can represent either electric or magnetic or thermal one – this is just a question of analogies.

**CircuitBuilder** is the main component of the library. It has the following features:

- Adding and maintaining the elements of the following element types to the circuit description:

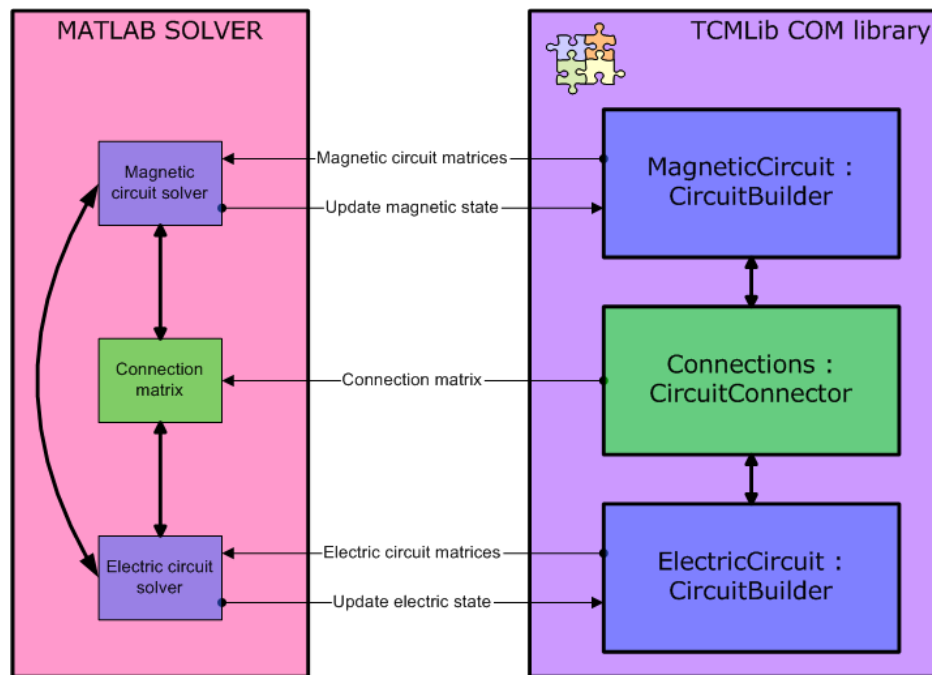


Figure 3.2: Interaction between TCMLib and Matlab

linear permeances, resistances, capacitors and inductances (last two for electrical circuits);

current and voltage sources;

all the elements above with the dependency of a particular parameter;

nonlinear elements specified by characteristics of  $I(U)$  or  $U(I)$ .

- Adding and maintaining the parameters of the circuit (for example, rotor angle), which the dependent elements' values are based on. In linear case the parameter's value is just applied to the element's value. In nonlinear case, the parameter's value is the argument for  $I(U)$  (or  $U(I)$ ) characteristic, associated with the element.
- Adding and maintaining the characteristics for the elements. One characteristic can be associated with many elements. This is necessary to maintain the group of equal nonlinear elements.
- Generation and providing circuit matrices, including Jacobi matrix components.
- "Tuning-up" features which allows the user to control the names of the types of elements.

### CircuitConnector

This component was designed in order to manage the connections between two circuits described by `CircuitBuilder` object. It provides the following features:

- Two connections with two `CircuitBuilder` objects, which represent, for instance, the electrical and magnetic circuits.

- Adding and maintaining the relations between the first and second circuits' branches.
- Providing the information to the solver about the correspondence matrix.

### 3.2.2 Matlab Solver general approach

This section presents the structure of the entire software realized in **Matlab v.7.0**. It contains the description of the software creation approach without any details of its particular realization.

**TurboTCM** being a rather complicated software was designed using an *Object Oriented Programming* (OOP) approach. But we decided to void using native class and object implementation realized in **Matlab**, since its realization is rather “heavy” and not so transparent. Thus a so-called “lite OOP” approach was used.

Most of the structures have so-called “*TurboTCM object form*”, which means that they behave like real objects with the help of associated member-functions. Anyway, there is a limit of this behaviour since there is no variable scope checking and inheritance mechanism implemented.

To realize OOP behavior most of the structures (with few exceptions) have special obliged fields:

**.Name** – defines the name of the structure (analogoy in OOP: class name).

**.Version** – defines the version of the structure as a string in the format: **TurboTCM.1** (1 – version number).

The **.Name** field allows checking the type of the structure in the functions' calls, while by means of the **.Version** field a backward compatibility mechanism is realized.

The functions linked to the specified structures and performing operations on its members are called “*member functions*” (like in OOP). The member functions have special name decoration: **StructureName\_FunctionName**, where: **StructureName** – the name of an associated structure, **FunctionName** – the name of a member function.

Moreover, each member function *must* have a maintained structure as the first input and first output arguments, declared with the same name. The type and version (for backward compatibility) of the structure given as the first argument is usually checked using the function **CheckTypeVersion**.

For each structure there is a *constructor* member function which has only output argument of the structure generated. This function is usually called **StructureName\_Create**. It creates all the fields used in the structure with default values (usually **[]**) and assigns the **.Name** field to a structure name and **.Version** field to the version number.

Sometimes, the constructor supports the second output argument which has the same fields as the structure, except that all of them are the strings with the fields' descriptions.

**Note.** Usually, the constructor is the function which provides all the information of its fields to the user in its help. So, if one wants to know the fields and their meaning for a structure, he should just type in the **Matlab** command line:

```
help StructureName_Create
```

Also, a structure may contain a *destructor* – a member function with the following name:

`StructureName_Delete.`

It is not required but may be usefull when the sturcture contains **ActiveX** and/or **Java** objects as members.

The following section presents global view of the basic structures and their interaction.

### 3.2.3 Matlab Solver structure

TurboTCM is divided into several logical parts which have their own particular purposes:

**Structure** – definition of all the structures used in TurboTCM. It aslo contains the most part of their member functions.

**Generation** – generation of the *Permeance Network Model* (PNM) based on the input parameters.

**Core** – calculation of the output modes and characteristics based on PNM generated.

**Services** – service functions which are widely used in all other parts of the software.

According to **Matlab** habits, the software is placed in a special folder – its *root* folder. The parts described above correspond to its subfolders. The GUI part of **TurboTCM** is placed in root folder.

Figure 3.3 shows the global view of the collaboration and interaction between different parts of TurboTCM. The following subsections will describe that interaction.

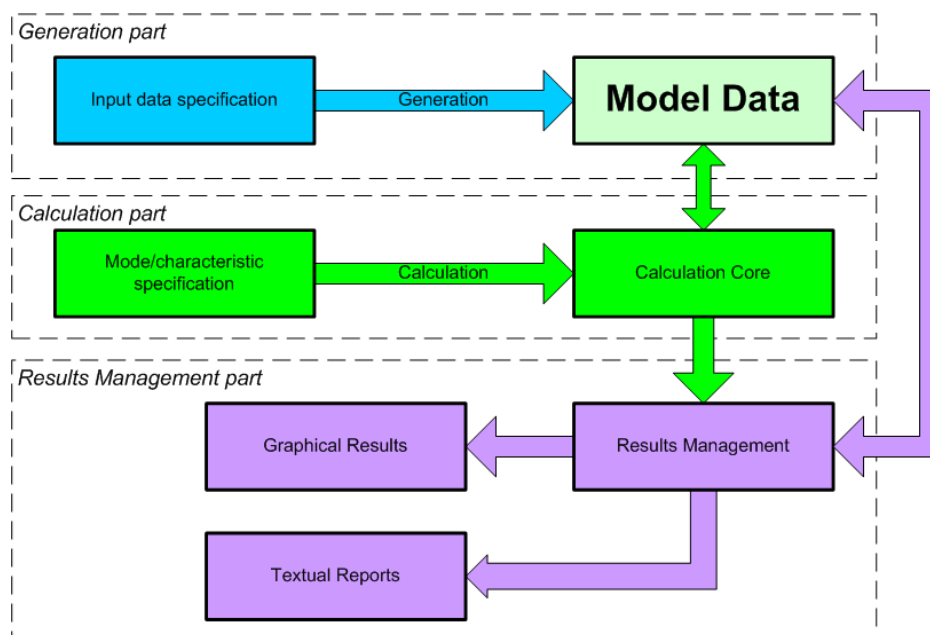


Figure 3.3: Collaboration between different parts of the software

## Input data specification

The input data of a turbogenerator are stored in the TCM object which is called **TCMProject**. The project of **TurboTCM** contains the parameters of the turbogenerator along with the simulation parameters. Besides, it stores the generated PNM and possible results. The structure of the input parameters of the project is shown on figure 3.4.

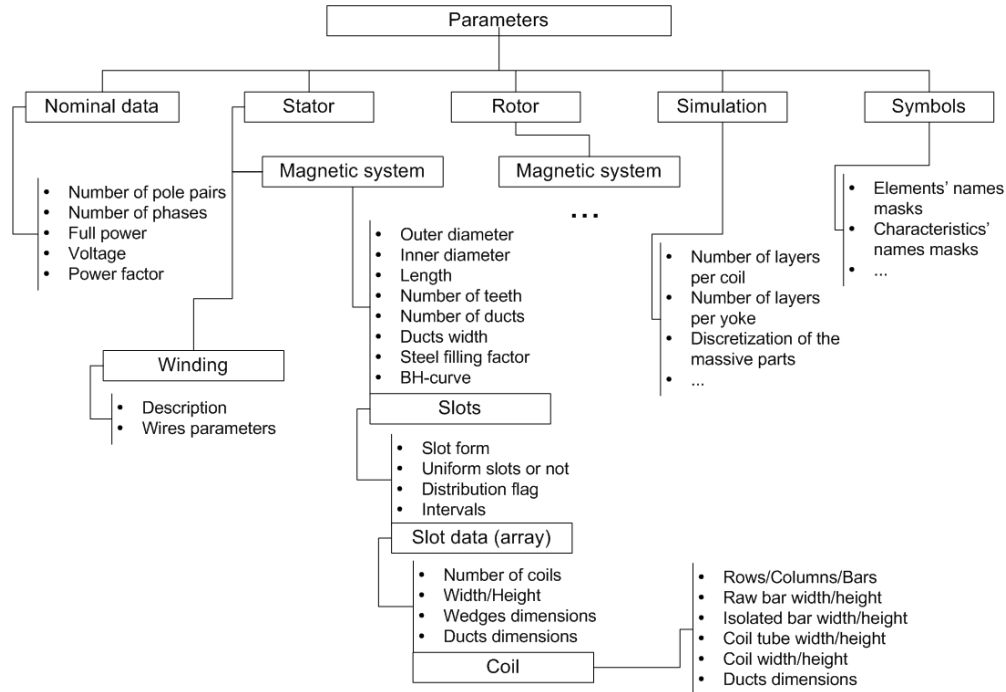


Figure 3.4: Input data specification

Input data contain *Nominal Data* of the machine, the parameters of its *Stator* and *Rotor*, *Simulation* parameters. The *Symbols* substructure contains special internal information concerning the PNM generation, like elements' and characteristics' symbol masks.

The description of stator and rotor of a machine is realized by means of the TCM object **MagneticSystemData**. It generalizes the description of *any* magnetic system of rotating machine. It describes the dimensions and distribution of slots, general dimensions of the magnetic part, winding parameters and distribution along with the material specifications.

## Model Data structure

According to the *Input Data Specification* which defines geometrical and other parameters of the turbogenerator, the main TCM object of calculation is generated – **ModelData**. That object reflects the current state of the PNM and is used to perform all the possible calculations of the model. The member functions of that object start with the name “MD\_” or “ModelData\_”.

The **ModelData** structure contains the following main information about the model:

**.cbm** – **CircuitBuilder** object containing magnetic circuit description, i.e. magnetic circuit elements, their relations, characteristics, dependencies, etc.

- `.cbe` – **CircuitBuilder** object containing electric circuit description.
- `.cc` – **CircuitConnector** object containing the magnetic-electric connection specification.
- `.Base` – The structure which contains the reference values for per-unit calculations.
- `.Mode` – The structure which describes the values of mode calculations (stator and rotor currents and voltages in complex form along with other necessary values).

Besides, though all necessary matrices can be obtained from **CircuitBuilder** objects, **ModelData** structure caches frequently used matrices (like electric and magnetic incidence matrices, etc) and the state matrices: voltages, currents, magnetic potentials, fluxes. Those last reflect the state of the model after each calculation. They are used to calculate the values for post processing after each state calculation. Additional information like number of iterations and progress callback functions is also provided.

### 3.3 Graphical User Interface

The graphical user interface (GUI) is designed for the creation of the project, PN-model generation according to the input data of turbogenerator, verification of the generated model, calculation of the operating modes and characteristics.

#### 3.3.1 Program Main Window

Typing the command **TurboTCM** in the command line of **Matlab** will open the main window of the program, shown on Figure 3.5.

The main window represents the project structure as a tree. It allows to set up the parameters of each part of the turbogenerator and parameters of simulation, analyze the parameters, generate the PN-model, analyze the model elements' characteristics, calculate the operating modes and characteristics. The project, generated model and the results can be stored in corresponding files.

#### Project files

Each saved project is represented at least by one file. This project file has a binary format and the extension `.tcmprj`.

If the project is saved after the model generation, another file is created. It contains the model description with extension `.tcmmdl`. Next time the project is loaded that file is loaded as well, thus the regeneration of the model is not necessary.

If the project has calculated results, the last are saved in separate file with extension `.tcmres`. Similarly to the model file, the results file is loaded along with the project next time.

#### 3.3.2 Setting up project data

The following data of turbogenerator must be defined in order to generate the model:

- common geometrical data of stator and rotor;

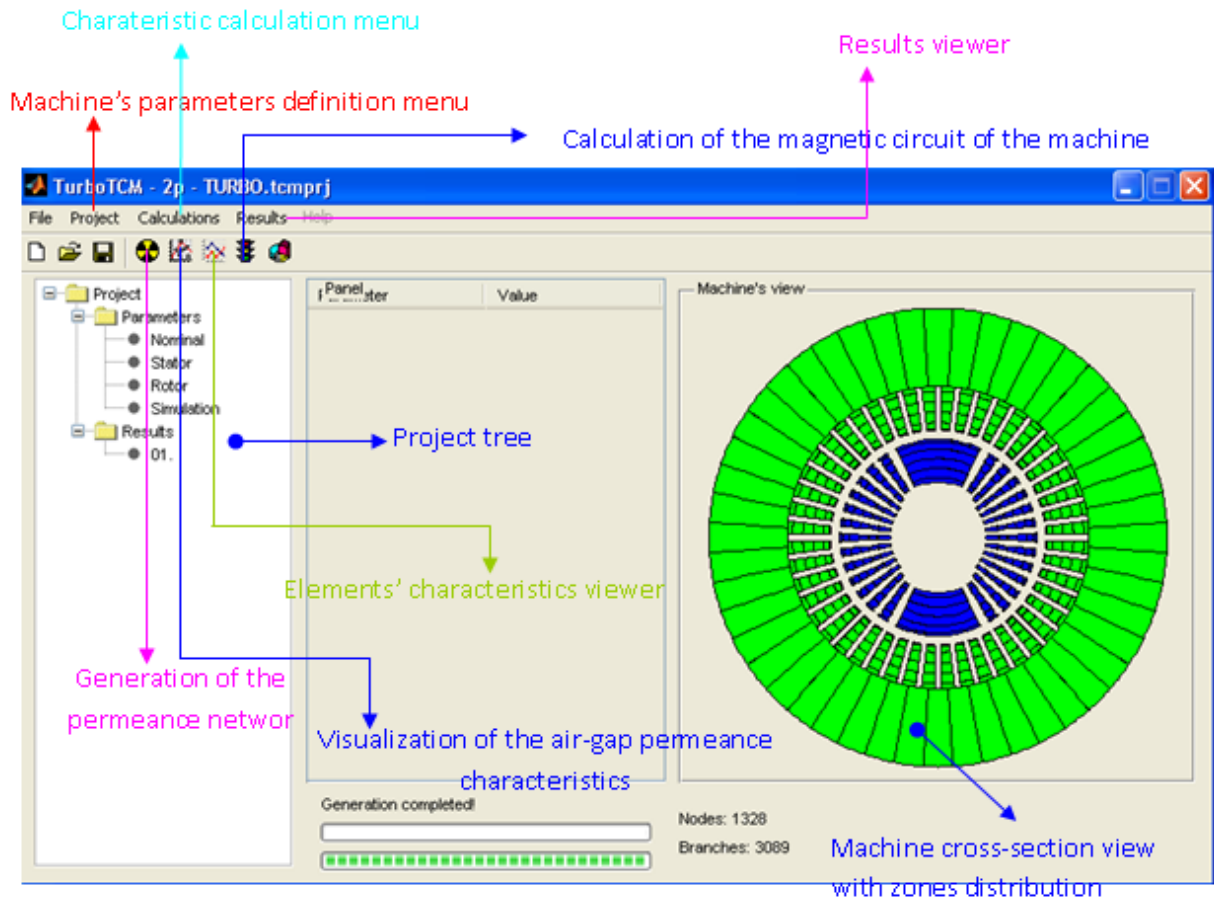


Figure 3.5: Program main window

- distribution and geometry of stator and rotor slots;
- winding parameters of stator and rotor;
- magnetic parameters of the cores;
- axial configuration of the turbogenerator;
- simulation parameters.

The parameters windows can be open using any following way:

- double-clicking the necessary item of a *project tree*;
- choosing the menu item in the menu *Project*.

### Machine's rated data

The window of rated data setup is shown on Figure 3.6. It allows to setup the following parameters:

- pole pair number;

Nominal p...

Number of pole pairs  
1

Full power, MVA  
63

Stator voltage, V  
11500

Power factor  
0.8

Excitation current, A  
675

Rotation speed, 1/min  
3000

OK Cancel

Figure 3.6: Setting up rated data

- full power of turbogenerator;
- rated linear voltage;
- rated power factor;
- supposed excitation current (it can be recalculated and replaced as soon as model is generated);
- rated rotation speed.

### Stator parameters

The stator parameters window is presented on Figure 3.7. The top-left fields allow to set up the basic dimensions of the stator magnetic system: external and internal (bore) diameters, full length of the magnetic system, number of slots (teeth). The *Ventilation* section allows to set the number and width of radial ventilation ducts. The *Material* section allows to set the lamination factor and load the BH-curve from the external file by pressing the button *Load BH-curve*. As soon as it is loaded it is shown in the right graph in the window.

TurboTCM supports two formats of BH-curve files:

- simple text format files, where the information is stored in two columns: the first one contains the values of field strength  $H$ , (A/m), the second one – values of flux density  $B$ , (T); each line forms one point of the curve;
- .bh-files, saved by VectorFields Opera 2D.



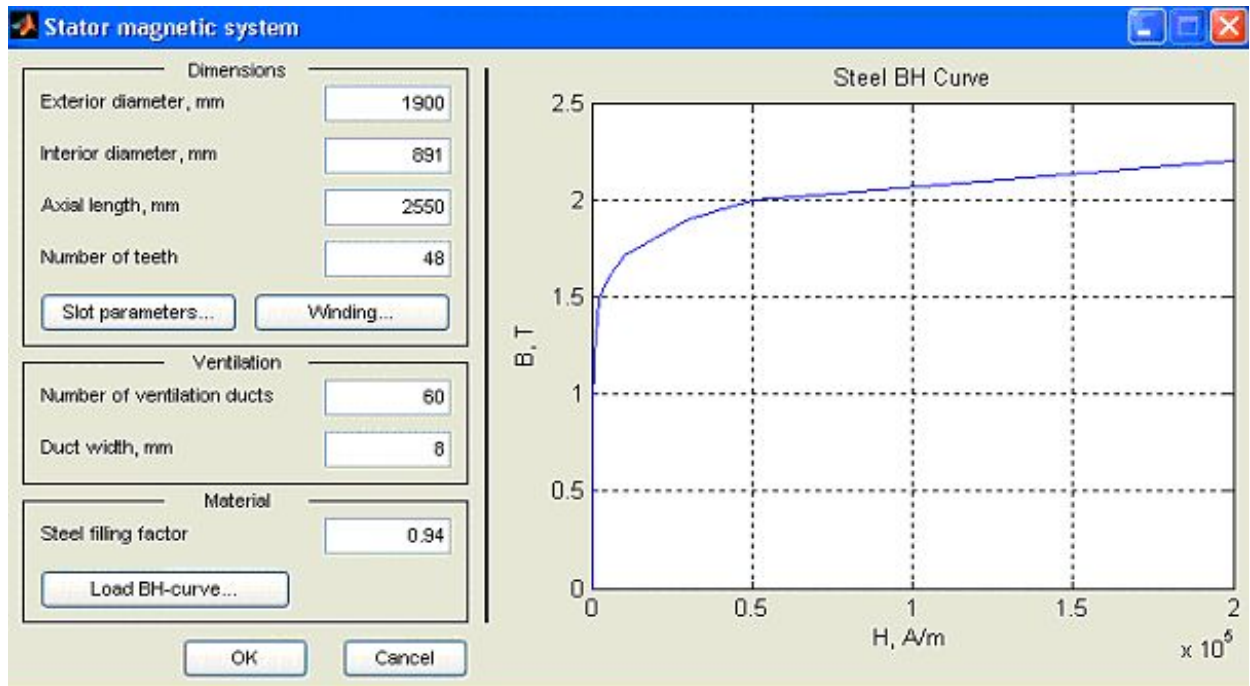


Figure 3.7: Stator parameters setup

The slot parameters and winding parameters can be defined by pressing the corresponding buttons.

### Slot distribution

The choice of slot type and their distribution in a magnetic system are defined in the window shown on Figure 3.8.

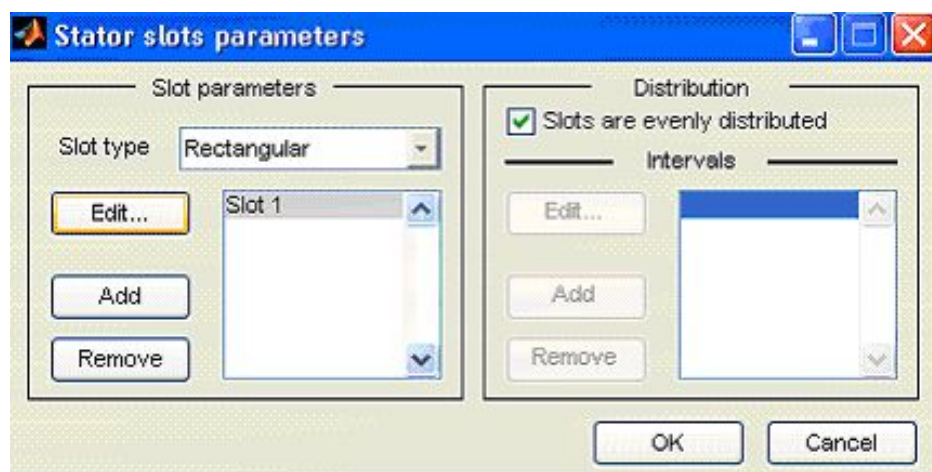


Figure 3.8: Setting up stator slot parameters

TurboTCM supports slot distribution symmetrically-defined relatively to one pole, i.e. the slots can have different parameters and even types between a pole and  $q$ -axis. This

feature is mostly used for the rotor definition, since stators usually have even and uniform slot distribution.

The buttons *Add* and *Remove* can be used to add or remove slots from the definition.

The *Distribution* section allows to define the angular distribution of the slots in the magnetic system. This feature will be discussed later in Section 3.3.2.

In order to set the slot parameters, at least one slot must be defined in the list. Thus the last slot cannot be deleted. Its parameters can be set using the button *Edit...*

### Slot parameters

The window shown on Figure 3.9 allows to define the slot parameters.

The figure shows a software window titled "RectangularSlotDialog". It contains three main parameter groups:

- Slot:**
  - Width, mm: 1 (24.3)
  - Height, mm: 2 (180.5)
  - Silt height, mm: 3 (9)
  - Ventilation duct width, mm: 4 (0)
  - Ventilation duct height, mm: 5 (0)
  - Number of coils: 6 (2)
  - Conductors per slot: 7 (2)
- Wedges:**
  - Bottom wedge height, mm: 8 (0.4)
  - Intercoil wedge height, mm: 9 (5)
  - Top wedge height, mm: 10 (4)
  - Top wedge width, mm: 11 (29)
  - Regulation wedge height: 12 (0.3)
  - Top wedge form: Trapezoidal
  - ☐ Top wedge is in silt
  - ☐ Top wedge is magnetic
  - Material characteristic...
- Coil:**
  - Coil width, mm: 13 (17.6)
  - Coil height, mm: 14 (76.5)
  - Number of rows: 15 (38)
  - Number of columns: 16 (2)
  - Number of bars: 17 (74)
  - Raw bar width, mm: 18 (8.5)
  - Raw bar height, mm: 19 (1.8)
  - Isolated bar width, mm: 20 (8.66)
  - Isolated bar height, mm: 21 (1.96)
  - Coil tube width, mm: 22 (8)
  - Coil tube height, mm: 23 (6)
  - Conductivity: [empty field]

On the right, a diagram shows a slot cross-section. Dimension 1 indicates the slot width, and dimension 2 indicates the slot height. The slot is filled with horizontal bars, and a blue line indicates the top wedge.

Figure 3.9: Defining slot parameters

The fields (1) – (7) serve to define general slot dimensions and number of coils in it. Parameters (8) – (12) define the wedge sizes along with the form of the top wedge. The coil parameters, including the number and dimensions of elementary bars, isolation and etc, can be defined in fields (13) – (23).

All the changes in geometrical parameters are immediately reflected on the view of the slot on the right side of the window.

#### Notes:

- Parameter (7) defining the number of wires per slot mustn't be less than number of coils in slot and divisible by them. That parameter determines the real number of turns in the winding.
- The product of the number of rows (15) and columns (16) of bars can differ from the entire number of bars in coil (17), because some coils may have some rows not filled completely by the bars. For example, for two-column coil the top and the bottom rows usually have only one bar.

## Rotor parameters

The parameters of rotor basically have the same structure as those of stator, thus here only the particularities of the rotor will be discussed.

The window for the parameters of the rotor is the same as that of stator, shown on Figure 3.7. Generally, the inner diameter of the rotor is zero. But main differences concern the parameters of slot distribution.

The peculiarity of the parameters of rotor slot distribution of two-poles turbogenerator is shown on Figure 3.10.

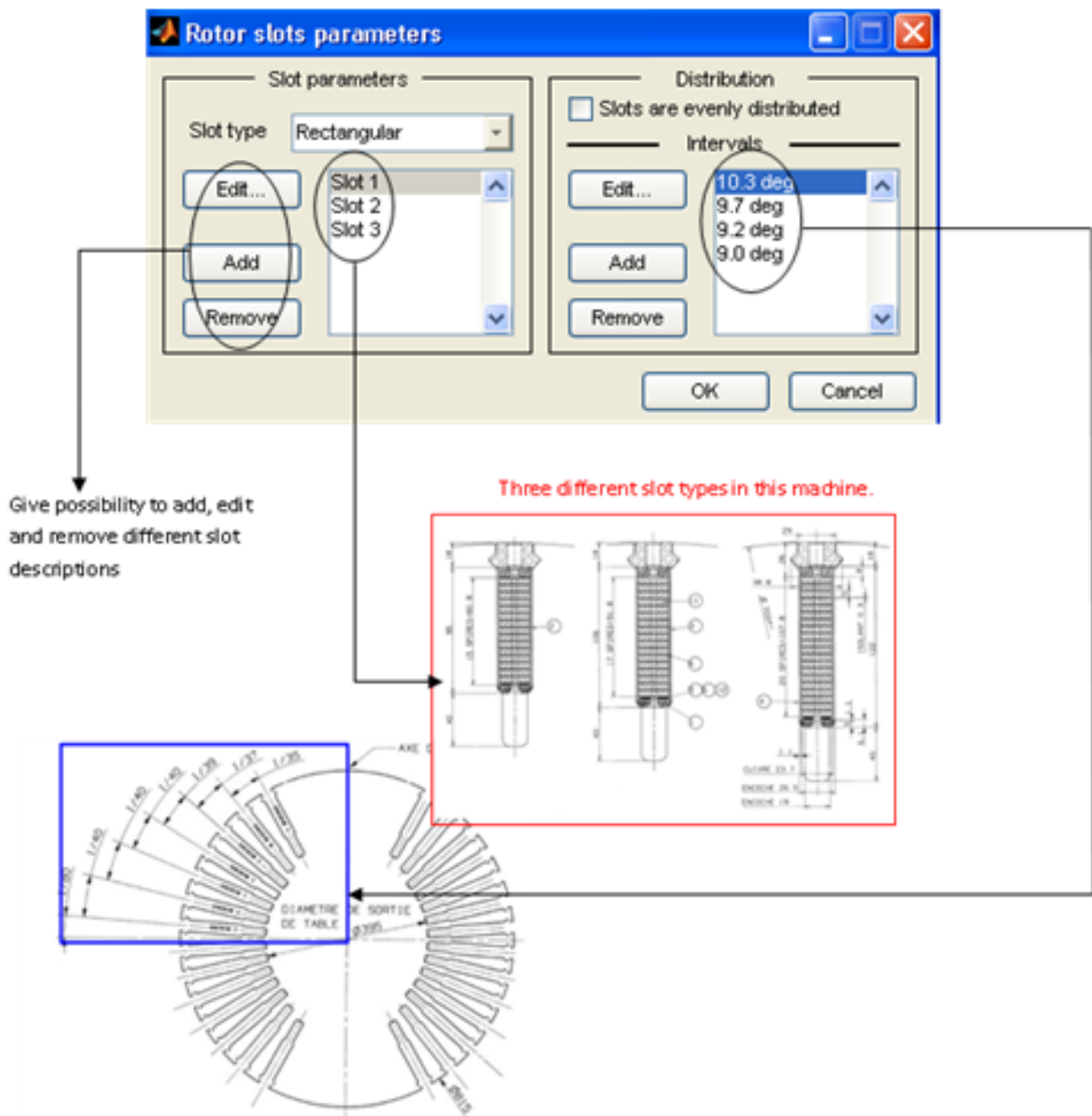


Figure 3.10: Slot distribution window for the rotor

The left part of the window allows to set *different slot configurations*; the right part –

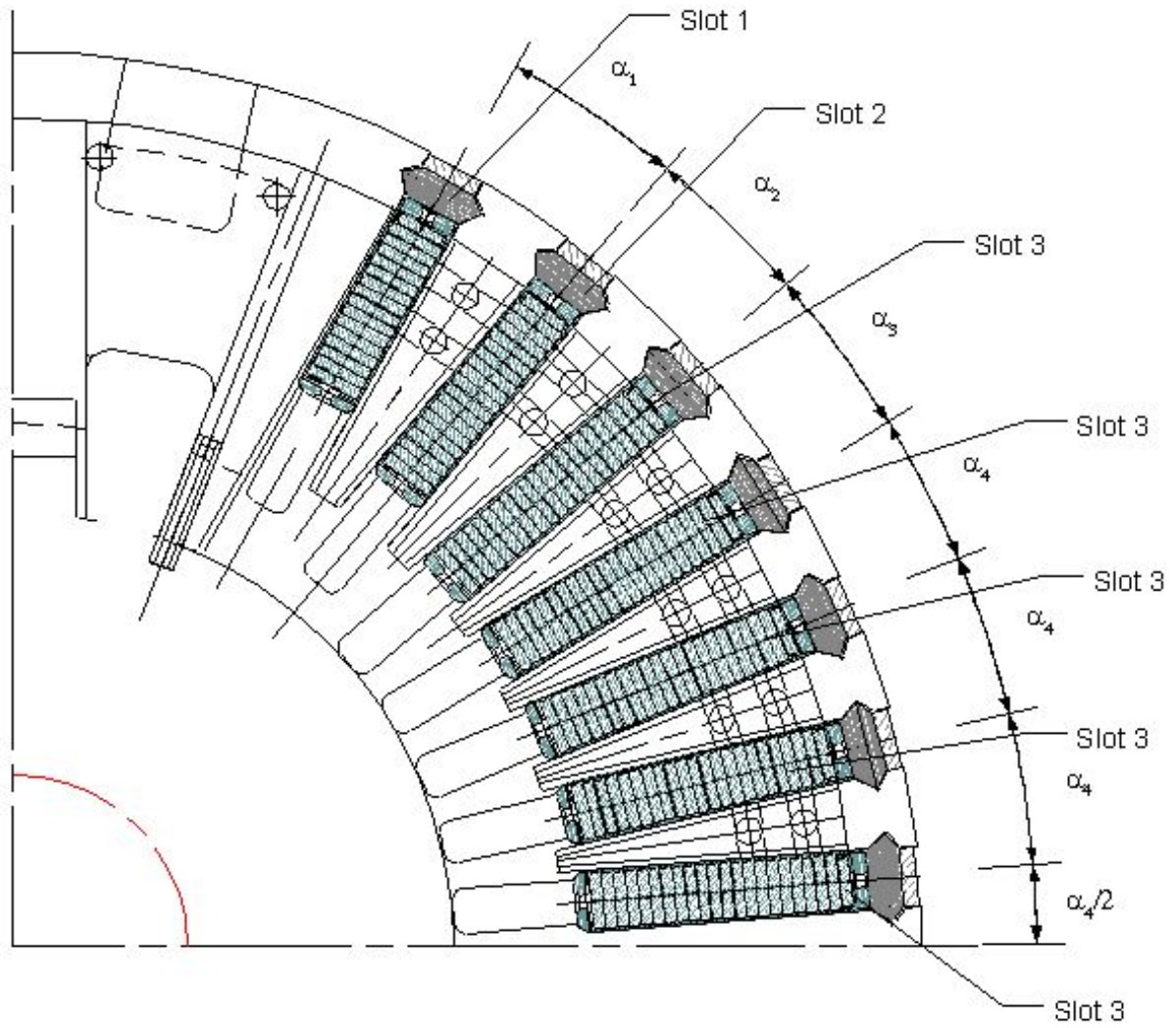


Figure 3.11: Rotor slot distribution

angular intervals between them (tooth pitches). For the rotor *at least one* interval must be defined – it is used to calculate the rotor pole pitch.

If more than one interval is specified along with more than one slot, their distribution is calculated symmetrically relatively to *the pole axis* and *between the pole and q-axis*.

Figure 3.11 presents the distribution of three different slots (Slot 1, Slot 2, Slot 3) with four different tooth pitches ( $\alpha_1$ ,  $\alpha_2$ ,  $\alpha_3$ ,  $\alpha_4$ ).

The number of possible variants of slots and tooth pitches is limited:

$$N_{lim} = \frac{Z_r}{4 \cdot p} \quad (3.1)$$

where  $Z_r$  – number of rotor slots,  $p$  – number of pole pairs.

The definition of the parameters of each slot is similar to the that of stator.

### Simulation parameters

Simulation parameters define the division of the magnetic systems of stator and rotor on layers. Window presented on Figure 3.12 allows to set the following parameters:

- number of layers in tooth zone of stator;
- number of layers in yoke zone of stator;
- number of layers in tooth zone of rotor;
- number of layers in yoke (core) zone of rotor (for the machines with  $p \geq 2$ ).

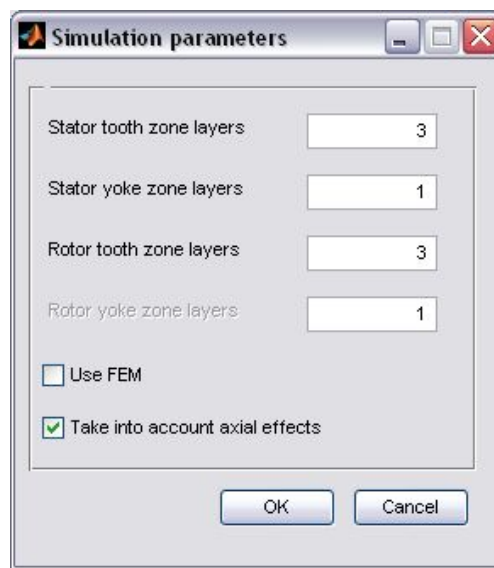


Figure 3.12: Simulation parameters window

The number of layers in tooth zones actually defines the number of slot leakage permeances per slot height without the slit. Besides, tooth zone always contains branches, representing tooth top parts (slit zone) and tooth top leakages.

The PN of a central zone of rotor is fixed and its discretization is defined by number of rotor slots (see Section 2.2.3 for details).

The *Use FEM* checkbox allows to chose the method of air-gap permeances calculation: finite element method with special boundary conditions according to TCM<sup>3</sup> or analytical method presented in section 2.2.4.

The *Take into account axial effects* checkbox allows to switch on/off taking into account the influence of ventilation ducts on the field of slots and air-gap of the machine according to the method described in Section 2.3

### 3.3.3 Model generation and its characteristic view

As soon as all input data describing turbogenerator are filled down, a PN-model must be generated. It can be realized by chosing the menu item *Calculations*→*Generate* in the main

<sup>3</sup>To use this feature a PDE Toolbox for Matlab must be installed.



window of the program (Figure 3.5) or by pressing corresponding button in the toolbar. After the model generation is finished cross-section of a machine will be shown on right side of window. This view provides generated zones of stator and rotor (the central part of the rotor is not shown on the view).

Upon the generation of the model the user is asked to recalculate excitation current for rated mode (Figure 3.13)

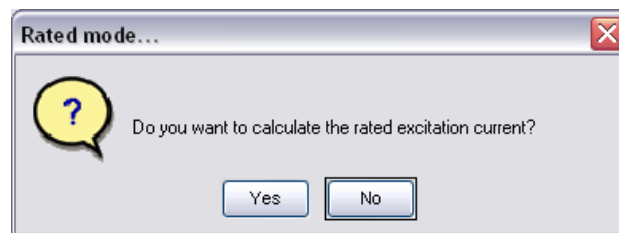


Figure 3.13: Calculation of excitation current

If the generation of the model was successful the menu items of characteristic visualization and calculation become available.

### Viewing air-gap characteristics

A window of the air-gap characteristic viewer is open by choosing menu item *Calculations* → *View airgap characteristics* (Figure 3.14).

The teeth of stator and rotor between which the user wants to see the characteristics can be chosen by mouse using the list boxes on the left side of the window. The user can choose either one stator tooth and one rotor tooth or several teeth from each core. The range of teeth can be chosen by mouse holding **Shift**-key and different teeth can be chosen holding **Ctrl**-key. Note that the first and middle teeth of rotor are considered to be poles.

The control panel on the top of the window allows to zoom in/out a part of the graph, shift it, switch on/off the legend, etc... A prepared graph can be shown in a separate standard figure **Matlab** window for its further printing or modification. It can be done using a button *Open in a new figure*.

### All model's characteristics viewer

Actually, all the model elements' characteristics (including nonlinear) can be viewed by choosing the menu item *Calculations* → *View all characteristics* (Figure 3.15).

The characteristics of elements (including air-gap) can be chosen according to their name from the list on the left of the window. In the example presented on Figure 3.15, only radial rotor pole characteristics are chosen.

The checkbox *Invert axes* allows to rotate the graphic view on 90°, i.e. swap  $x$  and  $y$  axes.

## 3.3.4 Calculating the modes and characteristics of turbogenerator

The following operating modes can be calculated using TurboTCM GUI:

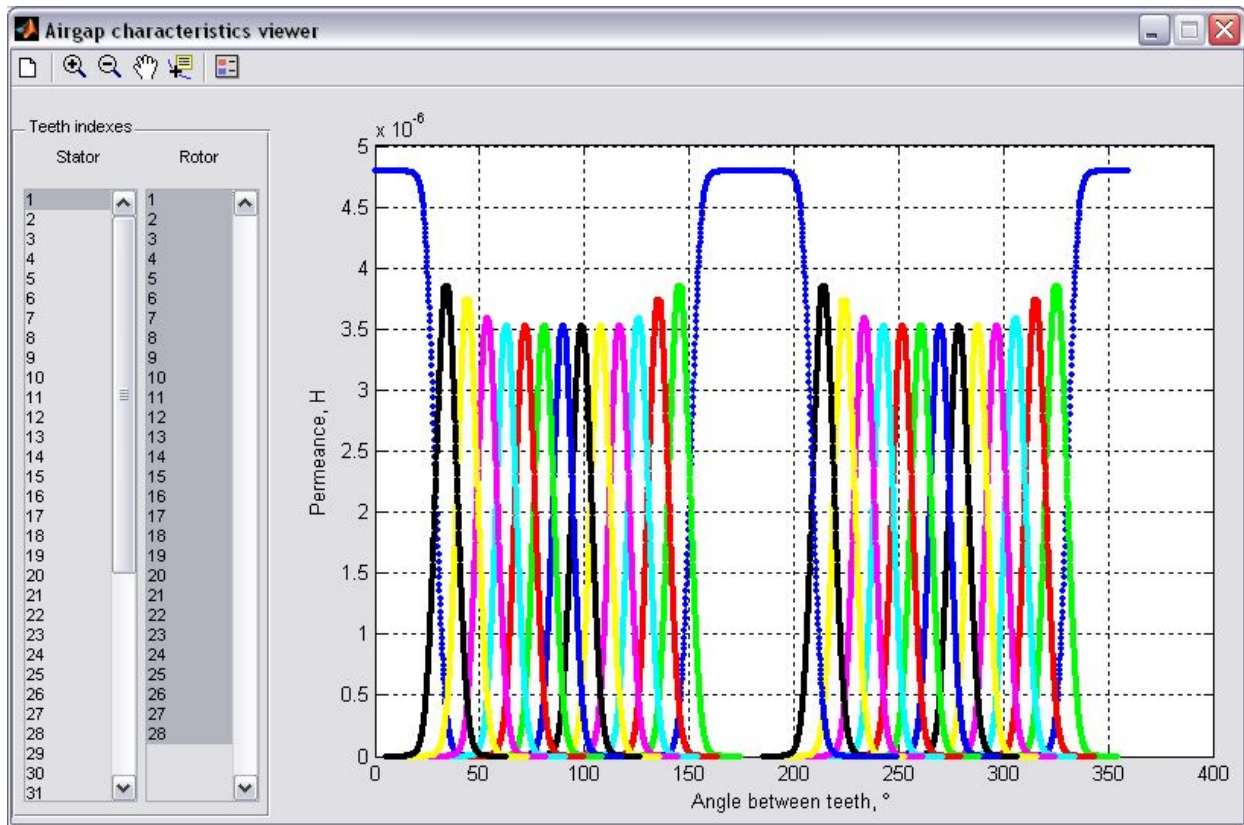


Figure 3.14: Air-gap characteristic viewer

- single operating mode of turbogenerator, defined by stator voltage and current and power factor;
- no-load characteristic;
- load characteristic of turbogenerator working on a simple charge;
- regulation characteristic of turbogenerator working for network;
- V-shaped characteristics of turbogenerator working for network;
- angular characteristics of turbogenerator working for network.

For each calculated characteristic the following information can be obtained:

- flux density and flux of air-gap, pole and rotor teeth, stator teeth and yoke;
- magnetic potentials of the air-gap, pole, rotor central core, stator and rotor tooth part, stator yoke;
- electromagnetic torque and load angle;
- parameters  $x_d$  and  $x_q$ ;
- etc...

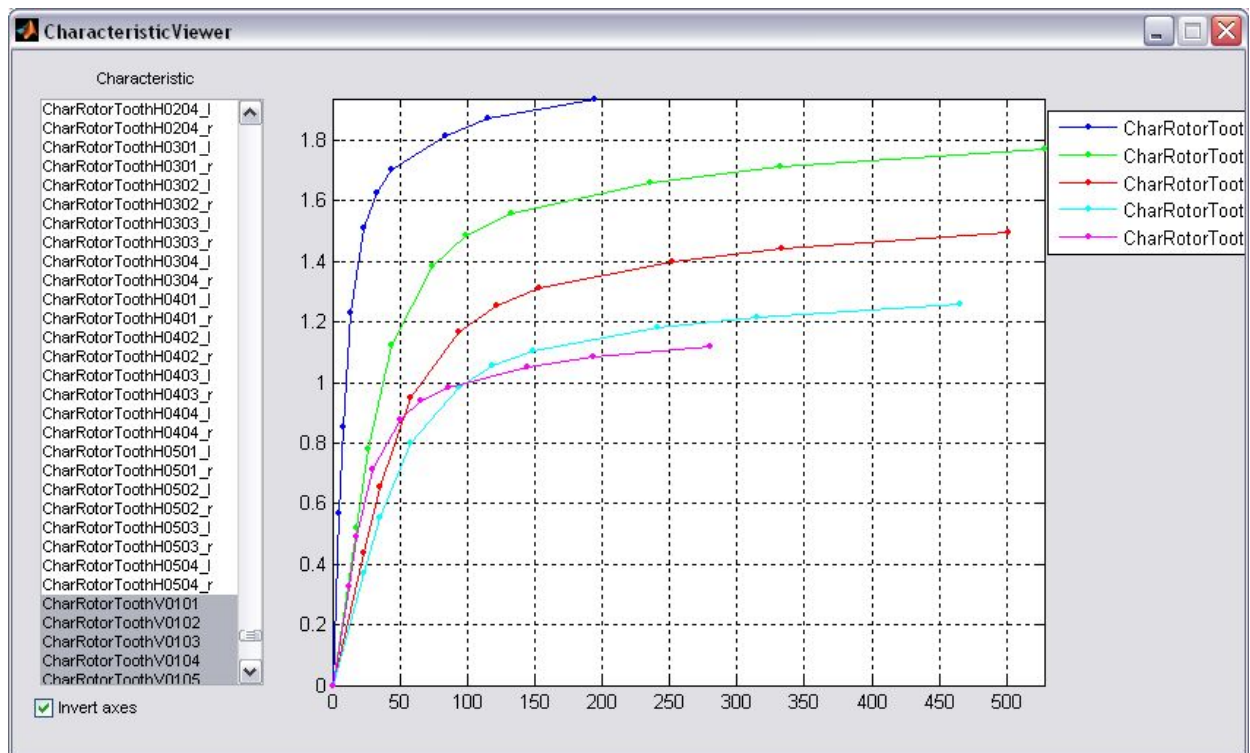


Figure 3.15: All characteristics viewer

Besides, the following parameters can be obtained for each point of each characteristic or operating mode:

- air-gap flux density spacial distribution;
- graphical view of the magnetic field parameters (magnetic potentials, flux density, fluxes) according to each element of PN.

The following sections provide the description of using GUI of TurboTCM to obtain the particular results. The last are presented further for different machines in Chapter 4.

### Operating mode calculation

The window allowing to calculate the operating mode of turbogenerator (Figure 3.16) can be called by choosing the menu item *Calculations* → *Mode Calculation* in the main window (or corresponding button in the toolbar).

This window allows to calculate one operating mode of the turbogenerator. In order to start the calculation the following fields must be set:

- *Mode type* – Stator voltage, current and power factor – calculation of the mode defined by stator voltage, current and power factor. In this case the excitation current will be obtained as a result.
- *Unit choice* – *Units* or *PerUnit* – defines if the calculation should be performed in regular units or per unit.



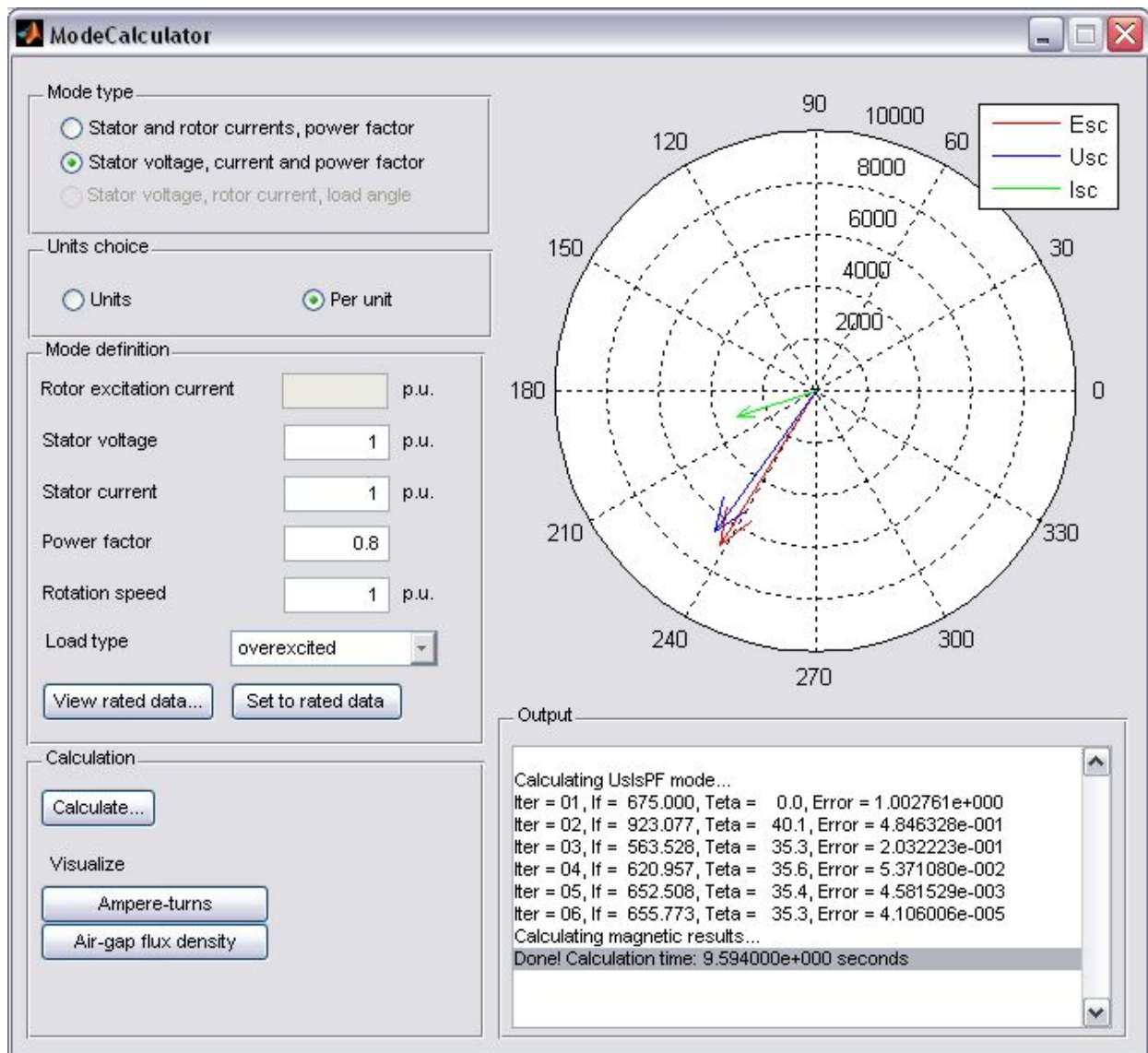


Figure 3.16: Operating mode calculation window

- *Mode definition* – defines the values of the mode: stator voltage and current, power factor (PF), rotation speed and load type. These fields can be filled down by rated values pressing the button *Set to rated data*. Pressing the button *View rated data...* allows to view the rated data of the turbogenerator.

Upon the definition of the values of the mode the calculation can be performed pressing *Calculate* button. A vector diagram on the top-right of the window will show the iteration process in “real-time”. The information about convergence will be displayed in *Output* window.

Finally the vector diagram will show the vectors of stator current  $I_{sc}$ , stator voltage  $U_{sc}$  and EMF “beyond the end-winding leakage”  $E_{sc}$ , obtained from the calculation.

As an example, several values can be observed upon the end of the calculation, like potential distribution in the elements of PN, i.e. elements’ ampere-turns (Figure 3.17, top) and flux density on the middle line of air-gap (Figure 3.17, down).

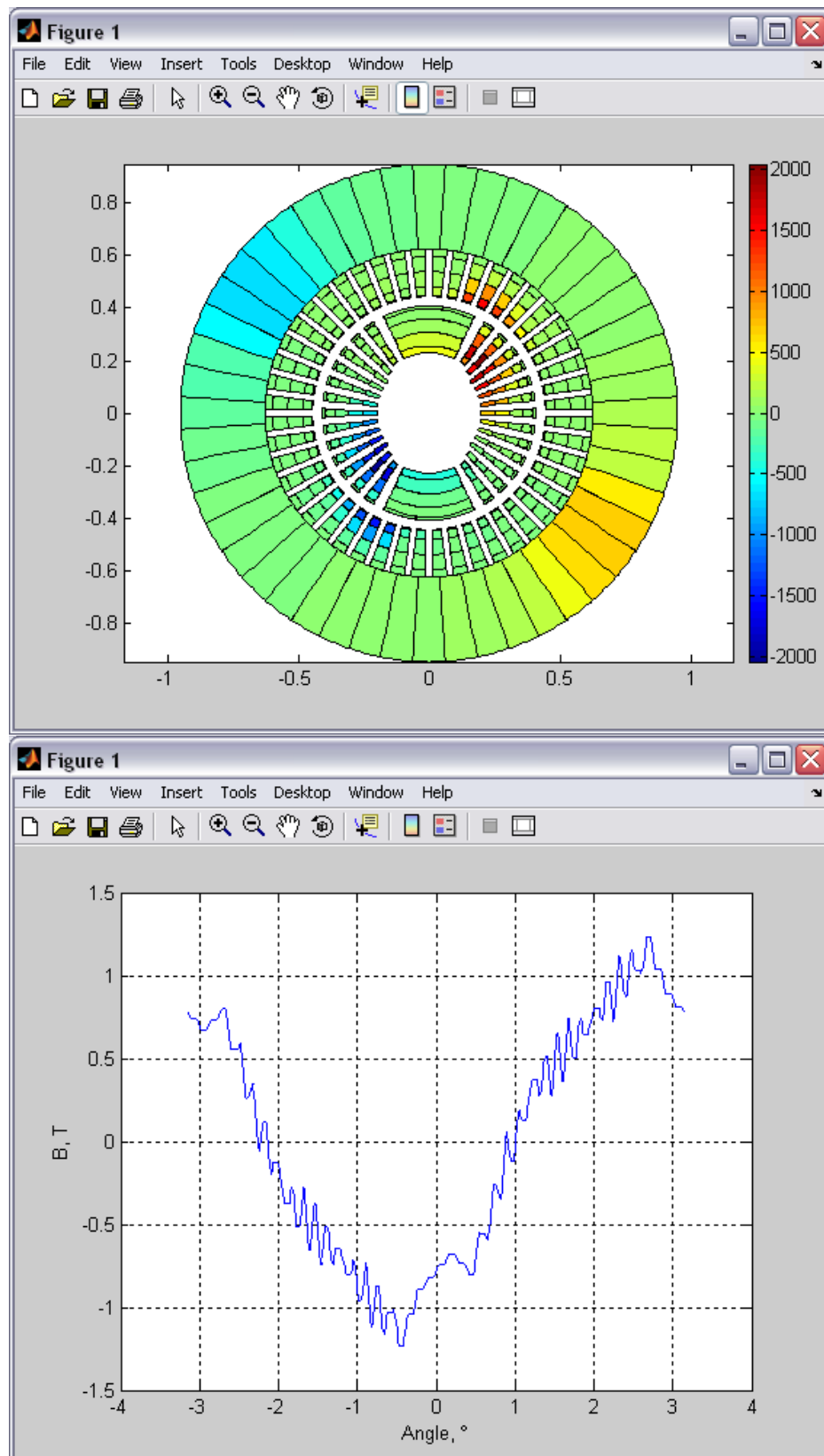


Figure 3.17: Ampere-turns of PN elements (top) and air-gap flux density (down)

After closing the calculation window, the results will be added to the result list of the main window.

### No-load characteristic

The no-load characteristic of turbogenerator is calculated as  $E_1 = f(I_f)$ , where  $E_1$  – stator winding EMF,  $I_f$  – turbogenerator excitation current. The rotation speed is constant. This is a direct problem, thus there is no need in additional iterative process.

Chosing the menu item *Calculations* → *No-load characteristic* opens a no-load characteristic parameters window (Figure 3.18). The excitation current must be set up as a vector, rotation speed – scalar. All the values must be set in per unit. The reference value for the excitation current is that calculated after the PN-model generation for the rated load. The calculation will start as soon as *OK* button is pressed.

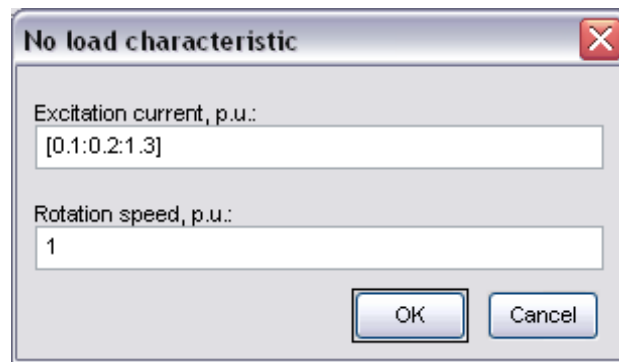


Figure 3.18: Input data for no-load characteristic

In case of succcessfull calculation the no-load characteristic will be added to the result list. It can be viewed by double-clicking on it in the result list.

**Note: setting vector values.** Vector values are widely used while setting the input data for calculations. The vector must be set using standard *Matlab* notation. Here are several examples:

- `[0.1:0.2:1.2]` – means a range of values from 0.1 to 1.2 with step 0.2.
- `[0.1:0.05:0.6 0.7:0.1:1 1.2]` – a range of values from 0.1 to 0.6 with step 0.05, then from 0.7 to 1.0 with step 0.1 and finally a single value 1.2.

For detailed information see the *Matlab* help.

### Load characteristic

The load characteristic is calculated on a single load for defined values of stator current, excitation current and power factor as  $U_s = f(I_s)$ , where  $U_s$  – stator voltage,  $I_s$  – stator current.

The calculation will start upon chosing the *Calculations* → *Load characteristic* menu and setting input data in the window shown on Figure 3.19). This window allows to define the vector of stator current values, excitation current, PF and rotation speed. All data must be defined in per unit.

**Attention!** The load type (inductive or capacitive) is defined by the *sign* of the PF: positive PF means active-inductive load, negative – active-capacitive. For the PF equal to 1 its sign is ignored.

The dialog box titled "Load characteristic" has a close button (X) in the top right corner. It contains the following input fields:

- Stator current, p.u.: [0:0.2:1.4]
- Excitation current, p.u.: 1
- Power factor: 1
- Rotation speed, p.u.: 1

At the bottom right, there are two buttons: "OK" and "Cancel".

Figure 3.19: Input data for load characteristic

Upon the end of calculation the characteristic will be added to the end of the result list and can be viewed from there.

### Regulation characteristic of turbogenerator

The regulation characteristic of turbogenerator on parallel work with network is calculated for fixed value of stator voltage and power factor as  $I_f = f(I_s)$ , where  $I_f$  – excitation current,  $I_s$  – stator current.

The calculation is launched from the menu item *Calculations* → *Regulation characteristic*. The input data window will show up (Figure 3.20) and allow to enter the value of stator current vector, stator voltage, PF and rotation speed. All data must be defined in per unit. The rules of setting load types were described in section 3.3.4.

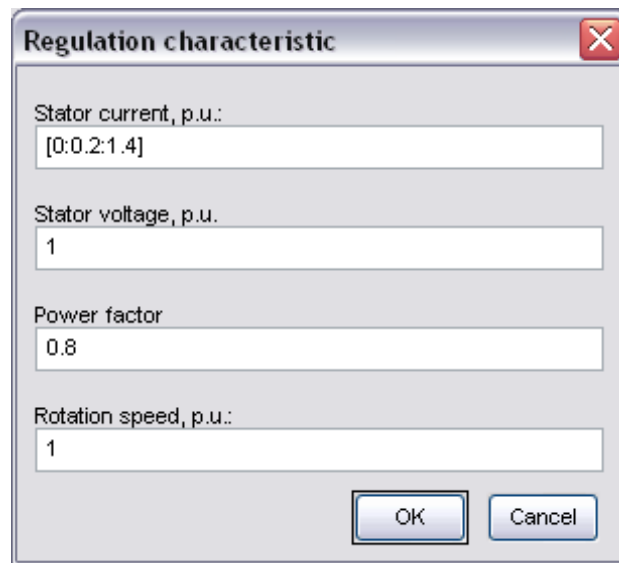
The calculated characteristic will be added to the end of the result list.

### V-shaped characteristics calculation

A V-shaped characteristic of turbogenerator is calculated for fixed values of stator voltage and active power as  $I_s = f(I_f)$ , where  $I_f$  – excitation current,  $I_s$  – stator current. The excitation current is given two ranges: underexcited and overexcited.

The menu item *Calculations* → *V-shaped characteristic* opens the input dialog (Figure 3.21) which allows to define the following values (per unit):

- vector of stator current values in underexcited zone;
- vector of stator current values in overexcited zone;
- stator voltage;



A dialog box titled "Regulation characteristic" with a close button (X) in the top right corner. It contains four input fields with labels and values:

- Stator current, p.u.: [0:0.2:1.4]
- Stator voltage, p.u.: 1
- Power factor: 0.8
- Rotation speed, p.u.: 1

At the bottom right, there are two buttons: "OK" and "Cancel".

Figure 3.20: Input data for regulation characteristic

- active power;
- rotation speed.

Note that the values of stator current in p.u. must not be less than defined active power in p.u. since such operating modes don't exist and these points will be excluded from the calculation.



A dialog box titled "V-shaped characteristic" with a close button (X) in the top right corner. It contains five input fields with labels and values:

- Stator current in underexcited zone, p.u.: [0.3:0.1:1.0]
- Stator current in overexcited zone, p.u.: [0.3:0.1:1.2]
- Stator voltage, p.u.: 1
- Active power, p.u.: 0.3
- Rotation speed, p.u.: 1

At the bottom right, there are two buttons: "OK" and "Cancel".

Figure 3.21: Input data for V-shaped characteristic calculations

### Angular characteristic calculation

The angular characteristic of turbogenerator is calculated for defined stator voltage and excitation current as  $P = f(\theta)$ , where  $P$  – active electric power,  $\theta$  – load angle.

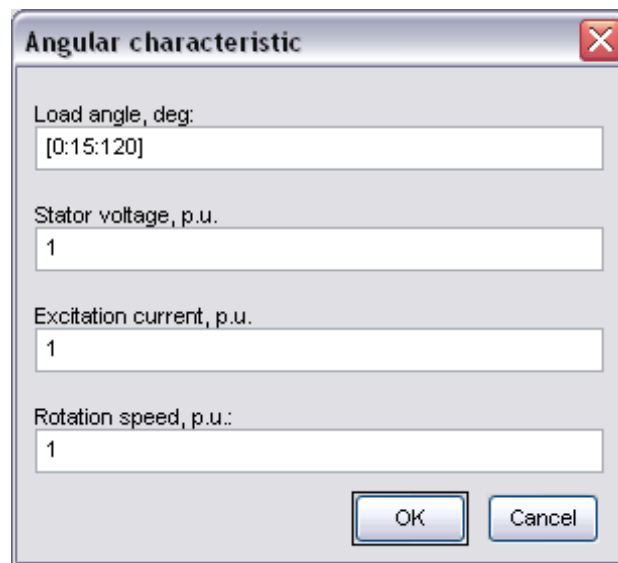
Similarly to the previous characteristic, that is launched from the menu item *Calculations* → *Angular characteristic* and input data dialog window (Figure 3.22).

The results of calculation are similarly stored in the end of the result list. Additional characteristics are shown in the results of the calculation (Figure 3.23): active and reactive power, stator current and PF as function of load angle. The red cross on angular characteristic marks its maximum, which load angle  $\theta_{max}$  corresponds for. That angle determines the range of stable work of turbogenerator. The value of  $\theta_{max}$  is shown under the active power graph.

## 3.4 Conclusion

This chapter presented the approach to software implementation of the methods expounded in Chapter 2. A description of the software package was given along with its capabilities.

The software was designed on two different levels: simulation core and almost independent graphical user interface. This conception allows to separate the tasks, gives the user flexible and convenient methods to create a project, enter a huge amount of machine's parameters, perform some calculations, view the results. From the other hand, it offers very flexible programming interface aimed to thoroughly use of all the capabilities of the model, creating user-defined scripts. The encapsulation of the calculation core gives the possibility to couple TurboTCM with the optimization supervisor (see Section 4.4 for examples) or any other software written in Matlab.



**Angular characteristic**

Load angle, deg:  
[0:15:120]

Stator voltage, p.u.  
1

Excitation current, p.u.  
1

Rotation speed, p.u.:  
1

OK Cancel

Figure 3.22: Input data for angular characteristic

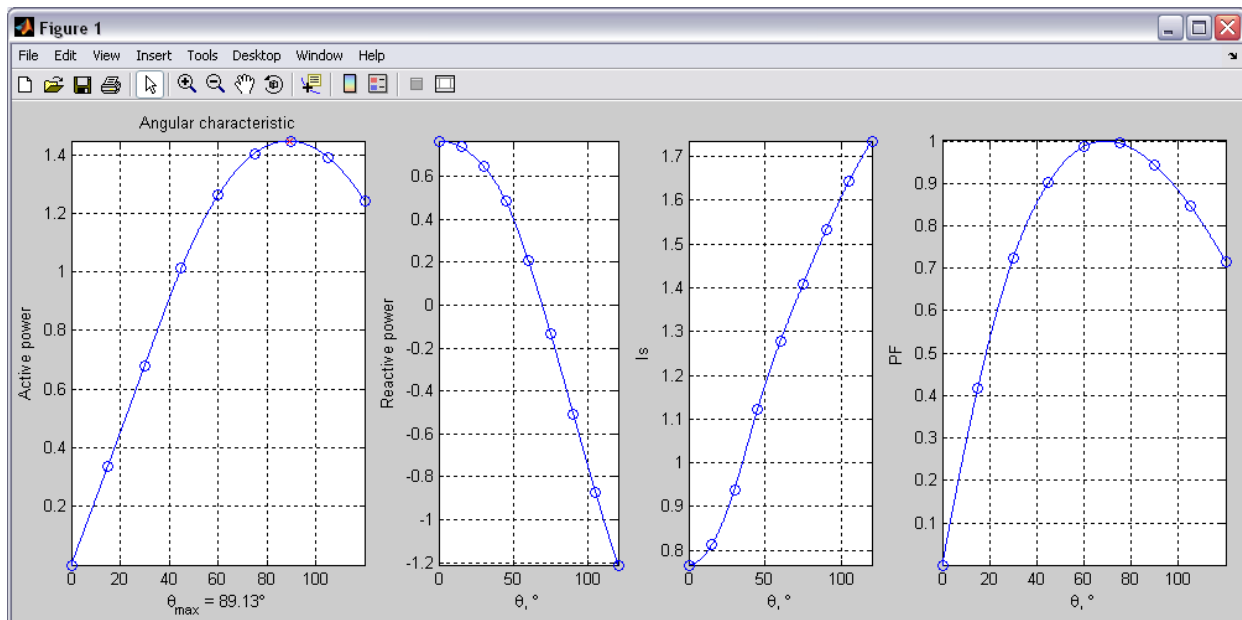


Figure 3.23: Results of angular characteristic calculation

# Chapter 4

## Application

The proposed approach was tested on several kinds of synchronous machines during the evolution of the software. Since the used method is rather universal, in the beginning a small synchronous electrical machine (3 kW) was produced in order to perform some adjustment of the method. The fluxes in different parts of the machines were calculated by TurboTCM and then compared with those from OPERA. No-load, short-circuit and load characteristics were compared with experimental results.

After the application to a small machine, the software was developed in order to be applied to two-poles turbogenerator. We were provided by Jeumont with experimental data in no-load and short-circuit cases for several machines. These results were compared with TurboTCM calculations.

The software allows calculating synchronous non-salient pole machines with any number of poles. In 4-pole turbogenerator case we had to extend a little bit the typical PN of the machine in order to reflect that particular case. The modified PN, some calculation and experimental results are also presented in this chapter.

### 4.1 Synchronous machine of 3kW

In the beginning, in order to “tune-up” the model of a synchronous machine, to reflect and verify its particularities, a small machine – prototype – was studied. The machine had the properities that are particular to turbogenerators, like different rotor slot pitches. For that machine the primary version of the software was realized. It took into account not so many input parameters as for turbogenerators but helped to define and optimize main structure of the software by means of try-and-error method.

#### 4.1.1 Machine description

The synchronous machine used in the study was constructed based on an asynchronous motor of 3 kW. The stator was left the same, while the rotor was produced complying with the specification reflecting the particularities of a turbogenerator.

The main parameters and dimensions of the machine are presented in Table 4.1. The stator of the machine has trapezoidal slots with the pouring winding. The rotor has slots with different slot pitches and is presented on Figure 4.1.



Rated data			
Total power		3000 VA	
Stator phase voltage		220 V	
Power factor		0.8	
Number of poles		2	
Stator data		Rotor data	
Outer diameter	164 mm	Outer diameter	92 mm
Inner diameter	94 mm	Shaft diameter	36 mm
Core length	110 mm	Core length	110 mm
Number of slots	24	Number of slots	16
Slot type	trapezoidal	Slot type	rectangular
Slot height	15.52 mm	Slot width	4 mm
Slot height	14 mm		
Slot width on top	9.45 mm		
Slit width	2.7 mm		
Slit height	0.68 mm	Number of turns	440
Number of turns	100		
		Slot pitches	17.14°/16.36°

Table 4.1: Dimensions of the 3kW machine

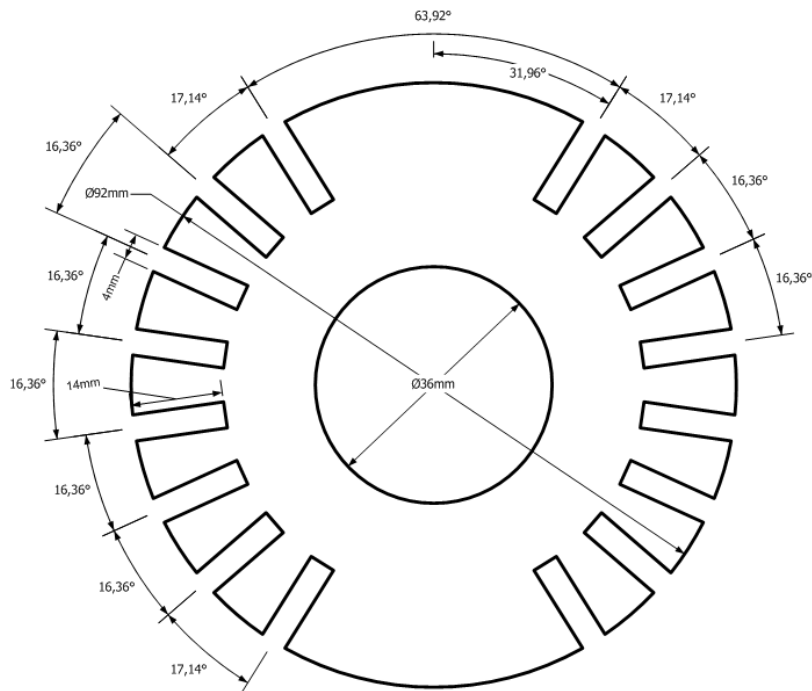


Figure 4.1: Rotor dimensions

The machine's shaft is made of a soft steel. It differs from the other part of the rotor. The BH-curves of stator, rotor and shaft materials are presented on Figure 4.2.

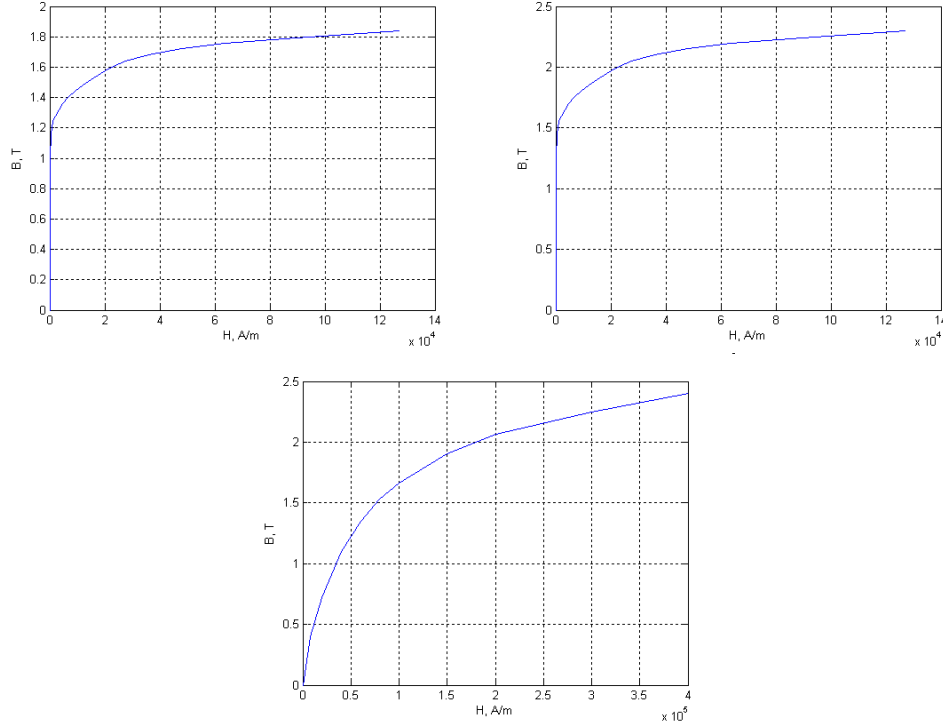


Figure 4.2: Steel BH-curves: rotor (left), stator(right) and shaft (bottom).

### 4.1.2 Machine's permeance network

The permeance network of the machine is generated using the method discussed in Chapter 2. The difference can be found in rotor: the shaft is modeled by an additional layer of nonlinear permeances.

Figure 4.3 shows a simplified rotor scheme, outlining the particularities of this model. Teeth permeances are shown on the figure while slot permeance branches are omitted. Permeances  $\Lambda_{yh1} - \Lambda_{yh8}$  represent the D-axis oriented branches corresponding to the yoke part of the rotor. Permeances  $\Lambda_{sh1} - \Lambda_{sh4}$  represent D-axis oriented branches corresponding to the shaft part of the rotor. Branches  $\Lambda_{yv1} - \Lambda_{yv5}$  and  $\Lambda_{sv1} - \Lambda_{sv3}$  represent Q-axis oriented flux corresponding to the yoke and shaft parts respectively. All D-axis oriented branches also contain the MFF-sources which are omitted on the figure.

### 4.1.3 Calculation results

In order to validate the model, the obtained results were compared with FE-calculation software OPERA-RM. A fragment of the OPERA model with generated mesh is shown on Figure 4.4. The mesh is rather complicated and irregular. The main part of energy conversion – the air-gap – has the finest mesh, since the gradient of flux density there is the highest. Special techniques must be applied to reflect the mutual movement of stator

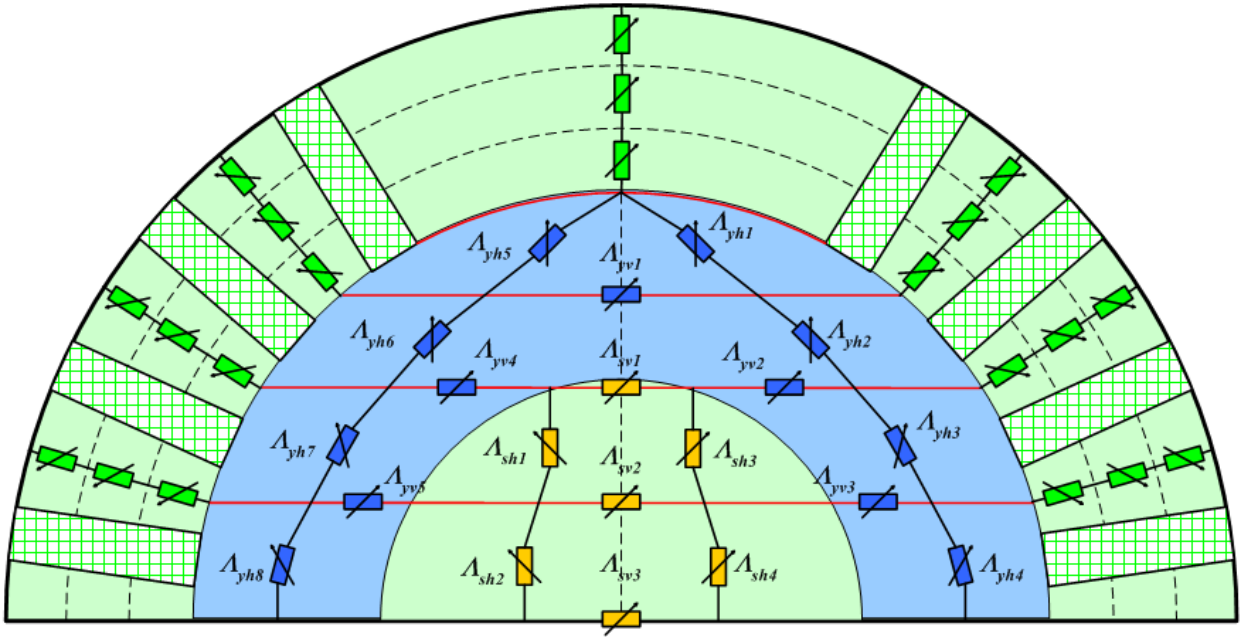


Figure 4.3: Rotor simplified scheme

and rotor cores, otherwise remeshing should be performed as soon as rotor position changes. From the other hand, the parts like stator and rotor teeth and yokes have also relatively high meshing, though flux density gradient is relatively small there. These factors increase calculation time while using finite element method, especially in load cases, when several rotation periods should be calculated to obtain only one point of the characteristic.

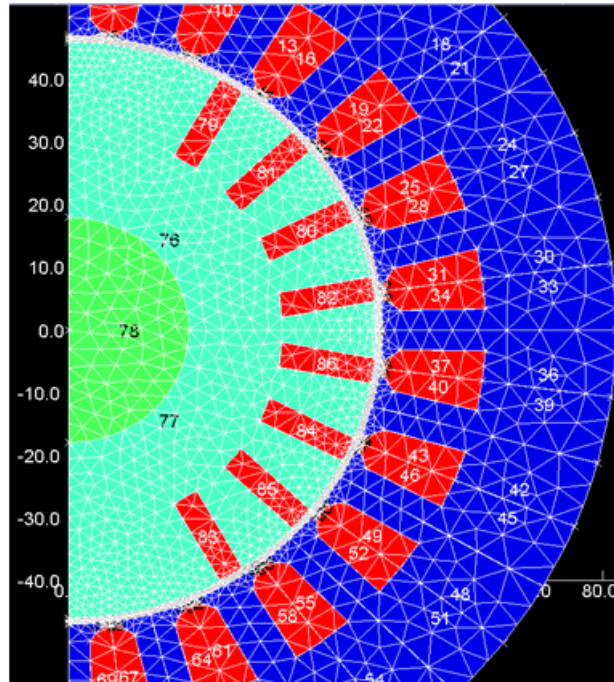


Figure 4.4: OPERA-RM model (fragment).

### Flux comparison

The flux comparison was performed in static mode calculation for different field currents. We compared the fluxes in the middle section of stator tooth aligned with rotor pole and the part of stator yoke where the flux was maximal. The results of calculations are presented in Table 4.2 and Figure 4.5. The maximal errors are 4,927% for tooth fluxes and 2,649% for yoke fluxes.

J,A	Teeth			Yoke		
	Opera	TurboTCM	Error	Opera	TurboTCM	Error
0,1	3,2660E-05	3,4264E-05	4,911%	1,1440E-04	1,1734E-04	2,567%
0,2	6,5310E-05	6,8528E-05	4,927%	2,2910E-04	2,3467E-04	2,433%
0,5	1,6330E-04	1,7132E-04	4,911%	5,7300E-04	5,8668E-04	2,388%
1,0	3,2660E-04	3,4264E-04	4,911%	1,1460E-03	1,1734E-03	2,388%
1,5	4,8910E-04	5,1278E-04	4,843%	1,7160E-03	1,7556E-03	2,305%
2,0	6,4890E-04	6,7881E-04	4,609%	2,2759E-03	2,3232E-03	2,076%
4,0	1,07700E-03	1,09277E-03	1,464%	3,63550E-03	3,59360E-03	1,153%
6,0	1,19500E-03	1,20593E-03	0,914%	3,95670E-03	3,88127E-03	1,906%
8,0	1,25800E-03	1,26192E-03	0,312%	4,15470E-03	4,05694E-03	2,353%
10,0	1,30450E-03	1,30199E-03	0,192%	4,30900E-03	4,19483E-03	2,649%

Table 4.2: Flux calculation results

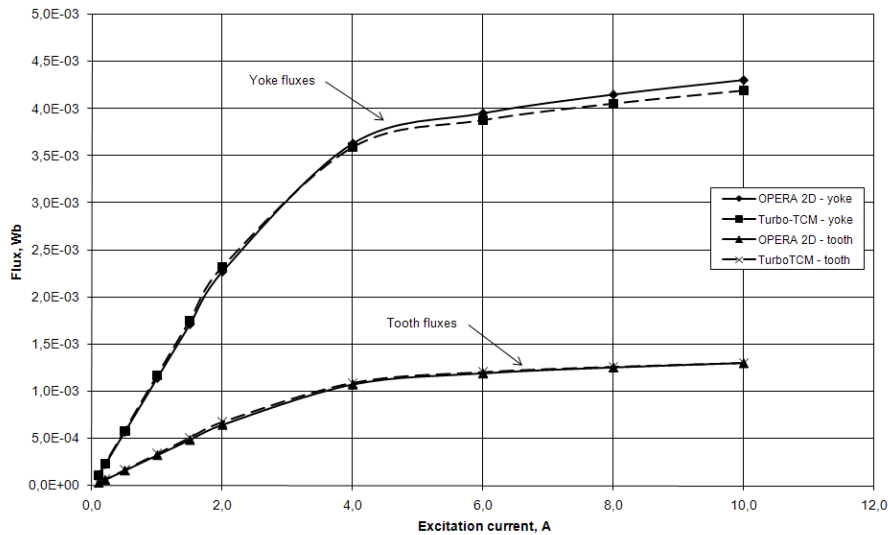


Figure 4.5: Fluxes comparison: TurboTCM – OPERA RM

### Static characteristics comparison

No-load and load characteristics are shown on Figure 4.6. TurboTCM result is compared with OPERA RM one. That finite element package performs the calculation of the EMF on a full period of rotation. The result is RMS value of the obtained EMF for different field currents. Maximal error is 6,39% for the field current of 20A.

For a fixed field current we obtained the load characteristic of the machine  $V_s(I_s)$  (Figure 4.6, right). The maximal error is 4,14% for stator current of 13A.

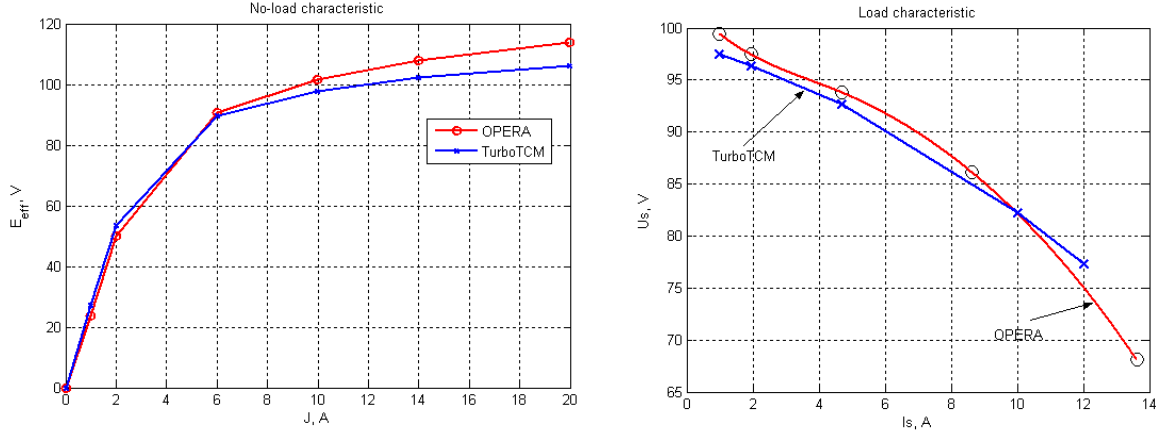


Figure 4.6: Noload (left) and load (right) characteristics: TurboTCM – OPERA RM

### Dynamic simulation

Figure 4.7 presents dynamic no-load calculations performed in OPERA RM and TurboTCM. EMF curves are shown on the left while their spectrum on the right. The data were obtained for 180 positions of the rotor in TurboTCM and 100 positions in OPERA RM for the field current of 10A. OPERA RM limits 100 positions per simulation, thus to obtain 180 positions we should have performed two simulations one by one.

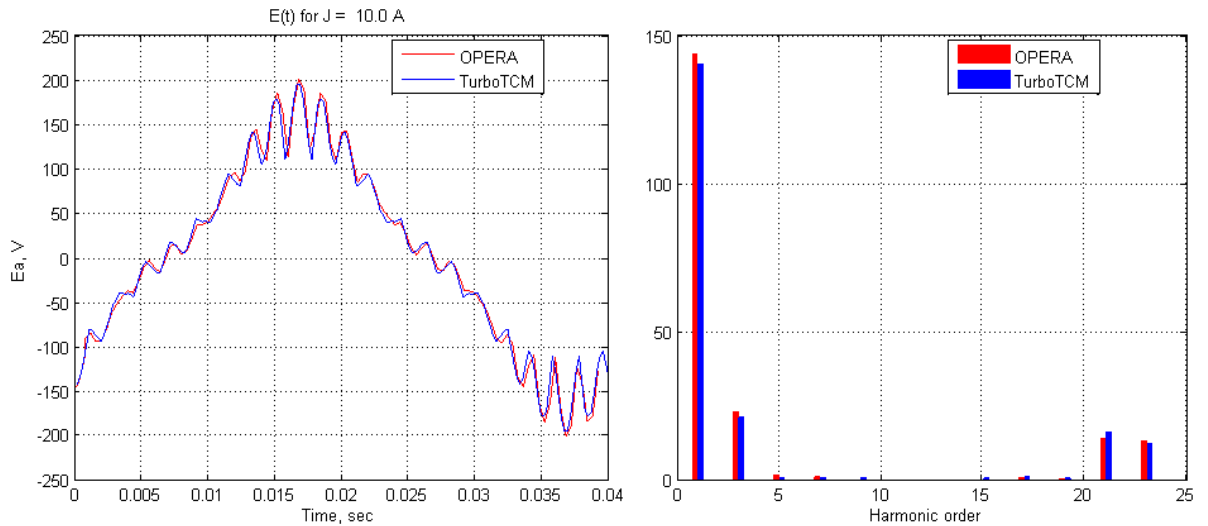


Figure 4.7: Dynamic calculation: TurboTCM – OPERA RM

Table 4.3 shows the calculation times in OPERA RM and TurboTCM for different field currents. The results show that even without saturation the time gain is 266,13 times, while in high saturated zone the gain becomes 672,13 times.

J, A	TurboTCM	OPERA RM	Difference, times
1	12,4sec	0h55min	266,13
10	18,1sec	3h06min	616,57
20	18,3sec	3h25min	672,13

Table 4.3: Calculation time comparison

### Experimental results

Experimental workbench shown on Figure 4.8 allows to obtain the experimental results for different modes. It consists of a generator prototype driven by a variable speed asynchronous motor with inverter which permit to run the machine on speed up to 3000 rpm. The acquisition equipment form the data channel to the computer.

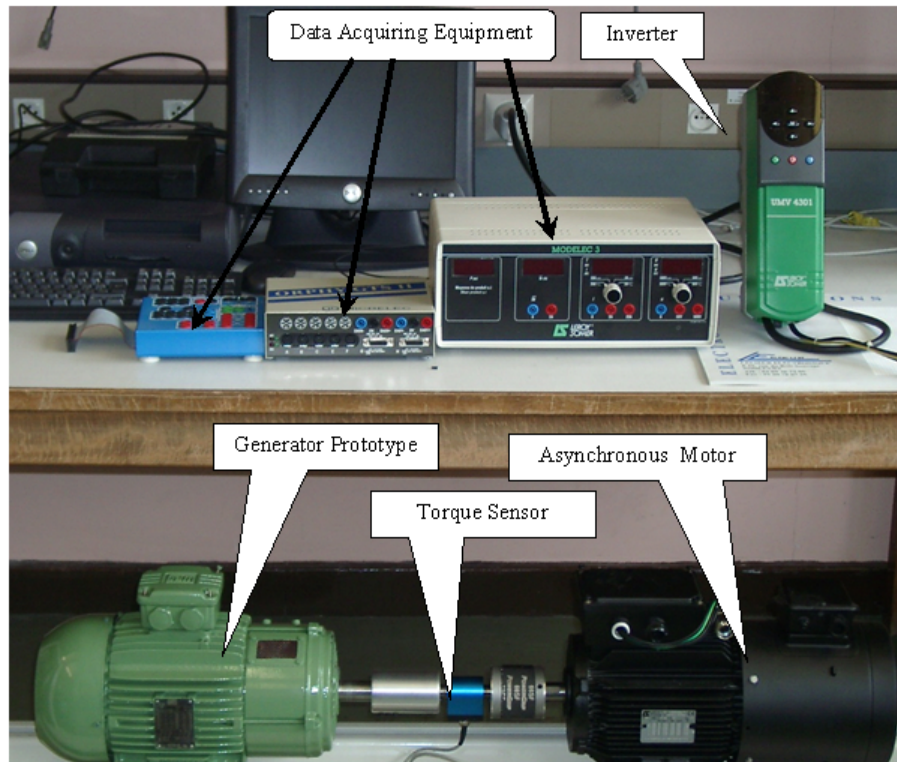


Figure 4.8: Experimental workbench

Two characteristics – noload and regulation – were obtained for the comparison (Figure 4.9). Simulation data show rather good correlation. But the remanent magnetization of the rotor causes additional error, which can be easily seen on a no-load characteristic and also affects the regulation characteristic. Besides, we had no information about the magnetic properties of the rotor and stator material, thus the BH-curves used for simulation were estimated.

Figure 4.10 presents the comparison of the EMF in dynamics. To the left one can see the EMF and its spectrum obtained by simulation while to the right – the experimental results. The amplitude, form and harmonic orders ( $h_3$ ,  $h_{21}$  and  $h_{23}$ ) are almost the same. Harmonics  $h_{21}$  and  $h_{23}$  are caused by tooth effects, since rotor slots are opened.

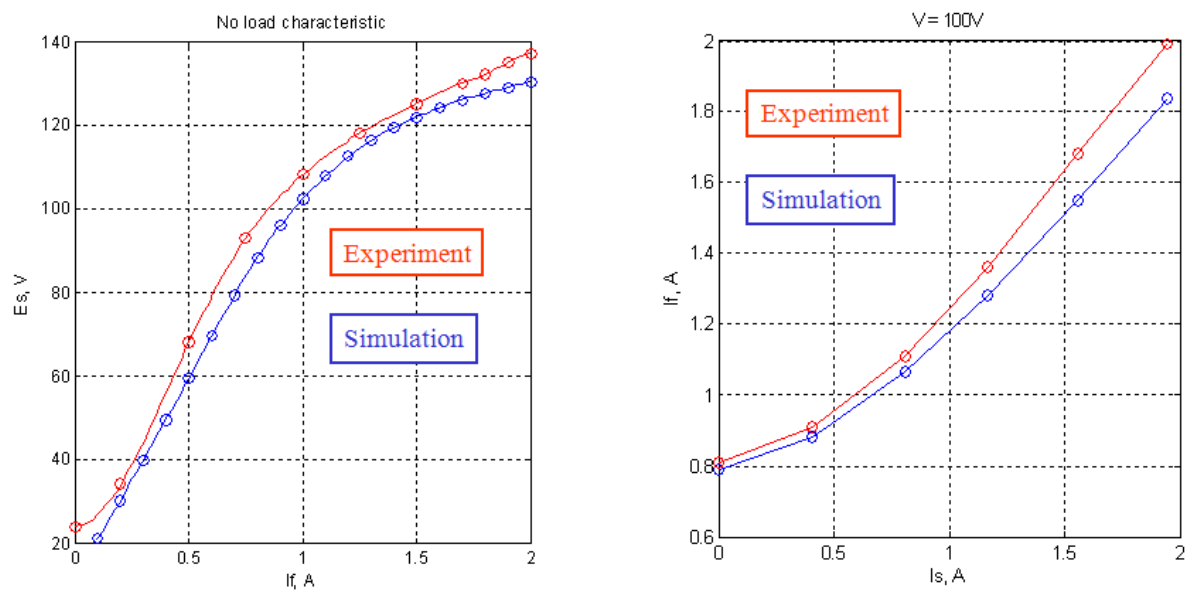


Figure 4.9: Static characteristics: comparison with experiment

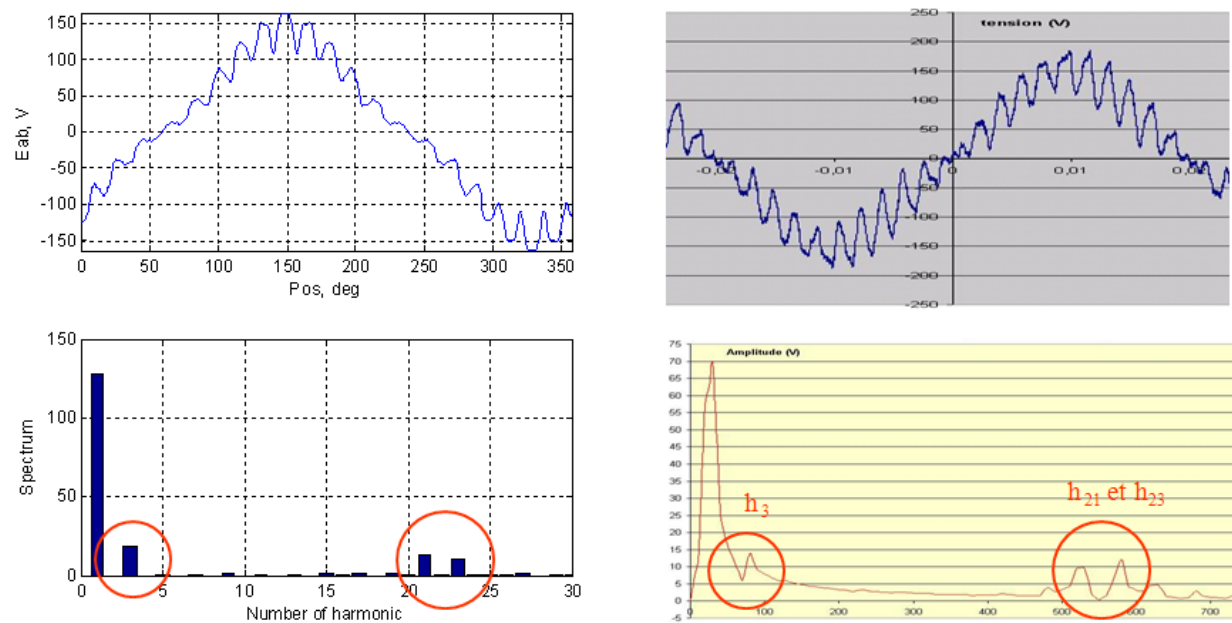


Figure 4.10: Rotation effect: experimental comparison



## 4.2 Two pole turbogenerator

This section presents the results of application of the approach to a two poles turbogenerator of 10-100 MW. Some of these results were presented in [42, 38, 40, 39, 41].

### 4.2.1 Machine description and its permeance network

The turbogenerators are driven by gas turbines having constant synchronous speed of 3000 or 3600 rpm. The range of machines of 10-100 MW have direct air cooling of rotor winding and indirect air cooling of stator.

Rotor has concentric winding stacked in massif magnetic shaft. The end windings are maintained by non-magnetic bands. Rotor slots have under-winding ducts and perforated conductors, thus having air flow from the cooling duct directed to the air-gap. Stator has three phase bar winding (two bars per slot) connected in the manner to realize necessary circuit and to obtain rated output voltage with ideally magnetized magnetic circuit and minimized voltage harmonics.

The end windings and coupling circuits are firmly supported and wedged to avoid the vibrations that damage the isolation. Copper magnetic shield protects the magnetic system of the induced currents caused by the magnetic field of end windings.

The PN of the turbogenerator is built using the principles explained in Chapter 2.

### 4.2.2 Calculation results

In order to validate the model, the obtained results were compared with experimental data in no load case and short circuit case<sup>1</sup>. Since the experimental result under load were not provided, the rated mode was compared with other calculations by Potier method and by means of native Jeumont software TurboB. TurboB, TurboB2 and TurboB4 are the software packages realized in Fortran and devoted to the calculation of 2-poles, 4-poles and n-poles turbogenerators. They implement analytical approach of turbogenerator's characteristics calculation and are in industrial use in Jeumont.

In order to study several turbogenerators Jeumont proposed an internship to the student of ENSEM<sup>2</sup> Ryth LY. The cases included the machines complying the range of 10-100 MW were studied.

The parameters of studied machines are shown in the following table:

#### No-load case

No-load characteristic of a machine present stator voltage regarding excitation current without any load.

Comparison data of no-load characteristics of the machines are presented in Appendix B in tables B.1-B.2, where:  $I_f$  – excitation current, A;  $E_{exp}$  – measured EMF, V;  $E_{tcm}$  – calculated EMF, V;  $Error$  – relative error, per cent. Graphical representation of the characteristics is given on figures B.1-B.8.

---

<sup>1</sup>Here and further all the measurements and machine parameters were provided by Jeumont Industry Framatome ANP.

<sup>2</sup>Ecole Nationale Supérieure d'Electricité et de Mécanique Nancy.



Name	Full power	Stator voltage	Frequency	Power factor
Machine 1	63.000 MVA	11500 V	50 Hz	0.80
Machine 2	33.625 MVA	11000 V	50 Hz	0.80
Machine 3	50.900 MVA	11000 V	50 Hz	0.80
Machine 4	34.375 MVA	13800 V	50 Hz	0.80
Machine 5	51.375 MVA	11500 V	50 Hz	0.80
Machine 6	66.667 MVA	11000 V	50 Hz	0.90
Machine 7	41.688 MVA	11000 V	50 Hz	0.80
Machine 8	31.529 MVA	13800 V	60 Hz	0.80

Table 4.4: Studied machines' parameters.

First points of all characteristics show big difference (the error is up to 92 percent) between calculation and experimental results, caused by remanent magnetization of the rotor which was not taken into account. In some cases (machines 1 and 3) the magnetization level is so high that leads to completely absent correlation between measured and calculated data. In fact, the direction of the remanent magnetization is always unknown, thus unpredictably affecting the whole characteristic.

Another difference can be found in the saturated part of the no-load curve (for example, Figure B.7). That difference occurs because of the insufficient data points of the BH-curve of stator and rotor steels: only 3-5 points of the curves were provided.

Mean absolute values of the errors are shown for each machine in the following table. Cases 1 and 3 have the biggest errors in the set (highlighted in bold).

Machine:	<b>1</b>	2	<b>3</b>	4	5	6	7	8
Error:	<b>7,11%</b>	2,41%	<b>16,46%</b>	1,03%	1,35%	1,67%	3,45%	2,47%

### Short-circuit case

Short circuit characteristic of a machine is obtained by measuring stator current while applying different excitation currents and stator voltage equal to zero (short circuit). In this case the field of the machine is orientated in q-direction.

Comparison data of short circuit characteristics of the machines are presented in Appendix B in tables B.3-B.4, where:  $I_s$  – stator current, A;  $I_{fexp}$  – measured excitation current, A;  $I_{ftcm}$  – calculated excitation current, A; *Error* – relative error, per cent. Graphical representation of the characteristics is given on figures B.9-B.16.

In short circuit mode the machine's magnetic system stays mostly linear, thus the calculation error is diminished. The comparison of the mean values of the errors is shown in the following table<sup>3</sup>:

Machine:	1	2	3	4	5	6	7	8
Error:	1,96%	0,38%	6,72%	2,71%	1,08%	1,21%	0,84%	0,37%

### Rated mode comparison

Since we had not been provided with experimental data for any mode in charge, the calculation results obtained in TurboTCM were compared with that of TurboB and that obtained

<sup>3</sup>The value of the error for the machine 8 is obtained without taking into account the first point since excitation current less than 1 A cannot be measured. See tables B.3-B.4 for details.

by Potier method. The table 4.5 shows the comparison for the rated mode, where:  $V_s$  – stator phase voltage,  $I_s$  – stator phase current,  $\cos\varphi$  – power factor,  $N$  – rotation speed.

The results show rather big errors between TurboB and TurboTCM. From the other hand, the error between Potier calculation and TurboTCM is small. The effect might be caused by a difference of the calculation methods of TurboB and TurboTCM, in particular, the method of taking into account nonlinear BH-curve of the machine.

In addition, it's possible to determine electromagnetic torque calculated by TurboTCM:

$$T_{TCM} = \frac{1}{2} \cdot \sum U^T \cdot \frac{\partial \Lambda}{\partial \theta} \cdot U \quad (4.1)$$

where:  $U$  – magnetic potential differences,  $\Lambda$  – permeances,  $\theta$  – rotor angle.

It's possible to compare the result with the classical relation for the rated point neglecting losses:

$$T_{EM} = \frac{S \cdot PF}{\Omega} \quad (4.2)$$

where:  $S$  – full power, VA,  $PF$  – power factor,  $\Omega$  – angular rotation speed, rad/sec.

The calculation error for rated mode is negligible:

$$T_{TCM} = 1.006 \cdot T_{EM} \quad (4.3)$$

### Working mode characteristics

TurboTCM allows to calculate a big variety of static characteristics of turbogenerators. Here some calculation results are presented without their validation.

**Regulation characteristic** is calculated for a constant stator voltage and load type varying stator current. Figure 4.11 shows three characteristics for different load types – capacitive, active and inductive – and rated voltage. Here:  $I_f$  – excitation current,  $I_s$  – stator current.

**V-shaped characteristic** is calculated for a constant active power and stator voltage, varying stator current. A set of V-shaped characteristics for machine 1 for different values of active power is shown on Figure 4.12, where:  $I_f$  – excitation current, p.u.,  $I_s$  – stator current, p.u.,  $P$  – active power, p.u. The calculation time of that whole set of characteristics is *less than 12 minutes* on a computer Pentium IV, 1300 MHz, 784 MB RAM.

**Additional results** can be obtained for any point of any characteristics. It was interesting to illustrate the variance of  $x_d$  and  $x_q$  parameters of the turbogenerator. These values were calculated by the method described in Section 2.5.2. The regulation characteristic of machine 1 for inductive load with power factor 0,8 and corresponding variation of  $x_d$  and  $x_q$  are shown on Figure 4.13. The resulting dependence of these parameters on the operating mode of the machine illustrates that real geometry of the turbogenerator was taken into account.

Machine	$V_s, V$	$I_s, A$	$\cos \varphi$	$N, \text{rpm}$	Excitation current, A		Error	
					TurboB	TurboTCM	TurboB	Potier
Machine 1	6639,50	3162,90	0,8	3000	729	651,80	<b>-10,59%</b>	
Machine 2	6350,90	1764,90	0,8	3000	756	736,10	-2,63%	
Machine 3	7967,40	1438,10	0,8	3600	505	451,51	<b>-10,59%</b>	
Machine 4	6350,90	2671,60	0,8	3000	720	703,12	-2,34%	-1,82%
Machine 5	6639,50	2579,20	0,8	3000	662	595,73	<b>-10,01%</b>	-1,88%
Machine 6	6350,90	3499,10	0,9	3000	696	630,46	-9,42%	
Machine 7	6350,90	2188,10	0,8	3000	599	520,46	<b>-13,11%</b>	
Machine 8	7967,40	1319,10	0,9	3600	591	548,61	-7,17%	-0,56%

Table 4.5: Rated mode calculation comparison.

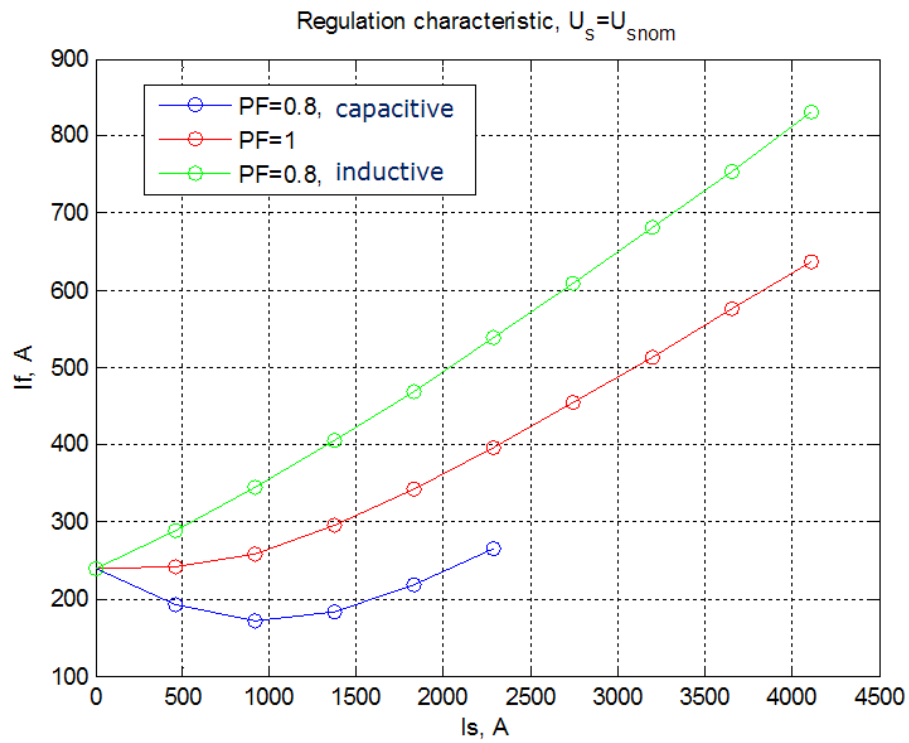


Figure 4.11: Regulation characteristic of machine 1.

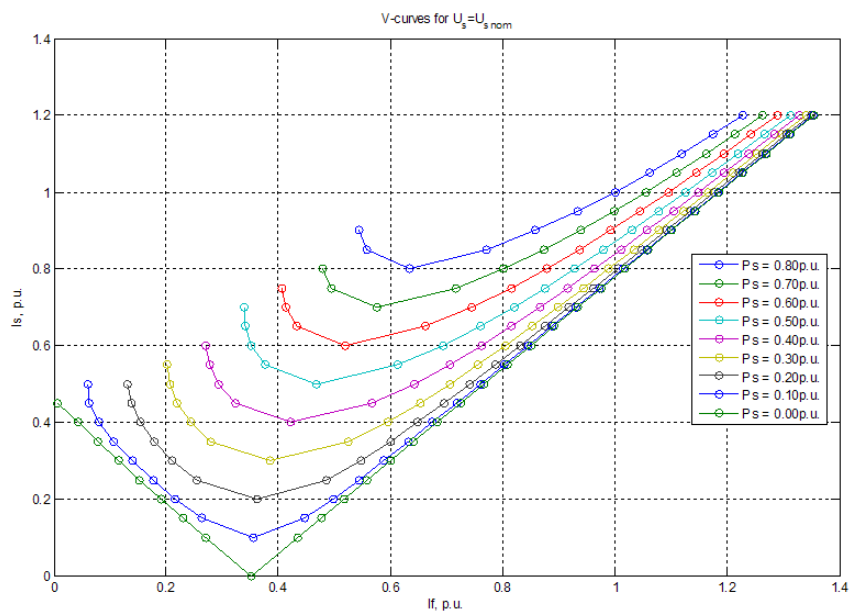


Figure 4.12: V-shaped characteristic of machine 1.

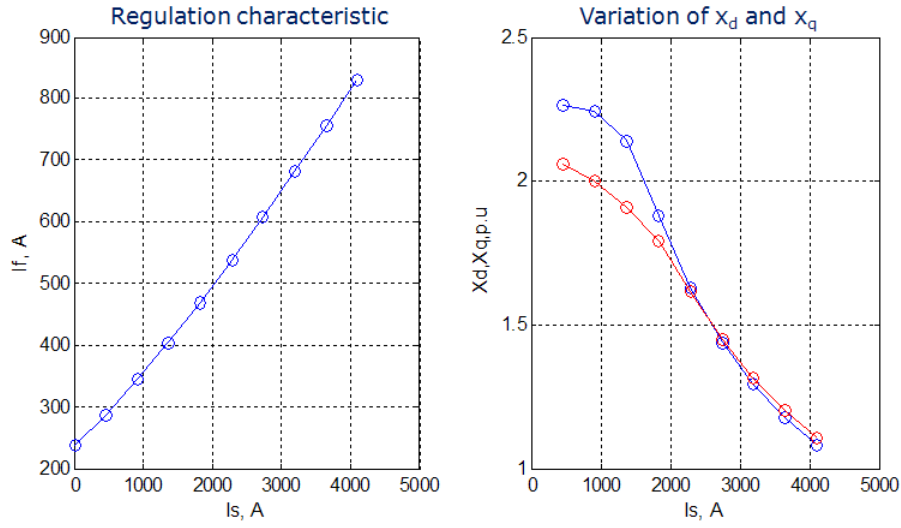


Figure 4.13: Regulation characteristic of machine 1 and variation of its  $x_d$  and  $x_q$  parameters.

**Flux density distribution** in the air-gap sometimes can be very useful for an engineer, for example, in surface loss calculations. Although TurboTCM does not use that distribution and its calculation is based only on winding flux linkages, it implements that option. The following figures show flux density distribution in the middle of the air-gap for three different cases: no-load (Figure 4.14), rated mode (Figure 4.15) and short-circuit mode (Figure 4.16). The flux distribution is shown on the left side of each figure along with its spectrum under. The pictures to the right show the distribution of the ampere-turns in the elements of the PN of the machine corresponding to each case. In all cases on the spectrum one can see the influence of stator and rotor tooth harmonics (39 and 41). Rather symmetric picture in no-load mode is changed in rated mode, thus reflecting the armature reaction, which is even bigger in short-circuit mode.

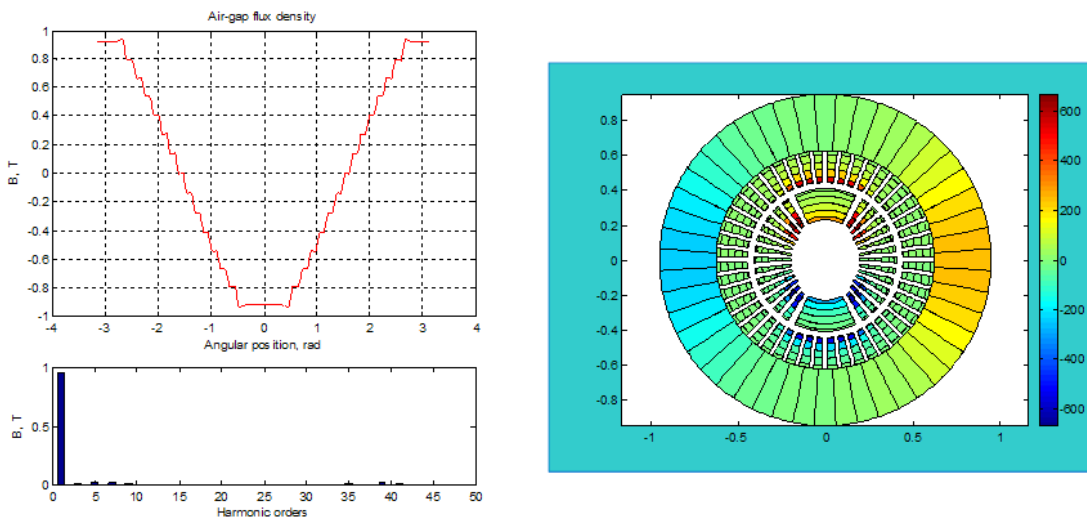


Figure 4.14: No-load air-gap flux density distribution.

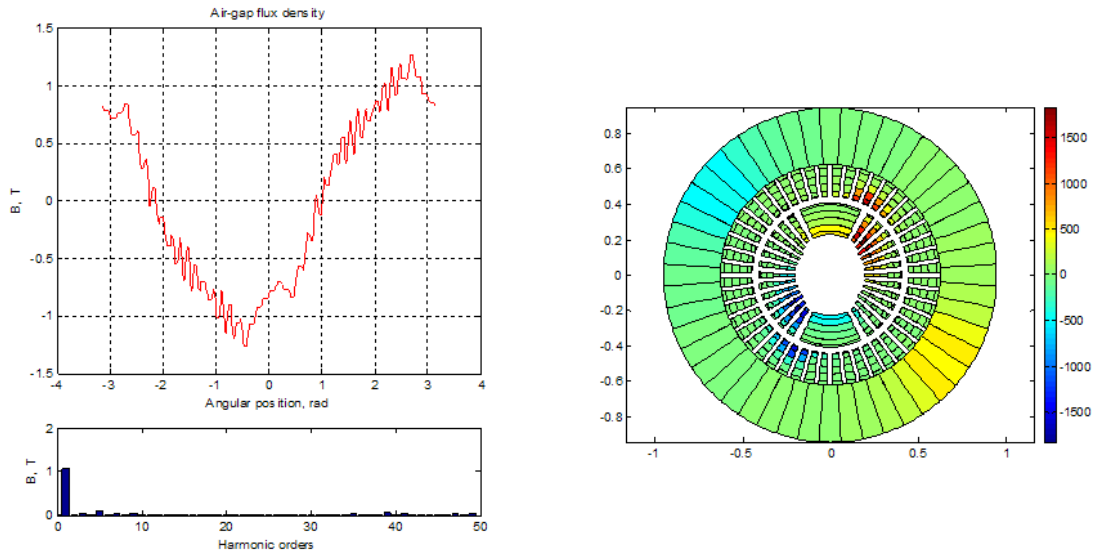


Figure 4.15: Rated mode air-gap flux density distribution.

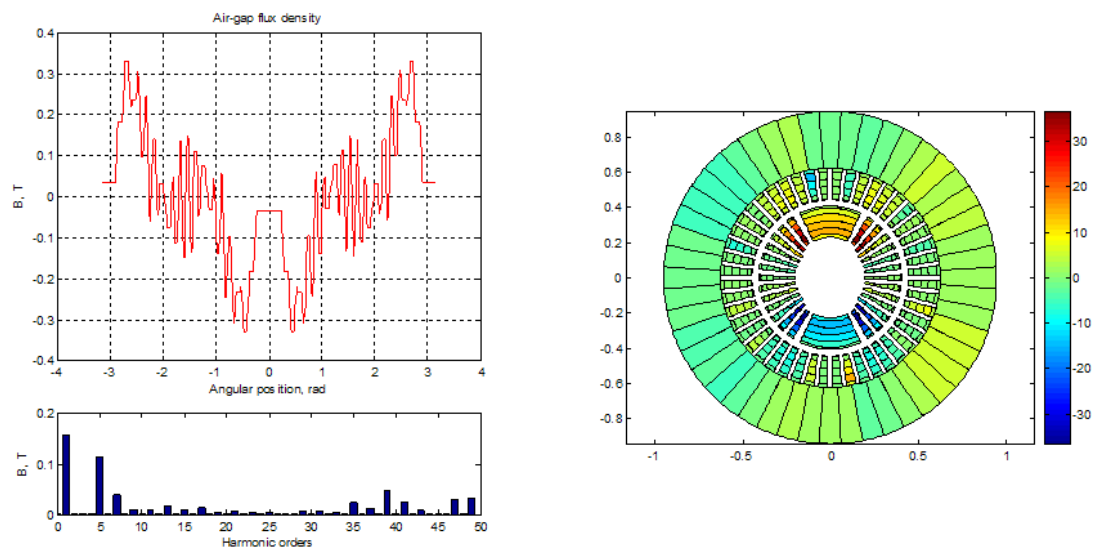


Figure 4.16: Short-circuit mode air-gap flux density distribution.

### 4.3 Multi-pole turbogenerator

This section presents the application of TurboTCM to the 4-pole machine of the same power range 10-100 MW. The construction of the PN of multi-pole generator was discussed Section 2.2.3.

One of the advantages of TurboTCM is the possibility of incorporating different geometries of the machines and their parts. Adaptive PN allows to take into account almost any slot types, rotor forms without additional programming or with small add-on code in Matlab, depending on the complexity of the problem.

Here the PN of a specific 4-pole case is shown and some calculation results are presented.

#### 4.3.1 Jeumont 4-pole turbogenerator

Although the PN of the 4-pole turbogenerator doesn't differ too much from that of n-pole generator, there are some particularities in its rotor, which are specific only for 4-pole configuration. The machine which parameters were provided by Jeumont Industry has laminated core with a hole in the center, where it is attached to the solid shaft with arms (see Figure 4.17). That hole is used for rotor ventilation in radial direction. The arms and shaft can not be neglected since in 4-pole configuration the flux also passes by them.

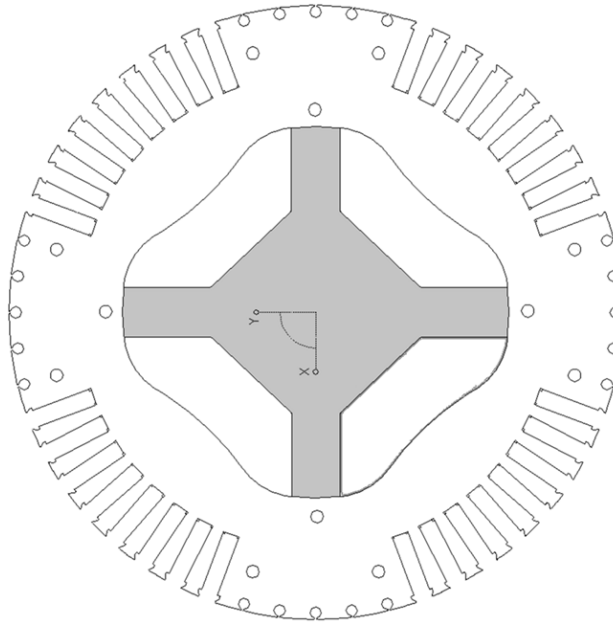


Figure 4.17: Rotor of the 4-pole turbogenerator.

The method of taking into account that special rotor configuration was realized by David Bonnet<sup>4</sup>, whose internship was devoted to the implementation of 4-pole machine as a module of TurboTCM.

Figure 4.18 shows the definition of the rotor zones. The minimal and maximal diameters define the limits of the new yoke zone. Additional BH-curve is given for the arm and

---

<sup>4</sup>David BONNET was a student from Ecole Nationale Supérieure d'Ingenieurs de Limoges, who passed his internship in Jeumont Industry and Ecole Centrale de Lille in 2005.

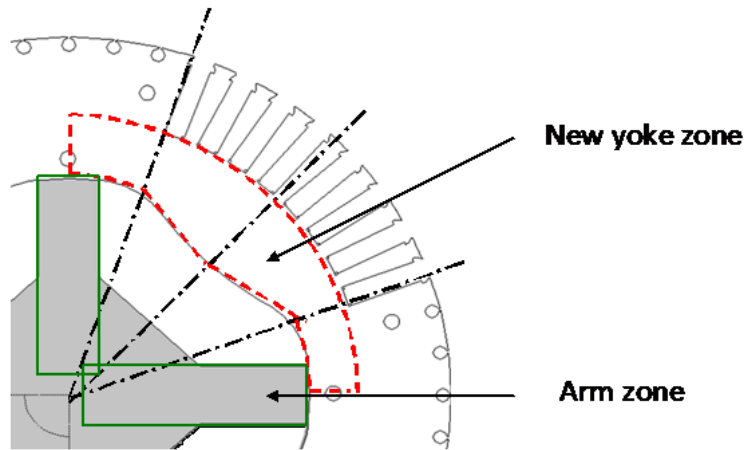


Figure 4.18: Taking into account rotor arms

shaft zones. The yoke zone in its turn is connected with tooth zone of the rotor which was not changed regarding the method described in Chapter 2. The distribution of the elements in the yoke, arm and shaft zones is illustrated on Figure 4.19. Red horizontal permeances implement the network of the yoke part between the poles (MMF sources are not shown here since they are placed regularly). Blue vertical permeances implement the arms. The common MMF source which combines all the currents of the above slots is placed between adjacent arms.

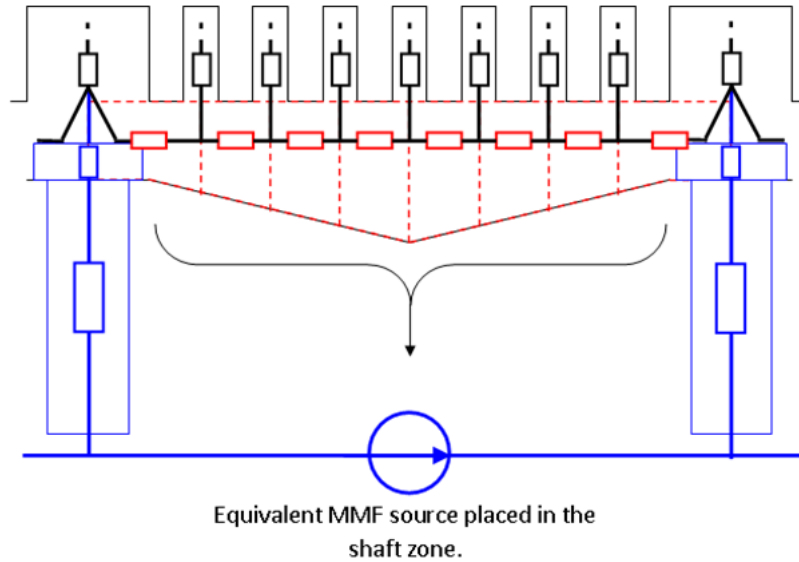


Figure 4.19: 4-pole rotor permeance network.

Figure 4.20 presents some no-load calculation results for the machine of full power  $S = 66667kVA$ , stator voltage  $U = 11kV$ , power factor  $\cos \varphi = 0.9$  and rotation speed  $3000rpm$ . The comparison was performed between linear and nonlinear calculations and experiment. The BH-characteristics of the arms and rotor were unknown and estimated, thus giving rather big error in non-linear case.



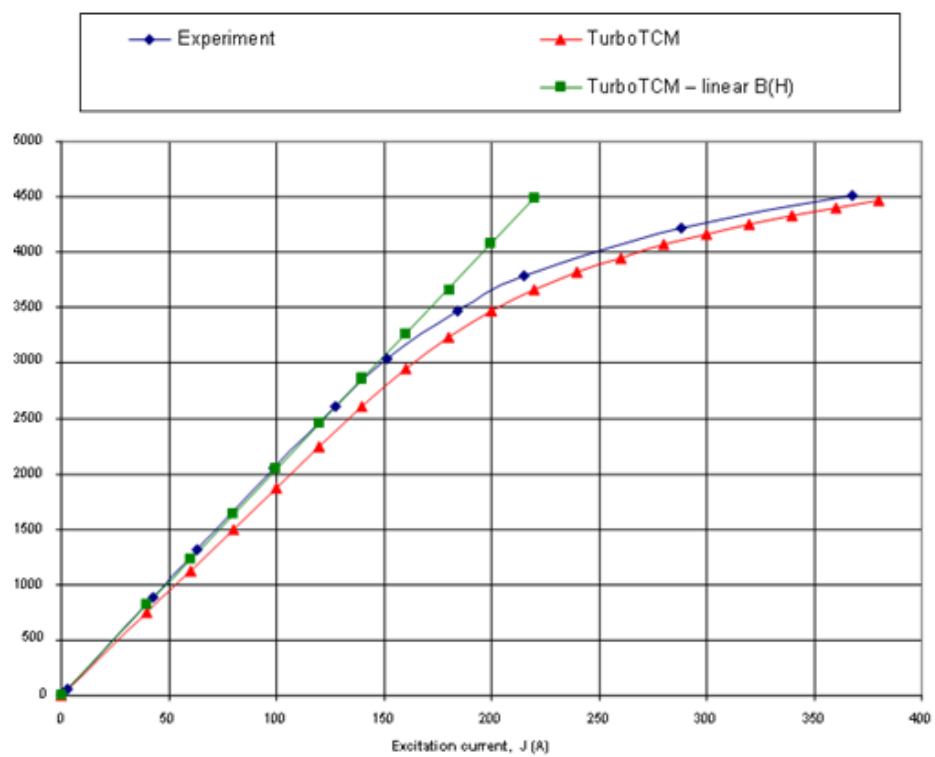


Figure 4.20: No-load characteristic comparison for 4-pole machine.

## 4.4 Optimization application example

In order to study the variation of different operating values (like EMF harmonics, torque, etc) depending on machine's geometrical parameters (like machine's length, tooth and yoke dimensions, pole dimensions and etc) **TurboTCM** was coupled with **Sophemis**. The last tool was designed in Ecole Centrale de Lille, L2EP by Stephan Vivier (see, for example, [57]) and implements experimental design approach.

The term “Experimental Design” is a methodology that is used for behavioral characterization of a system. It is based on modification and measurement of proper variables of a considered object, which comprises studied values along with their variation sources. Thus his method allows to determine the relationship between two types of variables: *the response* – studied physical values, and *the factors* – physical values that are defined by experimenter and influence the responses. To be more precise, it shows the links between responses and factors along with those between responses and factor interactions. This permits to build a model expressing the response in function of the factors.

First we present the objective of the study followed by some results. Other results can be found in [43].

### 4.4.1 Objective

Our objective was to demonstrate the use of **TurboTCM** together with an optimization supervisor, thus rather simple variables were chosen:

- $h_{s1}$  – stator tooth height;
- $b_{s1}$  – stator tooth width;
- $D_{i1}$  – stator boring diameter (affects air-gap value);
- $T_{p1}$  – rotor pole width.

Their variation limits are presented in the following table:

Factors	Lower bound	Upper bound
$h_{s1}$	$h_{s1} - 10\%$	$h_{s1} + 10\%$
$b_{s1}$	$b_{s1} - 10\%$	$b_{s1} + 10\%$
$D_{i1}$	$D_{i1} - 5\%$	$D_{i1} + 5\%$
$T_{p1}$	$T_{p1} - 10\%$	$T_{p1} + 10\%$

The chosen responses are:

- $K_{hB3}$  – 3rd order harmonic of the air-gap flux density in no-load;
- $K_{hE3}$  – 3rd order harmonic of the stator EMF in no-load;
- $K_{hE1}$  – the fundamental of the no-load stator EMF;
- $I_f$  – excitation rotor current in no-load.

The chosen factor set is a complete set of 3 levels with 4 factors which leads to 81 experiments.

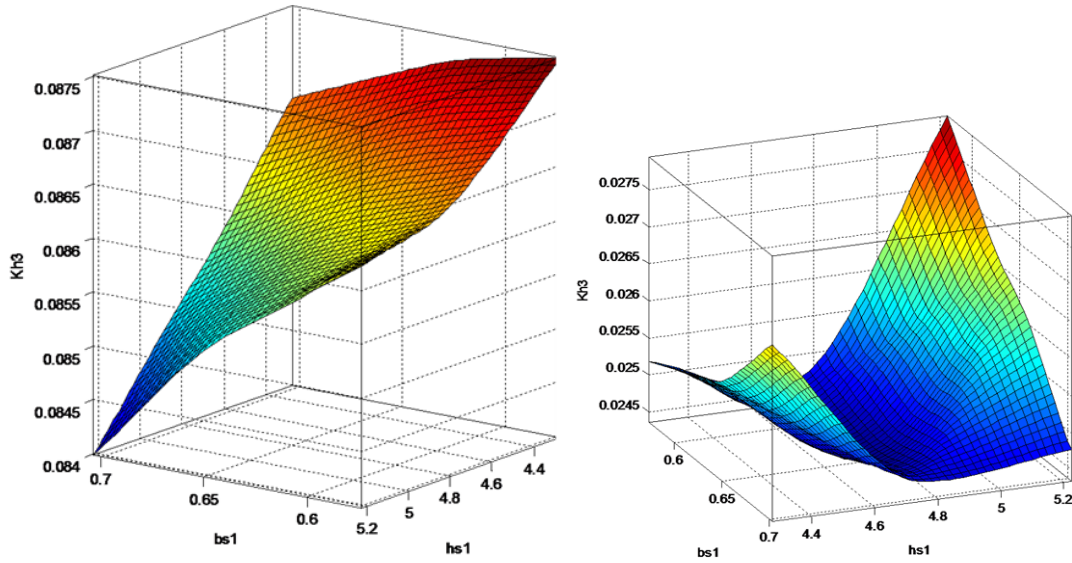


Figure 4.21:  $K_{hB3}$  for  $T_{p1}$  min (left) and  $K_{hB3}$  for  $T_{p1}$  max (right)

#### 4.4.2 Calculation results

Results are obtained for a fixed diameter  $D_i = 1.05D_{i1}$  and, thus, maximal value of the air-gap. Therefore, one can see that if the pole width increases, the 3rd harmonic of air-gap flux density decreases. The right picture on the Figure 4.21 shows very interesting result of the *minimum* of the 3rd harmonic.

The following results present the analysis of the 3rd and 1st harmonics of stator EMF. Figure 4.22 shows the influence of the stator tooth height and width on these values. Lower surfaces on that figure correspond to smaller  $T_{p1}$ .

It took 25 minutes to perform 81 simulations on Pentium IV, 1.9GHz and that time includes also the network regeneration time, since the parameters of its elements change depending on the variable values.

The calculation of excitation current  $I_f$  was performed for the same 4 parameters with only two extreme values of the diameter and the results are shown on Figure 4.23. The lowest surface corresponds to the minimal value of the pole width. The results are rather obvious: excitation current depends on the value of the air-gap, the pole width is in inverse proportion with that current. The value of  $I_f$  increases with increase of the stator tooth height since (stator yoke decreases in that case).

### 4.5 Conclusion

The aim of this chapter was to validate the approach and the software and to present some additional possible application.

On the very first stage of the thesis we implemented a model of a small generator, which had a particular rotor with slot distribution specific for turbogenerators. The results were validated by experiment and compared with the calculation by FEM. The comparison

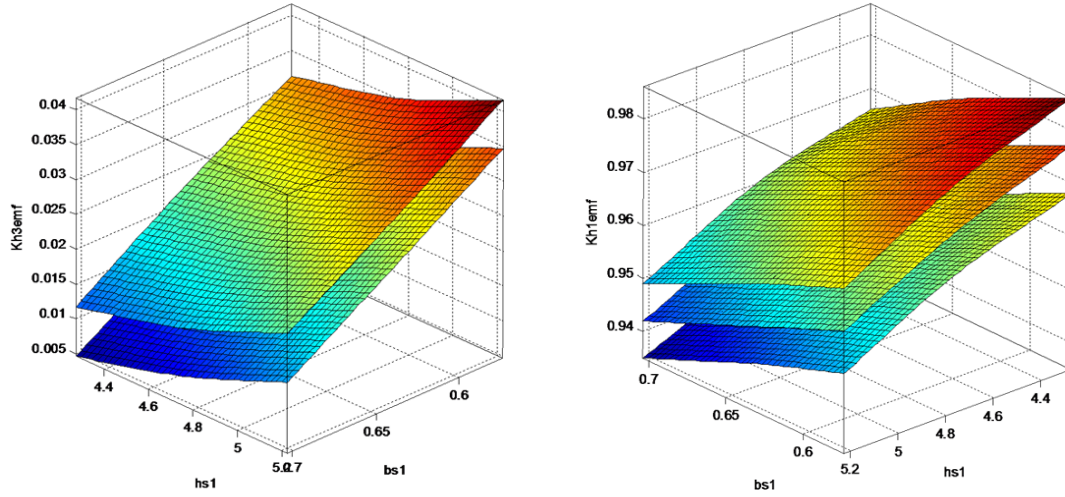


Figure 4.22:  $K_{hE3}$  (left) and  $K_{hE1}$  (right) for different  $T_{p1}$ .

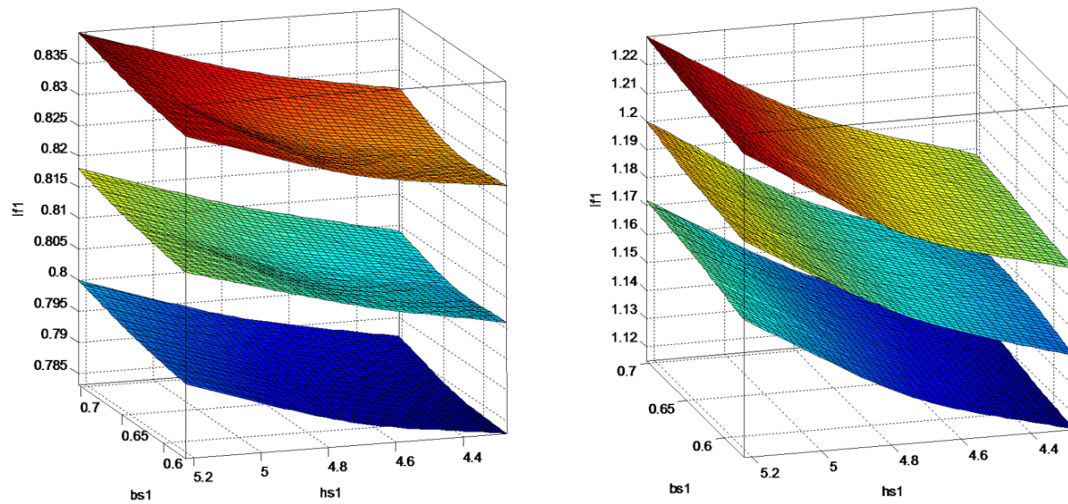


Figure 4.23:  $I_f$  for  $D_{i1}$  min (left) and  $D_{i1}$  max for different  $T_{p1}$ .

gave an acceptable results while the gain in calculation time regarding FEM-calculation was of order of 600 times. We obtained all the expected effects in the simulation like tooth harmonics of EMF, saturation, etc. From the other hand, we found out that the method is very sensitive to the material characteristics, thus the last must be obtained and measured carefully.

The software was then developed to implement a 2-pole turbogenerator model taking into account all its parameters including axial heterogeneity effects. The calculation results were compared with experimental data for eight different machines in no-load, short-circuit cases and rated operating mode. In some cases the provided test results were obtained on machines with remanent rotor magnetization, which affected the experimental data leading to significantly bigger errors while comparing them with simulation. Also we presented the results of calculation of different machine's characteristics. Although nowadays regular methods use linear dependency for  $x_d$  and  $x_q$ , our calculations show their variation in different operating modes.

An application of the approach and the software to 4-pole turbogenerator demanded additional changes to the PN. The shaft and support arms were taken into account along with variable section of the rotor yoke. It highlights the modifiability of **TurboTCM**, the easiness of reflecting different geometries of a machine using adaptive PN. Some comparison results were given.

Finally, we introduced the coupling of **TurboTCM** with optimization supervisor **Sophemis**, implementing experimental design method. That coupling allows to determine influencing factors, that can help to limit the number of variables for turbogenerator computer aided design. Using the response surface permits to determine an equivalent model, which can be used in optimization. The results and calculation time open good perspectives for further use of the model coupled with optimization software.

# Conclusion and perspectives

In this work we proposed a rapid, flexible optimization-oriented approach and realized a tool to calculate the operating modes and characteristics of turbogenerators 10-100 MW using the concepts of “virtual prototyping”. That approach is based on a theoretically validated tooth contour method. The method was developed in order to implement the complex geometrical structure of modern turbogenerators, take into account their particularities, generalize and automatize the approach of PN generation. The software **TurboTCM** was realized, which gives flexible possibilities to turbogenerator characteristics calculation and can be coupled to an optimization supervisor or other calculation tool in Matlab.

In the first chapter we presented the overview of the problem of electromagnetic machines’ analysis, existing methods that solve different aspects of the problem: from basic conventional approaches to modern numeric solutions. Since our method is based on permeance networks, we paid more attention on highlighting the existing solutions in that field.

The second chapter describes general approach in details. The theoretical basis and the way of permeance network construction, calculation of its parameters were shown without links to any particular type of the machines. However, we couldn’t completely abstract away from the particularities of turbogenerators, the complexity of their structure, thus giving variable topology model of the rotor and some calculation algorithms in respect to them.

The main idea of the approach is to *exploit the particularities of a machine to minimize the number of the network elements*. The formed calculation method represents a development of the combined approach to electrical machine analysis existing from the dawn of electromechanics. On the first stage we divide the volume of the machine onto zones with independent magnetic fields and well-expressed boundaries. Then we form a non-planar discrete scheme of the magnetic system. On a coupling stage we introduce the MMF sources representing slot currents into the scheme. And on final stage we perform iterative calculation of the flux linkages.

The precision of air-gap permeances calculation dictates the precision of the whole model. The approach doesn’t insist on the way of that calculation: it can be either finite element or analytical or any other method. We introduced the analytical approximative approach giving the possibility to calculate air-gap permeance characteristics rapidly and with high precision.

We showed that special techniques must be implemented to properly reflect axial heterogeneity of magnetic cores while using a model “in-plane”. Although general way of taking it into account is rather simple, one should remember that different parts of the machine are differently influenced by that heterogeneity. We showed five characteristic zones of a machine and described the implementation of the approach on the level of permeance network parameters. However, the proposed method is rather general and *can be easily used*

with other methods of machine's characteristic calculations, even FEM (in plane).

The use of adaptive PN construction helps to take into account complicated geometries of magnetic cores, irregular slot structure and distribution. The implementation of the algorithm allows to pass to other slot geometries and even rotor or stator geometries with minimal software modification using "add-on" principle.

Fixed rotor algorithm described in Section 2.5 offers rapid steady-state calculations, as a compromise between precision and calculation time. Anyway, for thorough harmonic analysis rotor rotation is easily implemented.

Chapter 3 presents the implementation of the software **TurboTCM**, created in Matlab. The separation of the software on two levels – mathematic core and graphical user interface – leads to the advantage of using the core in a couple with any other software, like optimization supervisors, leaving the function of project creation and results management to the user interface. Besides, the core itself gives very flexible control of the whole model and its behavior. The separation of the objects which are the circuit containers and couplers facilitates the future coupling with other possible models.

In the beginning the software was tested on a small 3 kW synchronous generator, which was specially constructed to give the possibility of model tuning. The results were compared with finite element analysis and experimental data and showed good correlation.

Then a two-pole turbogenerator model was realized and tested on several different machines of the selected power range. The no-load, short-circuit characteristics and some modes under load were compared with experimental results and gave relatively small errors in most cases. The cases of great errors are explained by high remanent magnetization of the rotors of these machines which can be easily seen in the beginning of their no-load curves. Besides, we realized the model of a four-pole turbogenerator with a particular construction of the rotor, which demanded additional permeance network modification.

Finally, we realized the coupling of **TurboTCM** with the optimization supervisor and performed some tests on simple variables. The simplicity of model creation and coupling with other tools proved the effectiveness of the approach and the modularity of the software in the tasks of optimization, demonstrating high speed of response surface determination.

The developed approach and designed software give the possibilities to further development and extension of the model by multi-physical phenomena. The architecture of the tool is open for its future extension by vibrational, acoustic and especially thermal models.

The following points show our perspectives in the nearest future:

- Expand the application of the approach and designed software to other types of machines. The implementation of **TurboTCM** already allows to take into consideration cores of *any* geometry.
- Concerning asynchronous machines: interesting results can be achieved by coupling the magnetic permeance network with thermal equivalent circuits and their joint calculation. This work is already an object of a CDD (Contrat de Durée Déterminé) "Futurelec3 – operation 1-bis" which started in October 2006. Normally, multiphysical models are based on linear magnetic models which take into account only the permeances of air-gap. It seems to be more realistic to replace them by a PN model of an asynchronous motor, which allows to avoid many restrictions.
- Improve the calculation of slot leakage permeances and air-gap permeances. There are many methods of air-gap permeance determination exist. They must be compared

together within unique calculation tool. This is rather big domain of work since the tool must be rebuilt generic.

Taking into account the rotation allows to extend the model to perform in future transient analysis of the turbogenerators taking into account the Foucault currents in massive parts of the machines.





# Appendix A

## Matlab Solver functions

This chapter presents a list of main functions of TurboTCM and their brief descriptions.

### A.1 General functions

General functions concern first of all TurboTCM project management. An empty project can be created by `TCMProject_Create` function. If the project was generated by GUI and saved in the file, then `TCMProject_Load` function can be used to load the project.

In order to use the saved project and calculate the model, `ModelData` must be generated first. And it must be regenerated each time the input parameters are changed. The following example shows how to use it:

```
Prj = TCMProject_Load('..\2p - TURBO.tcmprj'); % load a project
P = Prj.Parameters; % Extract the parameters to the variable P
MD = GenerateModelData(P); % Generate model data

%--- Calculate nominal point
[MD, If, Teta, exitflag, Esc, Usc, Isc, Psi] = ...
    MD_Calc_UsIsPF(MD, Usnom, Isnom, N.PF, Rs, Xse, N.Speed, 'Teta', pi);
%--- Obtain a TORQUE
M = MD_GetTorque(MD);
%--- Change any parameter you want
P.Stator..... = ....
%--- Regenerate model data
MD = GenerateModelData(P);
%--- Obtain another TORQUE
M = MD_GetTorque(MD);
%--- Etc.....
```

## A.2 Calculation functions

### A.2.1 Mode calculation functions

The following functions perform mode calculation based on fixed-rotor model described in Section 2.5.

**MD\_CalcEMF** – calculates the no-load mode defined by excitation current, stator current, its angle and speed.

**MD\_Calc\_IfIsPF** – calculates the mode defined by excitation current, stator current and power factor. The values of the stator voltage and load angle are returned.

**MD\_Calc\_UsIsPF** – calculates the mode defined by stator voltage, current and power factor. The values of the excitation current and load angle are returned.

**MD\_CalcFluxLinkageFixedRotor** – calculates phase and complex flux linkages for the specified excitation current, stator current and its angle. (This function is used in **MD\_CalcEMF**).

### A.2.2 Characteristic calculation functions

These functions return the characteristic in the form of **TRMD – TCMResultsMagneticData** structure. It contains one or several calculation points of the magnetic system and has the following fields:

- Basic fields:

**Title** – a title of the characteristic or mode point;

**Type** – the type of the characteristic, which may be one of the following: 'point', 'noload', 'load', 'regulation', 'vshaped', 'angular';

**bPerUnit** – shows if input data and results are perunit; can be either true or false (default);

**nCharCount** – number of sequently calculated characteristics. Normally, it's 1 but can be more for a set of characteristics with different constants;

- Mode determining values:

**If** – excitation current, A;

**Isc** – complex value of stator current, A(rms) d-q;

**Usc** – complex value of stator phase voltage, V(rms) d-q;

**Esc** – complex value of stator phase EMF, V(rms) d-q;

- Magnetic circuit fluxes and potentials:

**Um** – magnetic branches' voltages, A;

**Im** – magnetic branches' fluxes, Wb;

**Vm** – magnetic nodes' potentials, A;

- Calculation results:

**Fdelta** – airgap flux on a pole pitch, Wb;  
**Fpole** – flux of the pole coming from airgap, Wb;  
**Bdelta** – airgap flux density on a pole pitch, T;  
**Bys** – stator yoke flux density, T;  
**Bzs(:)** – flux density of a stator tooth (array), T;  
**Bpole(:)** – flux density of a pole (array), T;  
**Byr(:)** – flux density in a pole yoke (array), T;  
**Uagp** – airgap ampere-turns, A;  
**Uys** – stator yoke ampere-turns, A;  
**Uzs** – stator teeth ampere-turns, A;  
**Upole** – rotor pole ampere-turns, A;  
**Uyr** – rotor yoke ampere-turns, A;  
**MMFex** – MMF of the excitation winding, A;  
**Te** – electromagnetic torque, N\*m;  
**Xd** – synchronous reactance in d-axis, Ohm;  
**Xq** – synchronous reactance in q-axis, Ohm.

**MD\_CalcLoadChar** - calculates the characteristic  $V_s(I_s)$  for the specified speed and excitation current.

**MD\_CalcRegChar** - calculates the characteristic  $I_f(I_s)$  for the specified speed and stator voltage.

**MD\_CalcVChar** - calculates the V-shaped characteristic -  $I_s(I_f)$  - for underexcited and overexcited stator currents specified, active power specified and the voltage specified.

## A.3 Low-level calculation functions

These functions can be used to set up and calculate a user-specified functioning mode of the machine.

**MD\_SetStatorCurrents** - sets up the phase currents of the stator for RMS value and the angle.

**MD\_SetRotorCurrents** - sets up the rotor excitation current.

**MD\_SetTheta** - sets up rotor position angle.

## A.4 Post-processing functions

These functions can be used to obtain additional values after calculating one point of the functioning.

**MD\_GetAGFluxDensity** - calculates the distribution of the normal component of a flux density in the air-gap.

`MD_GetPotentials` - calculates stator/rotor teeth potentials.

`MD_GetPotentialsComplexForm` - calculates stator/rotor teeth potentials in a complex form in plane DQ thus allowing to plot them using COMPASS function.

`MD_GetTeethFluxes` - returns the teeth fluxes of stator/rotor in the specified layer.

`MD_GetTorque` - calculates the electromagnetic torque.

# Appendix B

## 2-pole turbogenerator result comparison

This appendix presents the graphical and table representation of the two-pole turbogenerator calculation results. Table B.1-B.2 and Figures B.1-B.8 show no-load cases. Tables B.3-B.4 and Figures B.9-B.16 give short-circuit results and comparison.

Machine 1				Machine 2			
$I_f, A$	$E_{tcm}, V$	$E_{exp}, V$	Error	$I_f, A$	$E_{tcm}, V$	$E_{exp}, V$	Error
1,0	760	60,76	92,00%	37,5	2145	2116,32	1,34%
65,0	3380	3949,18	-16,84%	87,5	4789	4926,31	-2,87%
140,0	7600	8288,01	-9,05%	124,2	6706	6926,52	-3,29%
170,0	9140	9716,43	-6,31%	154,4	8202	8477,21	-3,36%
249,0	11500	11678,85	-1,56%	180,1	9309	9650,87	-3,67%
315,0	12430	12653,01	-1,79%	238,7	11004	11343,77	-3,09%
				298,2	12022	12176,83	-1,29%
				425,3	13258	13322,04	-0,48%
				555,9	13992	14169,80	-1,27%
Machine 3				Machine 4			
$I_f, A$	$E_{tcm}, V$	$E_{exp}, V$	Error	$I_f, A$	$E_{tcm}, V$	$E_{exp}, V$	Error
7,2	1860	569,24	69,40%	1,0	77,5	55,38	28,55%
28,9	3200	2284,87	28,60%	47,4	2746	2624,85	4,41%
36,1	3786	2854,11	24,61%	100,2	5580	5537,07	0,77%
72,3	6160	5714,16	7,24%	140,0	7674	7674,62	-0,01%
108,4	8360	8511,13	-1,81%	163,8	8875	8885,12	-0,11%
144,5	10600	11115,49	-4,86%	185,3	9920	9923,00	-0,03%
180,6	12678	13230,59	-4,36%	212,0	11000	11046,67	-0,42%
224,0	13800	14777,92	-7,09%	244,2	12150	12029,43	0,99%
310,7	15560	16656,80	-7,05%	261,0	12638	12448,56	1,50%
404,6	16600	18193,04	-9,60%				

Table B.1: No-load data comparison: machines 1-4.

Machine 5				Machine 6			
$I_f, A$	$E_{tcm}, V$	$E_{exp}, V$	Error	$I_f, A$	$E_{tcm}, V$	$E_{exp}, V$	Error
1,0	135	62,63	53,61%	1,0	141	58,46	58,54%
36,8	2325	2304,90	0,86%	35,0	2115	2046,11	3,26%
41,5	2595	2599,28	-0,16%	66,5	3900	3887,19	0,33%
59,5	3660	3726,60	-1,82%	99,5	5718	5786,33	-1,19%
83,0	5055	5192,75	-2,72%	132,0	7455	7574,81	-1,61%
114,5	6900	7103,36	-2,95%	157,5	8700	8857,16	-1,81%
130,0	7773	7996,17	-2,87%	180,0	9615	9795,60	-1,88%
185,5	10395	10401,32	-0,06%	230,0	11000	11086,14	-0,78%
225,0	11500	11514,86	-0,13%	296,3	12060	12082,87	-0,19%
275,3	12450	12530,27	-0,64%	394,5	12922	13178,19	-1,98%
358,5	13317	13486,03	-1,27%	490,0	13530	14022,50	-3,64%

Machine 7				Machine 8			
$I_f, A$	$E_{tcm}, V$	$E_{exp}, V$	Error	$I_f, A$	$E_{tcm}, V$	$E_{exp}, V$	Error
1,0	118	61,03	48,28%	1,0	180	69,92	61,16%
49,5	3027	3020,84	0,20%	32,7	2336	2286,41	2,12%
70,3	4233	4288,75	-1,32%	78,3	5340	5470,54	-2,44%
100,6	6000	6096,91	-1,62%	95,5	6454	6653,73	-3,09%
140,7	8183	8329,65	-1,79%	125,1	8370	8644,76	-3,28%
179,5	9750	10102,90	-3,62%	138,9	9364	9549,76	-1,98%
233,0	11000	11493,53	-4,49%	170,9	11114	11452,15	-3,04%
289,0	11745	12312,42	-4,83%	200,2	12460	12893,70	-3,48%
390,0	12614	13403,34	-6,26%	242,0	13800	14170,33	-2,68%
432,7	12906	13804,36	-6,96%	315,3	15250	15383,07	-0,87%
				445,0	16520	16808,55	-1,75%

Table B.2: No-load data comparison: machines 5-8.



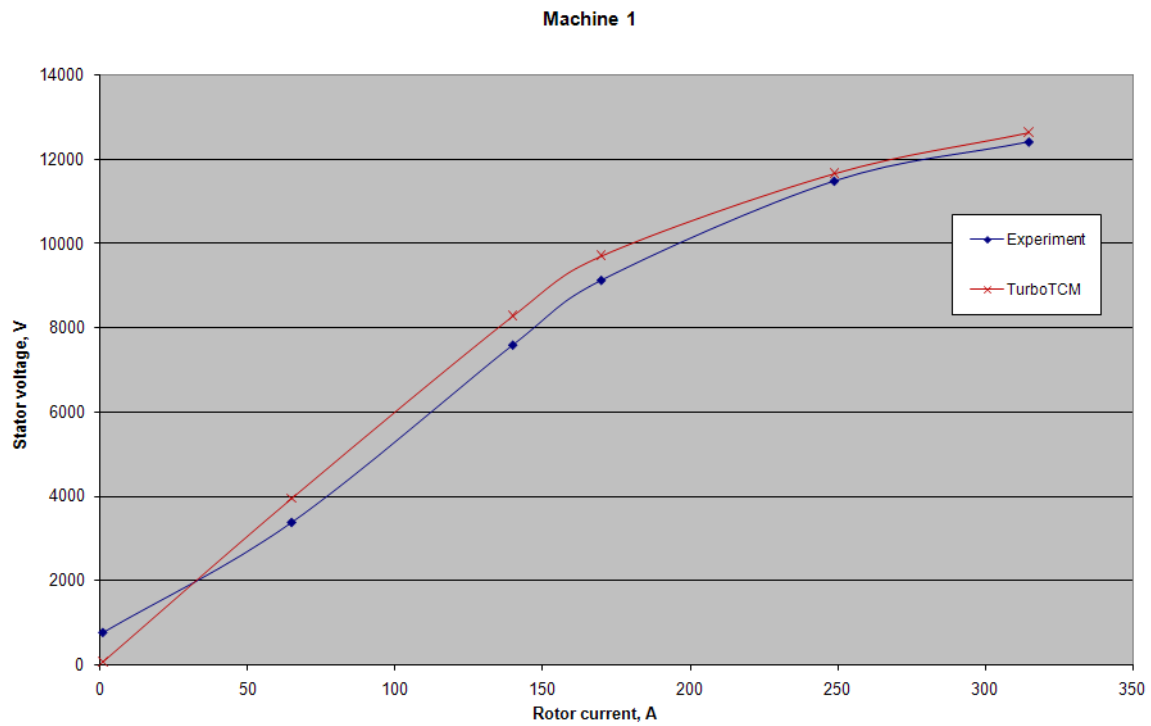


Figure B.1: No-load characteristic comparison: Machine 1.

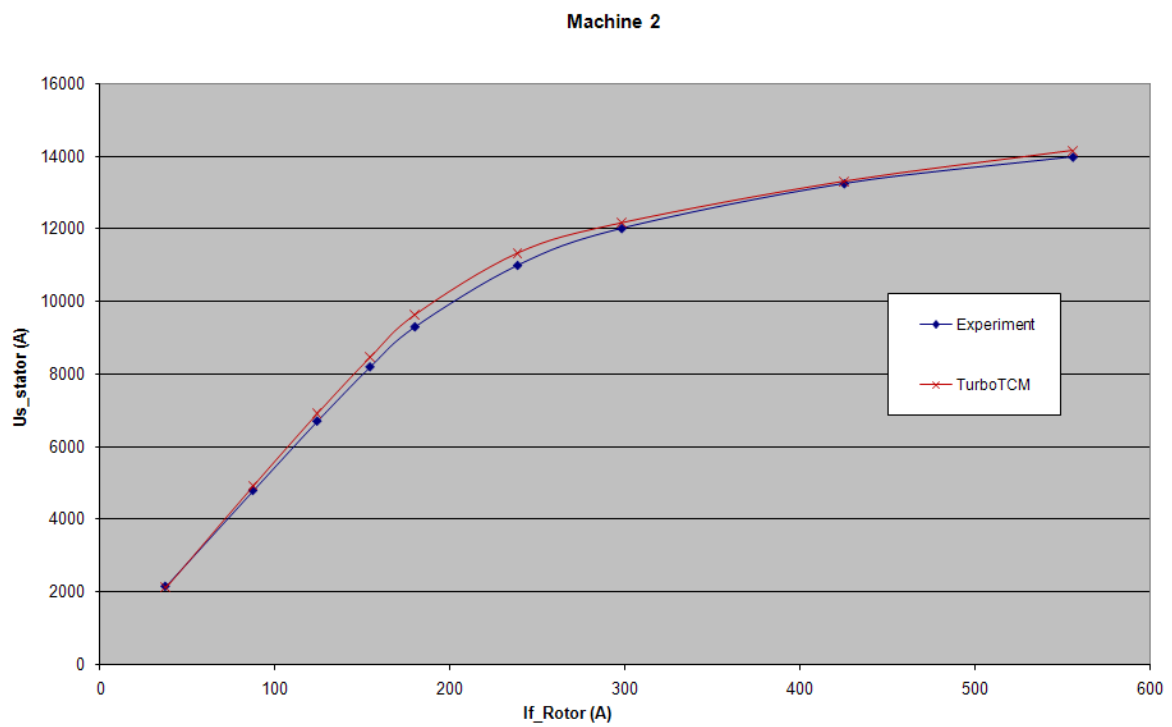


Figure B.2: No-load characteristic comparison: Machine 2.

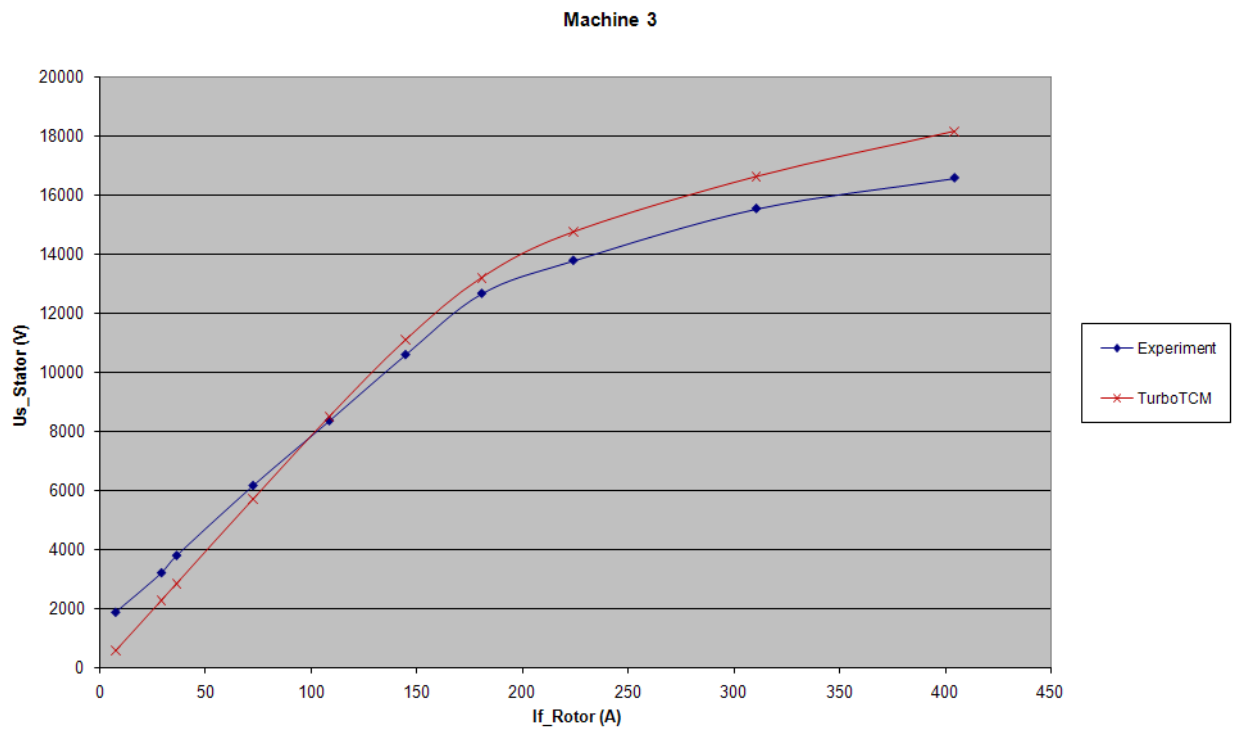


Figure B.3: No-load characteristic comparison: Machine 3.

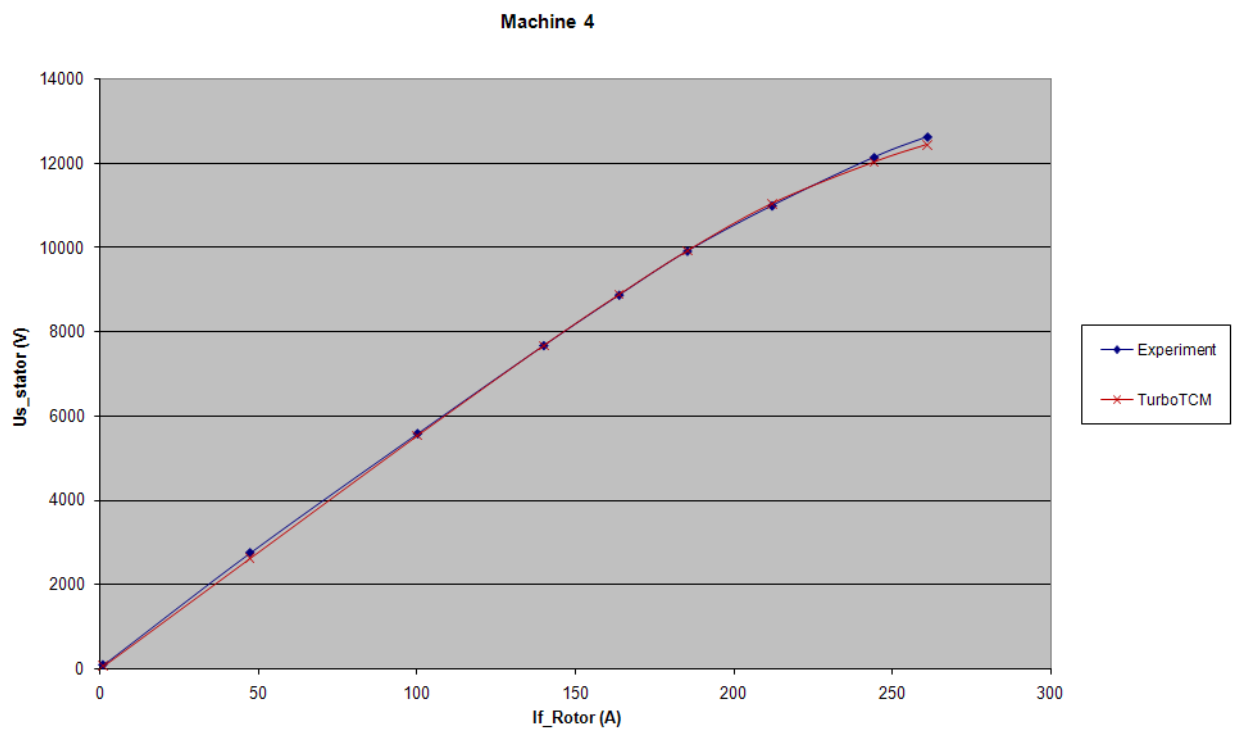


Figure B.4: No-load characteristic comparison: Machine 4.

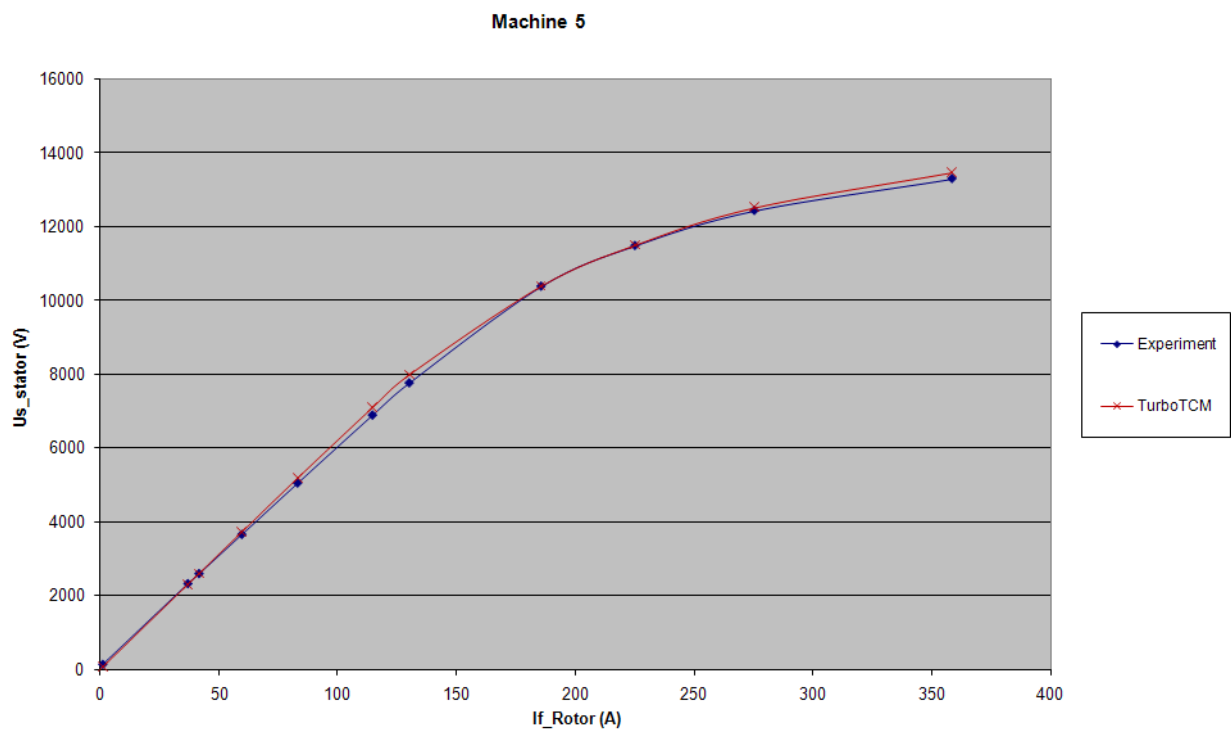


Figure B.5: No-load characteristic comparison: Machine 5.

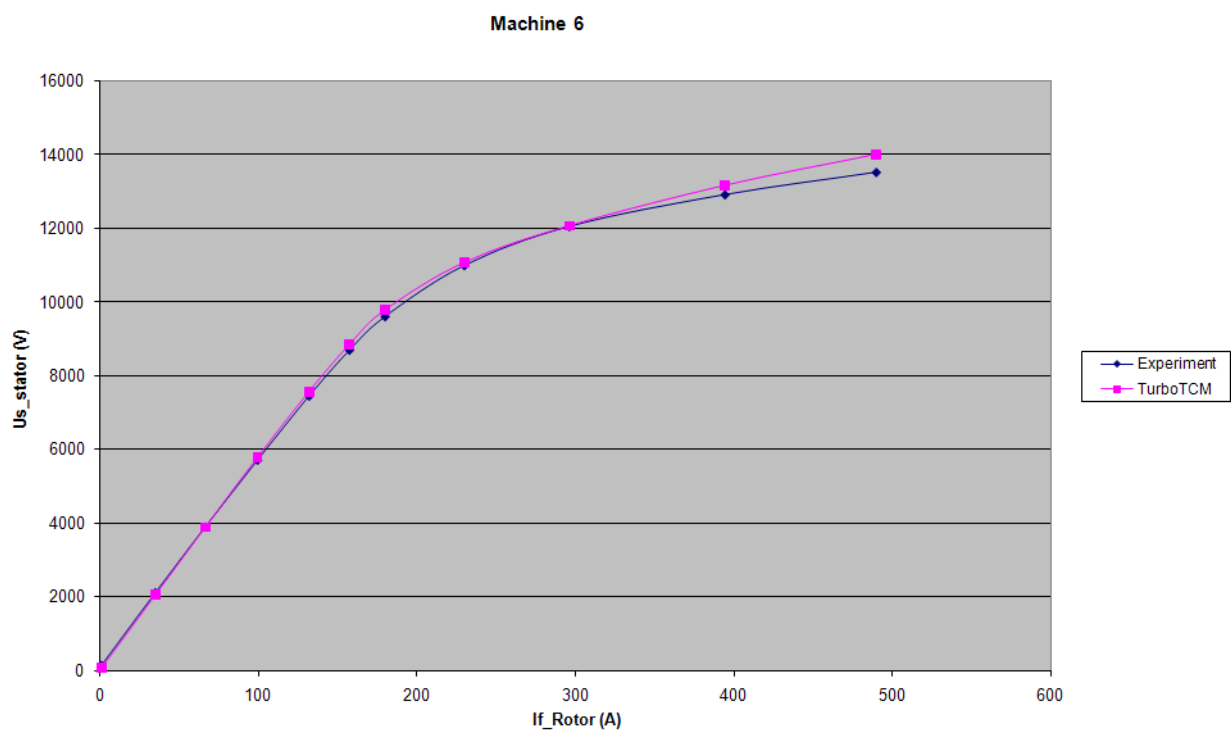


Figure B.6: No-load characteristic comparison: Machine 6.

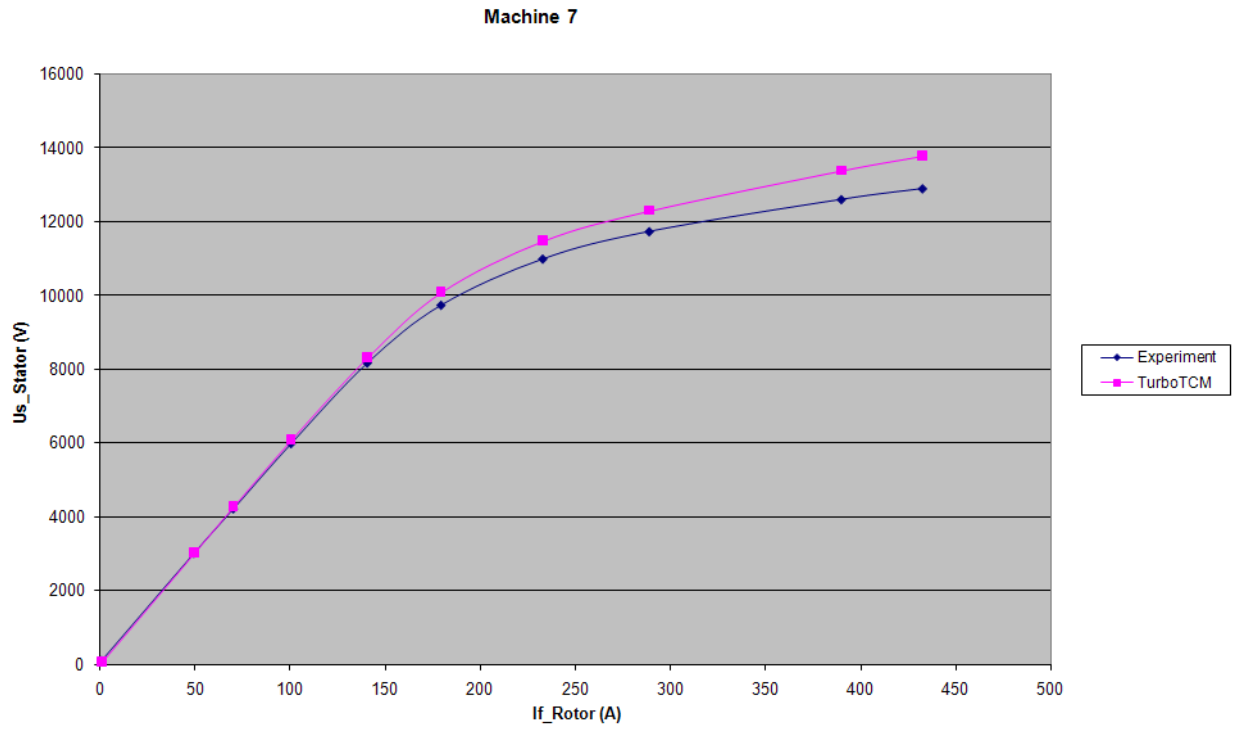


Figure B.7: No-load characteristic comparison: Machine 7.

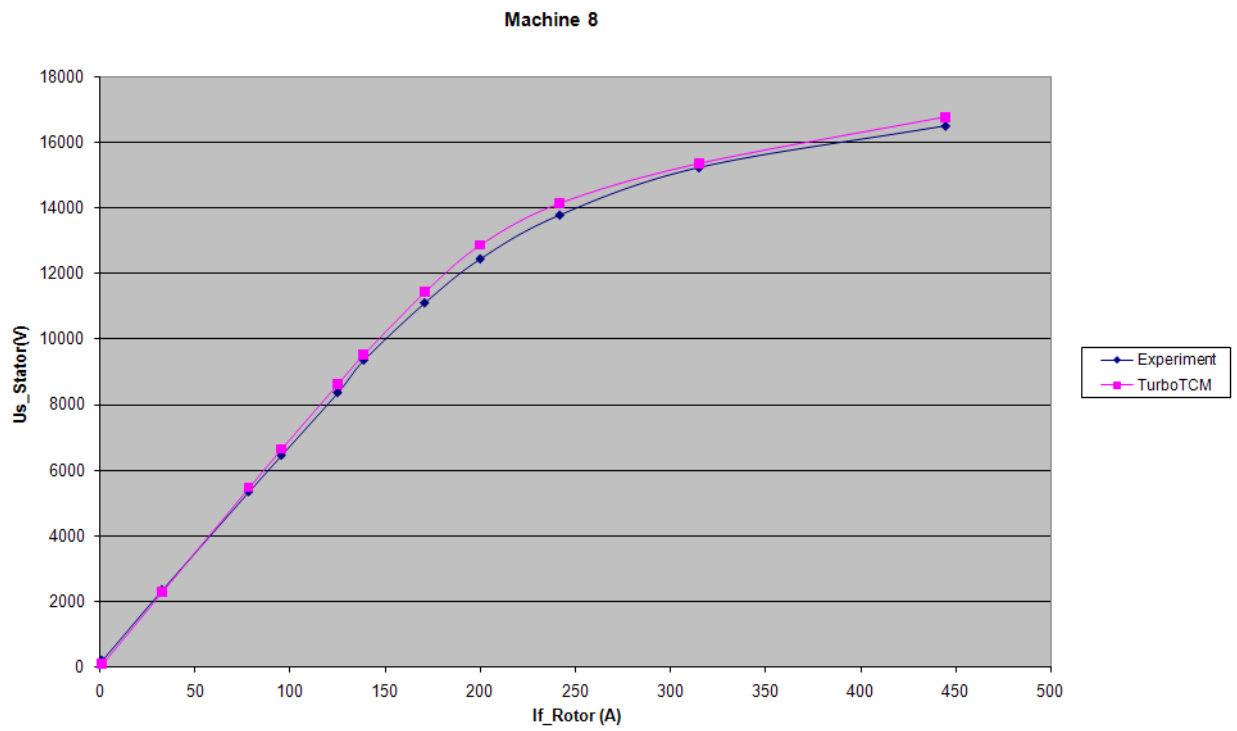


Figure B.8: No-load characteristic comparison: Machine 8.

Machine 1				Machine 2			
$I_s, A$	$I_{fexp}, A$	$I_{ftcm}, A$	Error	$I_s, A$	$I_{fexp}, A$	$I_{ftcm}, A$	Error
936	140,00	132,42	-5,42%	521	156,20	158,48	1,46%
1620	230,00	229,19	-0,35%	954	288,20	290,20	0,70%
2256	320,00	319,16	-0,26%	1241	376,90	377,51	0,16%
2808	400,00	397,26	-0,69%	1567	476,20	476,67	0,10%
3163	455,00	447,46	-1,66%	1765	536,50	536,91	0,08%
3552	520,00	502,52	-3,36%	1938	590,10	589,53	-0,10%
				2102	639,80	639,42	-0,06%
				2307	704,30	701,79	-0,36%
Machine 3				Machine 4			
$I_s, A$	$I_{fexp}, A$	$I_{ftcm}, A$	Error	$I_s, A$	$I_{fexp}, A$	$I_{ftcm}, A$	Error
364	59,00	76,11	29,00%	675	134,50	132,67	-1,36%
536	99,00	112,07	13,21%	1364	274,50	268,10	-2,33%
762	152,00	159,33	4,83%	1884	380,60	370,31	-2,70%
906	178,00	189,44	6,43%	2146	434,00	421,81	-2,81%
1051	211,00	219,76	4,15%	2418	488,90	475,28	-2,78%
1160	237,00	242,55	2,34%	2677	542,40	526,20	-2,99%
1280	263,00	267,64	1,77%	2948	597,90	579,50	-3,08%
1438	303,00	300,68	-0,76%	3207	651,00	630,45	-3,16%
1575	336,00	329,33	-1,98%	3330	676,20	654,65	-3,19%
1778	382,00	371,78	-2,67%				

Table B.3: Short circuit data comparison: machines 1-4.

Machine 5				Machine 6			
$I_s, A$	$I_{fexp}, A$	$I_{ftcm}, A$	Error	$I_s, A$	$I_{fexp}, A$	$I_{ftcm}, A$	Error
363	55,50	56,85	2,45%	470	62,30	65,55	5,21%
593	92,00	92,88	0,96%	1011	140,80	140,99	0,14%
921	144,50	144,26	-0,16%	1552	217,00	216,44	-0,26%
1298	204,20	203,31	-0,43%	1968	276,00	274,45	-0,56%
1678	264,50	262,83	-0,63%	2462	346,00	343,35	-0,77%
2025	320,00	317,19	-0,88%	2812	395,00	392,16	-0,72%
2374	376,30	371,85	-1,18%	3157	444,80	440,27	-1,02%
2579	410,00	403,97	-1,47%	3499	492,50	487,97	-0,92%
3000	475,90	469,91	-1,26%	3874	547,00	540,27	-1,23%
3260	518,00	510,64	-1,42%	4077	576,00	568,58	-1,29%
Machine 7				Machine 8			
$I_s, A$	$I_{fexp}, A$	$I_{ftcm}, A$	Error	$I_s, A$	$I_{fexp}, A$	$I_{ftcm}, A$	Error
493	78,30	79,89	2,03%	1	1,00	0,30	-70,23%
1100	178,50	178,26	-0,14%	377	110,80	112,24	1,30%
1522	247,50	246,64	-0,35%	556	164,50	165,53	0,63%
1920	313,50	311,14	-0,75%	787	234,00	234,21	0,09%
2188	357,00	354,57	-0,68%	1027	305,50	305,75	0,08%
2417	395,00	391,68	-0,84%	1111	331,00	330,76	-0,07%
2629	429,50	426,03	-0,81%	1246	372,50	370,95	-0,42%
2850	467,20	461,85	-1,15%	1364	407,00	406,08	-0,23%
				1488	444,00	443,00	-0,23%
				1550	463,00	461,45	-0,33%

Table B.4: Short circuit data comparison: machines 5-8.

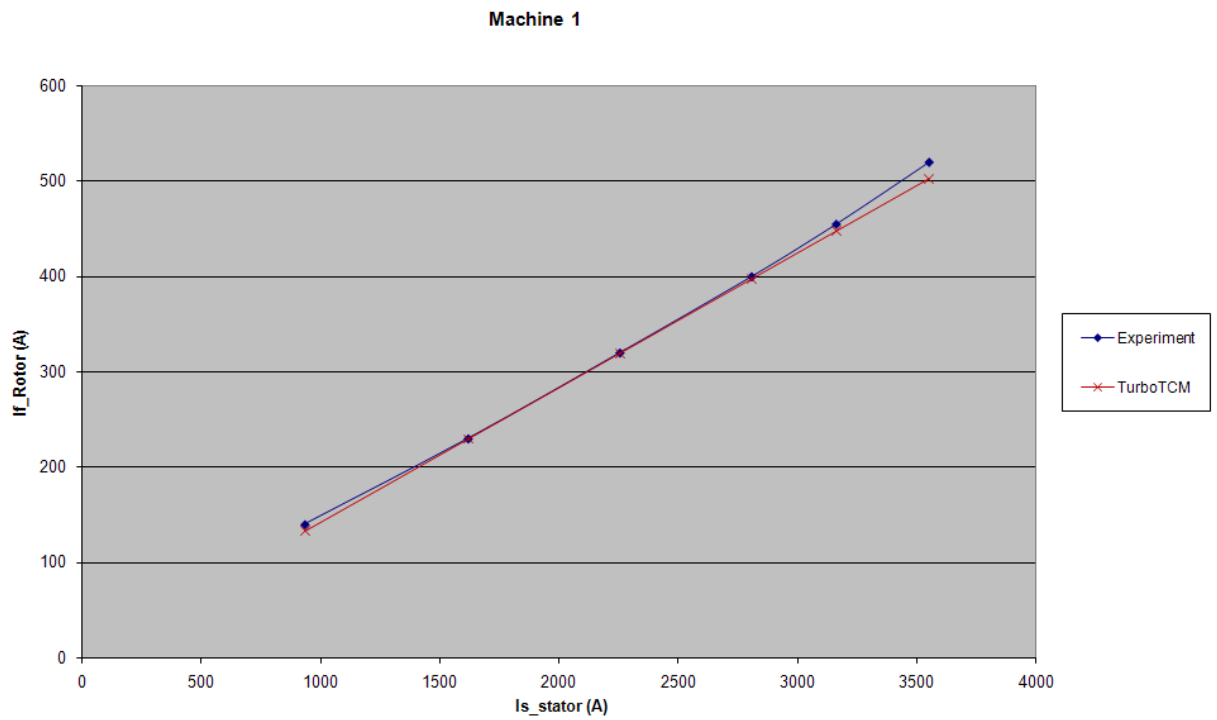


Figure B.9: Short circuit characteristic comparison: Machine 1.

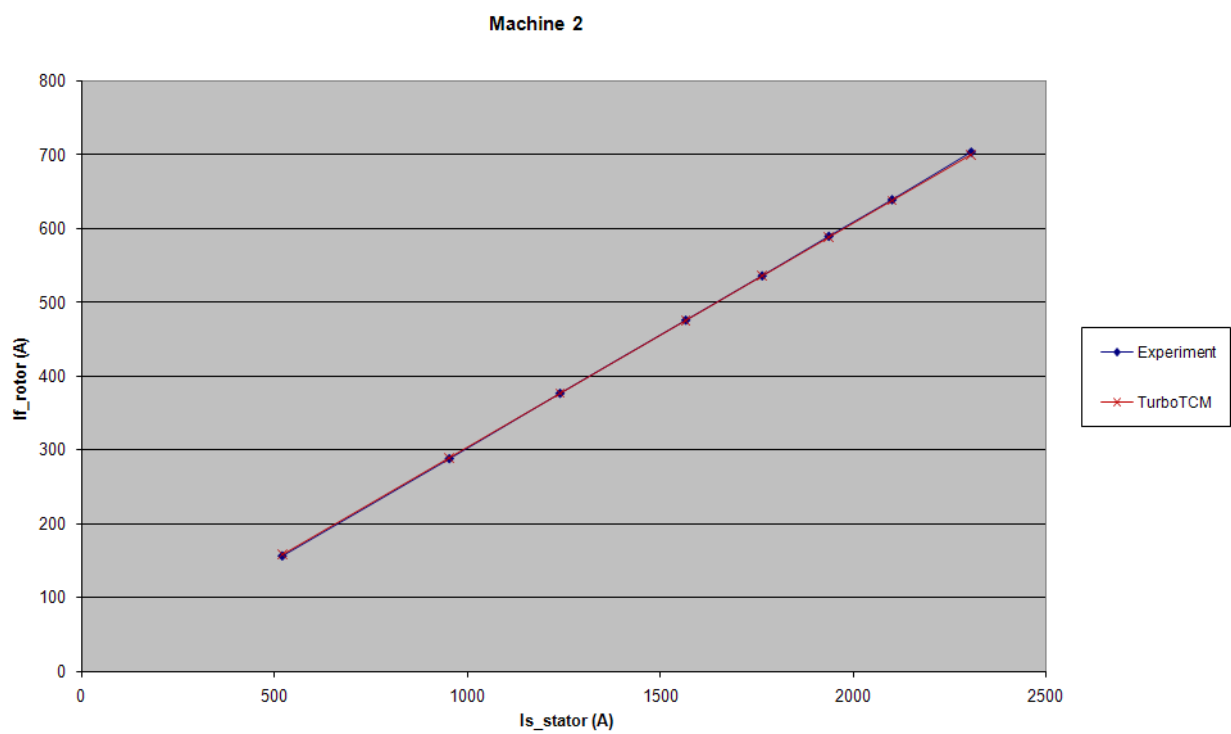


Figure B.10: Short circuit characteristic comparison: Machine 2.

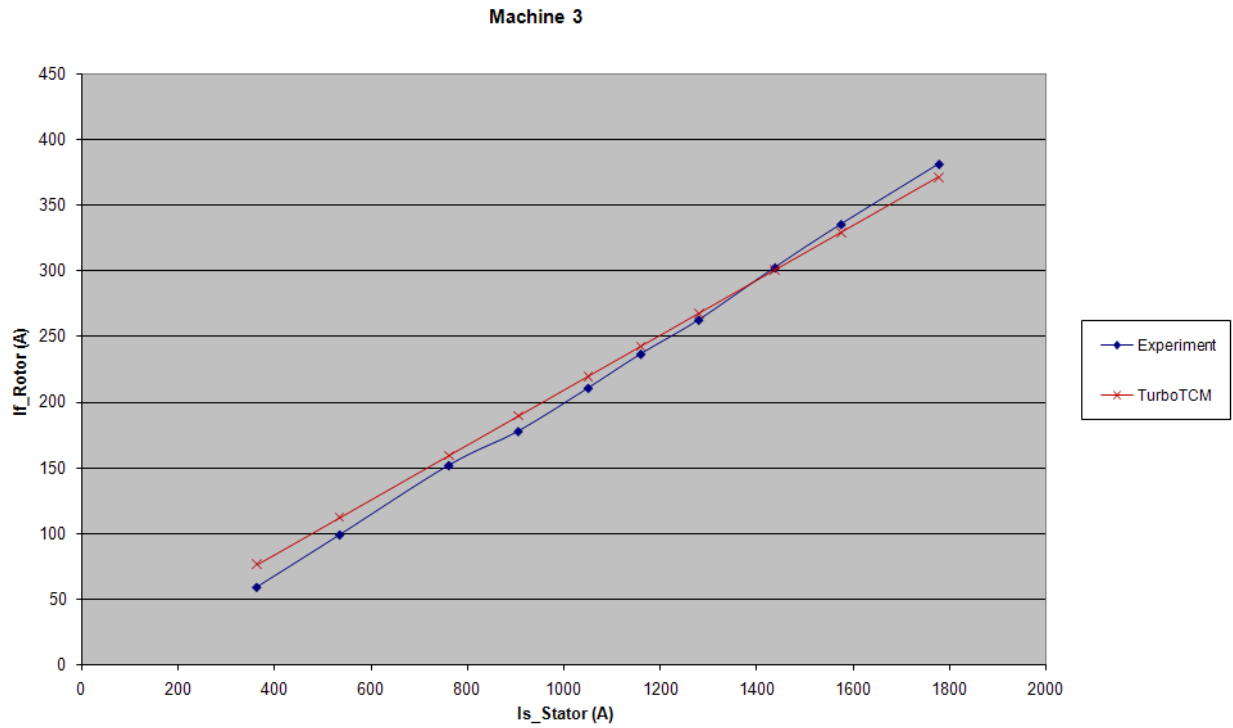


Figure B.11: Short circuit characteristic comparison: Machine 3.

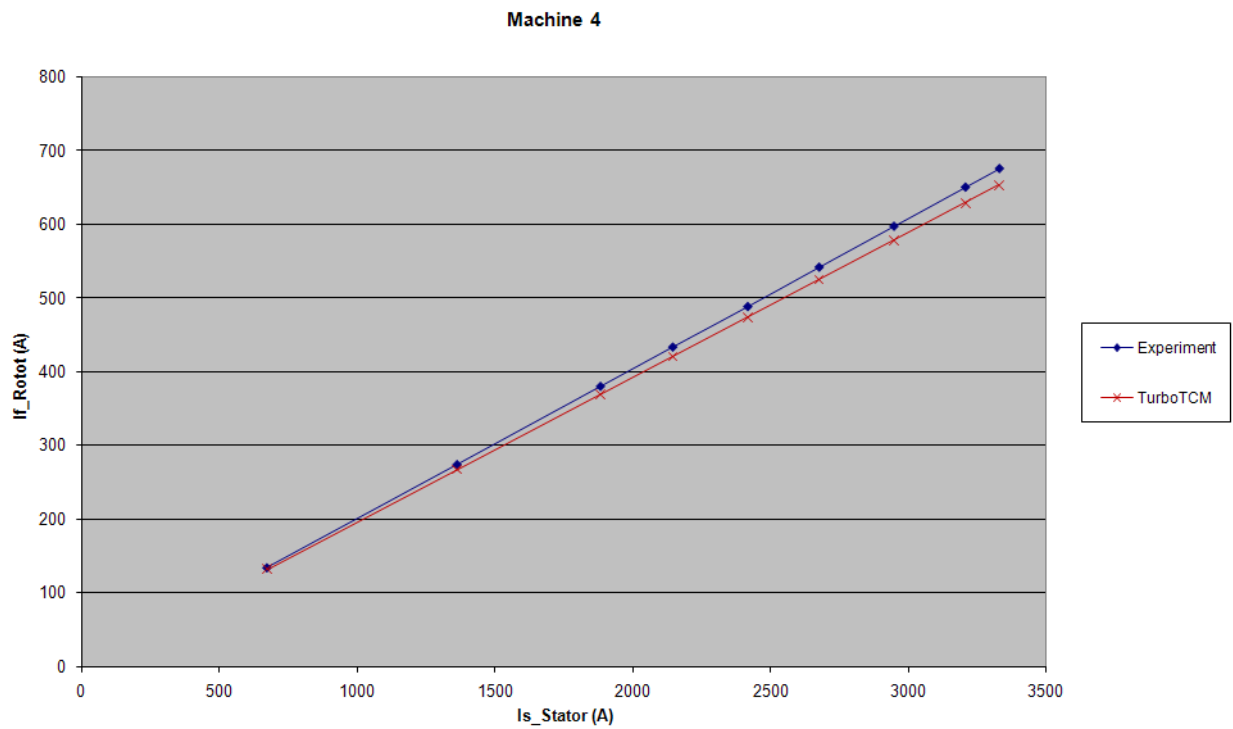


Figure B.12: Short circuit characteristic comparison: Machine 4.



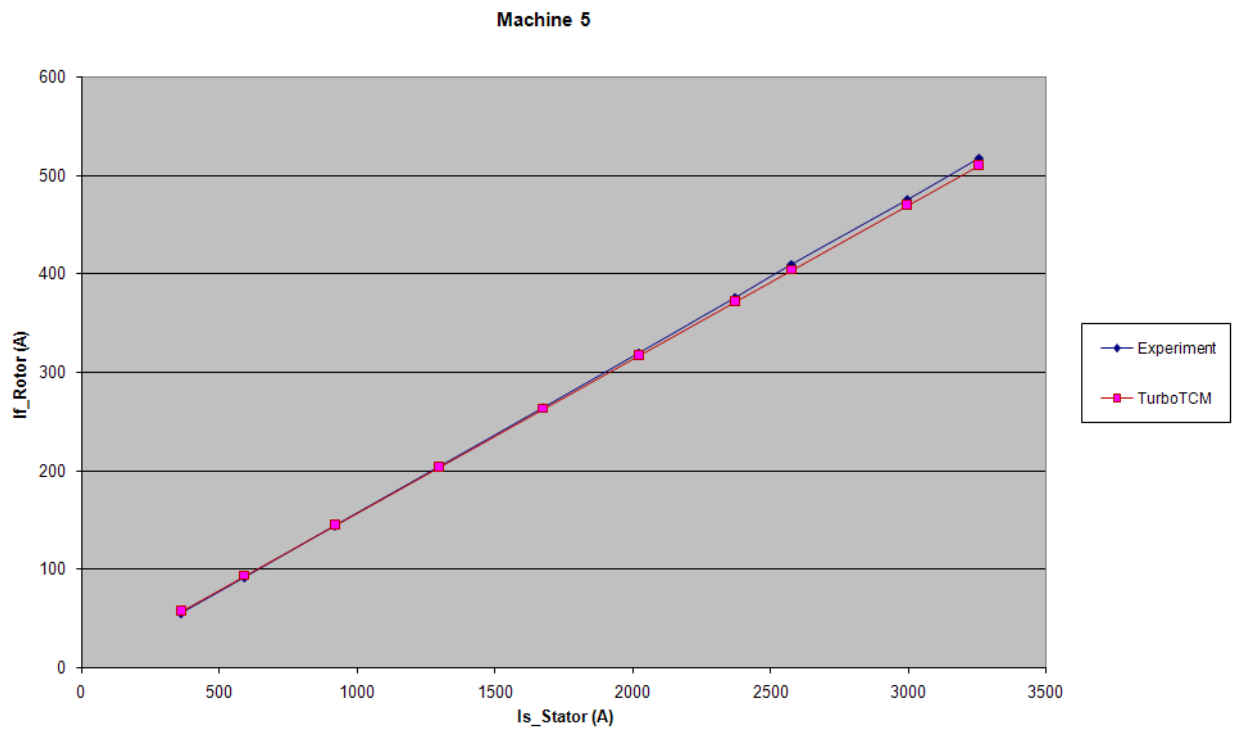


Figure B.13: Short circuit characteristic comparison: Machine 5.

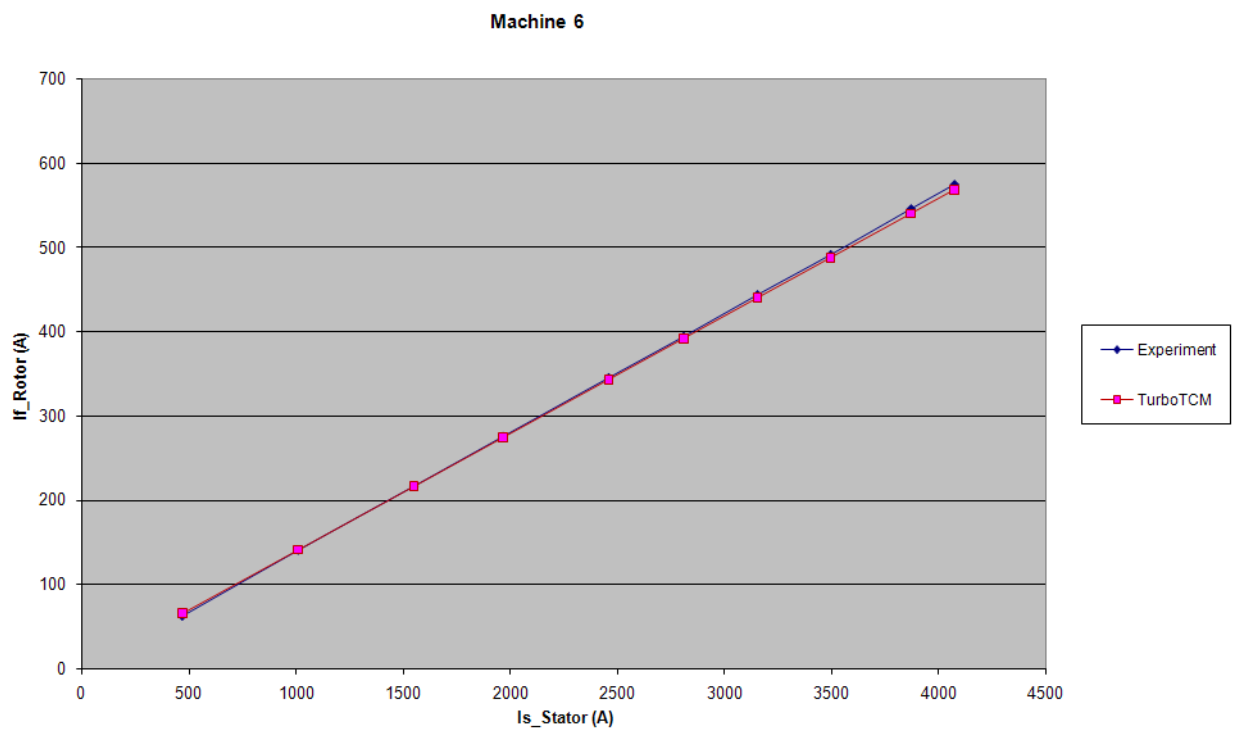


Figure B.14: Short circuit characteristic comparison: Machine 6.

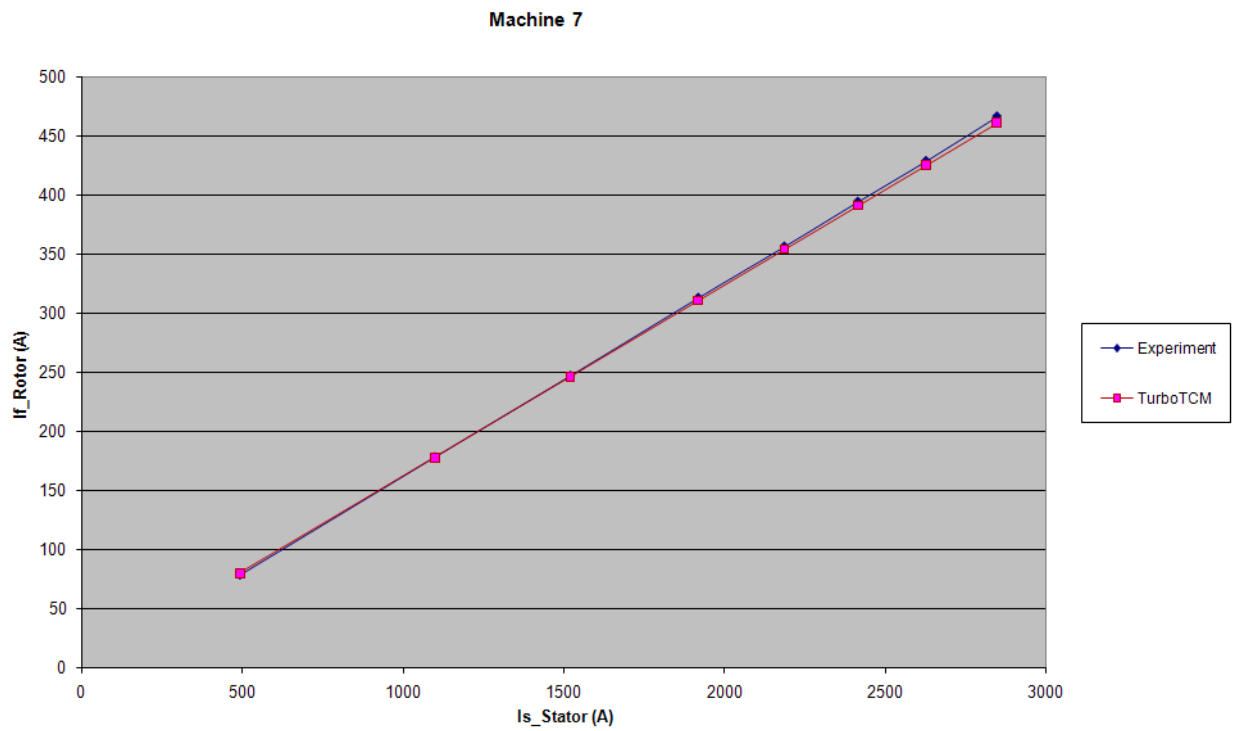


Figure B.15: Short circuit characteristic comparison: Machine 7.

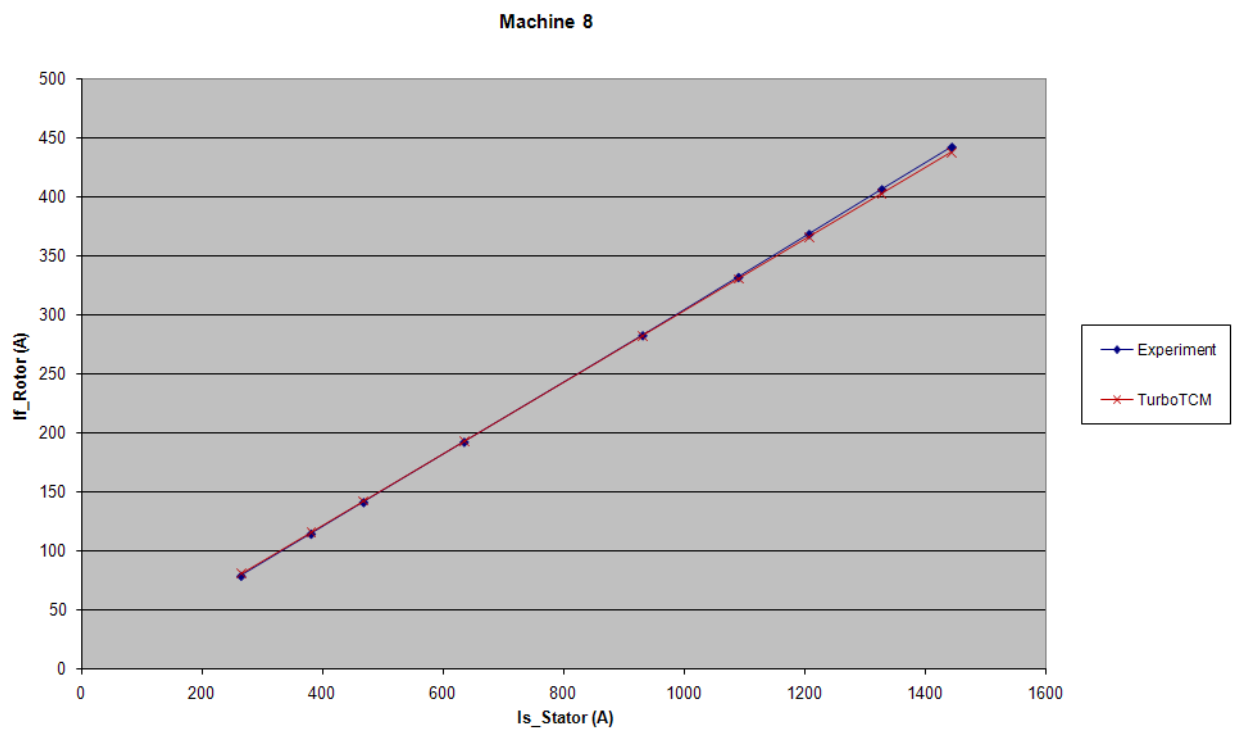


Figure B.16: Short circuit characteristic comparison: Machine 8.



# Bibliography

- [1] Amine Ait-Hammouda. *Predimensionnement et etude de sensibilité vibro-acoustique des machines a courants alternatifs et a vitesse variable*. PhD thesis, Ecole Centrale de Lille, March 2005.
- [2] L. Albert. *Modelisation et optimisation des alternateurs a griffes. Application au domaine automobile*. PhD thesis, INPG, Grenoble, 2004.
- [3] Joao Pedro A. Bastos and Nelson Sadowski. *Electromagnetic Modeling by Finite Element Methods*. Marcel Dekker, Inc, New York, 2003.
- [4] Bekkouche Benaissa. *Calcul du champ magnetique par la methode des permeances de contour de dent. Application au demarrage des moteurs asynchrones*. PhD thesis, Universite des Sciences et de la Technologie d’Oran, Oran, Algeria, May 1995.
- [5] Grady Booch. *Object-Oriented Analysis and Design*. Addison Wesley Longman, second edition, 1994.
- [6] D. Box. *Essential COM*. Addison Wesley Longman, 1998.
- [7] Muzaffer Canay. *Equivalent circuits of synchronous machines as well as pre-calculation of their parameters with examples*. PhD thesis, Ecole Polytechnique de l’Universite de Lausanne, Lausanne, Swiss, 1968.
- [8] C.J. Carpenter. Magnetic equivalent circuits. *Proc. IEE*, (115):1503–1511, October 1968.
- [9] Augustin Delale, Laurent Albert, Laurent Gerbaud, and Frederic Wurtz. Automatic generation of sizing models for the optimization of electromagnetic devices using reluctance networks. *IEEE Transactions on Magnetics*, 40(2):830–833, March 2004.
- [10] C. Delforge. *Modelisation d’un actionneur asynchrone et de sa commande vectorielle par reseaux de permeances*. PhD thesis, Universite des science et technique de Lille, January 1995.
- [11] A. Demenko and J. Sykulski. Magneto-electric network models in electromagnetism. *ISEF*, September 2005.
- [12] V. Devanneaux. *Modelisation de la machine asynchrone par reseau de permeances, validation par le diagnostic*. PhD thesis, Universite de Picardie Jules Verne, November 2002.

- [13] B. Du Peloux de St Romain. *Modelisation des actionneurs electromagnetiques par reseaux de reluctances*. PhD thesis, INPG, Grenoble, 2006.
- [14] B. Ducharme. *Caracterisation et modelisation des circuits magnetiques - du global vers le local*. PhD thesis, Universite de Claude Bernard, Lyon I, 2003.
- [15] Jacek F. Gieras and Mitchell Wing. *Permanent Magnet Motor Technology. Design and Application*. Marcel Dekker, Inc., New York, second edition, 2002.
- [16] R.N. Hasanah, M. Markovic, M. Jufer, and Y. Perriard. Slot-leakage inductance determination using schwarz-christoffel mapping. *Electrimacs-2005*, 2005.
- [17] Michel Hecquet. *Contribution a la modelisation des systemes electrotechniques par la methode des schemas equivalents magnetiques. Application a l'alternateur automobile*. PhD thesis, Universite des science et technique de Lille, January 1995.
- [18] Michel Hecquet. *Contribution a l'instrumentation de la demarche de conception des machines electrique. (HDR)*. PhD thesis, L'Universite des Sciences et Technologie de Lille, Decembre 2006.
- [19] Michel Hecquet and Pascal Brochet. Modelisation de l'alternateur automobile par un reseau de permeances couple a des circuits electriques. *Journal de Physique*, (3):1099–1116, August 1996.
- [20] Michel Hecquet and Pascal Brochet. Time variation forces in a synchronous machine using electric coupled network model. *IEEE Transactions on Magnetics*, 34(5):3656–3659, September 1998.
- [21] A. V. Ivanov-Smolensky. Tooth contour method and its application to a non-saturated electrical machine taking into account double-sided saliency. *Electrichestvo*, 9:18–28, 1976.
- [22] A. V. Ivanov-Smolensky. *Electrical Machines*. Energy, Moscow, 1980.
- [23] A. V. Ivanov-Smolensky, J. V. Abramkin, A. I. Vlasov, and V. A. Kuznetsov. *Universal Method Of Electromagnetic Processes Calculation In Electrical Machines*. Energoatomizdat, Moscow, 1986.
- [24] H. Jerance. *Reseaux de reluctances et diagnostic des machines electriques*. PhD thesis, ENSIEG, Grenoble, November 2002.
- [25] Bo-nan Jiang. *The Least-Squares Finite Element Method. Theory and Applications in Computational Fluid Dynamics and Electromagnetics*. Springer-Verlag, New-York, 1998.
- [26] V.A. Khvostov. *Computer calculation of the magnetic field in the active zone of a turbogenerator taking into account saturation*. PhD thesis, Moscow Power Engineering Institute, Moscow, 1977.

- [27] V. A. Kuznetsov and Pascal Brochet. A general numerical modeling of electromagnetic process in electromechanical systems. *The International Journal for Computation and Mathematics in Electrical and Electronic Engineering (COMPEL)*, 22(4):1142–1154, 2003.
- [28] Vyacheslav Kuznetsov. *General Method of Calculation of Magnetic Fields and Processes in Electric Machines Having Discrete Space-Distributed Windings*. PhD thesis, Moscow Power Engineering Institute, Moscow, 1990. Technical Science Doctoral Thesis.
- [29] Lev D. Landau and Evgeniy M. Lifshitz. *The classical Theory of Fields*, volume 2 of *Course of Theoretical Physics*. Nauka, Moscow, seventh edition, 1988.
- [30] M. Latreche. *Modelisation magnetique et thermique des machines electriques par des schemas equivalents*. PhD thesis, INP Toulouse, 1987.
- [31] M. Liwschitz. Calcul des machines electriques. *SPES*, II, 1967.
- [32] M. Markovic, M. Jufer, and Y. Perriard. Analyzing an electromechanical actuator by schwarz-christoffel mapping. *IEEE Transactions on Magnetics*, 40(4), July 2004.
- [33] F. Marthouret. *Developement de modeles dynamiques comportementaux de circuits magnetiques*. PhD thesis, INSA de Lyon, Lyon, 1995.
- [34] K. Nakamura, K. Kimura, and O. Ichinokura. Electromagnetic and motion coupled analysis for switched reluctance motor based on reluctance network analysis. *EPE - PEMC*, 2005.
- [35] V. Ostovic. *Dynamics Of Saturated Machines*. Springer-Verlag, 1989.
- [36] V. Ostovic, J.M. Miller, V.K. Garg, R.D. Schult, and S.H. Swales. A magnetic equivalent circuit based on performance computation of a lundell alternator. *IEEE Transactions on Industry Applications*, 35(4), July/August 1999.
- [37] J. Perho. *Reluctance network for analysing induction machines*. PhD thesis, University of Helsinki, Helsinki, Finland, December 2002.
- [38] Dmitry Petrichenko, Michel Hecquet, Pascal Brochet, Vyacheslav Kuznetsov, and Daniel Laloy. Numerical modelling of a turboalternator using tooth contours method: Cad application. *ICEM*, October 2004. CD-ROM.
- [39] Dmitry Petrichenko, Michel Hecquet, Pascal Brochet, Vyacheslav Kuznetsov, and Daniel Laloy. Design and simulation of turbo-alternators using coupled permeance network model. *COMPUMAG*, June 2005. CD-ROM.
- [40] Dmitry Petrichenko, Michel Hecquet, Pascal Brochet, Vyacheslav Kuznetsov, and Daniel Laloy. Development of the turbo-alternator simulation software. *ELECTRIMACS*, April 2005. CD-ROM.
- [41] Dmitry Petrichenko, Michel Hecquet, Pascal Brochet, Vyacheslav Kuznetsov, and Daniel Laloy. Tooth contour method applied to design of turboalternators: development of cad software. *COMPUMAG*, June 2005. CD-ROM.

- [42] Dmitry Petrichenko, Michel Hecquet, Pascal Brochet, Vyacheslav Kuznetsov, and Daniel Laloy. Design and simulation of turbo-alternators using coupled permeance network model. *IEEETransMag*, 42:1259–1262, April 2006.
- [43] Dmitry Petrichenko, Michel Hecquet, Pascal Brochet, Vyacheslav Kuznetsov, and Daniel Laloy. Permeance network method coupling with experimental design in order to optimize turbogenerators. *ICEM*, September 2006. CD-ROM.
- [44] William H. Press, Saul A. Teukovsky, William T. Vetterling, and Brian P. Flannery. *Numerical Recipes in C. The Art of Scientific Computing*. Cambridge University Press, second edition, 1999.
- [45] M. Rakatovao. *Un modele operationnel complet pour l'alternateur a griffes dans le domaine automobile*. PhD thesis, INP, Grenoble, 1996.
- [46] Carlos Ramirez. *Plate-forme numerique d'essais pour machines electriques de puissance*. PhD thesis, Ecole Polytechnique Federale de Lausanne, Lausanne, 2003.
- [47] Herve Roisse. *Contribution a la modelisation des systemes electrotechniques par la methode des reseaux de permeances couples. Application aux machines synchrones a aimants permanents*. PhD thesis, L'universite des sciences et technologies de Lille, Lille, January 1998.
- [48] H. Roters. *Electromagnetic devices*. John Wiley and Sons, New-York, USA, 1941.
- [49] Filtz R.V. *Mathematical basis of the electromechanical converters theory*. Naukova Dumka, Kiev, 1979.
- [50] G. Shepherd and B. King. *Inside ATL*. Microsoft Press, 1999.
- [51] G. A. Sipajlov, E. V. Kononenko, and K. A. Khorkov. *Electrical Machines (Special Course)*. Vysshaya Shkola, Moscow, second edition, 1987.
- [52] F. Sixdenier, B. Ducharne, J.P. Masson, L. Morel, and M.A. Raulet. Coupled programming: “finite elements” – “dynamical hysteresis flux tubes” for non-homogeneous circuits modeling. *COMPUMAG*, July 2003.
- [53] G.R. Slemon. An equivalent circuit approach to analysis of synchronous machines with saliency and saturation. *IEEE Transactions on Energy Conversion*, (5):538–545, September 1990.
- [54] S. Srairi, J. Farook, A. Djerdir, and Miraoui A. The magnetic network modeling of a permanent magnet motor with consideration of the saturation and heating effects. *ISEF*, September 2005.
- [55] Bjarne Strastrup. *The C++ Programming Language*. Addison Wesley Longman, third edition, 1997.
- [56] J. Turowski. *Ch.4, “Reluctance networks” in Computational Magnetism, J. Sykulski*. Chapman and Hall, New York, USA, 1996.

- [57] Stephan Vivier, Michel Hecquet, Amine Ait-Hammouda, Mark Goueygou, Pascal Brochet, and A. Randria. Experimental design model applied to a multiphysical model: treillis designs for a multidimensional screening study. *The International Journal for Copmutation and Mathematics in Electrical and Electronic Engineering (COMPEL)*, 24(3):15, 2005.
- [58] Jiri Vlach and Kishore Singhal. *Computer Methods For Circuit Analysis And Design*. Van Nostrand Reinhold Company Inc., New York, 1983.



# **Contribution à la modélisation et à la conception optimale des turboalternateurs. (résumé en français)**

**Par Dmitry Petrichenko**

C.N.R.T. Réseaux et Machines Electriques du Futur (Projet 'Archimed').  
L2EP, Ecole Centrale de Lille  
JEUMONT SA (AREVA NP)

**Mots-Clefs** : réseau de perméances, méthode de contours de dents, turboalternateurs, CAO des machines.

**Keywords** : permeance network, tooth contour method, turbogenerator, CAD of electrical machines.

## **I. Introduction**

### **Contexte :**

Dans les complexes industriels, les cahiers des charges sont de plus en plus exigeants en terme de performances et d'optimisation économique des installations de production électrique. Dans certains cas, on cherchera à minimiser les courants de court-circuit pour soulager les organes de coupure ; au contraire dans d'autres cas, on veillera à limiter les chutes de tension transitoires. Les moyens de calcul rapides permettant de dimensionner les machines, basés sur des modèles analytiques n'ont pas toujours la précision nécessaire. Les méthodes de calcul par Eléments Finis permettent d'optimiser des parties locales de la machine, mais deviennent trop lourds d'utilisation s'agissant de dimensionner des équipements pour répondre aux appels d'offre de matériel de moyenne puissance.

La méthode proposée par L2EP de Lille et le MPEI de Moscou, basée sur l'emploi des réseaux de perméances, a retenu l'attention de Jeumont SA pour développer un nouveau logiciel dans le cadre du CNRT « Réseaux et Machines du Futur » de Lille. Cette méthode permet de conserver la rapidité d'exploitation et d'améliorer la précision de calcul en adaptant facilement le réseau de perméances à la configuration étudiée.

Le travail développé est ouvert aux méthodes d'optimisation ainsi qu'à la prise en compte de régimes dynamiques.

### **Objectif :**

L'objectif de ce travail concerne le développement d'un outil complètement 'automatisé' permettant dans un premier temps la modélisation des turbo-alternateurs.

Notre idée est de se reposer sur un réseau de perméances paramétrées établi à partir de calculs analytiques et en ce qui concerne l'entrefer, l'utilisation de la Tooth Contour Method (TCM) [1], [2] ou la méthode de contour de dents. Le couplage électrique, magnétique ainsi que mécanique, la saturation, le mouvement et les effets tridimensionnels sont pris en considération.

L'objectif à long terme est de mettre au point d'un outil de conception optimale électromagnétique de turbo-alternateurs de 10 à 100 MW, d'un modèle numérique d'une part, d'un progiciel sur PC d'autre part.

Cet outil, développé sous Matlab, nous fournit très rapidement le circuit magnétique, en quelques secondes, et la possibilité d'effectuer des calculs :

- en statique, exemple : calcul des grandeurs comme la tension et le courant débité pour un point de fonctionnement nominal,
- ou en dynamique, exemple : détermination de l'allure temporelle de la tension de sortie.

La réalisation de l'outil est présentée, incluant la méthode de calcul du circuit, développée en C++, et le solveur développé sous Matlab. Celui-ci génère automatiquement le réseau de perméances paramétré.

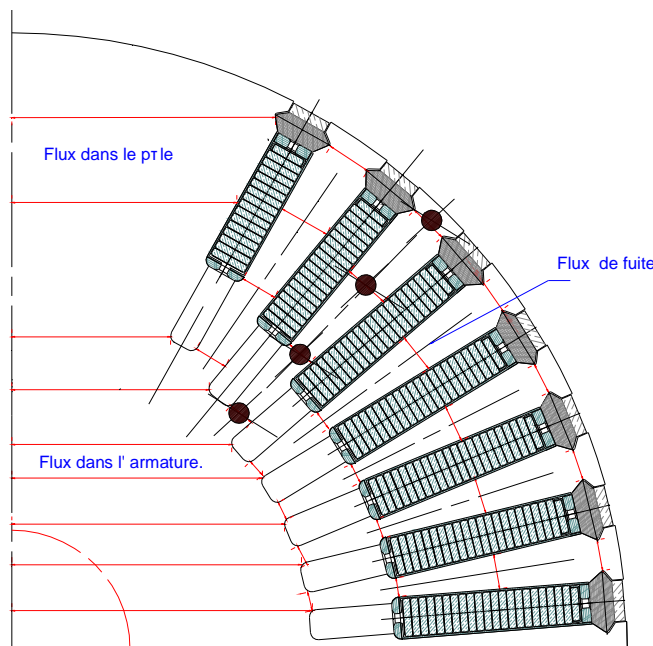
### ***Difficultés liées à l'étude des turbo-alternateurs :***

Le premier point a été la prise en compte du nombre de paramètres géométriques et électriques qui varient entre 250 et 300 en fonction de la finesse retenue pour l'étude. Sur la figure 1, une partie du rotor est présentée où l'on doit intégrer les différentes formes d'encoches, mais aussi la possibilité de relever le flux et l'induction en de nombreux points.

La deuxième difficulté est le nombre de phénomènes à prendre en compte. Les principaux concernent:

- La prise en compte des événements (canaux de ventilations),
- les têtes de bobines et des écrans magnétiques,
- l'association des différentes parties mécaniques (joints...)
- le bobinage (prise en compte des isolants et des cales entre plans)
- la présence ou non de cales d'encoche magnétique ou semi-magnétique.

Ainsi, un réseau de perméances adapté à ces paramètres a été défini. Ce réseau devait être déduit automatiquement. La démarche de constitution du réseau de perméances est rappelée ci-dessous.



### ***Choix de la méthode :***

Différentes méthodes existent pour la modélisation des machines électriques et le calcul de champ en commençant par la méthode des éléments finis : précise mais pour des modélisations 3D avec prise en compte du mouvement sur ce genre de machine les temps de calculs deviennent très pénalisants, supérieur à plusieurs heures.

Notre objectif à long terme étant de développer un outil de CAO des turbo-alternateurs, il est préférable de privilégier un outil avec des temps de calculs réduits (de l'ordre de la minute).

Ainsi, une autre approche que l'on peut classer entre les méthodes numériques et analytiques concerne la Permeance Networks Method (PNM) ou la méthode des réseaux de perméances. L'avantage de la PNM

est de réaliser un bon compromis entre le temps de calcul et la précision. Différentes techniques de calculs du réseau existent, surtout en ce qui concerne les perméances d'entrefer :

- celles utilisant des méthodes analytiques uniquement, par exemple [3], [4],
- celles reposant sur des calculs E.F. en statique et permettant d'avoir une grande précision sur le réseau de perméances obtenu, surtout en ce qui concerne des machines complexes et 3D [5], [6], [7].
- et celles utilisant la T.C.M. (Tooth Contour Method).

La T.C.M. ou méthode de contour de dents est basée sur une représentation théorique du champ dans l'entrefer à partir de la somme des champs magnétiques obtenus par des éléments spéciaux que l'on appelle « contour de dent ». Sur l'exemple donné Fig. 2, le 'contour de dent' stator concerne uniquement une dent stator entourée par des conducteurs disposés dans les encoches adjacentes. Au rotor, la discrétisation ou 'contour de dent' dépend de la géométrie, celle-ci imposant un réseau de perméances plus ou moins complexe.

La détermination du champ autour d'une dent est obtenue en utilisant des conditions limites particulières, en supposant que la perméabilité du fer stator et rotor est nettement supérieure à celle de l'air. Uniquement trois à quatre dents sont choisis pour la détermination des perméances en plaçant nos conditions limites directement sur les bords de la dent (Fig.2). Ainsi, la détermination est très rapide et ne nécessite pas la machine complète.

L'allure présentée  $\lambda_{sr}(b_{sr})$  de la perméance mutuelle entre le contour de dent stator  $s$  et le contour non alimentée du rotor  $r$  (potentiel scalaire égal à 0) est obtenue comme une fonction de la position relative  $\lambda_{sr}(b_{sr})$  [8]. Afin de valider cette allure, des calculs sur OPERA-2D (code éléments finis) [9] en statique ont été nécessaires [10].

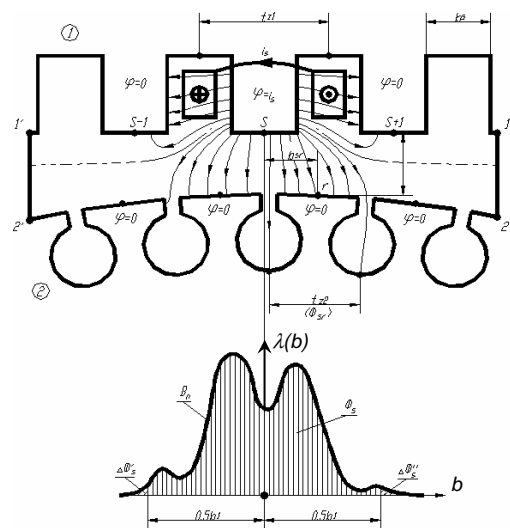


Fig. 2 : Représentation du contour de dent (1 seule dent 'alimentée')

La saturation est ensuite insérée au niveau de chaque perméance dans notre réseau et la méthode de Newton-Raphson permet de déterminer le flux ou le potentiel magnétique dans le circuit magnétique.

### Présentation du réseau de perméances :

Le réseau de perméances du système magnétique est généré automatiquement à partir des paramètres géométriques. La structure générale du stator et du rotor est présentée sur la figure suivante (Fig. 3).

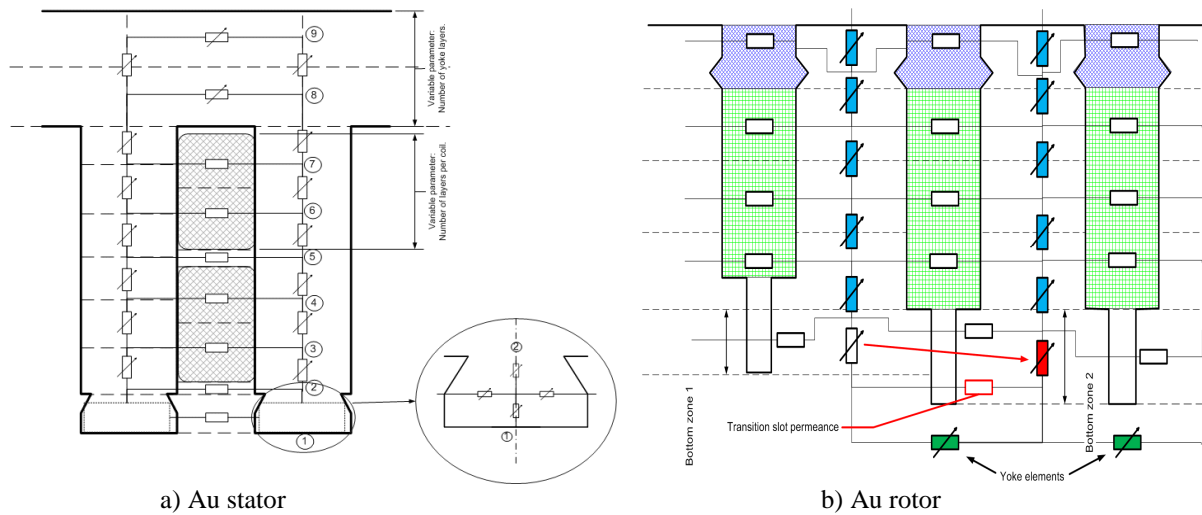


Fig. 3: Partie du réseau de perméances

Le nombre de subdivisions de la culasse statorique et des dents est variable. Cette variation sur la densité du réseau est possible au stator et au rotor. Elle permet d'intégrer plus précisément le problème des saturations locales. Cette décomposition a une influence, bien évidemment, sur le temps de calcul.

Le rotor d'un turbo-alternateur (Fig. 1) peut être très sophistiqué avec différentes formes d'encoches et de dents avec des profondeurs variables. Ces différentes formes sont prises en considération par une analyse fine des zones afin de trouver le meilleur découpage.

La Fig. 3.b montre le circuit magnétique équivalent de dents rotorique. L'utilisateur définit uniquement le nombre de subdivisions. La complexité de géométrie est traitée par l'outil.

#### *Couplage électrique – magnétique :*

Les sources de force magnétomotrice (MMF) sont placées au niveau des branches horizontales : Fig. 4 (non représentées sur les deux figures précédentes). Elles permettent le couplage électrique-magnétique.

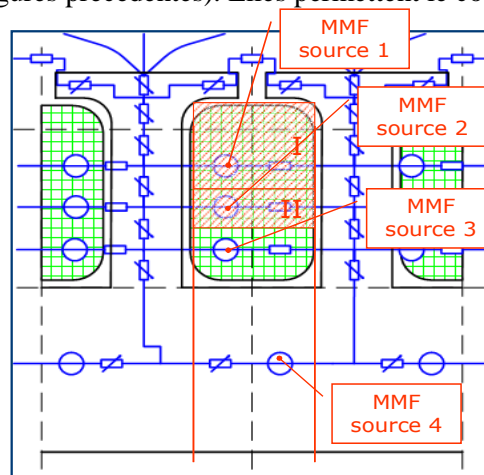


Fig. 4: Source de force magnétomotrice

Pour exemple, la source MMF1 est déterminée à partir de la 'région' de bobinage I, puis la source MMF2 à partir de la région de bobinage I & II, etc....

Des détails du circuit complet avec le couplage et la description du système d'équations sont donnés dans la référence [10].

Notre réseau est construit sur une période électrique uniquement et dans ce modèle équivalent, les courants induits au rotor ne seront pas considérés.

### Prise en compte des effets 3D :

Dans le cas de l'étude des turbo-alternateurs, la prise en compte de la 3ème dimension est nécessaire en vue d'intégrer les phénomènes suivants comme les canaux de ventilations ou les effets d'extrémités. En effet, l'influence des canaux de ventilations situés au stator et/ou au rotor est à prendre en considération dans le réseau de perméances.

Pour cela, un calcul de la longueur réelle du fer et l'utilisation de relations analytiques pour la prise en compte des effets d'extrémités sont placés directement dans le calcul des perméances. Ce point est détaillé dans la référence [11].

## III. Réalisation de l'outil

Une présentation des différentes parties de notre outil, appelé « TURBO-TCM » est donnée sur la Fig. 5. En ce qui concerne les données d'entrée, la fiche électrique et magnétique du turbo-alternateur est nécessaire et doit contenir : les dimensions stator et rotor, le nombre d'encoches stator et rotor, leurs dimensions, la description complète du bobinage stator et rotor, les caractéristiques des matériaux, les spécifications du circuit électriques, etc.

A partir de toutes ces informations, un circuit magnétique équivalent paramétré est défini, mais aussi le circuit électrique et les équations de couplage. La définition de ce réseau couplé peut être réalisée automatiquement ou manuellement (par exemple, durant la phase de test de l'outil).

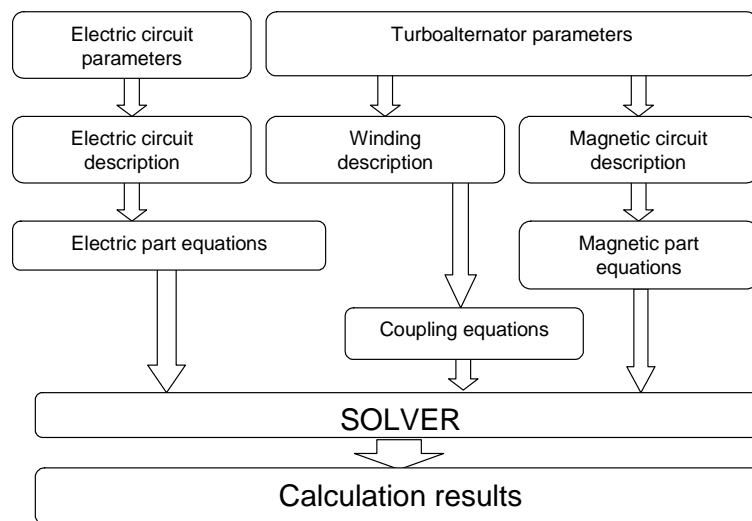
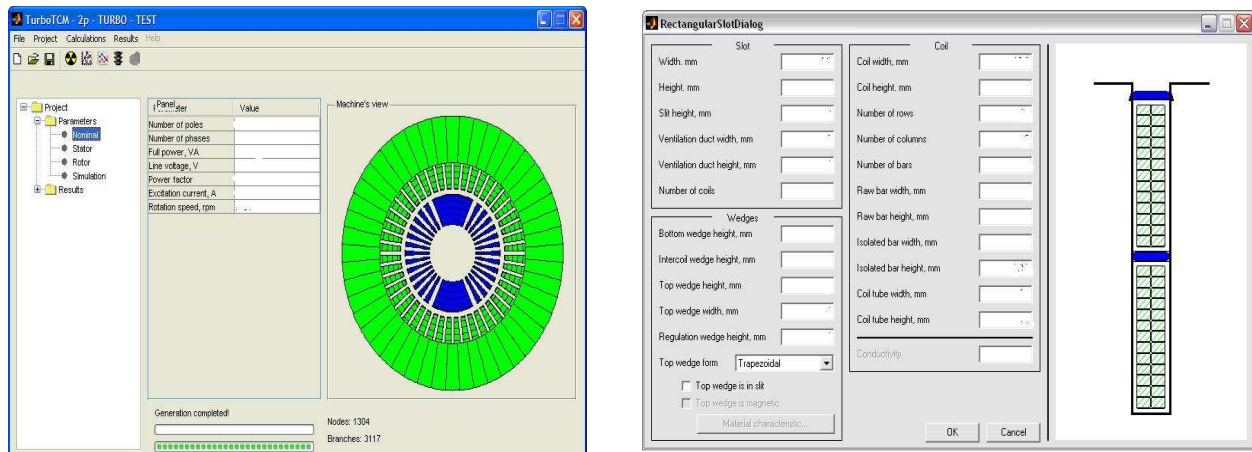


Fig. 5 : Structure de l'outil.

Ainsi, le système d'équations matricielles [10] peut être traité. Ces différentes '*parties*' correspondent à un modèle objet défini sous Visual Studio C++ .NET et utilisant la technologie 'Component Object Model' (COM). Celles-ci sont ensuite compilées comme une librairie '*type library* : TCMLib'.

L'avantage de cette démarche est de pouvoir générer et manager en temps réel le réseau paramétré tel que les éléments 'caractéristiques électrique ou magnétique', les paramètres du circuit, etc. Ces composantes 'TCM-Lib' peuvent être traitées par n'importe quel solveur. Dans notre cas, nous utilisons Matlab.

En ce qui concerne l'implantation sous Matlab, une interface graphique (Graphic User Interface) a été réalisée et sur la figure suivante, nous présentons une partie de l'interface utilisée pour les 'Données d'entrée' :



(pour des raisons de confidentialité, les données ont été supprimées)  
(exemple : encoche statorique)

Fig. 6 : Interface graphique : données d'entrée.

Différents algorithmes existent permettant de calculer les régimes en statique et dynamique de la machine. L'effet de saturation est réalisé par un algorithme bien connu : Newton-Raphson.

#### IV. Application à une machine synchrone 2 pôles

Une première machine disposant d'un rotor identique à celui d'un turbo-alternateur a été conçue en vue de valider notre modèle. La machine a une puissance de 3kW avec un rotor modifié. Celui-ci a la configuration suivante :

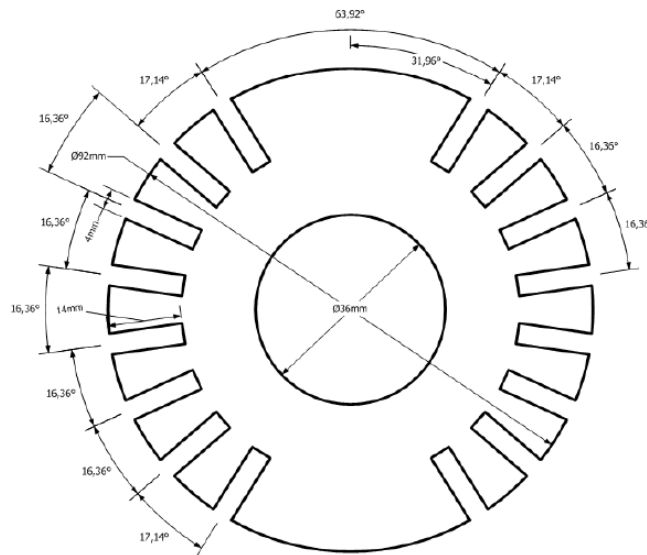


Fig. 7 : rotor 2 pôles (prototype de faible puissance)

La machine a un entrefer d'1mm et est composée de 24 encoches au stator et 14 au rotor avec une distribution non-régulière. Les caractéristiques  $b(h)$  sont différentes au stator et au rotor.

Nos simulations sont comparés aux résultats obtenus par un logiciel éléments finis, vue de la  $\frac{1}{2}$  machine Fig. 8 en utilisant OPERA-2D-RM : rotating machine, afin de valider le flux traversant une dent par exemple, mais aussi aux résultats expérimentaux.

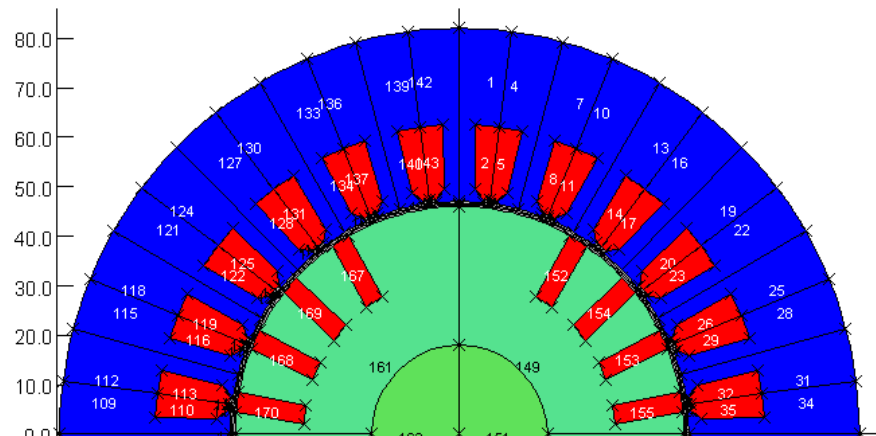


Fig. 8 : ½ machine 2 pôles (prototype de faible puissance)

Une première comparaison entre les simulations OPERA et le TURBO-TCM des flux au niveau de la carcasse et dans une dent en statique à vide et en charge a été réalisée. La Fig. 9 compare les flux au niveau d'une dent statorique alignée avec l'axe du pôle rotorique, et au niveau de la culasse où le flux est maximal.

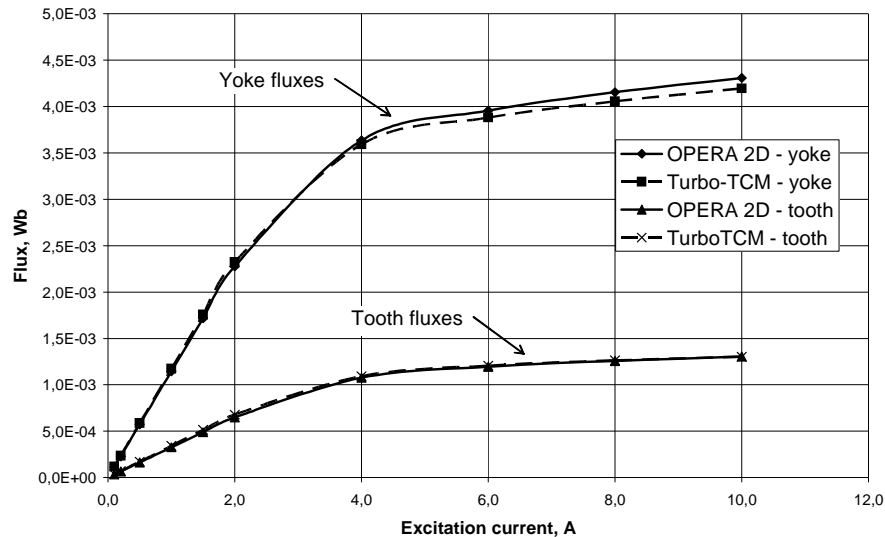


Fig. 9 : Comparaisons Turbo-TCM et OPERA : flux de dent et de culasse.

L'écart est relativement faible, l'erreur maximale sur le flux de dent est 4.9% et de 2.6% pour le flux de culasse. La figure suivante présente la caractéristique à vide  $E$  (la force électromotrice) fonction du courant d'excitation  $j$ . L'erreur maximale est de 6.6% obtenu pour le courant  $j$  maximal (20A).

Le FEM est obtenu par la méthode de rotor fixé. Cette méthode est utilisée pour obtenir tous les caractéristique de la machine en statique.

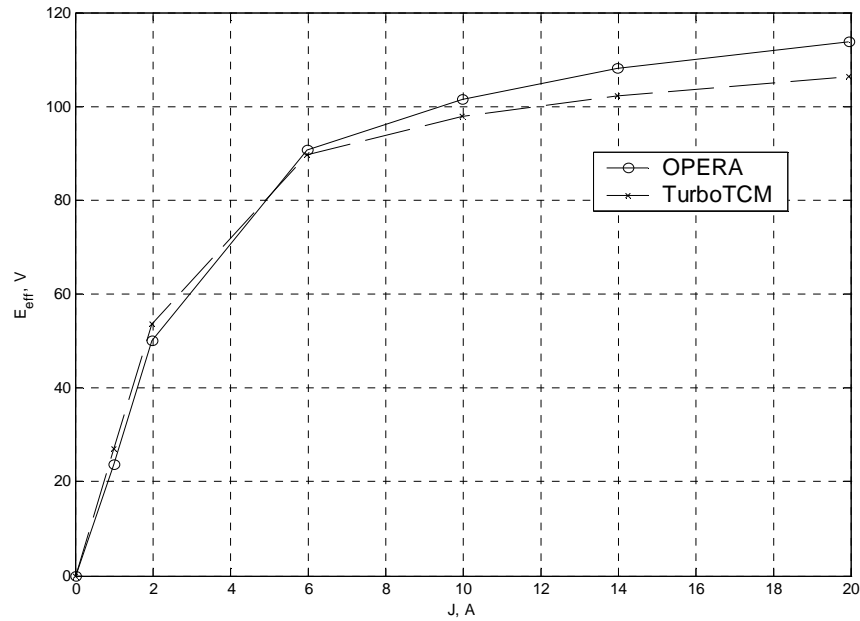


Fig. 10 : Caractéristique à vide  $E(j)$  de la machine synchrone

A présent, la caractéristique en charge est présentée.

La comparaison en charge est donnée sur la Fig. 11 présentant la caractéristique  $U_s$ , tension statorique entre 2 phases, fonction de  $I_s$ , courant dans une phase statorique. L'erreur maximale est de 4.1% pour un courant stator de 13A.

Les simulations obtenues sont très satisfaisantes et présentent un bon compromis temps de calcul – précision. En effet, le temps de calcul pour obtenir la caractéristique  $E(j)$  ou  $U_s(I_s)$  est de 10-15 secs.

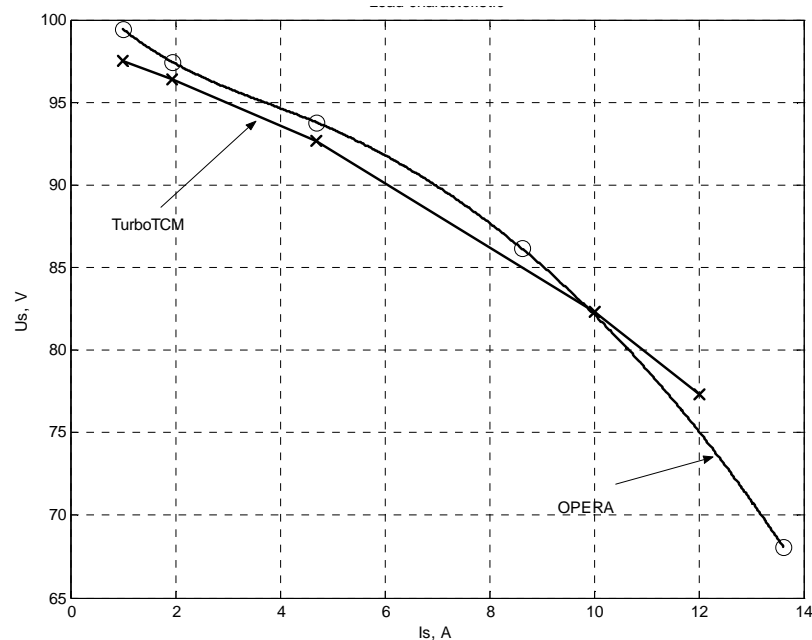


Fig.11 : Caractéristique en charge  $U_s(I_s)$

La comparaison en 'dynamique' : avec prise en compte du mouvement est donnée sur la Fig. 12. Le mouvement demande plusieurs points de simulations. Avec TURBO-TCM, 180 positions sont considérées pour une période. Avec OPERA-RM, seulement 100 positions sont données, le nombre de points de sortie



étant limité pour un calcul. La figure présente la fem à vide  $E$  (Volt) en fonction du temps (sec.) pour un courant d'excitation de 12 A (machine saturée).

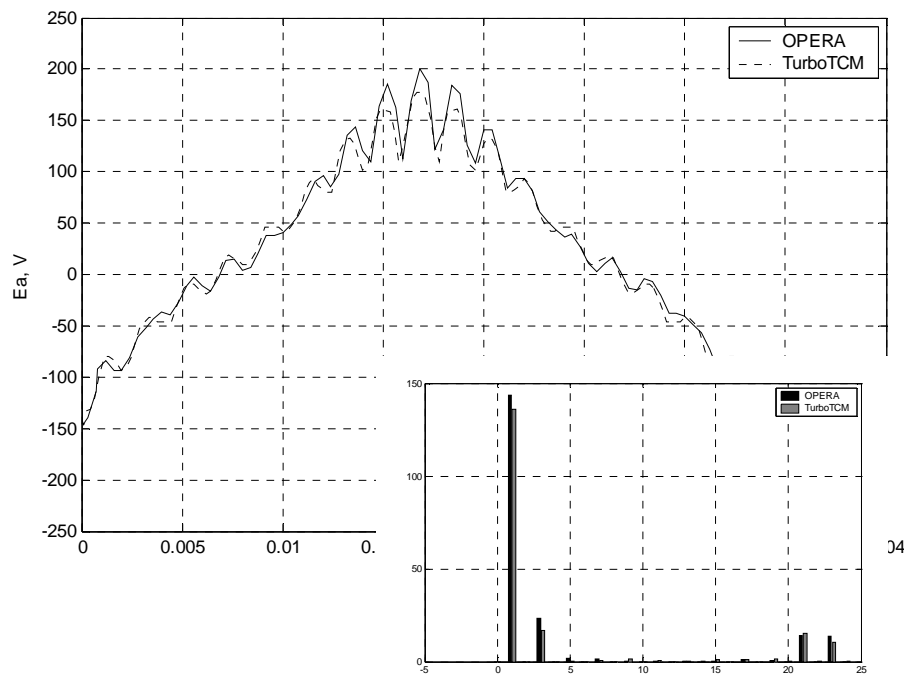


Fig. 12 : Résultats de simulations avec le mouvement.

La Table 1 présente le temps de calcul entre OPERA and TurboTCM sachant que le calcul par réseau de perméances compte 180 positions au lieu de 100 pour OPERA.

Table 1 : Temps de calcul

J, A	TurboTCM	Opera	Rapport sur le temps de calcul
1	12,4 sec	0h 55min	266,13
10	18,1 sec	3h 06min	616,57
20	18,3 sec	3h 25min	672,13

Ci-dessous, quelques résultats expérimentaux viennent renforcer la validité de notre modèle ‘réseau de perméances’. La comparaison de la courbe à vide calculée et expérimentale est présentée sur la Fig. 13, à gauche. Le résultat pour caractéristique de réglage est présenté sur la Fig. 13, à droite.

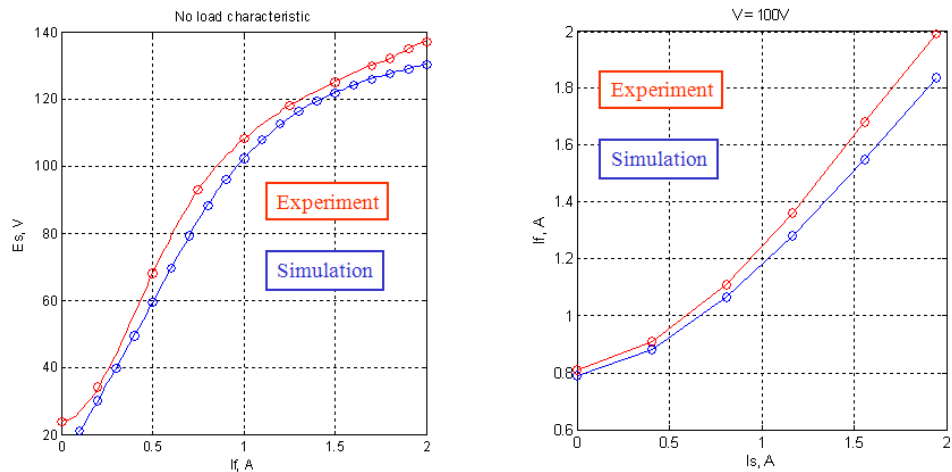


Fig. 13 : Comparaison de résultats de simulation et expérimentaux.

#### IV. Application au turbo-alternateur 2 pôles

Les turbo-alternateurs de la gamme industrielle (10 à 100 MW) sont entraînés par des turbines à gaz ou à vapeur tournant aux vitesses de synchronisme, 3000 ou 3600 tr/min. Le refroidissement par air est direct pour le bobinage rotorique dont les conducteurs sont ajourés pour laisser l'air se propulser depuis un canal sous encoche vers l'entrefer. Le stator est en refroidissement indirect, l'air circulant au travers des événements ménagés entre les paquets de tôles du circuit magnétique (figure ci-dessous).

Les bobinages rotoriques sont concentriques, logés dans des encoches taillées dans l'arbre massif magnétique. Les têtes de bobines sont maintenues par des frettes en acier amagnétique.

Le bobinage statorique triphasé est réalisé en barres (2 par encoches) connectées entre elles de façon à réaliser les circuits souhaités pour obtenir la tension de sortie nominale avec un circuit magnétique idéalement magnétisé et pour minimiser les harmoniques de tension.

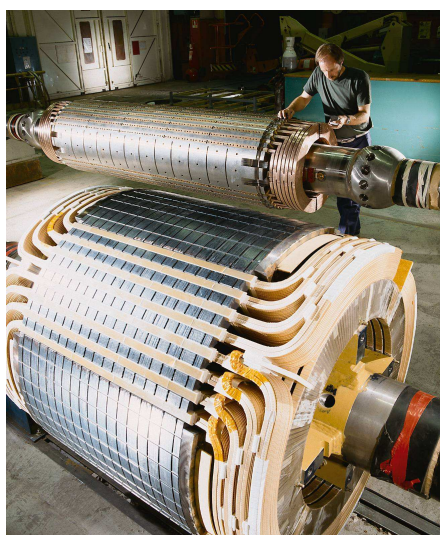
Les barres isolées de la masse par un mur isolant micacé sont constituées de brins de cuivre isolés les uns des autres, de dimensions optimisées et disposés en compensation Roebel pour minimiser les pertes Joules supplémentaires de type field et de circulation.

Les développantes et les circuits de couplage sont fermement supportés et calés pour éviter les vibrations qui endommagent les isolants.

Le circuit magnétique est réalisé en tôles à très faibles pertes, isolées et posées à joints décalés. Des tirants et les doigts d'extrémité permettent d'obtenir un serrage de la tôle magnétique entre deux plateaux de forte épaisseur pour éviter les vibrations et le bruit associé. Les plateaux en acier magnétique sont protégés du champ magnétique développé par les courants dans les têtes de bobines par des écrans de flux en cuivre.

Les caractéristiques dimensionnelles et les propriétés physiques de ces éléments constructifs constituent les données d'entrée du code de calcul développé.

Des extensions du code permettront également de dimensionner des machines à rotor cylindrique à polarité multiple (4 pôles, N pôles).



*Carcasse et stator d'un alternateur 4 pôles*

*Rotors bobinés d'un alternateur 4 pôles (en premier plan) et d'un turboalternateur 2 pôles (en arrière plan)*

#### **Caractéristiques à vide :**

Quelques résultats obtenus en régime permanent sont présentés ci-dessous. La méthode utilisée est détaillée dans les références [11], [12].

La Fig. 14 présente la tension à vide obtenue par Turbo-TCM et obtenue expérimentalement (mesures réalisées par Jeumont SA.). L'influence des effets 3D est donnée. L'erreur maximale est de 6,8% et de 0,3% pour le courant nominal.

La difficulté dans ce cas, est la prise en compte de la courbe  $b(h)$  « réelle » ayant une saturation importante au rotor mais aussi l'effet de magnétisation que l'on retrouve sur la caractéristique à vide réelle.

La Fig. 15 présente la caractéristique obtenue en court-circuit représentant le courant rotorique ( $I_f$ ) fonction du courant d'induit ou statorique ( $I_s$ ). Les résultats de simulation donnent de très bons résultats, erreur  $< 3.5\%$ . En effet, dans ce cas, il n'y pas d'effet de saturation.

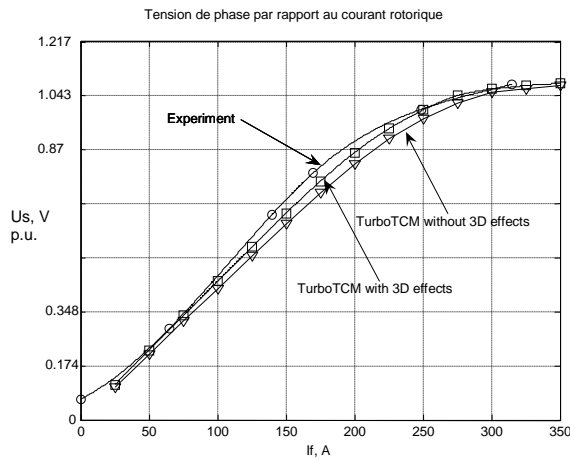


Fig. 14 : caractéristique à vide

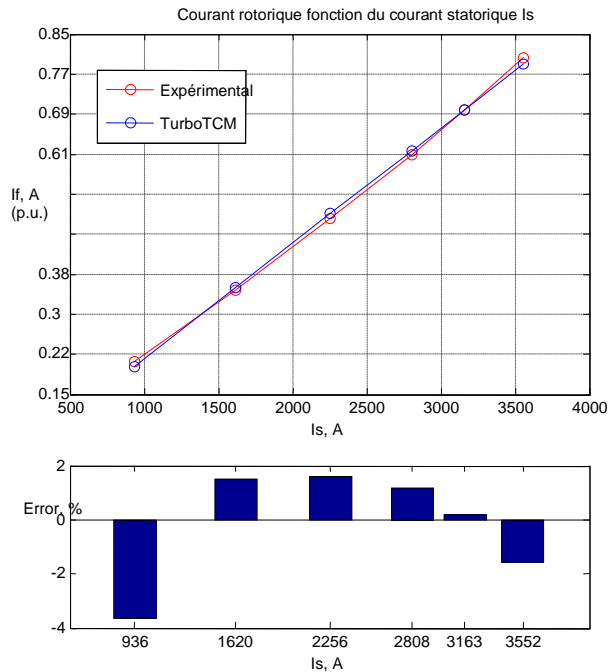


Fig. 15 : caractéristique en court-circuit.

L'analyse en dynamique (prise en compte du mouvement) est détaillée dans la référence [12]. L'intérêt est de pouvoir effectuer une analyse harmonique afin de vérifier par exemple que la tension de sortie de l'alternateur est parfaitement sinusoïdale ou de supprimer un harmonique en particulier au niveau de la fft de l'induction dans l'entrefer (Fig. 16).

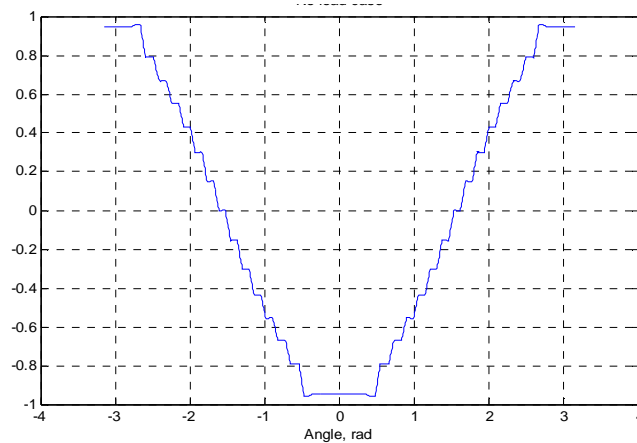


Fig. 16: Allure de l'induction dans l'entrefer (à vide)

Le temps de calcul pour une période est de l'ordre de la minute sur un pentium IV- 300MHz.

### Caractéristiques en charge :

Les figures suivantes (17 et 18) présentent les caractéristiques en charge d'un turbo-alternateur du marché industriel. Sur la Fig. 17, la tension de sortie  $U_s$  est fournie fonction du courant débité  $I_s$  pour 3 valeurs de  $\cos \varphi$  (PF). Les courbes en V sont données pour une tension de sortie nominale et pour différentes valeurs de puissance ( $P_s$ ).

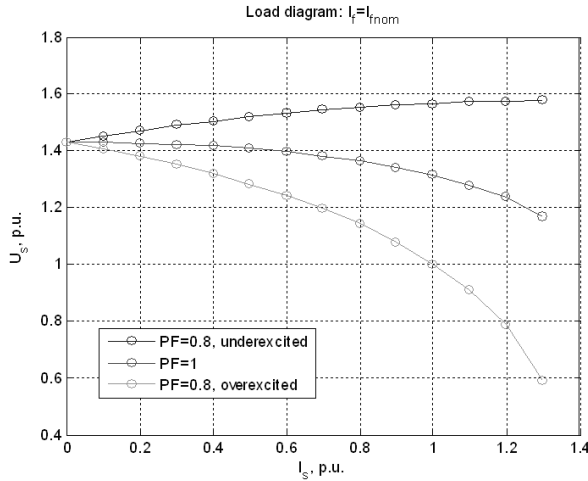


Fig. 17: Courbes  $U(I)$  pour différentes valeurs de PF

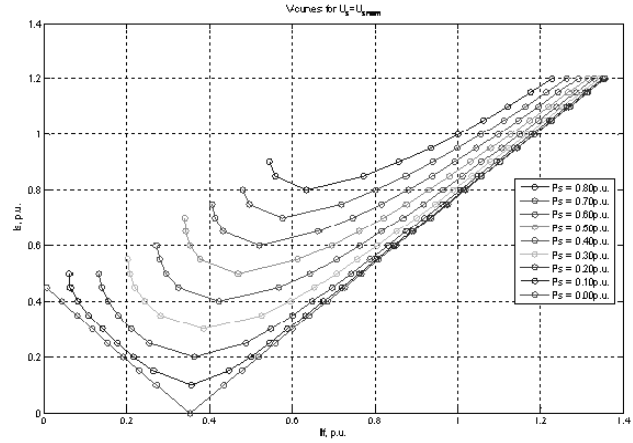


Fig. 18: Courbes en V pour différentes valeurs de puissance  $P_s$

Comme sur la Fig. 16, l'induction dans l'entrefer dans le cas d'un fonctionnement en charge est présentée sur la Fig. 19.

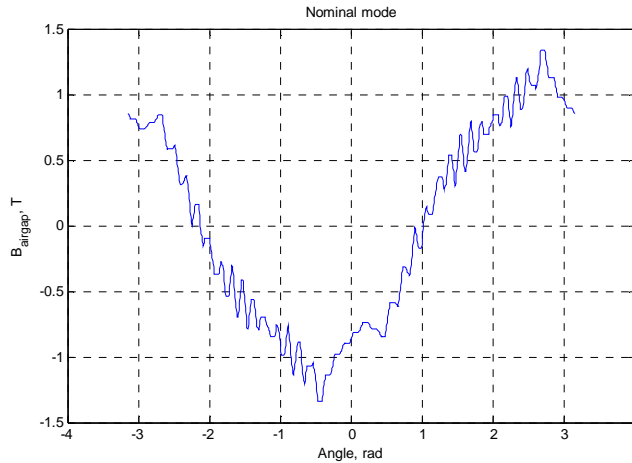


Fig. 19. Induction dans l'entrefer fonction de l'angle.

De plus, il est possible de déterminer le couple d'origine électromagnétique par l'outil 'TurboTCM':

$$T_{TCM} = \frac{1}{2} \cdot \sum U^T \cdot \frac{\partial \Lambda}{\partial \theta} \cdot U$$

Avec  $U$  – différence de potentiel magnétique,  $\Lambda$  – perméances,  $\theta$  – angle du rotor

Il est possible de comparer avec le calcul "classique" pour le point nominal (en négligeant le couple de pertes):

$$T_{EM} = \frac{S \cdot PF}{\Omega}$$

Avec  $S$  – la puissance apparente,  $PF$  – facteur de puissance,  $\Omega$  – vitesse de rotation en rad/sec

La différence entre ces deux calculs pour le point nominal est quasiment négligeable :

$$T_{TCM} = 1.006 T_{EM}$$

## V. Etude de sensibilité

Un autre avantage de 'TurboTCM', ayant un bon compromis entre le temps de calcul et la précision, il est possible d'étudier les variations de grandeurs d'entrée comme le diamètre, la longueur, etc..., fonction des caractéristiques de sortie.

Pour exemple, le couple électromagnétique produit par le turbo ainsi que la variation du courant rotorique sont considérés comme réponse. Seulement deux paramètres sont considérés :

- la hauteur de la culasse liée dans notre cas au diamètre (dia),
- la longueur de la machine (L).

Le domaine d'étude est défini par des intervalles de variations (Table 2).

TABLE 2: INTERVALLES DE VARIATION		
Facteurs	Niveau bas	Niveau haut
dia	dia - 5%	dia + 5%
L	L - 5%	L + 5%

Les figures suivantes (20 et 21) donnent l'influence de ces facteurs fonction des 2 réponses. Le nombre de points de simulations considérées pour représenter est de  $5*5$ , soit 25 simulations. Le temps de calcul est de l'ordre de 5 minutes pour obtenir ces surfaces de réponses.

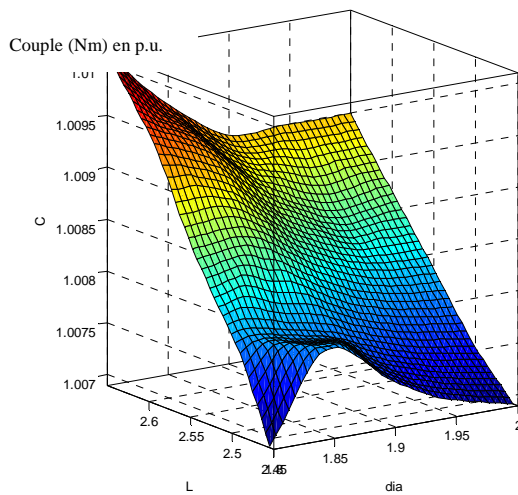


Fig. 20. Couple électromagnétique en p.u.

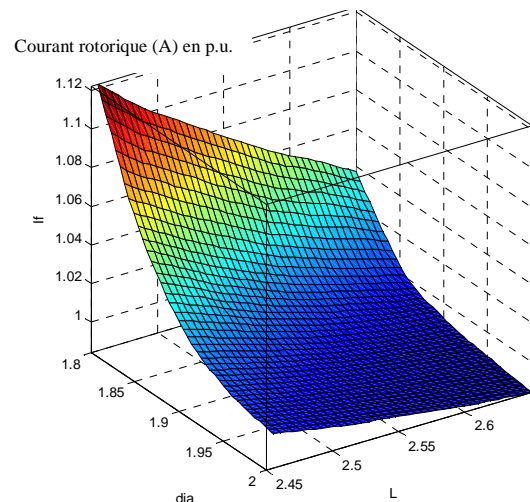


Fig. 21. Courant rotorique fonction en p.u.

Ces simulations sont réalisées dans des conditions nominales. Il est ensuite possible de choisir très rapidement en fonction du cahier des charges la hauteur de la culasse et la longueur du fer la plus intéressante par rapport au cahier des charges.

## VI. Conclusion & perspectives

Dans ce travail, un modèle de turbo-alternateurs a été présenté, basé sur la méthode de contour de dents. L'outil 'TurboTCM' développé sous Matlab permet de générer de façon automatique le réseau de perméances. Des simulations ont été comparées aux résultats expérimentaux et ont montré la bonne correspondance des résultats. Puis, certaines caractéristiques de sortie sont données montrant les possibilités de l'outil.

En réalisant un bon compromis entre le temps de calcul et la précision, nous pouvons envisager le couplage avec des outils d'optimisation. Dans un premier temps, une étude de sensibilité est fournie sachant que celle-ci peut être étendue à  $n$  facteurs influents.

Les perspectives sont nombreuses sur l'application d'un tel outil. Il nous reste à valider celui-ci sur ' $n$ ' turbo-alternateurs de puissances différentes mais aussi avec un nombre de pôles différents. Un de nos objectifs à court terme est de coupler l'outil avec la méthode des plans d'expériences [13], [14], permettant de considérer un grand nombre de facteurs, une première étape de 'Screening ou criblage' permettant de déduire les facteurs influents.

## REFERENCES

- [1] Ivanov-Smolenskii A., Kuznetsov V., "Universal Numerical Method for Simulating Electromechanical Converters and Systems", *Elektrichestvo*, Vol. 2000, No. 7, pp 24-34, July 2000, Moscow, Russia.
- [2] Kuznetsov V., Brochet P., "A general numerical modeling of electromagnetic process in electromechanical systems", *International Conference Electrical Machines (ICEM 2002)*, August 2002, Bruges, Belgium.
- [3] Ostovic V., "Dynamics of saturated machines", Springer-Verlag, 1989.
- [4] Worotynski J., Turowski M., and Mendrela E.A., "The accuracy of calculation of magnetic fields, inductance and forces in electromagnetic devices using the reluctance network method ", *Proc.ISEF'93*, Warsaw, pp159-162, 1993.
- [5] M. Hecquet, " Contribution à la modélisation des systèmes électrotechniques par la méthode des schémas équivalents magnétiques. Application à l'alternateur automobile", Thèse, Université des Sciences et Techniques de Lille, Janvier 1995.
- [6] M. Hecquet, P. Brochet, "Modélisation d'un alternateur automobile par un réseau de perméances couplé à des circuits électriques ", *Journal of applied Physics*. III, August 96, pp 1099-1116.
- [7] Hecquet M., Brochet P., "Time variation forces in a synchronous machine using electric coupled network model", *IEEE Trans. On Magnetics*, Vol. 34, No 5, pp 3656-3659, September 1998.
- [8] Ivanov-Smolenskii A. and authors, "Universal Method of Electromagnetic Processes Calculations in Electrical Machines", *Energoatomizdat*, 1986, Moscow, Russia.
- [9] Référence Manual of Vectors Fields : OPERA-2D RM; [www.vectorfields.com](http://www.vectorfields.com);
- [10] D. Petrichenko, M. Hecquet, P. Brochet, V. Kuznetsov, D. Laloy, 'Numerical modelling of a turboalternator using Tooth Contours Method: CAD application', *ICEM 2004, CD-Rom, Cracovie, 5-7 Oct. 2004*.
- [11] D. Petrichenko, M. Hecquet, P. Brochet, V. Kuznetsov, D. Laloy, 'Design and simulation of turbo-alternators using coupled permeance network model', *IEEE Trans on Magnetics*, Vol. 42, pp. 1259-1262, April 2006.
- [12] D. Petrichenko, M. Hecquet, P. Brochet, Vyacheslav Kuznetsov (MPEI), D. Laloy (Jeumont-Framatome), 'Design and simulation of turboalternators using Tooth contours method applied to design of turboalternators : developpement of CAD Software, ISEF'2005, Baiona, Espagne, 15-17Septembre 2005.
- [13] S. Vivier, "Stratégies d'optimisation par plans d'expériences et Application aux dispositifs électrotechniques modélisés par éléments finis", Thèse de doctorat, Université des Sciences et Techniques de Lille, Juillet 2002.
- [14] S. Vivier, M. Hecquet, A. Ait-Hammouda, M. Goueygou, P. Brochet, A. Randria, 'Experimental design method applied to a multiphysical model : treillis designs for a multidimensional screening study', ", *The International Journal for Computation and Mathematics in Electrical and Electronic Engineering (COMPEL)*, Special Issue, Vol. 24, No. 3, 15p, 2005.